



PROGRESS REPORT

ON THE ACTIVITIES AT THE
BUDAPEST RESEARCH REACTOR



BUDAPEST NEUTRON CENTRE
2013 - 2015

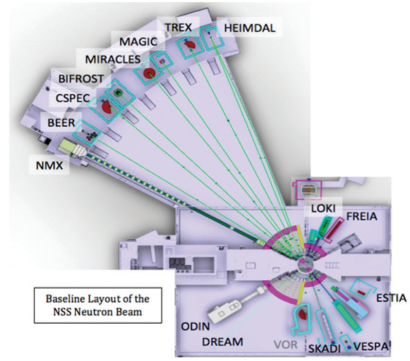


EUROPEAN SPALLATION SOURCE

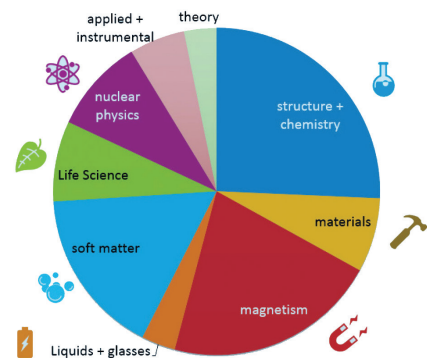
The European Spallation Source, ESS, will be built in Lund, Sweden. The ESS will be a world-leading multidisciplinary materials research centre. A neutron source for Europe's science community, the ESS facility can be likened to a super microscope, harnessing neutron beams to provide a superior research tool that can give us a greater in-depth understanding of materials at an atomic level.

Neutrons are excellent for probing materials on the molecular level – everything from motors and medicine, to plastics and proteins. Detailed studies are dependent on how many neutrons can be produced by a neutron source. This is a significant limitation for existing sources based on nuclear reactors. As a result, scientists and engineers have developed a new generation of neutron sources based on particle accelerators and spallation technology, a much more efficient approach. ESS will provide up to 100 times brighter neutron beams than existing facilities today. ESS will be a prominent part of the future landscape of European research infrastructures, providing experimental possibilities to researchers from academia as well as industry.

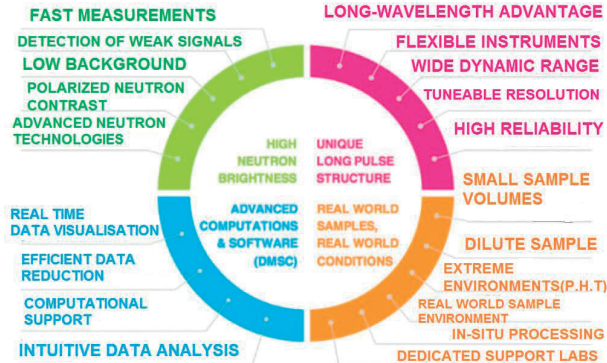
The ESS Baseline Layout for the First 16 Instruments



Neutron use per scientific topic



ESS opens new capabilities to science



<https://europeanspallationsource.se/>

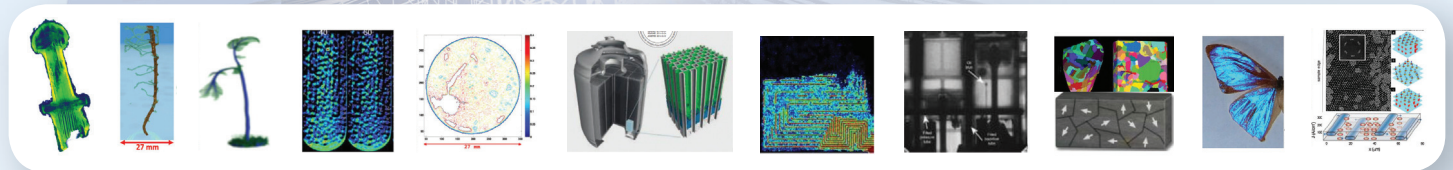
ESS TECHNICAL PARAMETERS

- Proton kinetic energy: 2 GeV
- Average bema power: 5 MW, 14 Hz
- Macro-pulse length: 2.86 ms
- Average macro-pulse current: 62.5 mA
- Rotating Tungsten target (2.5 m diameter x 10 cm height, 7500 Tungsten bricks)
- Target He gas-cooling
- 2 type of moderators (liquid H₂, water)
- Linac length: 602.5 m
- Maximum annual operation: 6.000 h

Timeline of ESS:



archeology-agriculture-material science-engineering materials-geoscience-life science-magnetic phenomena



BrightnESS is a EU-funded project within the Horizon 2020 Research and Innovation programme in support of the ESS, a partnership of several European nations working together to build the world's next-generation neutron science facility.



PARTNERS: 18 EU PARTNERS • 11 COUNTRY • 36 MONTH BUDGET: 20MEuro



PROGRESS REPORT

ON THE ACTIVITIES AT THE
BUDAPEST RESEARCH REACTOR



BUDAPEST NEUTRON CENTRE
2013–2015

Budapest Neutron Centre Progress report 2013 - 2015

Edited by R. Baranyai, E. Nagy

L. Rosta

Budapest, November, 2016

Postal address and contact persons:

Centre for Energy Research,
Hungarian Academy of Sciences
1121 Budapest, Konkoly Thege u. 29-33.

Hungary

Dr. Rózsa F. BARANYAI

Phone: 36-1-392-2799

Fax: 36-1-395-9293

e-mail: baranyai.rozsa@energia.mta.hu

Wigner Research Centre for Physics
Hungarian Academy of Sciences
1121 Budapest, Konkoly Thege u. 29-33.

Dr. László ROSTA

Phone: 36-1-392-2789

Fax: 36-1-392-2501

e-mail: rosta.laszlo@wigner.mta.hu

Location:

Budapest Research Reactor
1121 Budapest, Konkoly Thege út 29-33
KFKI, Bld, 10.

Cover page:

Team of Budapest Neutron Centre at Budapest Research Reactor Hall.

The publishing of this Progress Report was sponsored by BrightnESS EU supported project. Hungary is founding member of ESS ERIC and active participant of ESS constructing project.

The publishing was also sponsored by MIRROTRON and ANTE industrial companies, BNC partners in neutron instrumentation development projects.

Progress Report

CONTENTS

PREFACE	7
1. BUDAPEST RESEARCH REACTOR	8
2. INTERNATIONAL SCIENTIFIC ADVISORY COUNCIL	11
3. USER SELECTION PANEL	12
4. RESEARCH HIGHLIGHTS	14
4.1. "BEADS FROM HEAVEN" - NEUTRON TECHNIQUES REVEAL FIVE-THOUSAND-YEAR-OLD IRON SMITHING SKILLS	14
4.2. THE COMBINATION OF NEUTRON IMAGING AND PROMPT-GAMMA ACTIVATION ANALYSIS	19
4.3. NEW PROMPT FISSION GAMMA-RAY DATA IN RESPONSE TO THE OECD/NEA HIGH PRIORITY REQUEST	21
4.4. ATOMIC STRUCTURE OF AMORPHOUS MATERIALS STUDIED BY NEUTRON DIFFRACTION	23
4.5. SANS STUDY OF NANOSCALE STRUCTURE OF LOW-CARBON STEEL AFTER ROLLING WITH SHEAR	26
4.6. EXPERIMENTAL RESULTS ON IRRADIATED SAMPLES IN THE FRAMEWORK OF MATTER PROJECT	30
5. DETAILED RESULTS	34
6. INSTRUMENTS	138
6.1. PSD – NEUTRON POWDER DIFFRACTOMETER WITH POSITION SENSITIVE DETECTORS	138
6.2. MTEST DIFFRACTOMETER	140
6.3. TOF – HIGH RESOLUTION TIME-OF-FLIGHT POWDER DIFFRACTOMETER	142
6.4. YS-SANS – SMALL ANGLE NEUTRON SCATTERING INSTRUMENT YELLOW SUBMARINE	144
6.5. FSANS – TIME OF FLIGHT SMALL ANGLE NEUTRON SCATTERING INSTRUMENT	146
6.6. REF – COLD NEUTRON REFLECTOMETER	148
6.7. GINA - NEUTRON REFLECTOMETER WITH POLARIZATION OPTION	150
6.8. ATHOS - COLD NEUTRON TREE-AXIS SPECTROMETER	152
6.9. TAST/HOLO - THERMAL NEUTRON TREE-AXIS SPECTROMETER AND NEUTRON HOLOGRAPHIC INSTRUMENT	154
6.10. RAD – STATIC/DYNAMIC THERMAL-NEUTRON AND X-RAY IMAGING STATION	156
6.11. NORMA - NEUTRON OPTICS AND RADIOGRAPHY FOR MATERIAL ANALYSIS	158
6.12. BIO – BIOLOGICAL IRRADIATION CHANNEL	160
6.13. PGAA – PROMPT GAMMA ACTIVATION ANALYSIS	162
6.14. NIPS - NEUTRON-INDUCED PROMPT GAMMA-RAY SPECTROSCOPY	164
6.15. DÖME LOW-LEVEL GAMMA-SPECTROSCOPY FACILITY	166
6.16. BAGIRA4 – REACTOR IRRADIATION LOOP	168
6.17. RNAA – REACTOR-NEUTRON ACTIVATION ANALYSIS	170
7. EDUCATION	173
8. EVENTS	176
9. PUBLICATIONS	179
APPENDIX	188

PREFACE

The Budapest Neutron Centre (BNC) is the research organisation for the open access utilisation in science and technology for the Budapest Research Reactor (BRR) facilities. It is a consortium of neutron research laboratories of two institutions of the Hungarian Academy of Sciences: the **Centre for Energy Research (MTA EK)** and the **Wigner Research Centre for Physics**. BNC has a staff of nearly 120 people, it is governed by its Board of Directors and the legal representation is provided by MTA EK. BRR is one of the largest research infrastructure in Central Europe. This is the base for domestic and international user community to serve for exploratory and applied research in many fields of science and technology as well as for methodical developments in neutron beam and irradiation techniques. After a major refurbishment in 1993, this 10 MW reactor is now expected to be operated by 2023. From early 2012 only 20% enriched uranium-235 fuel is used.

The reactor has 10 horizontal beam tubes, one of the tangential beam tubes is equipped by a liquid H₂ cold neutron moderator. Three supermirror guides transport neutrons to the measurement sites in the guide hall. A thermal guide serves for a high resolution time-of-flight diffractometer. The reactor is operated in 10 days cycles, 12-14 cycles/year. Currently 17 experimental stations are serving for users: diffraction, small angle scattering, inelastic scattering, radiography/irradiation, in-beam gamma capture and in-pile irradiation facilities are available.

BNC is an open access facility for the domestic and international user community – the suit of neutron beam instruments are assisted by a professional team of scientists and engineers for experimental services. Research proposals can be submitted twice a year, an international selection panel takes care of the review of the proposals, even “fast-track” processing of proposals is possible thanks to the electronic communication. BNC has been involved in several former EU Framework Programs, currently three H2020 projects are being implemented with our partnership (BrightnESS, SINE2020 and IPERION CH). An important part of the experimental work presented in this Report was performed with the support of the last access program (NMI3-II). One of the success stories of this

period is the CHARISMA project completed in 2014. This was another transnational access type project for the investigation of objects of cultural heritage. 50 experiments – nearly twice as much as it was programmed – have been performed showing the growing interest in this field for non-invasive neutron techniques. One of the presented highlights (4.1) is also related to archaeology: The meteoritic origin and smelting of the “mankind’s earliest iron pieces” (5300 years old beds from Egypt) was proved by BNC’s neutron and X-ray techniques. The publication of this discovery was followed by an unusually for neutron works wide appearance in the world press (Times, Le Monde, Herald Tribune...).

The instrument development program was progressed, the new focusing small angle scattering spectrometer F-SANS was completed and entered the user program. The combined use of PGAA with neutron tomography, first proposed at BNC, has met considerable interest in the user community; another highlight article in this booklet (4.2) presents interesting results of this type of experiments. BNC’s international training program – the yearly one-week school with hands-on training on our spectrometers – continues to be a success: we clearly monitor the experimental proposals coming from new users having attended CETS (see details on the Central European Training School in section 8).

This Progress Report contains most of the relevant experiments performed at BNC during the past 3 years. It serves also as information for the users: A table of experimental stations is given in the Appendix. The call for proposals including the conditions how one can make use of the EC travel support is regularly advertised on the web (www.bnc.hu). The BNC website offers also the possibility of reading reports on BNC activities, e.g. the present Report. This booklet gives also the description of our experimental stations. A list of publications concerning this three years activity is also attached.

Budapest, September 2016.

Ákos Horváth
Chairman of the BNC
Board of Director

1. BUDAPEST RESEARCH REACTOR



📖 *Bird view of the Budapest Research Reactor*

The Budapest Research Reactor (BRR) as other research reactors in the world, plays a vital role for the society, producing radioisotopes for medical purposes (cancer detection and treatment), for industrial applications and neutron beams for fundamental and applied research.

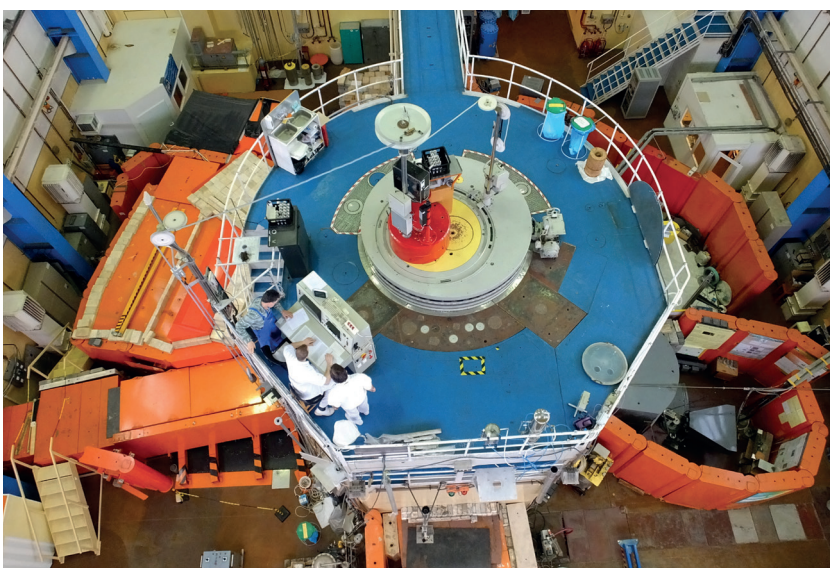
BRR is light water cooled and moderated tank type reactor, uses low enriched uranium (LEU) fuel. It produces continuous neutron flux 2.1×10^{14} neutrons per second per cm^2 with a thermal power of 10 MW.

The reactor operates for a 10 day cycle, followed by a short weekend break. After 10 reactor cycles,

a refueling outage comes, when the spent fuel assemblies are replaced with fresh ones. In addition there is a longer shutdown to carry out the necessary inspection and maintenance. Normally, there are 10 cycles per year providing 120 days for science.

BRR's operational staff collaborate with their international colleagues to share information and knowledge directly or through international cooperation and forums. BRR hosted the annual meeting of the Regional Advisory Safety Committee for Research Reactors in Europe (EURASC) during 2015. The participants discussed their experience on the safety issues including particular protection against internal and external hazards and neutronic and thermalhydraulic safety criteria for research reactors. BRR is a founder member of the Eastern European Research Reactor Initiative (EERRI), which is a coalition of nine reactors from the Central-European region. During the autumn of 2015 the 11th EERRI Research Reactor Group Fellowship Training Programme was organized. From the 6 week training programme 4 weeks were held in Budapest. Participants came from Jordan, Saud Arabia, Nigeria, Tanzania, and South Africa to improve their knowledge on the field reactor physics, reactor operation, nuclear measurements techniques, safety and environmental issues.

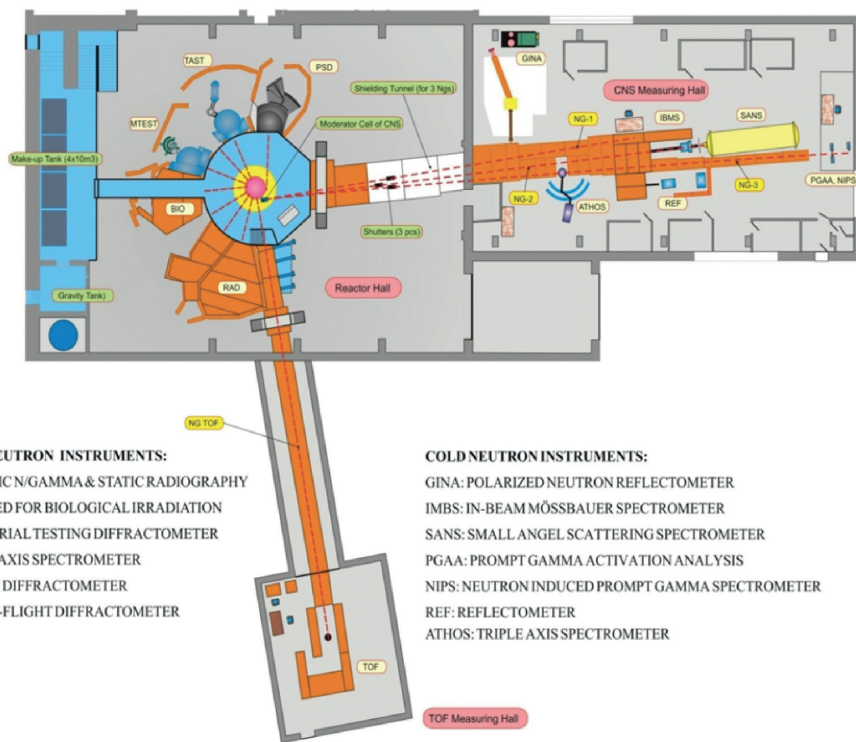
BRR is used by members of the scientific, medical, environmental and industrial communities, as well



📖 *Top view of the research reactor*

as Hungarian Universities. The research reactor generates neutrons with using nuclear fission of uranium for a wide range of scientific investigations. The Budapest Neutron Centre (BNC) coordinates the scientific utilization of the research reactor. 15 neutron instruments are offered in the user programme; from these 13 instruments are installed directly to the beam ports of the reactor or to the thermal and cold neutron guides, 2 of them are placed in the vertical irradiation

laboratory practice for studying nuclear-based techniques. Specialized course was developed for the geologist students of Eötvös Loránd University to introduce nuclear analytical techniques to their education. To train the young scientist and attract new users BNC organizes the Central European Training School on Neutron Scattering on regular basis. The school provides insight into neutron scattering, element analysis and imaging techniques



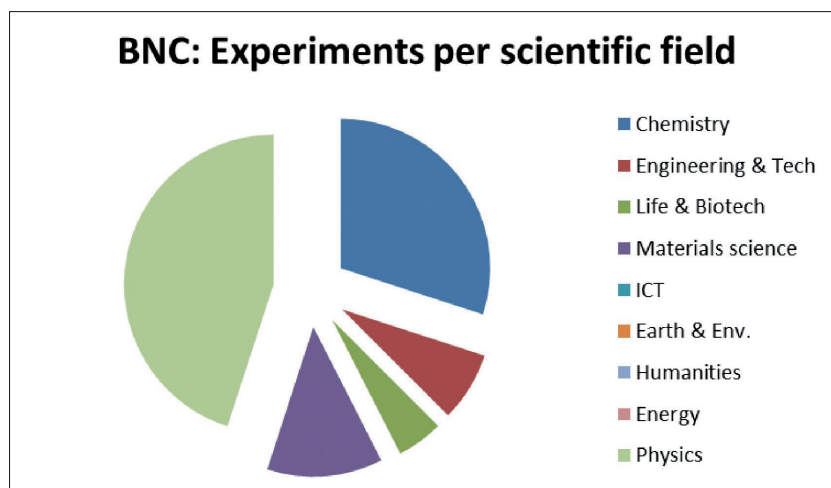
Layout of the BRR's facilities

channels. BNC provides access to the international neutron user community through the peer-review arrangement. Local scientists assist researchers and industrial users to find out the appropriate neutron techniques that meet their research needs. Research at BNC using neutrons addressing issues of chemistry, physics, engineering & technology, life science and material science, see the figure of Experiments per scientific field.

and their applications to study the structure and dynamics of condensed matter. The Budapest Research Reactor is open to the public. Members of the local communities and high school and university students are invited to visit and learn more about the amazing nuclear science.

BNC is a member of the European network of neutron centres and a partner in the EU Framework Programme projects (NMI3-II, CHANDA, IPERION, SINE2020, BrightNESS).

BNC is strongly committed to train the future professionals. In cooperation with Hungarian universities (Budapest University of Technology and Economics, Eötvös Loránd University, Pannon University) BNC accommodates students for



*Progress
Report*

2. INTERNATIONAL SCIENTIFIC ADVISORY COUNCIL

Aksenov, Victor L.	PNPI "Kurchatov Institute"	Russia
Avdeev, Mihail	FLNP Dubna	Russia
Faragó, Béla (chair)	Institute-Laue-Langevin	France
Geue, Thomas	Paul-Scherer Institute	Switzerland
Ioffe, Alexander	Jülich Centre for Neutrons	Germany
Jentschel, Michael	Institute-Laue-Langevin	France
Mezei, Ferenc	Wigner RCP/ESS Lund	Hungary/Sweden
Mikula, Pavol	INP Rez	Czech Republic
Pépy, Gerard	LLB Saclay	France
Révay, Zsolt	TUM Munich	
Rogante, Massimo	Rogante Engineering	Italy
Roszbach, Matthias	FZ-Jülich	Germany
Rosta, László	Wigner RCP	Hungary
Rumyancev, A. Yu	Foreign Ministry	Russia
Russina, Margarita	Helmholz Zentrum Berlin	Germany
Schober, Helmut	Institute-Laue-Langevin	France
Present ex-officio		
Baranyai, Rózsa	MTA EK	Hungary
Belgya, Tamás	MTA EK	Hungary
Füzi, János	Wigner RCP	Hungary
Horváth, Ákos	MTA EK	Hungary
Lévai, Péter	Wigner RCP	Hungary
Szentmiklósi, László	MTA EK	Hungary

3. USER SELECTION PANEL

Pépy, Gerard	Laboratoire Leon Brillouin,	France
Strunz, Pavel	INP Rez	Czech Republic
Godfrey, Evelyne	Uffington Heritage Watch	UK
Raisanen, Jyrki	University of Helsinki	Finland
Krakovszky, Ivan	Charles University	Czech Republic
<i>T. Bíró, Katalin (co-chair)</i>	Hungarian National Museum	Hungary
Roszbach, Matthias	Forschungszentrum Juelich GmbH	Germany
Jentschel, Michael	Institute Laue-Langevinw	France
Makai, Mihály	Budapest Technical University	Hungary
<i>Geue, Thomas (chair)</i>	Paul-Scherer Institute	Switzerland
Grósz, Tamás	Chemical Research Centre	Hungary

*Research
Highlights* | **4.**

4.1. “BEADS FROM HEAVEN” - NEUTRON TECHNIQUES REVEAL FIVE-THOUSAND-YEAR-OLD IRON SMITHING SKILLS

László Rosta¹, Tamás Belgya², György Káli¹, Zoltán Kasztovszky², Zoltán Kis², Imre Kovács³, Boglárka Maróti², László Szentmiklósi², Zoltán Szőkefalvi-Nagy³, Albert Jambon⁴, Thilo Rehren⁵

¹ Wigner Research Centre for Physics, Hungarian Academy of Sci., Institute for Solid State Physics and Optics

² Centre for Energy Research, Hungarian Academy of Sciences

³ Wigner Research Centre for Physics, Hungarian Academy of Sci., Institute for Particle and Nuclear Physics

⁴ Université Pierre et Marie Curie, Paris

⁵ University College London, Qatar, a UCL department at Hamad bin Khalifa University, Doha.

Abstract

In August 2013 the publication of a new study in *Journal of Archaeological Science* appeared which reveals that 5000 year old Egyptian iron beads have been found to be made from hammered pieces of meteorites [1]. The experimental work was performed at the Budapest Neutron Centre (BNC). The nature and origin of humankind's earliest iron artefacts has been a matter of debate for over a century. This discovery not only demonstrates successful nuclear analytical methodology to uncover trace elements after complete corrosion, but also proves that already in the fourth millennium BC metalworkers had mastered the smithing of meteoritic iron, an iron-nickel alloy much harder and more brittle than the more commonly worked copper.

The paper focuses on the earliest known iron artefacts: nine small beads securely dated to circa 3200 BC, from two burials in Gerzeh, northern Egypt. It highlights that these beads were made from meteoritic iron, shaped by being careful hammered into thin sheets before being rolled into tubes. The iron beads were strung into a necklace together

with other exotic minerals such as lapis lazuli, gold and carnelian, revealing the status of meteoritic iron as a special material on a par with precious metal and gem stones.

Using various neutron techniques at BNC – complemented by X-ray spectroscopy analysis – the ability to determine the nature of material even after complete corrosion of the iron metal has been demonstrated. In contrast to former investigations of the beads which involved only surface analysis, taking advantage of the deep penetration but non-invasive nature of the neutron techniques used, the authors were now able to get a more detailed insight into material features. Prompt-gamma activation analysis, neutron diffraction and neutron radiography revealed features such as the elemental composition, crystal/amorphous structure and the internal topology of the beads, respectively. Particle induced X-ray emission has also complemented to the full understanding of compositional data showing that the beads were made from meteoritic iron. This study was also reviewed in the Hungarian archaeology e-journal in 2013 [2].

Introduction

The nature and origin of mankind's earliest iron artefacts have remained a matter of uncertainty and dispute ever since their excavation in 1911, in a predynastic cemetery near the village of el-Gerzeh in Lower Egypt. A total of nine tubular iron beads were retrieved from the cemetery, all from two closed archaeological contexts, and so of secure

date. Four beads were found in their original order as strung into a necklace with tubular lapis lazuli, carnelian, agate, and gold beads (Petrie et al. 1912) [3]; this tomb also contained three more iron beads, a limestone mace-head, a copper harpoon, and a small ivory vessel, a mudstone fish-shaped palette, an ivory spoon, a flint bladelet, two stone vessels,

and twelve ceramic vessels. Two more beads were from another tomb, containing the most diverse materials in the entire cemetery: lapis lazuli, obsidian, gold, carnelian, calcite, chalcedony, steatite, faience, garnet, serpentine (Fig.1).

Since both tombs are securely dated to Naqada IIC-III A, c 3400-3100 BC, the beads predate the emergence of iron smelting by nearly 2,000 years, and other known meteoritic iron artefacts by more than 1,000 years, giving them an exceptional position in the history of metal use. Their early date makes it reasonable to assume that they were made from meteoritic iron; while the tombs were undisturbed, the intrusion into the tomb of man-made iron through taphonomic processes or contamination during excavation cannot be excluded entirely. Here we present positive proof of a meteoritic origin of these beads (Fig. 2.), strengthening the argument that these are indeed the earliest known examples of iron metal worked by humans.

Meteoritic iron has several characteristics that distinguish it from smelted iron. Most prominent are the large crystal grain size and Widmannstetter texture, elevated bulk concentrations of nickel (1 to 10 wt%), cobalt (1000 to 10,000 ppm) and germanium (mostly 200 to 400 ppm), and the presence of mineral phases such as schreibersite ($[\text{Fe,Ni}]_3\text{P}$), troilite $[\text{FeS}]$ and sphalerite $[\text{ZnS}]$. Some of these characteristics, however, are not diagnostic. While germanium has not been found in smelted iron above c 10 ppm,

Experimental techniques and results

We analysed the three beads currently held at the UCL Petrie Museum of Egyptology in London, UK for their composition and surviving structure using non-invasive methods. Earlier analysis by pXRF indicated an elevated nickel content of the surface of the beads in the order of a few per cent, and their magnetic property suggested that iron metal may be present in their body. Following this, prompt-gamma activation analysis (PGAA), particle-induced X-ray emission (PIXE), neutron radiography (NR), and time-of-flight neutron diffraction (ToF-ND) were used [4] to characterise surface and body of the beads, at the laboratories of the Budapest Neutron Centre.

By ToF-ND testing for grain size and crystal lattice structure of any metallic phases present in the beads,



Figure 1. Collection of stone and faience beads from Tomb 67. Modern re-stringing, without the iron beads.



Figure 2. Photographs of three of the originally nine iron beads from Gerzeh, Lower Egypt. From left UC10738, UC10739 and UC10740. Petrie Museum of Egyptian Archaeology. (Photo by Gianluca Miniaci)

nickel and cobalt are common alloying elements in modern steel, and have been found in similar concentrations in some ancient smelted iron. Elevated phosphorus and sulphur concentrations are also found in smelted iron. The chemical and microstructural characteristics of meteoritic iron may also be distorted or lost through extended working of the metal or corrosion during burial.

no metallic form of iron was found. No definite Bragg peaks were observed, consequently they should consist of a larger number of low symmetry crystalline phases (probably with non-uniform



Figure 3. The time-of-flight neutron diffractometer (ToF-ND) at the thermal neutron beam-line No.1, with the new large area back-scattering detector bank.

chemical compositions, as oxides), imperfectly crystallized or amorphous compounds (these occur typically at hydroxides) and/or hydrogen in any other form. This is considered typical for the corrosion products of iron.

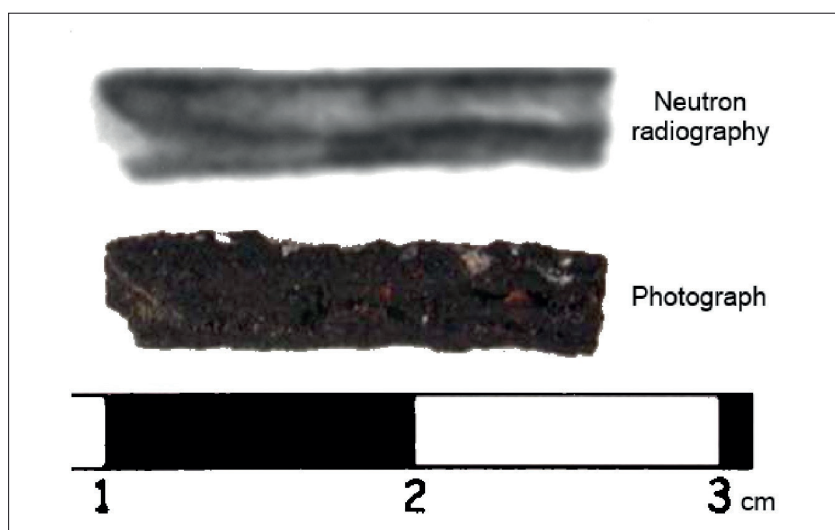
Neutron radiography revealed the original shapes and bulk morphology of the artefacts and details of their manufacture. All three artefacts have a central hole along their long axis, not visible during visual inspection due to their corrosion. These images demonstrate that the beads were made from rolled iron sheet, with areas of overlapping metal visible at the centre of the seam and V-shaped tapering at one end of bead UC10740 (Fig. 3). This would have required repeated hammering with intermittent annealing, a technique also documented for pre-Columbian Hopewellian meteoritic iron beads (McCoy et al. 2008) [5].

PGAA showed that the beads consist predominantly of iron and oxygen in broadly similar amounts, which is consistent with their corroded state. Of more interest, the beads contain between 2.8 and 4.1 wt% nickel, 0.6 to 1.0 wt% phosphorus, and 1700 to 2400 ppm cobalt (Table 1.) Small amounts of light elements (hydrogen to manganese) are thought to represent corrosion and soil particles incorporated from the burial environment. PIXE analysis of the beads' surfaces (Fig.5.) confirmed the presence of iron as the main element, followed by nickel at an estimated 5 wt%. Individual spots have different concentrations of copper, lead, arsenic, zinc and manganese, reaching several hundreds of ppm.

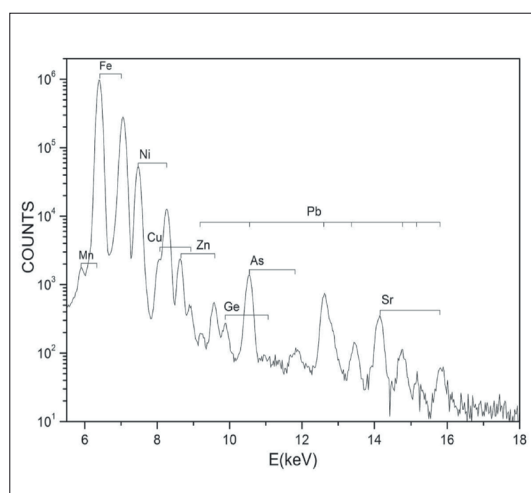
(The X-rays from lighter elements were filtered out to avoid disturbing pile-up peaks.) Two of the three beads showed spots with germanium above the detection limit estimated to be at c 30 ppm, and reaching up to c100 ppm in individual spots. Due to the elevated detection limit of 1000 ppm for germanium caused by the germanium content of the detector used in the PGAA measurements it was not possible to detect this element by PGAA in such low concentrations.

The most surprising finding of the neutron radiography images was the wrapped sheet-like internal structure, which was preserved in spite of the complete corrosion of the beads. The bulk contents of the beads in iron, nickel, cobalt, and phosphorus are consistent with meteoritic iron. Germanium levels as found by PIXE in selected areas on the surface of two of the beads reach about half the level common for meteorites, and much higher than those detected in smelted iron.

We explain the relatively lower level of germanium compared to fresh meteoritic iron with the selective oxidation and subsequent loss of germanium during smithing. Repeated heating and hammering would also have broken up any coarse-grained Widmannstaetten texture into irregular small ferrite grains, and destroyed the schreibersite crystals, partly homogenising the phosphorus content across the worked metal (McCoy et al. 2008) [5]. The diagnostic textural properties of meteoritic iron were therefore most likely already lost prior to the corrosion of the metal.



▲ **Figure 4.** Neutron image of the UC10740 iron bead, its in-side view and photo.



▲ **Figure 5.** PIXE spectrum of bead UC10740, showing Ka and Kb lines for main elements, including iron (Fe), nickel (Ni), and germanium (Ge).

Table 1

Composition of three iron beads from Gerzeh (UC10738-40), one partly corroded piece of meteoritic iron from Argentina (CdC3C), and two completely corroded medieval non-meteoritic iron samples (28848/12 and/1) for comparison. All data in weight percent, determined by PGAA. D.L. stands for detection limit.

Sample code element	D.L./ wt%	UC10738		UC10739		UC10740		CdC3C		28848/12		28848/1	
		Conc./ wt%	Abs. unc. ±	Conc./ wt%	Abs. unc. ±	Conc./ wt%	Abs. unc. ±	Conc./ wt%	Abs. unc. ±	Conc./ wt%	Abs. unc. ±	Conc./ wt%	Abs. unc. ±
H	0.0006	1.65	0.03	1.58	0.03	2.03	0.03	0.114	0.003	1.16	0.03	1.36	0.03
B	0.00005	0.0473	0.0009	0.0575	0.0010	0.0810	0.0012	<D.L.		0.00172	0.00004	0.00465	0.00010
Na	0.09	0.13	0.01	0.23	0.02	0.20	0.01	<D.L.		0.059	0.004	0.090	0.012
Mg	0.2	0.66	0.09	<D.L.		0.46	0.04	<D.L.		0.37	0.06	0.47	0.06
Al	0.05	0.18	0.07	0.31	0.02	0.10	0.03	<D.L.		0.12	0.02	0.06	0.02
Si	0.1	1.5	0.1	3.0	0.1	1.3	0.05	<D.L.		0.6	0.04	0.2	0.06
P	0.2	0.8	0.2	0.6	0.1	1.0	0.1	0.24	0.05	<D.L.		<D.L.	
S	0.05	0.2	0.02	0.2	0.01	0.2	0.01	0.11	0.01	0.063	0.007	<D.L.	
Cl	0.005	0.709	0.017	0.625	0.011	0.806	0.015	0.0050	0.0001	0.118	0.003	0.167	0.004
K	0.01	0.028	0.002	0.077	0.003	0.080	0.005	<D.L.		0.023	0.003	0.021	0.004
Ca	0.1	0.48	0.03	0.55	0.02	0.67	0.03	<D.L.		0.80	0.03	0.28	0.02
Ti	0.003	0.016	0.002	0.047	0.002	0.009	0.001	<D.L.		<D.L.		<D.L.	
Mn	0.008	0.023	0.003	0.0160	0.0004	0.050	0.001	<D.L.		0.008	0.0005	0.027	0.0007
Fe	0.2	50.2	0.4	48.7	0.4	48.5	0.3	64.1	0.2	60.2	0.2	60.0	0.2
Co	0.005	0.203	0.006	0.237	0.008	0.170	0.006	0.284	0.010	<D.L.		<D.L.	
Ni	0.2	3.55	0.10	4.10	0.10	2.75	0.06	4.88	0.15	<D.L.		<D.L.	
O (calculated)		39.6	0.1	39.7	0.1	41.6	0.1	30.3	0.1	36.5	0.1	37.3	0.1

Copper, zinc, arsenic and lead are not present in meteoritic iron at levels similar to those found on the surface of the archaeological beads, but can all occur in smelted iron. PIXE found significant amounts of these elements whereas PGAA did not detect them, because it has higher detection limits. We assume that the presence of these elements on the surface is a consequence of environmental contamination and electrochemical precipitation onto the corroding iron beads. Copper, arsenic and possibly lead are supposed to come from the large copper harpoon found in the same tomb. Alternatively, they could originate from contamination by copper tools used in the manufacture of the beads, as tongs or for rolling the metal around to shape the tubes. An environmental origin is assumed for boron and chlorine, both common in the saline soils of Egypt's desert into which the tombs were dug. The zinc content is inconclusive; it can either be due to environmental contamination or stem from zinc sulphide present in the original meteoritic metal.

Following the BNC experiments on the Petrie Museum's iron beads a recent study was published on the meteoritic origin of Tutankhamun's iron dagger blade (Fig. 6.) using portable x-ray fluorescence spectrometry [6]. This technique is



Figure 6. The iron dagger of King Tutankhamun (iron dagger Carter no. 256K, JE 61585 with its gold sheath). The full length of the dagger is 34.2 cm [6].

usually suitable only for surface or near-surface analysis of the artefacts.

Referring, however, to our study on absolutely non-destructive neutron analyses providing bulk compositional information about the whole objects of a similar meteoritic iron object with additional PIXE measurements, the x-ray surface analysis of this dagger can also be considered as a reliable approach. In fact, measurements performed by different methods on different pieces of artefacts complete each other. Hence, conclusions strengthened by two sides and techniques complementing each other can successfully answer given the scientific questions – even in the case of such popular subject as the fate of ancient arms of the mysteriously died young Egyptian King.

Conclusion

In summary, the composition of the beads is consistent with a meteoritic origin of the metal. The presence of significant amount of nickel detected in our measurements is a strong proof for this, and germanium as well, despite of its irregular and relatively low concentrations found. The really exciting outcome of this research is that we were for the first time able to demonstrate conclusively

that there are typical trace elements such as cobalt and germanium present in these beads, at levels that only occur in meteoritic iron.

A new feature to understand was the atomic crystal/amorphous structure of the components, no metal structure was identified – the fact that the macroscopic topology of the objects were preserved

even after the complete chemical transformation (corrosion) during thousands of years. The direct image of the internal topology of the beads, revealing how they were rolled and hammered into form was a real breakthrough to realize that this is a very different technology from the usual stone bead drilling, and shows quite an advanced understanding of the metal smiths how to work this rather difficult material. The shape of the beads was obtained by smithing and rolling, probably involving multiple cycles of hammering and annealing, not by stone-working techniques such as carving or drilling used for the other tubular beads from this tomb.

It is assumed that recrystallization and homogenisation during hammering and annealing of the original meteoritic iron into sheet metal would have removed much of the original structure already prior to corrosion. Cycles of hammering and annealing were

used for producing similar beads during the Neolithic and Early Bronze Age using soft copper; however, these beads are the earliest smithed iron artefacts known and made from a material much more difficult to work. Composition and manufacturing technique rule out a sub-recent origin of the beads, confirming that they are not later intrusions into Gerzeh tombs 67 and 133 but indeed humankind's oldest known iron artefacts.

The comprehensive methodological approach by using non-invasive techniques presented in this study, based on the Budapest Neutron Centre's facilities might be an important reference to similar investigations on artefacts or other type of complex/composite materials requiring simultaneous information on the atomic level structure, macroscopic topology and chemical composition.

References:

1. Rehren T, Belgya T, Jambon A, Káli Gy, Kasztovszky Zs, Kis Z, Kovács I, Maróti B, Martínón-Torres M, Miniaci G, Pigott VC, Radivojevi M, Rosta L, Szentmiklósi L, Szőkefalvi-Nagy Z; 5,000 years old Egyptian iron beads made from hammered meteoritic iron, *J. Archaeological Science* **40**, 4785–4792 (2013)
2. Rosta L, Belgya T, Káli Gy, Kasztovszky Zs, Kis Z, Kovács I, Maróti B, Szentmiklósi L, Szőkefalvi-Nagy Z, Jambon A, Rehren Th; Proof of the Meteoritic Origin of Mankind's Earliest Iron Artefacts through Neutron and X-ray Analysis, *Hungarian archaeology e-journal 2013 WINTER*, http://www.magyarregeszet.hu/wp-content/uploads/2013/12/Rosta_13T.pdf,
3. Petrie/Wainwright/Mackay 1912. *The Labyrinth, Gerzeh and Mazghuneh*. British School of Archaeology in Egypt XXI. London.
4. Kasztovszky Zs, Rosta L, How can neutrons contribute to Cultural Heritage research? *Neutron News* **23**, 25-29 (2012)
5. McCoy TJ, Marquardt AE, Vicenzi EP, Ash RD, Wasson JT, Meteoritic metal beads from the Havana, Illinois, Hopewell Mounds: a source in Minnesota and implications for trade and manufacture. *Lunar and Planetary Science* **39** (2008)
6. Comelli D, D'Orazio M, Folco L, El-Halwagy M, Frizzi F, Alberti T, Capogrosso V, Elnaggar A, Hassan H, Nevin A, Porcelli F, Rashed M and Valentini G, The meteoritic origin of Tutankhamun's iron dagger blade, *Meteoritics & Planetary Science* 1–9 (2016)

4.2. THE COMBINATION OF NEUTRON IMAGING AND PROMPT-GAMMA ACTIVATION ANALYSIS

Z. Kis, L. Szentmiklósi, Zs. Kasztovszky, B. Maróti,

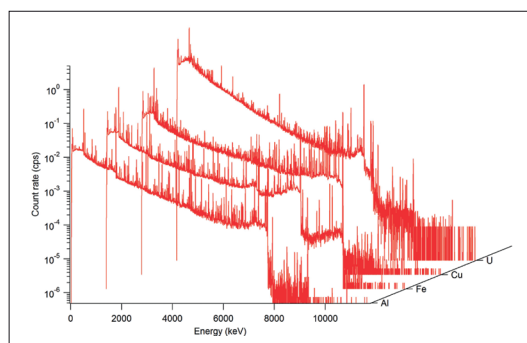
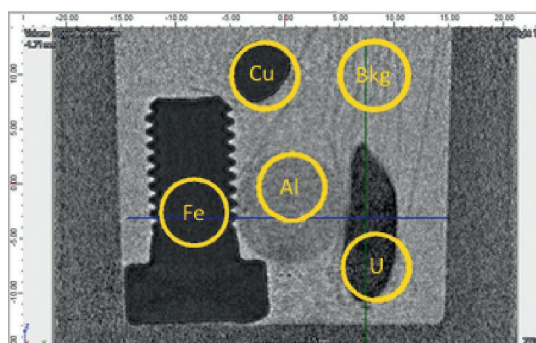
Centre for Energy Research, Department of Nuclear Analysis and Radiography

At the NIPS-NORMA facility, a novel non-destructive procedure has been developed to determine the distribution of major elements and visualize internal parts of heterogeneous objects by combining position sensitive prompt-gamma activation analysis (PGAA) and neutron radiography/tomography (NR/NT) into a unique facility [1]. A combination of these two methods saves substantial beam time in the NR/NT-driven PGAI (Prompt Gamma Activation Imaging) mode. Here the interesting regions are visualized and located first, and the time-consuming prompt-gamma measurements are made only where they are really needed. We present two case studies, from safeguards and archaeometry.

Lead Black Boxes - One of the missions of the Centre for Energy Research is to develop methodology for the characterization of any illicit radioactive or nuclear material. For a sealed object of unknown origin a preliminary screening is usually required to decide if a container is safe to open. As lead shield successfully attenuate gamma rays passive gamma counting for radionuclide identification may not be feasible. Conventional prompt gamma-ray activation analysis (PGAA), however, as an active interrogation technique, has already been successfully applied to reveal the presence of nuclear materials inside lead and iron containers. PGAA with a standard beam size (~cm), however, provided the average composition of the whole cavity volume of the container. Instead, we used NR/NT-driven PGAI, where – in addition to an in-situ visualization of the contents – a better selectivity and quantification could be achieved [2].

The element analysis capability of the method is demonstrated on a complex benchmark object, composed of a lead container (with a 6 mm wall thickness and 42 mm outer diameter), in which three copper spheres (d = 5 mm), an aluminum cylinder (d = 12 mm, L = 25 mm), an M6 size steel metric screw and uranium oxide powder (packed into a Teflon bag) were placed, and the container was sealed. The result of the NR/NT-driven measurement is twofold as both visual and chemical information are obtained. First, an excellent agreement was found between nominal and measured dimensions. This made it possible to precisely position the irradiation spots according to the radiographic image (Fig. 1).

The raw prompt-gamma spectra taken at the marked spots are good enough for a qualitative assessment. This quick screening can be achieved within a couple of hours, as rapid reporting time is an important requirement for a forensic method. Note the evenly rising baseline of the farthest prompt-gamma spectrum, as a first-glance evidence for the presence of fissile materials. For uranium, even the enrichment of the material can also be given from the ratios of peaks at 4060 and 6395 keV gamma energies. Limitations of the proposed technique are, however, the too low and too high neutron attenuation. The method is intended for the quantification of major elements only. The identification of uranium within a lead shield, or the differentiation between Fe and Cu would not be possible using the more conventional X-ray radiography because of the similar mass absorption coefficients.



◀ **Figure 1.** The positions of the collimated beam overlaid on the radiography images and the spectra measured at each spot, after background correction (from front to back: Al, Fe, Cu and U)

Egyptian sealed pottery - An Eighteenth Dynasty Egyptian sealed pottery has been investigated using computed tomography (CT) of various modalities (terahertz electromagnetic radiation, X-rays and neutrons) and NT-driven PGAI in order to analyze the bottle itself and its contents [3]. This multi-modal study emphasizes the complementarity and specificity of the three imaging methods, together with the position-sensitive elemental mapping technique, all of which are shown to be of a prime importance for historians and museum curators dealing with cultural heritage. Neutron imaging gave information about the way the object has been closed by a double stopper (clay and probably a ball of linen or some other string-

like organic material) and provided a more accurate representation of the mobile and heterogeneous content, probably consisting of germinated herbal seeds (Fig. 2).

The elemental composition of three different parts of the jar (labeled by Full, Void and Plug) was determined with NT-driven PGAI (Fig. 2a). Due to the uncertainty in the self-absorption corrections only a semi-quantitative elemental composition for the inner content could be given. The amounts of the characteristic elements for ceramics (Na, Mg, Al, Si, K, Ca, Ti, Mn, and Fe) were roughly the same in both 'Full' and 'Void' measurements. On the other hand, some elements characteristic of organic material (H, C, N, S, and Cl) show an excess in case of the 'Full' measurement, compared with that of the 'Void'. Furthermore, the composition of the plug also shows an excess of H, C, N, S, and Cl, which confirms the organic nature of the fabric. As a result, the content could consist of germinated seeds (or any other dried organic material) such as barley that was a staple cereal of ancient Egypt. It is concluded that the internal cork could be made of a ball of linen.

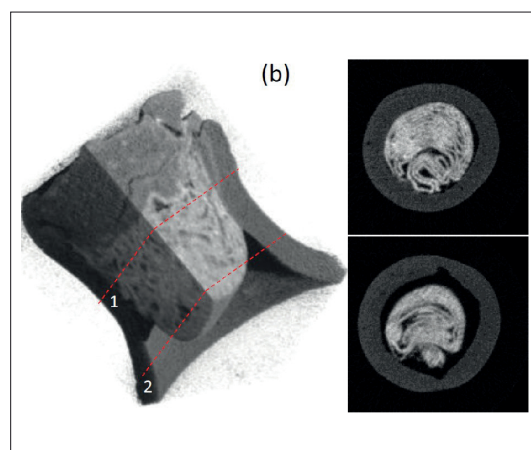
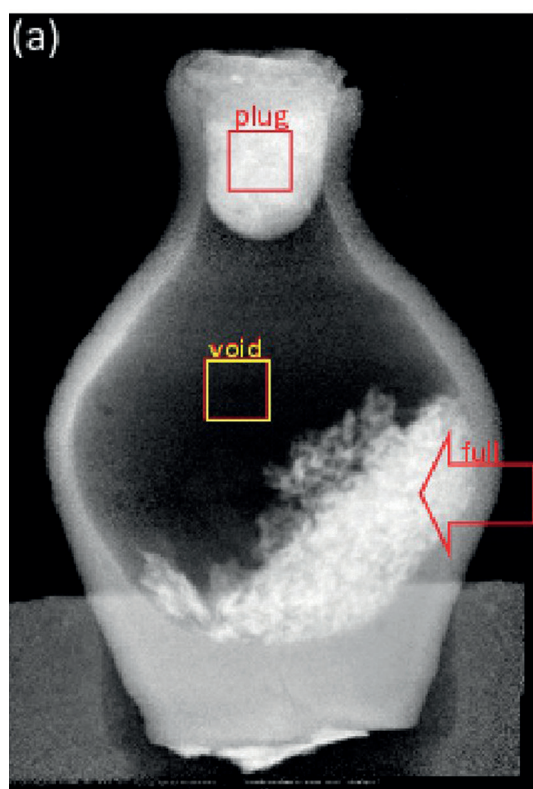


Figure 2. ▶

Neutron CT. (a) Global front view. (b) 3D representation of the cork. Axial views of the cork at the position 1 and 2 indicated in (b). (Abraham et al. 2014)

References:

- [1] Z. Kis, L. Szentmiklósi, T. Belgya, NIPS-NORMA station - A combined facility for neutron-based nondestructive element analysis and imaging at the Budapest Neutron Centre, Nucl. Instrum. Methods Phys. 779 (2015) 116–123.
- [2] L. Szentmiklósi, Z. Kis, Characterizing nuclear materials hidden in lead containers by neutron-tomography-driven prompt gamma activation imaging (PGAI-NT), Anal Methods. 7 (2015) 3157–3163.
- [3] E. Abraham, M. Bessou, A. Ziéglé, M.-C. Hervé, L. Szentmiklósi, Z.S. Kasztovszky, et al., Terahertz, X-ray and neutron computed tomography of an Eighteenth Dynasty Egyptian sealed pottery, Appl. Phys. A. 117 (2014) 963–972.

4.3. NEW PROMPT FISSION GAMMA-RAY DATA IN RESPONSE TO THE OECD/NEA HIGH PRIORITY REQUEST

S. Oberstedt¹, R. Billnert¹, A. Gatera¹, M. Vidali¹, F-J.Hamsch¹, A. Oberstedt², T. Belgya³, L. Szentmiklósi³, Z. Kis³

¹ European Commission, Joint-Research Centre, Institute for Reference Materials and Measurements (IRMM), Geel, Belgium

² Extreme Light Infrastructure - Nuclear Physics (ELI-NP) / Horia Hulubei National Institute for R&D in Physics and Nuclear Engineering (IFIN-HH), Bucharest-Magurele, Romania

³ Centre for Energy Research, Hungarian Academy of Sciences, Budapest, Hungary

With the potential of more advanced nuclear reactors in the near future, a better understanding of the entire fission process is needed. Since four out of six of the impending reactors that have been selected by the Generation-IV International Forum (GIF) are fast reactors, an innovative core design is required to be able to handle the excessive heat from the fission process. In order to model these cores, a better understanding of the released heat from the common reactor isotopes is crucial. Present knowledge regarding this heat release implies that approximately ten percent of the total energy released in fission is due to γ -rays, of which around 40% originates from prompt fission γ -rays. An uncertainty of at most 7.5% is required with regard to the γ -heating in order to model these cores adequately, however, in evaluated data files γ -heating is underestimated by up to 28% for the neutron-induced fission of the main reactor isotopes, ^{235}U and ^{239}Pu . Therefore, these two isotopes (among others) have been included in NEA's high priority list for prompt fission γ -ray data, in particular new values for γ -multiplicity and mean energy are requested, as data in the evaluated files for both isotopes rely on results made in the early 1970's.

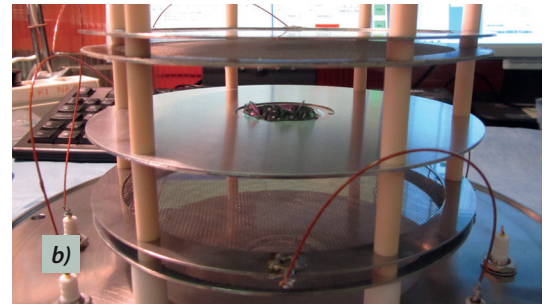
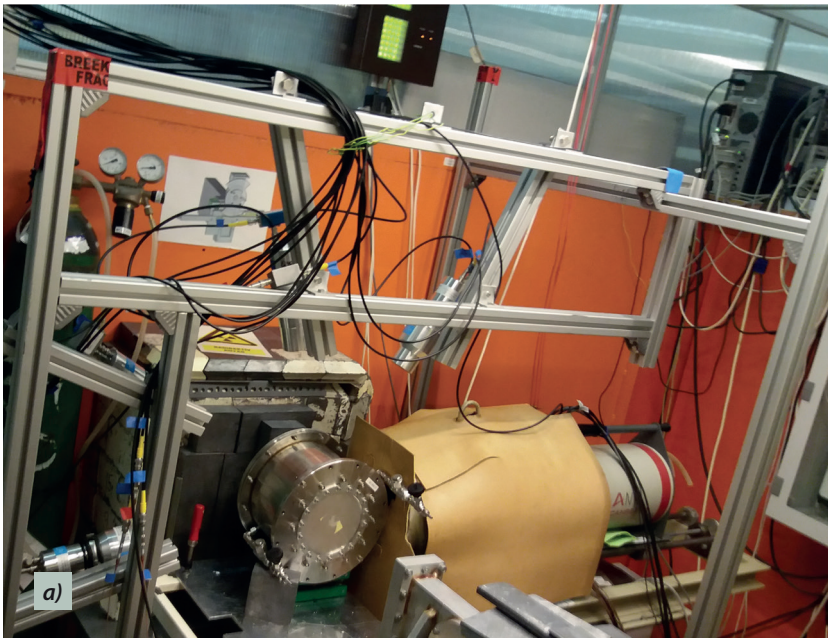
Instrumental development, especially the release of new lanthanide-halide scintillation detectors and the advent of digital data acquisition and signal processing techniques, offers nowadays a much more sophisticated approach to generate high-quality nuclear data. In order to make an independent verification of the historical data, we executed a series of experiments to measure prompt γ -rays from the neutron-induced fission on relevant reactions, such as $^{235}\text{U}(n_{\text{th}},f)$, $^{241}\text{Pu}(n_{\text{th}},f)$ and $^{239}\text{Pu}(n_{\text{th}},f)$.

As a proof of principle, and as a validation of the instrumentation, IRMM started studying the spontaneous

fission of ^{252}Cf since this reaction was measured in the early 1970's as well as very recently at LLNL. After having obtained this confirmation, the experiments were continued to measure prompt γ -ray spectra from slow neutron induced fission. Four campaigns with 6-10 days of beam time each were completed in February-March 2010, June 2012, June 2013 and November 2015 at the PGAA station so far, financed by the EU-funded EFNUDAT, ERINDA and CHANDA projects. These aim for a coordination of European efforts to exploit up-to-date neutron beam technology for novel research on advanced concepts for nuclear fission reactors and the transmutation of radioactive waste.

In the first measurement campaign photons were detected with a 3 in. \times 3 in. coaxial $\text{LaCl}_3:\text{Ce}$ scintillation detector, located at a distance of about 30 cm from a very thin ^{235}U target placed in the fission fragment spectrometer VERDI. The fast fission trigger was provided by a polycrystalline chemical vapor deposited (pcCVD) diamond detector. In a second run, an ultra-thin spectroscopic uranium sample of effective mass 640 μg was placed inside a twin Frisch-grid ionization chamber, which delivered the fission trigger. For ^{241}Pu , a sample with 40 μg mass and enrichment of 99.39 %, for ^{239}Pu , a target of 858 μg was used.

The coincident measurement of photons was accomplished with two coaxial $\text{LaBr}_3:\text{Ce}$ as well as two coaxial CeBr_3 scintillation detectors simultaneously, whose size (diameter \times length) is 2 \times 2 and 1 \times 2 inches, respectively. The response to γ -rays in the different lanthanide-halide detectors were simulated by means of the PENELOPE Monte-Carlo code. In each run the fission rate was about 5 kHz per sample that resulted in about 2 TB of raw data.

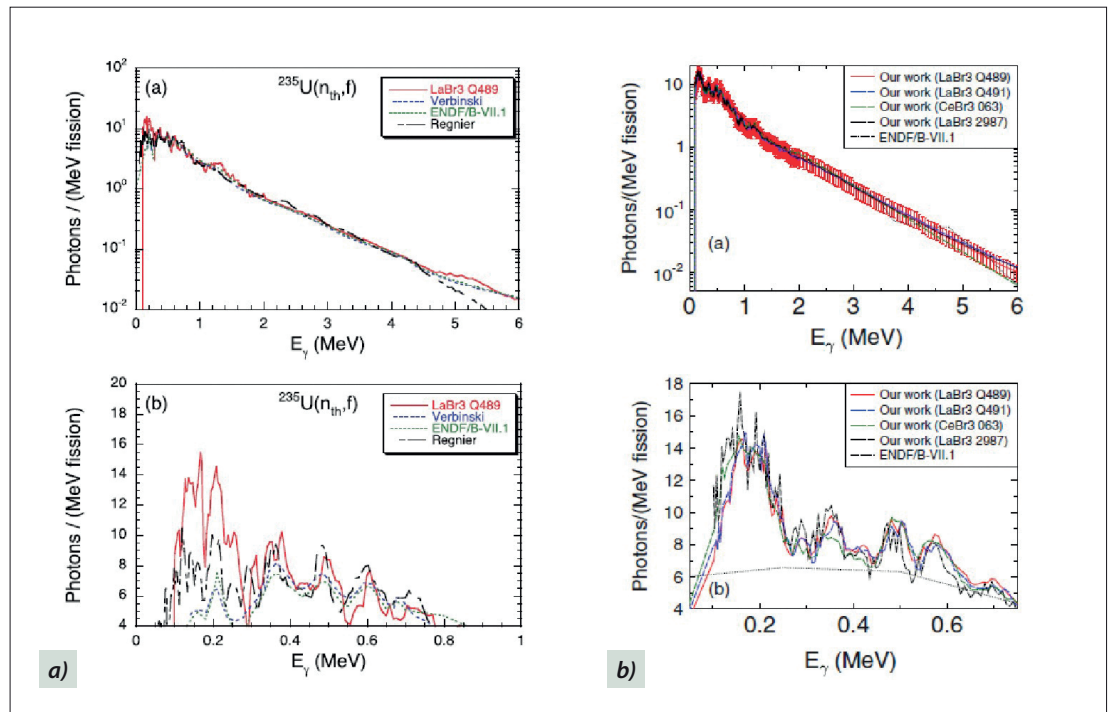


▲ **Figure 1.**

a) Frisch-grid ionization chamber and a set of scintillator detectors were installed at the PGAA station
 b) The target being mounted to the ionization chamber
 c) The experimental team setting up the fast digitizers

Figure 2. ▶

Unfolded prompt-fission γ -ray emission spectra from the reactions $n_{th}+^{235}\text{U}$ (a) and $n_{th}+^{241}\text{Pu}$ (b), in comparison to the literature. Lower panels show the first ~ 800 keV of the spectra magnified. The data analysis of the ^{239}Pu experiment is still in progress, results are expected to be published in 2016.



References:

1. A Oberstedt, T Belgya, R Billnert, R Borcea, T Bryå, W Geerts, A Göök, FJ Hamsch, Z Kis, T Martinez, S Oberstedt, L Szentmiklosi, K Takács, M Vidali. (2013) Improved values for the characteristics of prompt-fission γ -ray spectra from the reaction $^{235}\text{U}(n_{th},f)$. *Physical Review C* 87(5):051602.5
2. A Oberstedt, T Belgya, R Billnert, FJ Hamsch, Z Kis, TM Perez, S Oberstedt, L Szentmiklősi, K Takács, M Vidali. (2013) New prompt fission gamma-ray spectral data and its implication on present evaluated nuclear data files. *Physics Procedia* 47. 47:156-65. doi:10.1016/j.phpro.2013.06.023.
3. S Oberstedt, R Billnert, T Belgya, R Borcea, T Bryś, W Geerts, A Göök, F-J Hamsch, Z Kish, T Martinez Perez, A Oberstedt, L Szentmiklősi, M Vidali. (2014) New Prompt Fission γ -ray Data in Response to the OECD/NEA High Priority Request. *Nuclear Data Sheets* 119:225-8.
4. S Oberstedt, R Billnert, T Belgya, T Bryś, W Geerts, C Guerrero, F-J Hamsch, Z Kis, A Moens, A Oberstedt, G Sibbens, L Szentmiklősi, D Vanleeuw, M Vidali. (2014) High-precision prompt- γ -ray spectral data from the reaction $^{241}\text{Pu}(n_{th},f)$. *Physical Review C* 90(2):024618.6

4.4. ATOMIC STRUCTURE OF AMORPHOUS MATERIALS STUDIED BY NEUTRON DIFFRACTION

Margit Fábrián^{1,2}, Erzsébet Sváb²

¹ Centre for Energy Research, Hungarian Academy of Sciences, H-1525 Budapest P.O.B. 49, Hungary

² Wigner Research Centre for Physics, Hungarian Academy of Sciences, H-1525 Budapest P.O.B. 49, Hungary

Structure of glass matrix for radioactive waste conditioning

Understanding of the incorporation of actinides in borosilicate matrix used for nuclear waste storage is of a great importance for radioactive waste immobilization [1,2]. This study carried out on matrix glasses doped respectively with 30wt% UO_3 and CeO_2 , Nd_2O_3 used for chemical modelling of the actinides. Transuranium elements are not available therefore lanthanides chemically modeling them were used. Ce stays for the hazardous radioactive Pu, while Nd for Am and Cm. Samples were prepared from oxides: SiO_2 and B_2O_3 (^{11}B isotope) are strong network formers; Na_2O is a network modifier; BaO and ZrO_2 serve both as network modifier, glass and hydrolytic stabilizers. Based on the experience of our previous studies, new glassy samples were synthesized with the so-called 'Matrix' of composition $55\text{SiO}_2 \times 10\text{B}_2\text{O}_3 \times 25\text{Na}_2\text{O} \times 5\text{BaO} \times 5\text{ZrO}_2$ (mol%); into which the model compounds were added as oxides. The studied samples contained (70)w% Matrix and (30)w% UO_3 , CeO_2 or Nd_2O_3 . Neutron diffraction (ND) measurements were performed, indicates that the new compositions are stable glassy samples, no crystalline phase was detected. ND measurements were performed by the 2-axis PSD monochromatic neutron diffractometer ($\lambda_0=1.068 \text{ \AA}$; $Q=0.45\text{-}9.8 \text{ \AA}^{-1}$) [3] at the 10 MW Budapest research reactor. The

ND experimental $S(Q)$ data have been simulated by the reverse Monte Carlo (RMC) method [4], which is a widely used effective tool to model disordered structures. The RMC minimizes the squared difference between the experimental $S(Q)$ and the calculated one from a 3-dimensional atomic configuration. The convergence of the RMC calculation was good and the final $S(Q)$ matched very well the experimental structure factor (Figure 1).

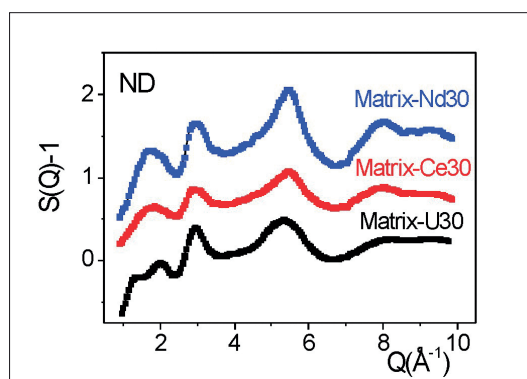


Figure 1. Neutron diffraction structure factors for Matrix-U30 (black), Matrix-Ce30 (red) and Matrix-Nd30 (blue) glasses and RMC fits (solid line). (The curves are shifted vertically for clarity.)

From the RMC simulation several first and second neighbor partial atomic pair-correlation functions, $g_{ij}(r)$ and coordination number distributions, CN_{ij} have been revealed with a fairly good stability and statistics. Figure 2 presents most important partial

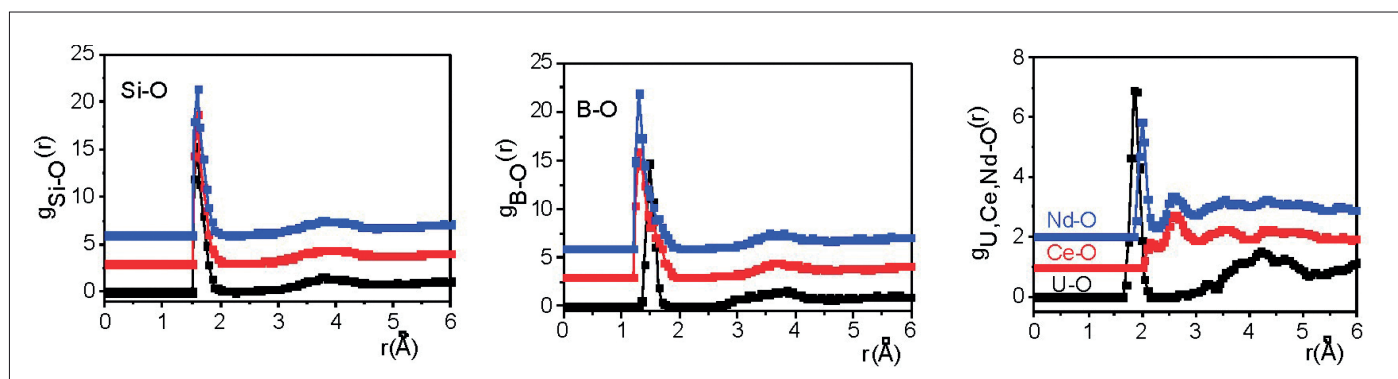


Figure 2. The Si-O, B-O and U,Ce,Nd-O partial atomic pair correlation functions from RMC modelling, for Matrix-U30 (black), Matrix-Ce30 (red) and Matrix-Nd30 (blue).

pair correlation functions, $g_{\text{Si-O}}(r)$, $g_{\text{B-O}}(r)$, $g_{\text{U,Ce,Nd-O}}(r)$ for the different concentrations. The atom pairs responsible for building up the glassy network show characteristic first neighbor distributions.

For Si-O a covalent bond length at 1.60 Å was revealed for all studied glasses, showing an excellent agreement within limit of error. For the B-O network we have established one broad peak at 1.50 Å, 1.35 Å and 1.33 Å from the Matrix-U30, Matrix-Ce30 and Matrix-Nd30, respectively. For U-O, Ce-O, Nd-O the first peak positions were possible to determine with a relatively high accuracy, because they do not overlap with other atomic pair distributions. The U-O correlation function shows a well resolved peaks at relatively short distances, centred at 1.86 Å. The Ce-O distribution function shows a broad peak at 2.13 Å. The Nd-O shows characteristic first neighbour distance at 2.00 Å. However the intensity of Nd-O

peak distribution is significantly higher than the Ce-O peak intensity, suggested that Nd atom shows better tendency to incorporate on the network structure.

For several glasses, it was found that the basic network structure consists of tetrahedral SiO_4 units and of mixed trigonal BO_3 and tetrahedral BO_4 . The BO_3 and BO_4 units are linked to SiO_4 , forming mixed $^{[4]}\text{Si-O-}^{[3]}\text{B}$ and $^{[4]}\text{Si-O-}^{[4]}\text{B}$ bond-linkages. Significant second neighbour atomic pair correlations have been revealed between uranium, cerium, neodymium and the network former (Si,B) atoms. From these results we may conclude that also for the doped glasses we have a stable basic network structure and uranium, cerium, neodymium accommodates in both silicate and borate site. This may be the reason of the observed good glassy stability and incorporation ability of the ions.

References:

- [1] K.S. Chun, S.S. Kim and C.H. Kang: Journal of Nuclear Materials 298 150 (2001)
- [2] C.M. Jantzen, K.G. Brown and J.B. Pickett: Westinghouse Savannah River Company Report, WSRC-MS-2000-00307 (2000)
- [3] E. Sváb, Gy. Mészáros, F. Deák, Materials Science Forum 228 247-252(1996)
- [5] R. L. McGreevy, L. Pusztai, Mol. Simul. 1 359-367 (1988)

Formation of mixed bond-angle linkages in zinc boromolybdate glasses

Zinc boromolybdate materials are known as low melting dielectric materials and they have high potential in several applications, due to their stable and unique structure with favourable optical properties. The glass formation tendency of MoO_3 - $\text{ZnO-B}_2\text{O}_3$ and of several other similar compositions has been explored and the optical spectroscopic features have been analysed by Dimitriev [1,2]. The structure characterization is challenging, as far as this system contains the conditional network former MoO_3 and the traditional network former B_2O_3 . In order get deeper insight into the network structure, including the inter-atomic distances and coordination distributions, we have undertaken neutron diffraction study combined with reverse Monte Carlo (RMC) modelling on the same system. Our interest is mainly focused on the characterization of the network former structural units and their bond-linkages forming the medium-range order. Especially interesting question is the role of ZnO, whether it acts as modifier or network former, not

yet investigated for this system, as far as we know. The amorphous $x\text{MoO}_3$ - 50ZnO - $(50-x)\text{B}_2\text{O}_3$, $x=10, 20, 30$ mol% samples have been prepared from commercial powders of reagent grade MoO_3 , ZnO and B_2O_3 . The B_2O_3 was isotopically enriched in ^{11}B -isotope (99.6%) in order to reduce the influence of the high neutron absorption of ^{10}B -isotope present in natural boron.

Neutron diffraction (ND) experiments were performed on the PSD diffractometer ($\lambda_0=1.068$ Å) [3] at the 10 MW Budapest research reactor in the momentum transfer range $Q=0.5$ - 10 Å $^{-1}$ on the 7C2 diffractometer at the LLB-CEA-Saclay ($\lambda_0=0.726$ Å) [4] was used in a broader Q -range up to 16 Å $^{-1}$. Simultaneous reverse Monte Carlo (RMC) [5] simulation of the two diffraction data sets was applied to generate reliable 3D atomic configurations and, to calculate the partial atomic pair correlation functions, nearest neighbor distances and coordination number distributions. The fit of the

RMC calculations was good, the final $S(Q)$ s matched very well the experimental ones, as they are shown in Figure 1. In order to get qualitative and some quantitative information for the local structure we have calculated the total atomic distribution function, $G(r)$ by sine-Fourier transformation shown in Figure 2.

The first- and second neighbor correlation functions, atomic distances and coordination numbers have been revealed, not yet reported for this system. It was found, that the first neighbor distances do not depend on concentration within error of limit, the actual values are $r_{B-O}=1.38 \text{ \AA}$, $r_{Mo-O}=1.72 \text{ \AA}$ and $r_{Zn-O}=1.97 \text{ \AA}$. In consequence, the average CN_{B-O} slightly increases with increasing B_2O_3 . For the Mo-O and for Zn-O coordination number distributions mainly 4-fold coordinated oxygen

atoms are obtained, the number of different types of neighbors is $< 5\%$. ZnO proved to be a network former, not a modifier as it is often reported in the literature for similar systems. From the analyses of the obtained structural parameters we have concluded that the glassy network is formed by trigonal BO_3 and tetrahedral BO_4 , MoO_4 , ZnO_4 groups. Concentration dependence was found for the BO_4/BO_3 fraction, it increases with increasing B_2O_3 content. We have concluded that only small amount of boroxol ring is present and it is supposed that the network is formed by organization of BO_3 and BO_4 groups into superstructure units, and partly by separated BO_3 triangles. The BO_3 and BO_4 units are linked to MoO_4 or ZnO_4 , forming mixed $[4]Mo-O-[3],[4]B$, $[4]Mo-O-[4]Zn$, $[3],[4]B-O-[4]Zn$ bond-linkages. Significant medium-range order exists up to $\sim 7 \text{ \AA}$.

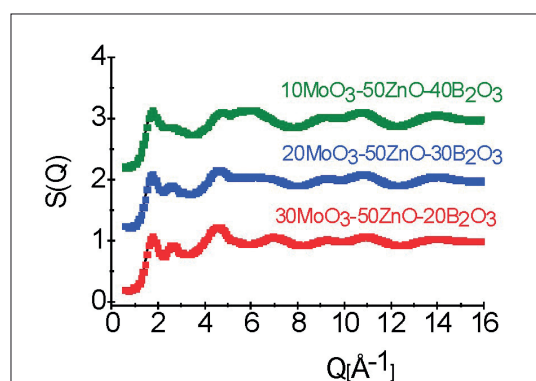


Figure 1. Neutron diffraction structure factor of molybdate samples, experimental data (symbols) and RMC simulation (solid line).

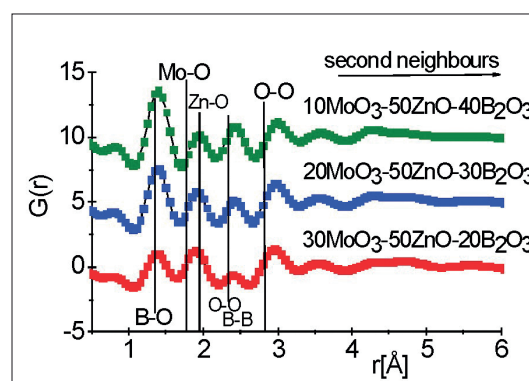


Figure 1. Total distribution functions, $G(r)$ calculated from $S(Q)$. (The curves are shifted vertically for clarity).

References:

- [1] L. Aleksandrov, T. Komatsu, R. Iordanova, Y. Dimitriev, *Optical Materials* 33, 839-845 (2011)
- [2] L. Alexandrov, R. Iordanova, Y. Dimitriev, K. Hamda, J. Ide, M. Milanova, *Advanced Materials Research* 39-40 37-40 (2008).
- [3] E. Sváb, Gy. Mészáros, F. Deák, *Materials Science Forum* 228 247-252(1996)
- [4] J. P. Ambroise, M. C. Bellissent-Funel, R. Rellissent, *Rev. Phys. Appl.* 19 731-734 (1984)
- [5] R. L. McGreevy, L. Pusztai, *Mol. Simul.* 1 359-367 (1988).

4.5. SANS STUDY OF NANOSCALE STRUCTURE OF LOW-CARBON STEEL AFTER ROLLING WITH SHEAR

A. Zavdoveev¹, A. Maksakova¹, E. Pashinska¹, A. Varyukhtin¹, A. Len², J. Füzi², L. Rosta²

¹ Donetsk Institute for Physics and Engineering named after A. A. Galkin, Kyiv, Ukraine

² HAS Wigner Research Centre for Physics, Budapest, Hungary

The rolling with shear is a new continuous severe plastic deformation (SPD) method which is applicable for steel treatment. Low breakage of wires, which reduces expenses for wire processing, can be achieved by intermediate softening annealing, resulting in higher plasticity. However the annealing increases the cost of processing and makes production more complex. The rolling with shear technology ensures high plasticity of the material without decreasing the strength. This gives opportunity to perform further cold drawing without intermediate softening annealing.

SEM and TEM techniques are adequate to give information about the formation of sub-micron voids; however remains opened the question whether these voids are introduced during the fracture process of the sample preparation [1, 2]. Therefore a non-destructive method, such as SANS is needed to make clear the origin of voids, cracks, pores. Samples processed with standard (ST) technology and with rolling with shear (RS) technology were measured at the Yellow Submarine SANS spectrometer in Budapest [3].

Steps of the ST (standard) technology

1. Heating of the billets to 1200°C.
2. Plastic deformation of the metal, which is accomplished at least twice at the temperature below the lowest critical point of the phase transformation. It takes place in the pairs of roll

grooves: 1. seam pass; 2. edging. The partial reduction is not less than 0.1.

3. Cooling: 1.5°C/min down to the end-temperature of the structure transformations.

RS (rolling with shear) technology

The steps of the ST technology are fulfilled, however the rolling inside the edging passes is made with

grooves displaced along the axis of rolls (Fig.1a,b) at the distance of 0,05 - 0,20 of the groove width.

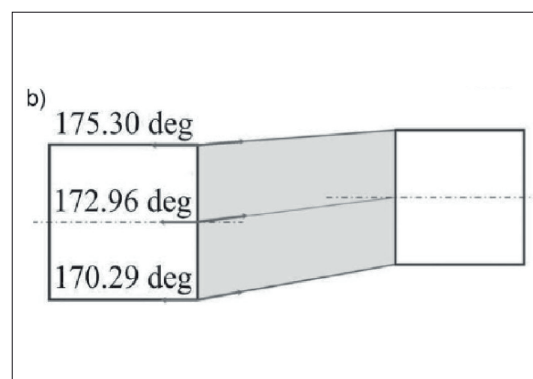
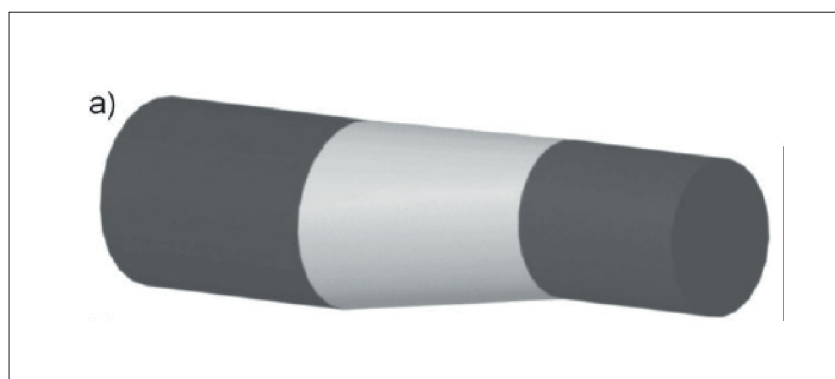


Figure 1.

a. View of the rolled rod. b. Displaced grooves displaced along the axis of rolls.

ST versus RS technology

The materials processed by RS-technology shows dislocation-free ferrite grains; the dislocation density within the bulk of a grain is three orders lower of that after ST-technology. Traces

of dislocation toward grain boundaries were observed (Fig. 2.). These indicate that intensified defect motion occurs during the process of deformation using RS-technology.

The strength characteristics of ST and RS rods are comparable, the plasticity of the RS rods is 60% higher than of the ST steel rods. Rolling with shear

of metal results in formation of uniaxial grains with low size dispersion [1, 2].

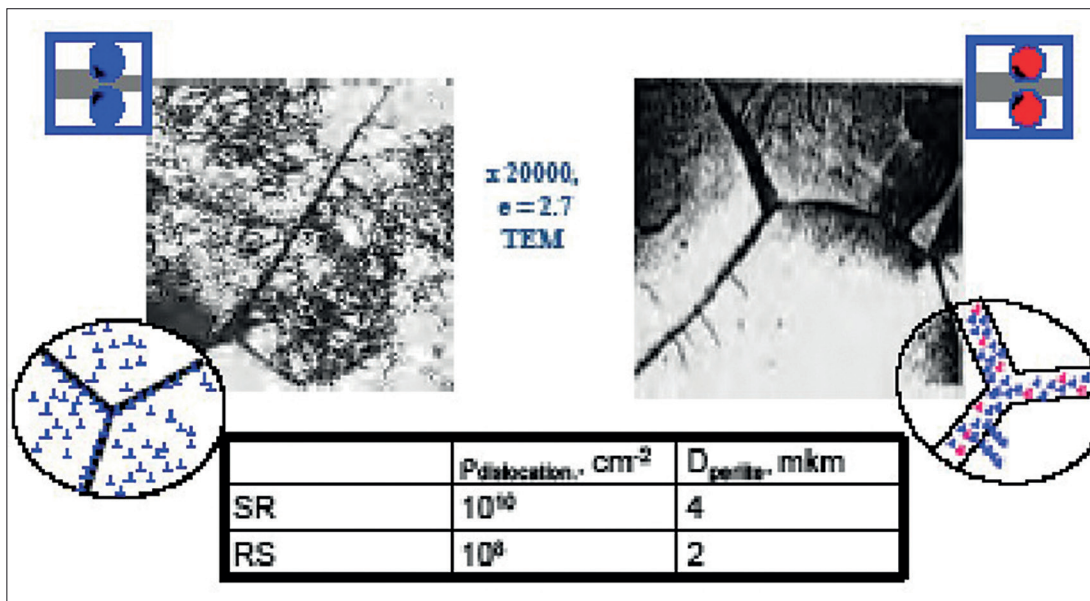


Figure 2. TEM images of steel rods produced by ST and RS technologies

Experimental

Two series of low carbon steel samples (Grade 08G2S) produced by ST and RS technologies were investigated. The chemical composition of the steel was: C: 0.08%, Mn: 1.87%, Si: 0.82%, S: 0.02%, P: 0.022%, Cr: 0.02%, Ni: 0.02%, Cu: 0.02%, N: 0.007%.

The samples (Fig. 3.) were measured at Yellow Submarine SANS machine at Budapest Neutron Centre at the whole available Q range: 0.007-0.4 Å⁻¹. The samples were placed perpendicular to the beam (Fig.4). The registered 2D scattering intensities for the samples with 6.5mm diameter are shown on Figure 5.

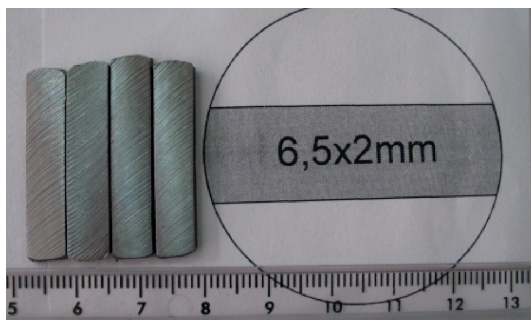


Figure 3. 2mm thick samples were cut from the 6.5mm diameter rods and placed into the neutron beam.

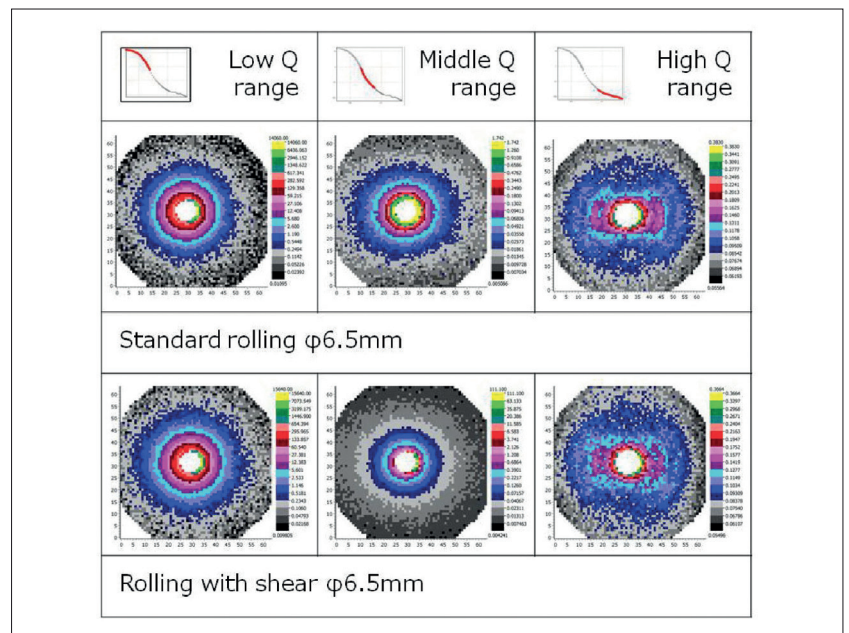
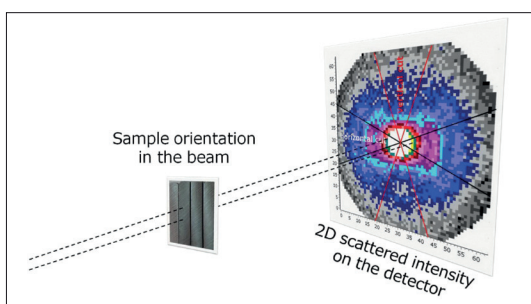


Figure 4. Samples orientation in the neutron beam

Figure 5. 2D SANS scattering intensities for three different scattering vector (Q) ranges

Data evaluation

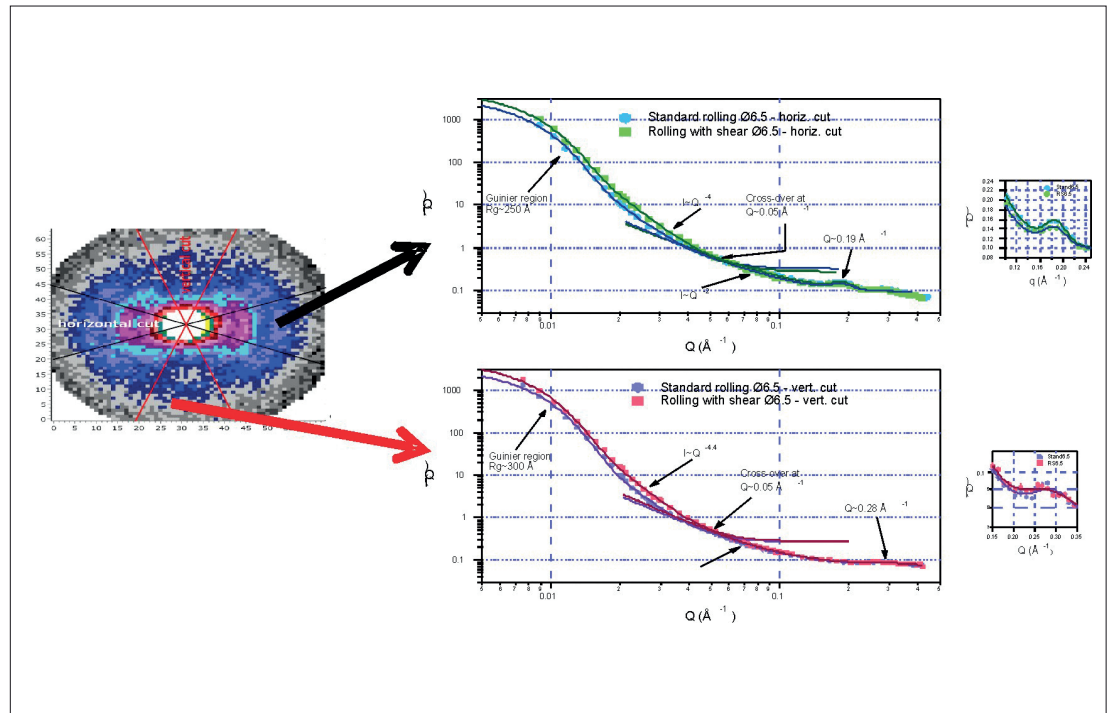


Figure 6. Horizontal and vertical 1D cuts from the 2D SANS intensities. The graphs represent the scattering vector values versus the intensities measured on the detector.

The horizontal and vertical orientations of the anisotropic SANS patterns were treated separately (Fig. 6). In both, ST and RS cases, the curves showed two different regions, with a given **cross-over point**. In the small Q value region a **Guinier type scattering together with a power-law scattering** was found, at large Q region besides the **power-law scattering with a different power exponent, a peak** could also be fitted (Fig. 6 and Tables 1 and 2).

The used fitting function was (Equation 1):

$$I(Q) = \text{Const1} \exp\left(-\frac{Q^2 R_g^2}{3}\right) + \text{Const2} \left(\frac{Q}{\arctan(Q R_g / \sqrt{6})}\right)^{-p} + bg \quad (1)$$

where R_g is the mean gyration radius of the scattering

objects, and p is the exponent characterizing the surface of the scatterers.

The Guinier type scattering was attributed to the nanometric sized pores, cracks and defects, while the power-law scattering in the large Q range region characterized the surface structure of the micrometric sized grains. The exponent above 4 is characteristic to surfaces with a gradual change in the neutron scattering length density of large surface areas. In the region of the large Q range a peak was found that gives the average repeating distance of the ferrite and iron-carbide layers within the perlitic grains (see Fig. 13). The power-law exponent between 1 and 2 is characteristic to the surfaces of the large and oriented (parallel to the wires axis) layers.

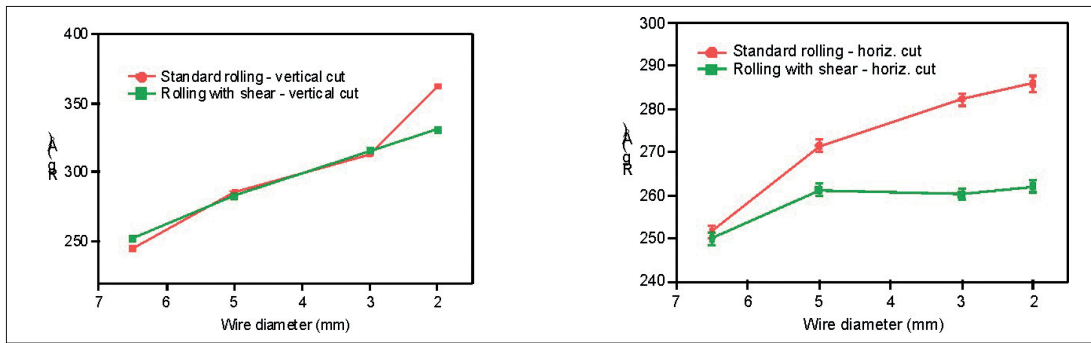
Figures 6 and 7 show the difference between the samples processed with standard rolling and rolling with shear technology. The average size of the defects (Fig. 6) is lower for both – horizontal and vertical – directions in the case of the RS technology, and the sizes decrease with the decreasing wire diameter. The repeating distances (Fig. 7) measured in the horizontal direction (=vertical cut) are slightly larger for the RS samples, that is attributed to a smaller deformation degree of the layers in the interior of the grains.

Table 1. Fitted parameters for the ST and RS steel samples – horizontal cuts

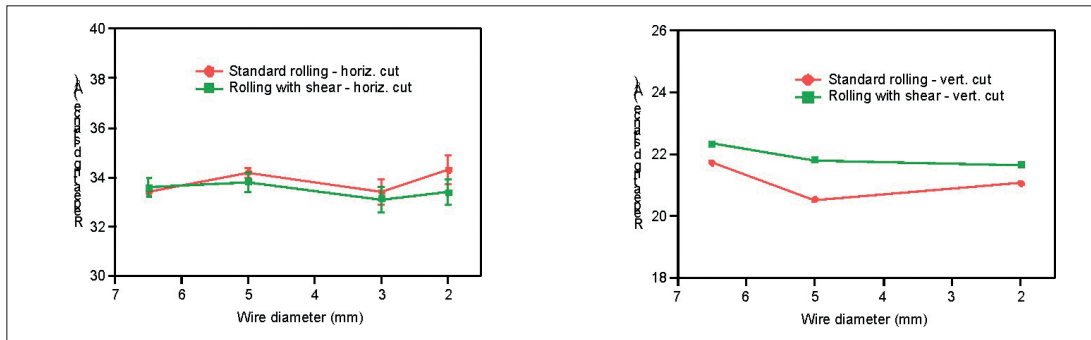
Sample HORIZONTAL	R_g (Å)	Power1	Repeating distance (Å) ($d=2\pi/Q$)	Power2
Stand6.5	252±1	3.99±0.04	33.4±0.2	2.1±0.2
Stand5	271±1	4.01±0.05	34.2±0.2	1.6±0.5
Stand3	282±1	4.45±0.05	33.4±0.5	1.0±0.5
Stand2	286±1	4.61±0.05	34.3±0.6	1.5±0.8
RS6.5	250±1	4.13±0.03	33.6±0.4	2.3±0.3
RS5	261±1	4.20±0.05	33.8±0.4	1.8±0.4
RS3	260±1	4.15±0.04	33.1±0.5	1.8±0.4
RS2	262±1	4.78±0.06	33.4±0.5	1.3±0.7

Table 1. Fitted parameters for the ST and RS steel samples – vertical cuts

Sample VERTICAL	R_g (Å)	Power1	Repeating distance (Å) ($d=2\pi/Q$)	Power2
Stand6.5	245±1	4.18±0.02	21.74±0.2	2.3±0.1
Stand5	286±1	4.45±0.03	20.53±0.7	2.1±0.3
Stand3	313±1	5.17±0.03	-	-
Stand2	362±2	5.36±0.03	21.08±0.5	2.8±0.8
RS6.5	252±1	4.36±0.02	22.36±0.4	2.4±0.1
RS5	283±1	4.61±0.03	21.82±0.4	2.7±0.2
RS3	316±1	5.03±0.03	-	-
RS2	331±2	5.70±0.04	21.67±0.5	3.0±0.6

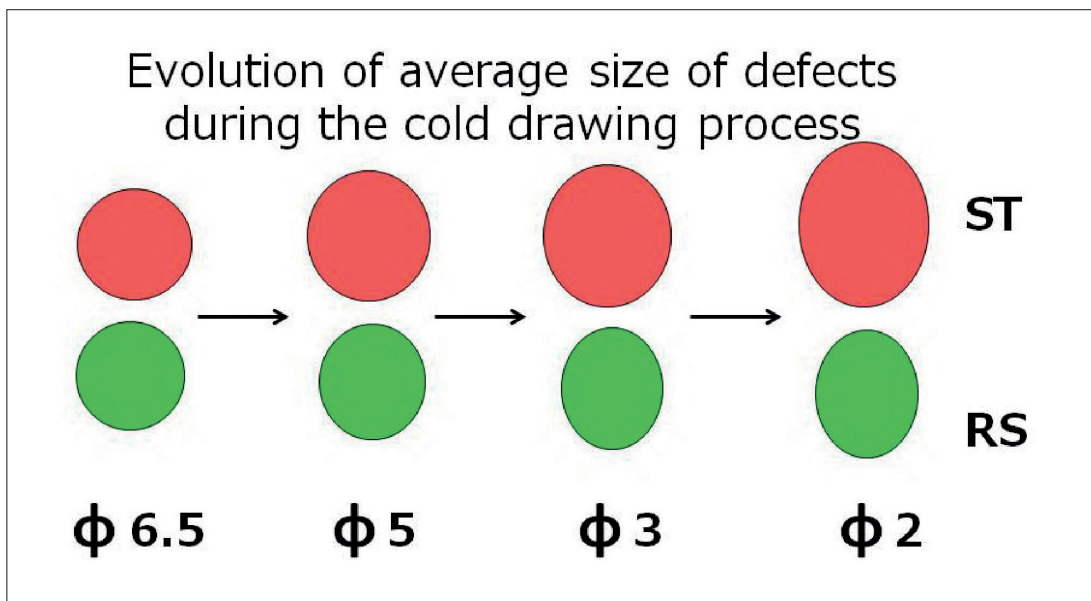


◀ **Figure 7.** Graphic representation of the R_g values in the horizontal (left) and vertical (right) direction



◀ **Figure 8.** Graphic representation of the repeating distance values for the horizontal (left) and vertical (right) directions.

SANS results confirm the dynamic healing of the nanosized defects during the cold drawing of the wires.



◀ **Figure 9.** Schematic representation of the evolution of average size of defects during the cold drawing process

References:

- [1] Pashinska E., *Physical and mechanical base of structure evolution at combined plastic deformation*, Veber, Donetsk, **2009**
- [2] Efimova Yu., *Formation of structure and properties of carbon steels at ECAP and further drawing*, PhD Thesis, Magnitogorsk, Russia, **2009**
- [3] A Len, A. Zavdoveev, A. Maksakova, E. Pashinska, A. Varyukhtin, Gy. Káli: SANS study of nanoscale structure of low-carbon steel after rolling with shear, Poster presentation on ECNS2015, Zaragoza, Spain, **2015**

4.6. EXPERIMENTAL RESULTS ON IRRADIATED SAMPLES IN THE FRAMEWORK OF MATTER PROJECT

Attila Kovács¹, Levente Tatár, Ferenc Gillemot

¹ Centre for Energy Research, Hungarian Academy for Science, Budapest, Hungary

As a prerequisite for standardization for materials used in future Generation IV reactors, the MATTER (MaTerial TEsting and Rules) project focuses on the research for candidate materials for these reactor types. Special attention is paid to P91 and 316LN type steels. 316L is a stainless steel, widely used in industry, with well-known properties. 316LN is a variant of the 316L steel, which satisfies the more severe requirements of the nuclear industry with more strict limits on impurities.

Our knowledge is more-or-less limited on the properties of these steels in the conditions of high temperature irradiations which correspond to the conditions present in Generation IV reactors. The objective of this work was to obtain experimental results on the tensile and fracture properties of 316LN steels after high temperature irradiations for different temperatures.

The first step in the preparation of the experimental work was an activity calculation to assure that by

the end of the project the specimens would not be too active to be handled during the experiments. In the 316LN steel the content of Ni and Cr is high. Thus after irradiation radioactive elements with high activity and long decay are produced. The need to finish the mechanical tests in the framework of the MATTER project, the estimated activation of samples, and the dose limit (4 μ Sv) for our lab limited the total irradiation time to 3 reactor cycles (campaigns).

From our project partners we have received a 316 LN plate containing weldment with gross dimensions of 400x200x15 mm. Full-size V-notched Charpy and miniature tensile specimens were cut from the plate, some of them containing only base metal and some of them containing weldment.

The irradiations were done in the Bagira3 irradiation rig which, unlike previous Bagira1 and Bagira2 rigs, can withstand much higher temperatures as the target holder is made of titanium alloy. Irradiation temperatures can be controlled between 150–650°C

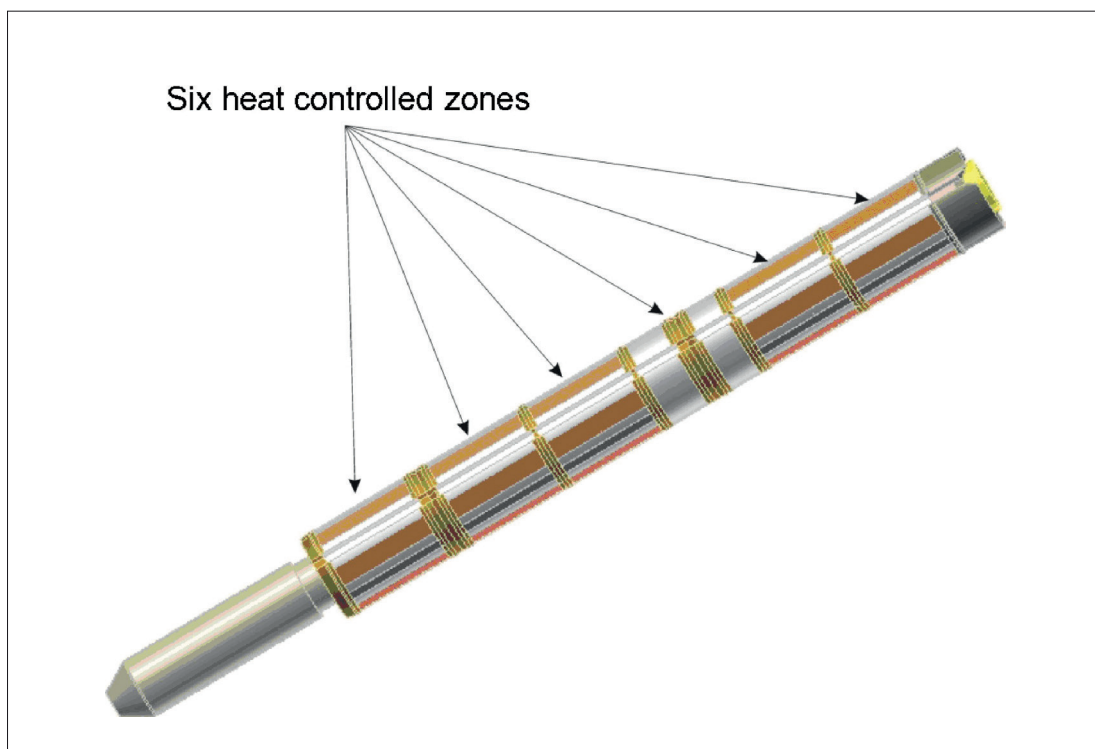
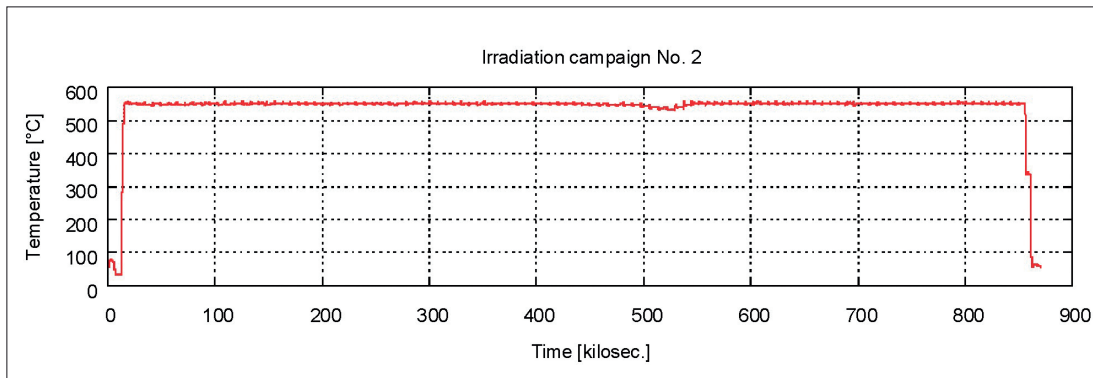


Figure 1. ▶
Specimen holder



◀ **Figure 2.**
Temperature evolution during the second irradiation campaign

	Base metal	Weldment
Before irradiation	300 HV	343 HV
After irradiation	256 HV	522 HV

◀ **Table 1.**
Hardness measurement results (average of individual measurements)

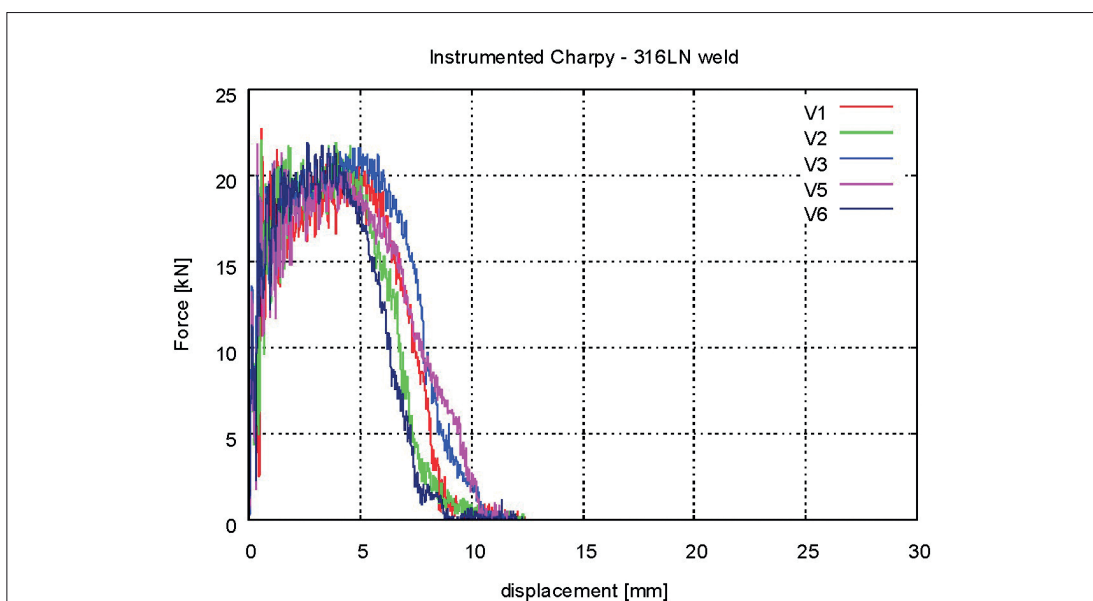
with gamma and electric heating and helium-nitrogen gas mix cooling. To fine-tune the temperatures, the electric heating is divided into six separately controlled zones, each of them having its own thermocouple and heating element. The rig has a detachable specimen holder, unique for each irradiation. The specimen holder used for the present irradiation is presented in Figure 1. The zone which corresponds to the miniature tensile specimens is clearly distinguishable.

Temperatures were recorded during the irradiation. Figure 2. shows the recorded temperatures during irradiation for the irradiation campaign no. 2. Time is presented in kiloseconds as it is a suitable unit for irradiation campaigns.

For the two materials (316LN and 316LN weldment) Vickers-type hardness measurements, Charpy impact and tensile tests were performed in both irradiated and initial state. Tensile tests were done at room temperature and at 550 °C. Fracture surfaces were examined too.

Table 1. shows the hardness before and after irradiations for both materials.

Standard V-notch Charpy measurements had been performed according to the ASTM requirements. Instrumented Charpy hammer has been used, loads and displacements were recorded. Typical Force-displacement curves are presented in Fig. 3.



◀ **Figure 3.**
Typical force-displacement curves during Charpy impact test for irradiated weld metal

Figure 4. ▶
 Ultimate tensile strength vs. temperature for unirradiated a) and irradiated b) 316LN base metal and weld

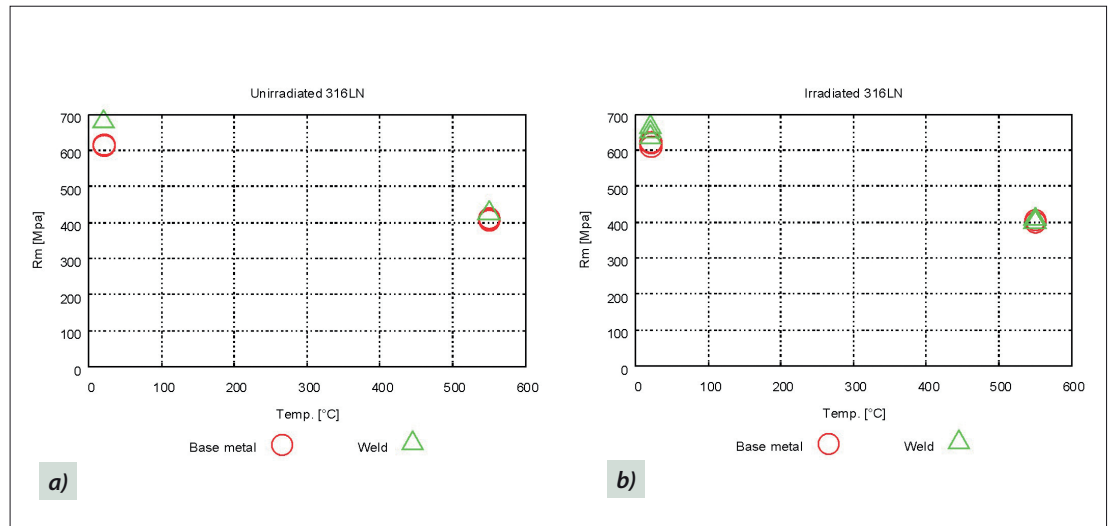


Figure 4. presents the variation of the ultimate tensile strength for unirradiated and irradiated base metal and weld.

In conclusion, with the currently obtained radiation damage at high temperature (550°C, approx. 0.05 dpa) both 316LN base metal and its weld remain in ductile

state, with only very slight changes in ductility. There is a small decrease of the hardness for the base metal (14%) and a more significant increase (34%) for the weld material. Examination of the fracture surfaces shows a clear distinction between the base metal and the weldment, but no clear distinction between irradiated and unirradiated samples.

*Detailed
results
(Experimental
reports)* | **5.**

<h1 style="margin: 0;">BNC</h1> <p style="margin: 0;">Experimental Report</p>	<i>Experiment title</i> Structural study of magnetocaloric material (MnAs) around the first order phase transition	<i>Instrument:</i> MTEST <i>Local contact:</i> Laszlo Temleitner
	<i>Principal proposer:</i> Lukasz Hawelek, Institute of Non-Ferrous Metals, ul. Sowinskiego 5, 44-100 Gliwice, Poland <i>Experimental team:</i> Lukasz Hawelek, L. Temleitner	<i>Experiment Number:</i> BRR_324 <i>Date:</i> 02-12, 16-26.04.2013

Objectives

Submitted objectives:

- study the phase transition of MnAs by neutron diffraction to identify the nuclear structure and their magnetic contribution

Verified objectives (the amount of the MnAs sample was too low):

- Impact of cobalt content on the crystallization pattern in the Finemet-type ribbons

Results

The neutron diffraction data were collected at the neutron powder diffractometer MTEST at Budapest Neutron Centre with the neutron wavelength $\lambda=1.4394 \text{ \AA}$. For further complementary analysis the XRD and ND data were converted from the 2θ to the Q scale representation by the following formula $Q=(4\pi\sin\theta)/\lambda$. The structural changes of the nanocrystalline phase were studied on samples with 58.8 and 65 molar percents of cobalt after annealing for 4 hours at 420 and 500°C. For lower temperature in the XRD and ND patterns the amorphous halos are clearly observed, whereas for higher temperature the α -(Fe,Co)Si phase and the cubic DO_3 phase coexist. The major Bragg peaks of both phases coincide with each other. For XRD data the volume fraction of nanocrystalline phase for studied samples was estimated from the integral intensities of reflections of the crystalline phase and the amorphous phase halo in Q range up to 10 \AA^{-1} . Then the amorphous part of the intensity was subtracted and then for such obtained intensity the Rietveld method analysis was performed for obtaining the lattice parameter a . The mean grain size of the nanocrystals was also estimated. It may be noted that the for the same annealing condition the lattice parameter of the α -(Fe,Co)Si phase decrease and the mean grain size increase as the Co concentration increases in agreement with the previous results [1,2]. The obtained results are presented in Figure 1.

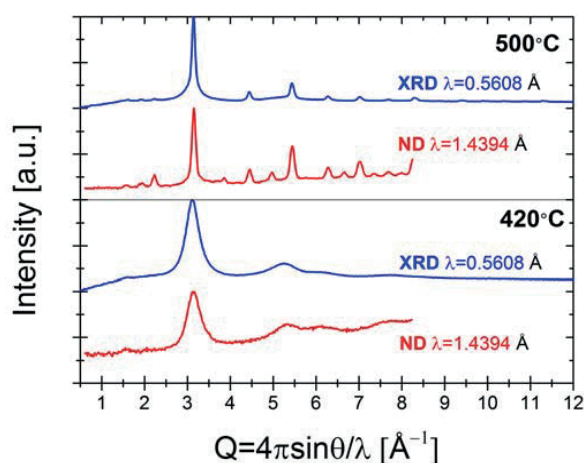


Figure 1. The XRD and ND diffraction patterns compared for Co-doped FINEMET amorphous ribbons.

References

- [1] K. Ruwali, A. Gupta, S.N. Kane, P. Duhaj, Mater. Sci. Eng. A 226-228, 729, (1997)
- [2] J.M. Borrego, C.F. Conde, A. Conde, J.M. Greneche, J. Non-Cryst. Solids 287, 120, (2001)

<h1 style="text-align: center;">BNC</h1> <p style="text-align: center;">Experimental Report</p>	<i>Experiment title</i> The structure of liquid perfluorodecalin with and without dissolved oxygen	<i>Instrument:</i> MTEST <i>Local contact:</i> L. Temleitner
	<i>Principal proposer:</i> Eckhard Spohr <i>Experimental team:</i> Eckhard Spohr, L. Pusztai, L. Temleitner	<i>Experiment Number:</i> BRR-359 <i>Date:</i> 19-29 Nov. 2013

Objectives

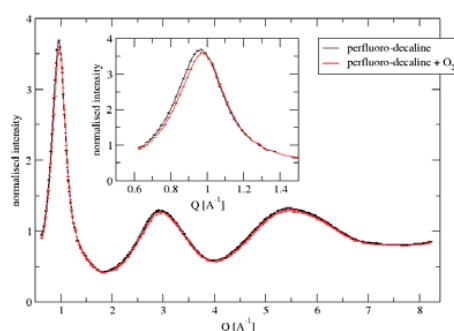
Perfluorodecalin is arguably the most widely used perfluorocarbon in medical and cosmetic applications. The pure substance is very convenient to deal with: it is an inert liquid at room temperature and the molecule itself is stable up to about 400°C. Most applications utilise its ability to dissolve large amounts of oxygen (100 ml of perfluorodecalin at 25°C will dissolve 49 ml of oxygen at room temperature and atmospheric pressure). The present proposal was initiated within the University of Duisburg-Essen by extensive investigations of the liquid as an oxygen carrier for vesicular deployment of trauma victims.

Interestingly, very little is known about the liquid structure of pure perfluorodecalin: to our best knowledge, no neutron diffraction experiment has been performed either on the neat or the oxygen-saturated liquid. The proposed experiment aims at determining the neutron weighted total scattering structure factor, $F(Q)$, of $C_{10}F_{18}$ with and without oxygen saturation. The main issues to resolve are (a) conformation of the molecules in the neat liquids; (b) nature of intermolecular correlations; (c) possible conformational changes on introducing oxygen; (d) environment of oxygen molecules.

Results

The measurement has been performed with the MTEST diffractometer using 1.44 Å neutrons, which made possible to perform the examinations under the 0.65–8.2 Å⁻¹ range in scattering vector. Two samples have been prepared: one without dissolved oxygen (degassed by syringe) and another one saturated with oxygen (0.022 mM/L). The samples have been sealed in a 6 mm thin-walled vanadium can designed for measurement of liquids. Results have been obtained by subtracting the intensities of empty can and transforming the measured datasets into Q-space.

According to the results, although slight the shift of the peaks is observable, the two curves behaves similar: the possible reason is the small difference in neutron coherent scattering lengths. These results are going to be interpreted with x-ray diffraction measurements and by means of molecular dynamics and Reverse Monte Carlo computer simulations. After that, we are planning to publish them in research periodical.



Journal of Alloys and Compounds, **615**
(2014), S203-S207.

<h1 style="margin: 0;">BNC</h1> <p style="margin: 0;">Experimental Report</p>	<i>Experiment title</i> Total scattering investigation of local structure around iron in FeV-based bcc-hydrides	<i>Instrument:</i> MTEST <i>Local contact:</i> Temleitner László
	<i>Principal proposer:</i> Henrik Mauroy <i>Experimental team:</i> Henrik Mauroy	<i>Experiment Number:</i> BRR-358 <i>Date:</i> 1-11 November 2014

Objectives

Ti-V-M (M = Cr, Mn, Fe, Co or Ni) bcc hydrides have excellent thermodynamics and decent hydrogen capacity (2-3 wt.%) [1]. Vanadium costs about 300 Euro/kg, about 10 times more than most other first row transition metals and is a severe limitation for utilization of Ti-V-M bcc alloys for hydrogen storage. A possible workaround is to utilize much cheaper ferrovandium alloys (FeV = Fe_{0.2}V_{0.8}) instead (about 30 Euro/kg). The reduction in price comes at the cost of lower hydrogen capacity. Kinetic and thermodynamic properties are also altered; however sometimes in a favorable way [2-4].

Total neutron and X-ray scattering experiments coupled with RMC modelling are powerful tools to extract information about short-range atomic order in hydrides [5-8]. For the bcc-hydrides it is desirable to investigate the distribution of the metal atoms to see what kind of tetrahedral sites are available for hydrogen occupation and which of these sites are actually preferred. The local structure around the Fe atoms is of particular interest and may give clues to the destabilizing effect Fe has on the thermodynamics of the Ti-V-hydride phase and is the main subject we wish to investigate in this experiment. Neutron scattering, using deuterated samples, is a key to structure determination of hydrides due to the negligible x-ray scattering power for hydrogen. Neutrons are also particularly advantageous for the present materials to distinguish the different metal elements from each other because their coherent scattering lengths differ to a great extent, being negative for Ti and Mn, negligible for V and positive for D, Fe, Zr and Nb.

Results

Total neutron scattering data were collected at MTEST for three samples with the compositions Ti_{0.4}Nb_{0.55}Fe_{0.05}, Ti_{0.7}V_{0.25}Fe_{0.05}D_{1.843} and Ti_{0.63}V_{0.27}Fe_{0.1}D_{1.73}. RMC modelling with the RMCPOW program revealed a strong tendency for Fe atoms to be surrounded by Fe, thus forming Fe-nanoclusters with extents of a few nanometers. This explains the reduced H-capacity of Fe-containing bcc alloys since Fe is not a hydride-forming element and interstitial sites coordinated solely by Fe are thus not favourable for hydrogen or deuterium occupation. Moreover, the models obtained from MTEST data show a significant but clearly lowered deuterium concentration in the Fe clusters.

For comparison, total scattering data have also been obtained at the GEM instrument at ISIS. RMC modelling with RMCprofile shows the tendency of Fe-clustering, but in addition the models show that almost no deuterium atoms are situated in the Fe-cluster. The comparison is interesting as it shows that strong short-range ordering features can be well modelled by low-Q reactor data (Fe-Fe correlations strongly influence the pair-distribution function due to the large scattering cross-section of Fe), while more subtle features can be missed or incompletely modelled.

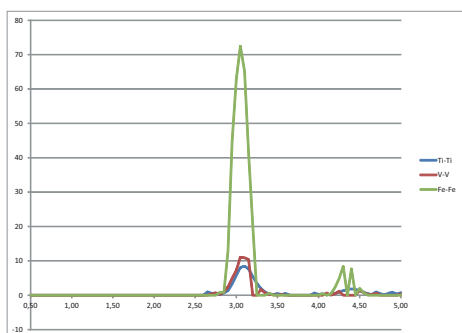


Fig. Metal-metal partial pair distribution functions of Ti_{0.7}V_{0.25}Fe_{0.05}D_{1.843} obtained from RMC modelling with MTEST data for showing strong tendency of Fe clustering.

<h1 style="margin: 0;">BNC</h1> <p style="margin: 0;">Experimental Report</p>	<i>Experiment title</i> Structural study of magnetocaloric (Mn,Fe)₂(P,As) compounds around the first order phase transition	<i>Instrument:</i> MTEST <i>Local contact:</i> Laszlo Temleitner
	<i>Principal proposer:</i> Lukasz Hawelek, Institute of Non-Ferrous Metals, ul. Sowinskiego 5, 44-100 Gliwice, Poland <i>Experimental team:</i> Lukasz Hawelek, L. Temleitner	<i>Experiment Number:</i> BRR_384 <i>Date:</i> 2-12.09.,7-17.10.2014

Objectives

The project objective was to perform the temperature dependent neutron diffraction (ND) measurements for two different samples MnFePAs-type magnetocaloric materials below and above their Curie temperatures (temperature of magnetic phase transformation) determined previously using magnetic measurements. The ND measurements should be done for further Rietveld-analysis using series of high-resolution, low-Q measurements (with 1.45 Å wavelength) and for real-space analysis, high-Q range (with 0.88 Å wavelength).

Results

During this beamtime the neutron diffraction experimental has been performed on two powder samples with chemical composition as follows: sample1 - Mn_{1.0}Fe_{1.0}P_{0.35}As_{0.65}, sample2 - Mn_{1.0}Fe_{1.0}P_{0.35}As_{0.54}Si_{0.11} with different non-metallic As/Si ratio content. To achieve the proposal objectives the measurements for sample 1 has been performed below and above Curie temperature e. g. at 300K and 400K respectively. To obtain the best relation of resolution and scattering vector Q range the measurements has been done using two monochromators Cu(111) and Cu(220) that allow to reach the different Q range: up to 8 Å⁻¹ and 13 Å⁻¹. Because of the 10 times lower intensity of the scattered neutrons for Cu(220) monochromator setup in comparison to Cu(111), the higher Q value measurements were much more time-consuming. The Cu(111) monochromator is giving the wavelength 1.45 Å whereas the Cu(220) the wavelength 0.89 Å. To obtain the correct sample intensity, the intensity of the vanadium empty can (8 in diameter) was then subtracted from the measured intensity. Additionally for proper detector positioning in both monochromators setup the nickel powder as a pattern was measured. In the next part of this beamtime the sample2 was measured at the same two temperatures, below the Curie temperature at 300K and above the Curie temperature at 400K. The measured data using both monochromators at 300K and 400K after correction and combining in Q-scale for sample1 and sample2 is presented in Figure 1.

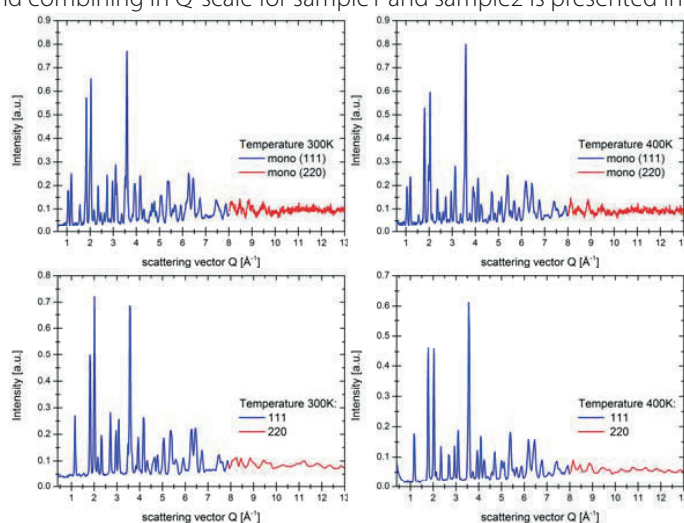


Figure 1. The Q-scale representation of the neutron diffraction intensity for sample 1 measured at 300K (left top) and 400K (right top) using Cu(111) and Cu(220) monochromators and for sample 2 measured at 300K (left bottom) and 400K (right bottom) using Cu(111) and Cu(220) monochromators.

The successfully obtained results are suitable for further comparative analysis of temperature dependant atomic structure evolution around the magnetoelastic transformation that coexists in the giant magnetocaloric effect in Fe₂P-type compounds. The data evaluation and comparative analysis is still in progress.

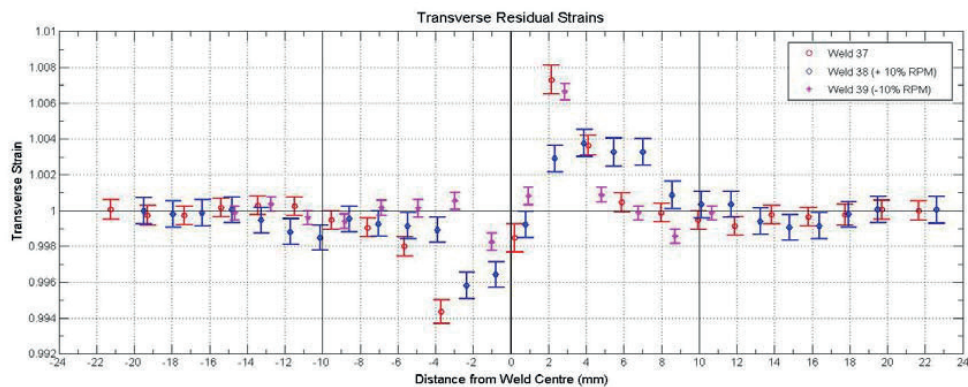
<h1 style="margin: 0;">BNC</h1> <p style="margin: 0;">Experimental Report</p>	<i>Experiment title</i> The effect of Friction Steel Welding on the size distribution of nanoparticles in ODS MA956	<i>Instrument:</i> MTEST <i>Local contact:</i> László Temleitner
	<i>Principal proposer:</i> Huw Dawson <i>Experimental team:</i> Huw Dawson, Enrique Jimenez-Melero	<i>Experiment Number:</i> BRR-411 <i>Date:</i> 11-21 November 2014, 13-16 January 2015

Objectives

The intended experiment title was 'The Effect of Friction Stir Welding on the residual stress distribution in MA956 ODS steel'. The objective was to measure the residual stresses present in MA956 steel plates after bead-on-plate friction stir welding, using neutron diffraction. It was also hoped to measure how the distribution and magnitudes of the stresses were affected by the welding parameters used. There were six welds in total that used parameters that varied their rotation speed, traverse speed and downforce of the tool used.

Results

Although it was possible to view changes to the residual stress across the welds it was not possible to measure them to an accurate level. This was most likely due to the fact that the welded plates were not perfectly flat and had a slight bow. It was not possible to align the plate well enough or to continually correct for the changing orientation of the plate with respect to the detector. Therefore there was a systematic error in the results. It was attempted to correct the data after the experiment but it was not possible to fully remove the error. The best final results attained are shown below.



Future measurements have confirmed that there should not be a negative strain from 0 to -4 mm from the weld centre.

It was also not possible to measure the strains in the longitudinal direction so only the transverse strains could be measured and not the residual stress.

<h1 style="margin: 0;">BNC</h1> <p style="margin: 0;">Experimental Report</p>	<i>Experiment title</i> Local atomic order in light metal-based amorphous metallic alloys	<i>Instrument: MTEST</i> <i>Local contact:</i> <i>László Temleitner</i>
	<i>Principal proposer:</i> Rafał Babilas <i>Experimental team:</i> Rafał Babilas, László Temleitner	<i>Experiment Number:</i> BRR-446 <i>Date:</i> 4-9 November 2015

Objectives

The aim of the project was complex determination of the local structure in the samples of light metals-based amorphous alloys ($Mg_{60}Cu_{30}Y_{10}$, $Mg_{60}Cu_{25}Y_{10}Ni_5$, $Mg_{65}Cu_{20}Y_{10}Zn_5$, $Ca_{50}Mg_{20}Cu_{30}$) by using the Reverse Monte Carlo (RMC) technique due to specific arrangements of atoms in each kind of alloy. The RMC models in studies of the short-range order (SRO) in metallic glasses were prepared with emphasis on the information from neutron diffraction (ND) measurements. The use of MTEST instrument was very important to obtain results necessary to precise the local atomic ordering and to prepare realistic structural models in these proposed disordered alloys.

Results

The neutron diffraction data for the studied multicomponent alloys in an as-cast state was obtained. The diffraction patterns of the studied samples showed a broad diffraction halo indicating the formation of an amorphous structure. In order to determine atomic configurations in the short-range order regions the ND experimental data were fitted by the Reverse Monte Carlo method. The total structure factors $S(Q)$ s obtained from neutron diffraction results and from the RMC calculation were prepared for the scattering vector Q in the range $1-10 \text{ \AA}^{-1}$. Excellent fits with experimental and calculated $S(Q)$ s were obtained, so the model $S(Q)$ suitable agrees with the experimental ND data. The partial pair distribution functions from the final RMC structural models were obtained. All the PDFs exhibit sharp and distinct first peaks.

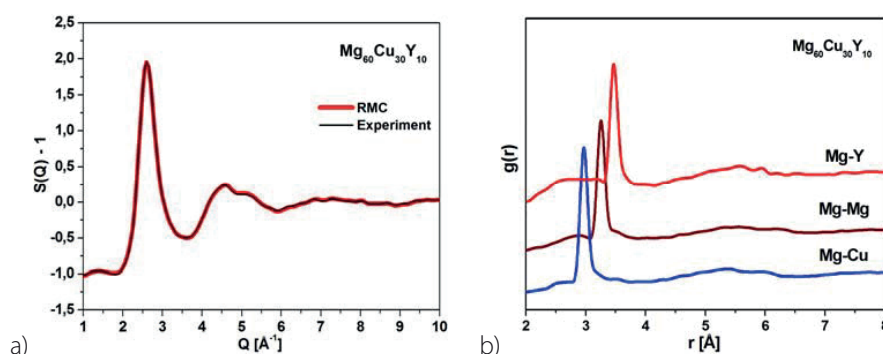


Fig. 1. Experimental and RMC fitting structure factors (a) and partial PDFs (b) for $Mg_{60}Cu_{30}Y_{10}$ metallic glass.

The partial PDFs were also used to determine the inter-atomic distance of selected atoms, which is defined as the radial distance corresponding to the first peak. The peak positions of Mg-Mg, Mg-Cu and Mg-Y partial PDFs are found at 3.25, 2.95 and 3.45 \AA , respectively for the $Mg_{60}Cu_{30}Y_{10}$ metallic glass (Fig.1). The RMC model was used for analysis of the local structure of the studied glasses. The resulting configuration of 8000 atoms was represent by the output boxes. From the boxes a layer of 5 \AA in thickness was selected in order to visualize atomic arrangement. The selected regions demonstrate that there are some kinds of atomic clusters in disordered configuration of atoms. In selected configurations of atoms in the 2D representation the presence of pentagons and hexagons was observed as representation of SRO regions.

<h1 style="margin: 0;">BNC</h1> <p style="margin: 0;">Experimental Report</p>	<i>Experiment title</i> Network structure of new molybdate glasses by neutron diffraction and reverse Monte Carlo modelling	<i>Instrument</i> PSD_1 <i>Local contact</i> M. Fábrián
	<i>Principal proposer:</i> K. Kiril <i>Experimental team:</i> M. Fábrián, E. Sváb; K. Kiril	<i>Proposal No.</i> BRR_309cont. <i>Date(s) of Exp.</i> February-March 2013

Objectives

Rare-earth molybdate phases are known to exhibit a great variety of important physical properties including high ion and electron conductivity of fast oxide ion conductors derived from the parent oxide $\text{La}_2\text{Mo}_2\text{O}_9$ (LAMOX family, $(\text{Sm}_2(\text{MoO}_4)_3, \text{LiLn}(\text{MoO}_4)_2, \text{Ln}=\text{Nd, Pr, Ho})$.

In contrast to the most molybdates with relatively well-characterised crystalline structures, the preparation and structural information on amorphous molybdate systems is not ample. The main problems of the preparation of molybdate glasses without modifier ions or participation of classical network formers are connected with the high crystallization tendency of the components. The aim of this work is to get a deeper insight into the structural network characteristics of new series of molybdate conditional glass former containing modifiers Nd_2O_3 , MgO and classical glass former B_2O_3 .

Results

The nominal composition of the glasses are $90\text{MoO}_3\text{-}10\text{Nd}_2\text{O}_3$ (hereafter referred to as $\text{Mo}90\text{Nd}10$), $80\text{MoO}_3\text{-}15\text{Nd}_2\text{O}_3\text{-}5\text{MgO}$ ($\text{Mo}80\text{Nd}15\text{Mg}5$), $75\text{MoO}_3\text{-}12.5\text{Nd}_2\text{O}_3\text{-}12.5\text{MgO}$ ($\text{Mo}75\text{Nd}12.5\text{Mg}12.5$) and $50\text{MoO}_3\text{-}25\text{Nd}_2\text{O}_3\text{-}25\text{B}_2\text{O}_3$ ($\text{Mo}50\text{Nd}25\text{B}25$) (mol%). In order to get information about the structure and chemical bonding from the neutron diffraction data, two types of measurements were carried out. Neutron diffraction experiments were carried out at the 10 MW Budapest research reactor using the PSD diffractometer [1] and at the 7C2 diffractometer in LLB/Saclay [2]. As a first step of data evaluation the total reduced correlation function, $G(r)$ was calculated by the usual Fourier transformation, are shown in Fig. 1.

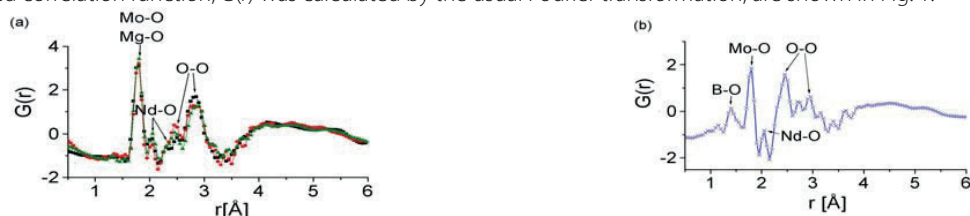


Figure 1. Experimental neutron total reduced distribution function, $G(r)$: a) $\text{Mo}90\text{Nd}10$ (black), $\text{Mo}80\text{Nd}15\text{Mg}5$ (red), $\text{Mo}75\text{Nd}12.5\text{Mg}12.5$ (green) and b) $\text{Mo}50\text{Nd}25\text{B}25$ (blue) glasses obtained by Fourier transformation from the corresponding $S(Q)$.

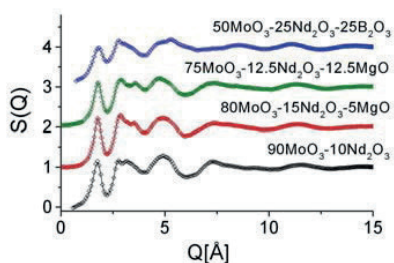


Figure 2. Experimental data (colour) and RMC simulation (solid line)

The experimental $S(Q)$ data have been simulated by the RMC simulation technique [3]. Using reasonable cut-off distances and connectivity constraints in the RMC simulation procedure, we have obtained very good agreement between the experimental and the calculated $S(Q)$ data, are presented in Figure 2. From the RMC modelling the partial atomic correlation functions $g_{ij}(r)$ and the coordination number distributions CN_{ij} have been revealed. Formations of MoO_4 units were established with 1.80Å Mo-O distance. In the binary glass MoO_4 (55%) and MoO_6 (25%) structural units were revealed.

In ternary systems mainly MoO_4 units are present, and with decreasing MoO_3 concentration, the ratio of MoO_6 units roughly decreases. For the B-containing ternary glasses B-O first neighbour distance was obtained at 1.40Å , the B-O network is formed by BO_3 and BO_4 groups. Mixed $\text{MoO}_4\text{-BO}_4$ and $\text{MoO}_4\text{-BO}_3$ linkages form pronounced intermediate-range order.

References

- [1] E. Sváb, Gy. Meszaros, F. Deak *Mater. Sci. Forum* 228 (1996) 247; <http://www.bnc.hu/>
- [2] J. P. Ambroise, R. Bellissent *Rev. Phys. Appl.* 19 (1984) 731; <http://www-llb.cea.fr/en/>
- [3] R.L. McGreevy, L. Pusztai *Mol. Simul.* 1 (1988) 359

<h1 style="margin: 0;">BNC</h1> <p style="margin: 0;">Experimental Report</p>	<i>Experiment title</i> Comparative study on the influence of different activators (Mn^{2+}, Eu^{3+}, Ce^{3+}) upon the nanostructure evolution of the host matrix willemite phosphors	<i>Proposal No.</i> PSD_2 <i>Local contact</i> M. Fábíán
	<i>Principal proposer:</i> Z. Dudás <i>Experimental team:</i> M. Fábíán, Gy. Mészáros, Z. Dudás	<i>Experiment Number</i> BRR_357 <i>Date:</i> March 2013

Objectives

The willemite ($\alpha\text{-Zn}_2\text{SiO}_4$) based phosphors has successful applications as color-emitting materials in lamps, cathode ray tubes, flat panel displays, electroluminescent and optoelectronic devices and more recently, radiation detectors in medical imaging systems. $\alpha\text{-Zn}_2\text{SiO}_4$ under ordinary conditions crystallizes in the phenacite structural type and belongs to the rhombohedral space group R-3. Zinc silicate phosphors consists in willemite solid solutions in the $\text{Zn}_2\text{SiO}_4 - \text{Me}_2\text{SiO}_4$ system, where Zn^{2+} ions are substituted by different metal ions in willemite crystalline network. We have started to investigate a new Willemite system doped with Mn^{2+} , Eu^{3+} , Ce^{3+} ; by using the 'PSD' neutron diffractometer [1]. The main purpose of this work is study to investigate the influence of different activator type (Mn^{2+} , Eu^{3+} , Ce^{3+}) and charge compensator (Li^+ or K^+) upon the structural parameters of the willemite host lattice by neutron diffraction measurements.

Results

Neutron diffraction patterns were collected at room temperature on 13 compositions. The measurements were performed in thin walled vanadium sample holder, using cylindrical sample geometry. The powder specimens about 2.5-3g samples was measured about 12-14h depending on the compositions and the quantity. Background measurement was also carried out. Were measured the following 6 specimens, $\text{Zn}_2\text{SiO}_4:\text{Mn}$, $\text{Zn}_2\text{SiO}_4:\text{Tb}$, $\text{Zn}_2\text{SiO}_4:\text{Eu}(-6,-8,-9)$, $\text{Zn}_2\text{SiO}_4:\text{Ce}(-1,-2,-3)$, $\text{Zn}_2\text{SiO}_4:\text{CM}(-1,-2)$, and $\text{Zn}_2\text{SiO}_4:\text{H}(-1,-11000)$. The behaviour of the ions (Mn^{2+} , Eu^{3+} , Ce^{3+} , Tb^{3+}) doped into crystal lattice of Zn_2SiO_4 is closely related to the luminescent properties of the obtained willemite samples as a color-emitting phosphor. For the neutron diffraction the samples were chosen according to their luminescent emission, in the present case measured samples give the best luminescent emission.

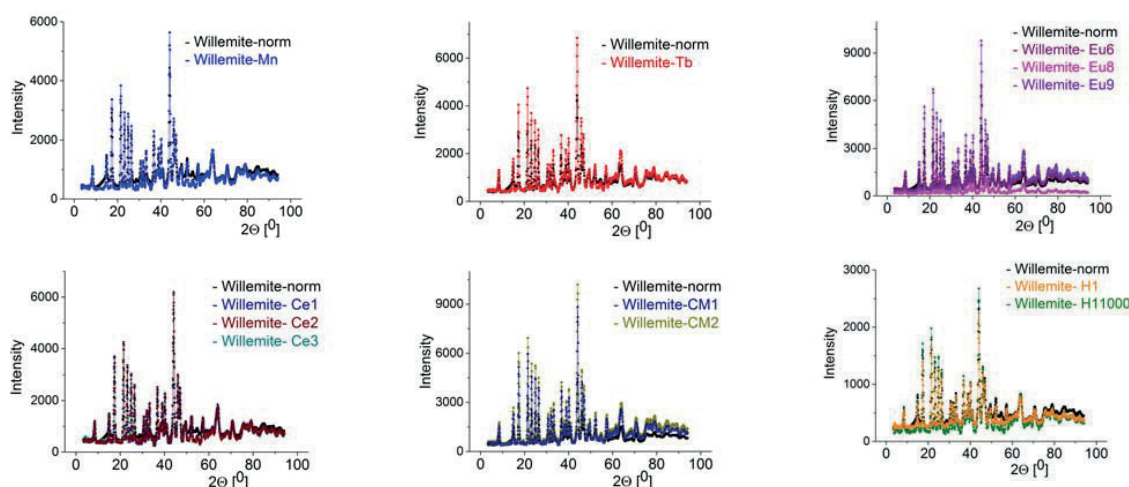


Figure 1. Neutron diffraction patterns on the studied Willemite samples doped with Mn^{2+} , Tb^{3+} , Eu^{3+} , Ce^{3+} ions.

The measured samples proved to be crystalline, exception the poor willemite, where appear mixed phases, together amorphous and crystalline character. For all studied samples the neutron diffraction results seems to be valuable for further data treatment, show in Figure 1.

Data analysis of the ND pattern was performed, the structure factor are calculated. The neutron diffraction results are in good correlation with the X-ray diffraction measurements.

Future prospects: Publication is in progress.

References

[1] E. Svab, Gy. Meszaros, F. Deak *Mater. Sci. Forum* 228 (1996) 247; <http://www.bnc.hu/>

<h1 style="margin: 0;">BNC</h1> <p style="margin: 0;">Experimental Report</p>	<i>Experiment title</i> Structure study of new steel compositions	<i>Proposal No.</i> PSD_3 <i>Local contact</i> M. Fábán
	<i>Principal proposer:</i> M. Rogante <i>Experimental team:</i> M. Fábán, M. Rogante	<i>Experiment Number</i> 1_IH <i>Date:</i> May 2013

Objectives

The Ni-based alloys are used for their outstanding corrosion and high temperature resistance. Many are metallurgically related to the austenitic stainless steels but are much more highly alloyed, particularly with nickel, chromium and molybdenum in order to enhance their corrosion resistance. These alloys are used resist extremely corrosive conditions in the energy, power, chemical and petrochemical industries.

Results

Neutron diffraction (ND) studies on new steel samples were performed at the 10 MW Budapest research reactor using the 'PSD' neutron powder diffractometer [1]. Monochromatic wavelength of $\lambda_0=1.067 \text{ \AA}$ was used. The diffraction spectrum was measured in the momentum transfer range of $Q= 0.95-9.8 \text{ \AA}^{-1}$. The disc specimens were about 3-4 g, 10 mm diameter and 1 mm thickness. The studied samples were measured with the similar time, each with 3 hours.

The ND pattern shows that the specimens are crystalline. In the ND experiments the intensity curves are fairly similar for all two samples, differences may be observed only in the fine details, especially in different intensity of the basic peaks. This indicates that the basic characteristics of the metal-metal network do not show significant differences in dependence of the compositions. The preparation mode and the different temperatures causes slight changes, this may be observed in the intensities. Especially, the small (pre)peak gets more pronounced in case of higher temperature, see sample 26NiCrMoV-A in the Figure 1(a).

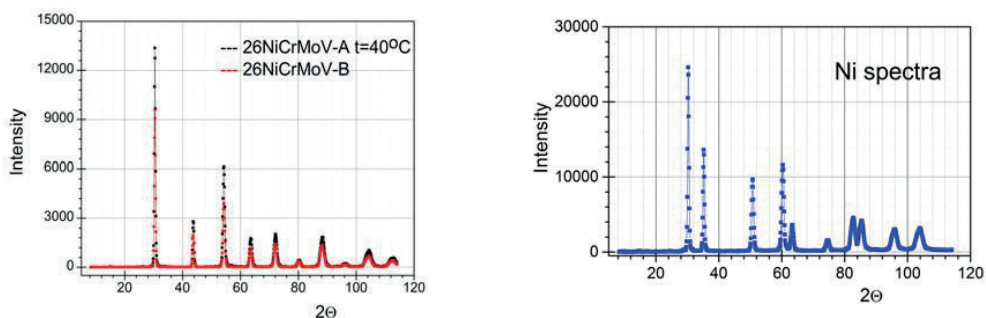


Figure 1. Figure X. Neutron diffraction measurements on the studied samples a.) 26NiCrMoV-A($t=40^\circ\text{C}$) and 26NiCrMoV-B and b.) Reference Ni sample.

The samples contain in all two cases at the same percentage Ni atom. Ni atom has very strong neutron scattering parameters, most important is the neutron scattering length, $\langle b \rangle_{\text{Ni}}=1.434 \cdot 10^{-12} \text{ cm}$, therefore we use the pure Ni measurements for the reference data. In the Ni measurements we calculate with the same methods the intensity and we obtain stable peaks with good resolution. Figure 1(b) show intensity for the investigated pure Ni sample. We compare the samples spectra (26NiCrMoV-A and B) with the Ni spectra, and we can identify the Ni peaks in the studied samples. First main peak come in the 30.4° , this is the first basic Ni peak, and another similar peak in our samples which correspond to the Ni is around 63° and 104° .

Future prospects: Publication is in progress.

References

[1] E. Svab, Gy. Meszaros, F. Deak *Mater. Sci. Forum* 228 (1996) 247; <http://www.bnc.hu/>

<h1 style="margin: 0;">BNC</h1> <p style="margin: 0;">Experimental Report</p>	<i>Experiment title</i> The influence of the Ce³⁺ concentration and the thermal treatment temperature upon the nanostructure evolution of the host matrix willemite phosphors	<i>Proposal No.</i> PSD_4 <i>Local contact</i> M. Fábíán
	<i>Principal proposer:</i> S. Sorescu <i>Experimental team:</i> M. Fábíán, S. Sorescu	<i>Experiment Number</i> BRR_357 <i>Date:</i> December 2013- January 2014

Objectives

In the past few decades the majority of the researches focused on the development of willemite based phosphors to be used in cathode ray tube, plasma display panels, three-dimensional color displays, electrochemical devices, memory devices and optical sensors. More recently these materials were successfully applied like dielectric ceramics for wireless applications and also like biomaterials.

It is well known that the willemite possesses a rhombohedral structure, wide energy band gap, semi-conducting properties and excellent chemical stability. Willemite has an excellent potential as a multi-color emitting phosphor over the whole visible light region depending on the nature of the guest ion. The luminescent behavior of the obtained phosphors is closely related to the type and quantity of the activator ions. The luminescence emission of Eu³⁺, Tb³⁺, Mn²⁺, Ce³⁺ activated α -Zn₂SiO₄ covers the red, yellow, green, and blue domain of the visible spectrum, respectively.

Results

The present work aims to investigate the influence of the doping concentration of the trivalent Cerium ions upon the crystalline structure of the willemite as host material. 0.5 to 5 percent of Cerium (III) ions were used to dope the Zn₂SiO₄. The phosphor powders were prepared using the simple wet-chemical sol-gel method combined with furnace firing at 300, 500, 700, 800, 900 and 1000 °C.

Neutron diffraction studies on willemite doped samples were performed at the 10 MW Budapest research reactor using the 'PSD' neutron powder diffractometer [1]. Monochromatic wavelength of $\lambda_0=1.069$ Å, momentum transfer range of $Q=0.95-9.8$ Å⁻¹. The results revealed a clear relationship between the Ce³⁺ concentration and the thermal treatment temperature upon the crystalline size and the atomic arrangement on the crystalline network. With the increasing of the Cerium doping concentration the crystalline size is increasing from 38.8 nm for the 3% mole percent of Ce³⁺ (the lowest value) to 53.5 nm (highest value) for the 4% mole percent. The value of the all other samples were situated 40.5-47.5 nm.

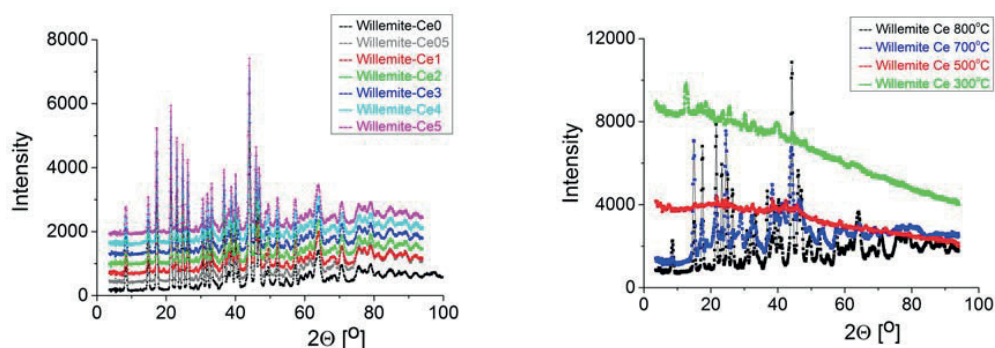


Figure 1. Neutron diffraction patterns on the studied Willemite doped with Ce³⁺ in function of concentration and temperature.

The effect of the thermal treatment temperature upon the crystalline size of the 1 mol% doped sample were determined, see Fig 1. Until 500°C no crystallinity of the samples were determined. The willemite starts to crystallize from 700°C with a size of 32.7 nm. Increasing the thermal treatment temperature the crystalline size it is increasing 36.4 nm for 800°C, 42.5 nm for 900°C and 48.7 nm for 1000°C. Unfortunately, for almost all samples cerianite impurities were determined.

Future prospects: Publication is in progress.

References

[1] E. Sváb, Gy. Meszaros, F. Deák *Mater. Sci. Forum* 228 (1996) 247; <http://www.bnc.hu/>

BNC Experimental Report	<i>Experiment title</i> Neutron diffraction of Zr-1%Nb fuel cladding material	<i>Proposal No.</i> PSD_5 <i>Local contact</i> M. Fábíán
	<i>Principal proposer:</i> M. Fábíán <i>Experimental team:</i> M. Fábíán, Z. Hózer	<i>Experiment Number</i> 2_IH <i>Date:</i> February 2014

Objectives

During a LOCA accident at high temperature the oxidation process of zirconium alloy claddings in steam creates an external oxide layer on the tube surface and produces hydrogen. A part of the hydrogen can be absorbed by the metal. The oxide layer, the oxygen and hydrogen content degrades the mechanical properties of the cladding it mostly results in the embrittlement of the alloys. The embrittlement can lead to the failure of the fuel rods under accidental conditions, especially during the reflooding of the hot nuclear core. The cladding material of Western type PWRs is Zircaloy alloy, the Russian design VVER reactors apply Zr-1%Nb cladding. There are differences between the mechanical properties and corrosion resistance of these alloys: the Zircaloy has higher mechanical strength and the Zr-1%Nb (E110) has better corrosion resistance during normal operation. In the present work comparative studies were carried out to investigate the differences at high temperature steam corrosion processes and to determine the effect of the corrosion on the embrittlement of E110 and E110 OCs alloys. We tested with neutron diffraction, to obtain the basic nature of these alloys.

Results

Neutron diffraction measurements were carried out on the medium resolution PSD neutron diffractometer. The wavelength of the monochromatic neutron beam was 1.07 Å. The diffractometer is based on a ³He linear position sensitive detector system that allows simultaneous detection of scattered data over an angular range of 25°. The range of 2θ was 9.2°-113.2°. For the measured samples E110 and E110-OCS, based on the Zr-1%Nb material, the neutron diffraction data could be well described by the hexagonal α-Zr, space group: P6₃/mmc. The results show that under applied physical and mechanical effects the E110 tubes not pronounced conspicuous differences.

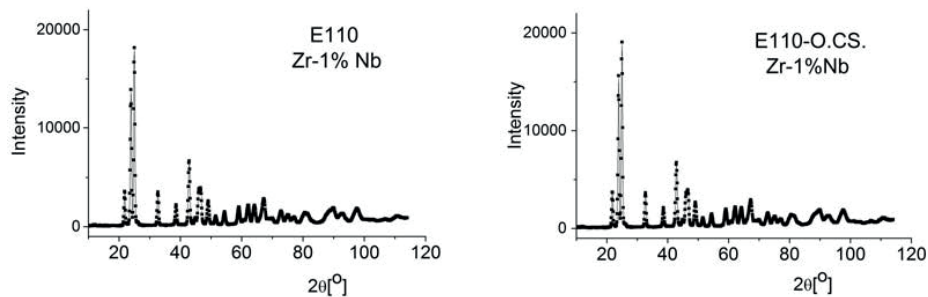


Figure 1. Neutron diffraction spectrum of Zr-1 at%Nb.

Neutron diffraction data analyses have revealed that the E110 and E110 OCs materials can be described by α-Zr structure.

References

[1] Svab E, Meszaros Gy, Deak F 1996 *Mater. Sci. Forum* **228** 247 and <http://www.bnc.hu/>

<h1 style="margin: 0;">BNC</h1> <p style="margin: 0;">Experimental Report</p>	<i>Experiment title</i> Development of glass matrix for radioactive waste conditioning	<i>Proposal No.</i> PSD_6 <i>Local contact</i> M. Fábíán
	<i>Principal proposer:</i> M. Fábíán <i>Experimental team:</i> M. Fábíán, E. Sváb	<i>Experiment Number</i> 2_IH <i>Date:</i> October-November 2014

Objectives

The most feasible and accepted way for storage of high-level radioactive waste (HLW) is the vitrification process, where the active elements are melted and poured into glass form, and thereafter deposited in the deep geological formation, where the objective is to retain the radionuclides in the host rocks, and to block access to the biosphere. Understanding of the incorporation of actinides in borosilicate matrix used for nuclear waste storage is of a great importance for radioactive waste immobilization. This study carried out on matrix glasses doped respectively with 10 and 30wt% CeO₂ and Nd₂O₃ used for chemical modelling of the actinides. Neutron diffraction measurements and Reverse Monte Carlo simulations were performed.

Results

The composition of the investigated glassy specimens are 90(70)wt% [55SiO₂·10B₂O₃·25Na₂O·5BaO·5ZrO₂] + 10(30)wt% CeO₂, Nd₂O₃ (hereafter referred as Matrix-Ce10(30), Matrix-Nd10(30), respectively). The investigations and results are presented parallel for the mentioned four samples. B₂O₃ was isotopically enriched with ¹¹B-isotope (99.6% enrichment) in order to reduce the influence of the high neutron absorption of ¹⁰B present in natural boron. Actinides are not available, therefore for chemical modelling of the actinides we use lanthanides, used as their complementary elements. Ce stays for the hazardous radioactive Pu, while Nd for Americium and Curium. Neutron diffraction measurements were performed in a momentum transfer range $Q=0.45-9.8 \text{ \AA}^{-1}$ measured by the 2-axis PSD monochromatic neutron diffractometer ($\lambda_0=1.068 \text{ \AA}$) [1] at the 10 MW Budapest research reactor. The experimental structure factors, $S_{EXP}(Q)$ data have been simulated by the RMC method [2]. The RMC technique minimizes the squared difference between the experimental, $S_{EXP}(Q)$ and the calculated, $S_{RMC}(Q)$ one by moving the atoms randomly. The convergence of the RMC calculation was good and the final $S(Q)$ matched very well the experimental one. Fig. 1 displays the neutron experimental and the calculated $S(Q)$ for the glassy samples, for the Matrix-Ce10(30), Matrix-Nd10(30) samples.



Figure 1. Neutron diffraction total structure factors for Matrix-Nd10(30) (blue) and Matrix-Ce10(30) (magenta) glasses and RMC fits (solid line).

It was established that the basic network structure consists of tetrahedral SiO₄ units and of mixed trigonal BO₃ and tetrahedral BO₄ units, the basic network structure of the simple and matrix glasses similar than doped glasses. For the Ce-O and Nd-O correlations characteristic distribution was detected at 2.13 Å and 2.00 Å, respectively. Furthermore, significant second neighbour atomic pair correlations have been revealed between cerium, neodymium and the network former (Si,B) atoms. From these results we may conclude that also for the doped glasses we have a stable basic network structure and cerium, neodymium accommodates in both silicate and borate site. This may be the reason of the observed good glassy stability and incorporation ability of the ions.

Future prospects: Publication is in progress.

References

- [1] E. Sváb, Gy. Meszaros, F. Deak *Mater. Sci. Forum* 228 (1996) 247; <http://www.bnc.hu/>
 [2] R.L. McGreevy, L. Pusztai *Mol. Simul.* 1 (1988) 359

<h1 style="margin: 0;">BNC</h1> <p style="margin: 0;">Experimental Report</p>	<i>Experiment title</i> Understanding the atomic structure of glass sealant materials assed by PSD diffraction	<i>Instrument:</i> PSD_7 <i>Local contact:</i> M. Fábíán
	Principal proposer: Allu Amarath Reddy Experimental team: M. Fábíán, A.A. Reddy	<i>Experiment Number:</i> BRR_407 <i>Date:</i> February 2015

Objectives: Glasses are known to be more stable at its room temperature within the short-range order. The stability of glass usually decreases and starts continuous devitrification with increasing temperature and or with the isothermal heat treatment at sufficient high temperature. In searching of suitable glass material, which can be potentially applied as a sealant for SOFCs, we have investigated a glass compositions within the system of CaO–MgO–Al₂O₃–SiO₂ (CMAS), CaO–Al₂O₃–SrO (CAS), SrO–Al₂O₃–SiO₂ (SAS) owing to their high chemical resistance. Use of PSD neutron diffraction technique for the newly designed glasses to obtain the clear information about the structure of glasses.

Results: Neutron diffraction measurements have been performed at the 10 MW Budapest research reactor using the two-axis 'PSD' diffractometer (monochromatic wavelength was $\lambda_0 = 1.068\text{\AA}$). The diffraction spectrum was measured in the momentum transfer range of $Q=0.95\text{--}9.5\text{ \AA}^{-1}$. The structure factor, $S(Q)$, from the raw experimental data obtained independently for the four samples, using the programme packages available at the facility are presented in Fig. 1. The neutron diffraction pattern shows that the specimens are fully amorphous, and no hydrogen was detected. The experimental $S(Q)$ data have also been simulated by the RMC method using the software package available. Partial atomic pair correlation functions, $g_{ij}(r)$, for SiO, AlO, MgO and CaO have been revealed from RMC simulations.

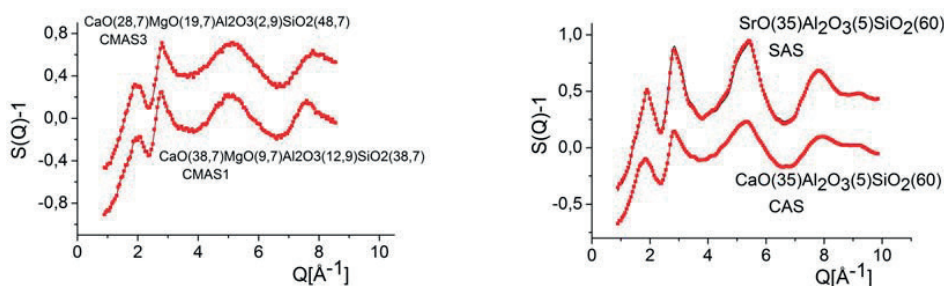


Figure 1. Neutron diffraction structure factor: experimental data (red symbols) and RMC simulation (solid line).

For the Si–O distribution we obtained a very characteristic peak at 1.60 and 1.62 \AA for CMAS1 glass and CMAS3 glasses respectively. In the case of CAS and SAS glasses the peak obtained at 1.6 \AA . The obtained Si–O distance for CMAS1, CAS and SAS glasses are less than the v-SiO₂ glass. The coordination number distribution shows that more than 98% of Si atoms are surrounded by four oxygen atoms. The actual average coordination numbers obtained from RMC modeling are 3.83, 3.7, 3.64 and 3.54 (± 0.15) for the CMAS1, CMAS3, CAS and SAS compositions, respectively. This indicates that the substitution of SrO for CaO in aluminosilicate glasses does not influence the Si–O bond length, however, it marginally influences the coordination number decreases from 3.64 to 3.54.

The Ca–O distribution contains a narrow peak at 2.3 \AA for CMAS1 glass whereas the peak appears at 2.35 \AA for CMAS3 glass. No changes were observed for AlO and MgO for which the peaks appeared at 1.75 \AA and 1.7 \AA respectively for both CMAS1 and CMAS3 glasses. The coordinatin number distribution indicates that aluminum exist in four fold coordination. The obtained results from PSD technique are highly helpful in order to obtain the clear information about the structure of glass. However, to comment in details about the role of Mg and Al further structural information based on MAS-NMR and Raman spectroscopy are needed and the corresponding experiments are under process.

Future prospects

The structure analysis is in progress.

<h1 style="margin: 0;">BNC</h1> <p style="margin: 0;">Experimental Report</p>	<i>Experiment title</i> Investigation of nature Boson peak and nanostructure by method inelastic scattering neutron in chalcogenide glasses As_2Se_3, $As_{40}Se_{30}S(Te)_{30}$, $As_{33}Se_{33,3}S(Te)_{33,4}$	<i>Instrument.</i> PSD_8 <i>Local contact</i> M. Fábrián
	Principal proposer: Rahim Alekberov Experimental team: M. Fábrián, R. Alekberov	<i>Experiment Number</i> BRR_435 <i>Date:</i> February/March 2015

Objectives

Chalcogenide glasses and glass-like semiconductors, based on the chalcogen elements As, S, Se and Te, have attracted much interest in recent years. These glasses show continuous change in physical properties by varying the chemical composition. The purpose of the present investigation is to study the new As_2Se_3 , $As_{40}Se_{30}S_{30}$, $As_{40}Se_{30}Te_{30}$, $As_{33}Se_{33,3}S_{33,4}$ and $As_{33}Se_{33,3}Te_{33,4}$ samples, and to undertake a systematic study of the glassy network structure by means of neutron diffraction. We intend to obtain in the first step information on the short range order, and in second step on the medium range atomic correlations.

Results

Neutron diffraction measurements have been performed at the 10 MW Budapest research reactor using the two-axis 'PSD' diffractometer ($\lambda_0=1.068 \text{ \AA}$) [1]. The diffraction spectrum was measured in the momentum transfer range of $Q=0.95-9.5 \text{ \AA}^{-1}$. The powder specimens of about 2-3 g/each were filled in a cylindrical vanadium sample holder of 8 mm diameter, 50 mm height and 0.07 mm wall thickness for the experiments.

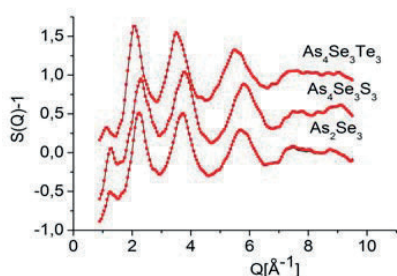


Figure 1. Experimental (red dots) and reverse Monte Carlo simulated (line) structure factors from RMC simulations.

The experimental $S(Q)$ data have been simulated by the RMC method [2] using the software package using the software package RMC++. The experimental $S(Q)$ factors are compared with those accumulated from the data of the RMC models of the corresponding glass compositions. The agreement of experimental and calculated scattering data was good. Comparisons between experimental and calculated structure factors are given in Fig 1. The neutron diffraction pattern shows that the specimens are fully amorphous, and no hydrogen was detected.

The partial atomic pair correlations, $g_{ij}(r)$ have been revealed from RMC simulation with a good reproducibility and acceptable statistics, and they are shown in Figs. 2.

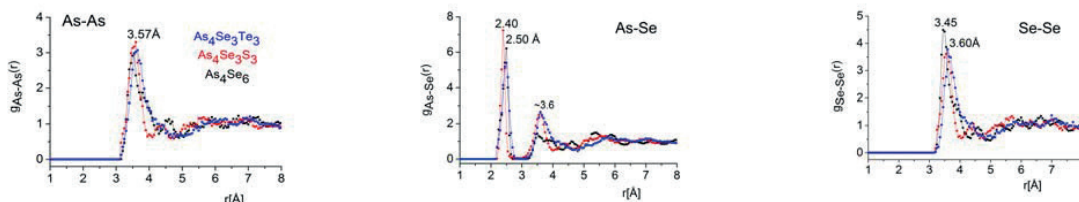


Figure 2. Partial atomic pair correlation functions obtained from the RMC modelling for the glasses.

In general, the curves for all the three compositions are almost the same within model errors. This suggests that substituting a part of Se by Te atoms does not change the basic network structure within the limit of experimental and modelling errors. For all three compositions, the As-Se correlation shows a rather sharp first neighbour distance at $2.4 \pm 0.1 \text{ \AA}$. In the $As_{40}Se_{30}S_{30}$ and $As_{40}Se_{30}Te_{30}$ glasses the possible As-As and Se-Se homopolar bonds have similar and characteristic broad peak at $3.6 \pm 0.1 \text{ \AA}$, while for the $As_{40}Se_{60}$ glass the peak shifted slightly to $3.45 \pm 0.1 \text{ \AA}$ in case of Se-Se. Addition of S,Te to As-Se network has negligible effect on As-Se bonds. Therefore, in the ternary As-Se-S and As-Se-Te systems the As-Se bond distance remains the same as in the binary As-Se system. The observed 2nd neighbour distance at 3.6 \AA for the As-Se bonds are an evidence for medium range ordering in both the binary and ternary glassy structures. It is established that substitution of Se by S, Te does not change the basic glassy network structure.

References

- [1] E. Svab, Gy. Meszaros, F. Deak *Mater. Sci. Forum* 228 (1996) 247; <http://www.bnc.hu/>
[2] R.L. McGreevy, L. Pusztai *Mol. Simul.* 1 (1988) 359

<h1 style="margin: 0;">BNC</h1> <p style="margin: 0;">Experimental Report</p>	<i>Experiment title</i> Neutron diffraction study of the structure of new molybdate glasses from the MoO₃-MeO_x system, Me=Cu,Ti and MoO₃-ZnO-B₂O₃ systems	<i>Instrument</i> PSD_9 <i>Local contact</i> M. Fábíán
	<i>Principal proposer:</i> R. Iordanova <i>Experimental team:</i> M. Fábíán, E. Sváb, M. Milanova	<i>Proposal No.</i> BRR_393 <i>Date(s) of Exp.</i> May/June 2015.

Objectives

Zinc boromolybdate glasses are known as low melting dielectric materials and they have high potential in several applications. Several network characteristics of the MoO₃-ZnO-B₂O₃ glass system have been reported in ref. [1] investigated by various optical spectroscopic methods, however, basic structural characteristics are still open question. The structure characterization is challenging, as far as, they consist of the conditional network former MoO₃, from the traditional network former B₂O₃, and the role of ZnO is a debate concerning its modifier or network former role. In the present work we aim to study the atomic scale short- and intermediate range order of ternary xMoO₃-50ZnO-(50-x)B₂O₃, x=10,20,30 mol% glasses synthesized by melt quench technique, prepared from B-11 isotope.

Results

In order to get information about the structure and chemical bonding from the neutron diffraction data, two types of measurements were carried out. Neutron diffraction (ND) experiments were carried out at the 10 MW Budapest research reactor using the PSD diffractometer [2] and at the 7C2 diffractometer in LLB/Saclay [3]. For the analysis of the ND data both the traditional Fourier transformation and the reverse Monte Carlo (RMC) [4] simulation techniques have been applied. RMC simulation was applied to generate a 3-dimensional atomic configuration, which is consistent with the experimental data. From RMC modeling the partial atomic pair correlation functions, coordination number distributions and three-particle bond angle distributions have been revealed. The fit of the RMC calculations was good, the final S(Q)s matched very well the experimental ones, as shown in Fig. 1.

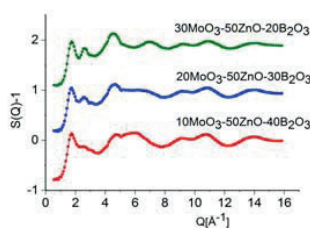


Figure 1. Neutron diffraction structure factor: experimental data (color symbols) and RMC simulation (solid line).

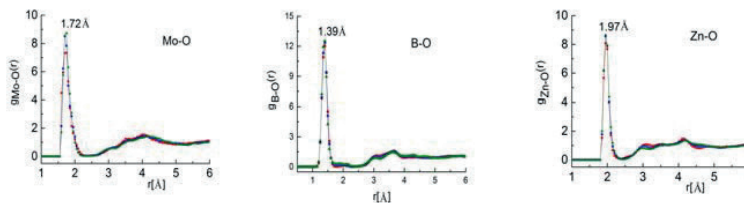


Figure 2. The Mo-O, B-O and Zn-O partial atomic pair correlation functions from RMC modeling.

The results show well-defined first neighbor distances for the Mo-O, Zn-O and B-O distributions (Fig. 2.). The first neighbor distances do not depend on concentration within error of limit. For the boron environment 3 and 4 coordinated atoms with mixed trigonal BO₃ and tetrahedral BO₄ structural units. ZnO proved to be a network former, not a modifier as it is often reported in the literature for similar systems. From the analyses of the obtained structural parameters we have concluded that the glassy network is formed by trigonal BO₃ and tetrahedral BO₄, MoO₄, ZnO₄ groups. Concentration dependence was found for the BO₄/BO₃ fraction, it increases with increasing B₂O₃ content. We have concluded that only small amount of boroxol rings are present and it is supposed that the network is formed by organization of BO₃ and BO₄ groups into superstructure units. The BO₃ and BO₄ units are linked to MoO₄ or ZnO₄, forming mixed ^[4]Mo-O-^{[3],[4]}B, ^[4]Mo-O-^[4]Zn, ^{[3],[4]}B-O-^[4]Zn bond-linkages. Significant intermediate-range correlations have been revealed for the second neighbor distances, indicating a stable and well-defined network. Significant medium-range order exists up to ~7 Å.

References

- [1] L. Aleksandorov, T. Komatsu, R. Iordanova, Y. Dimitriev, *Optical Materias* 33 (2011) 839
- [2] E. Sváb, Gy. Meszaros, F. Deak *Mater. Sci. Forum* 228 (1996) 247; <http://www.bnc.hu/>
- [3] J. P. Ambrose, R. Bellissent *Rev. Phys. Appl.* 19 (1984) 731; <http://www-llb.cea.fr/en/>
- [4] R.L. McGreevy, L. Pusztai *Mol. Simul.* 1 (1988) 359

<h1 style="margin: 0;">BNC</h1> <p style="margin: 0;">Experimental Report</p>	<i>Experiment title</i> Structure study of matrix glasses doped with uranium	<i>Proposal No.</i> PSD_10 <i>Local contact</i> M. Fábíán
	<i>Principal proposer:</i> M. Fábíán <i>Experimental team:</i> M. Fábíán, E. Sváb	<i>Experiment Number</i> 4_1H <i>Date:</i> November 2015

Objectives

The final and safe storage of radioactive waste materials is nowadays an existing problem to be solved urgently. The most feasible and accepted way for storage of high-level radioactive waste (HLW) is the vitrification process, where the active elements are melted and poured into glass form. Based on the experience of our previous studies, new glassy samples were synthesized with the so-called 'Matrix' composition $55\text{SiO}_2 \cdot 10\text{B}_2\text{O}_3 \cdot 25\text{Na}_2\text{O} \cdot 5\text{BaO} \cdot 5\text{ZrO}_2$ (mol%); into which the model compounds were added as oxides. Another successful preparation was the sample series with UO_3 added to the matrix; the final glassed contained 10, 20, 35 and 40 w% UO_3 .

Results

The composition of the investigated glassy specimens are $(100-x)[\text{Matrix}] + x\text{wt}\% \text{UO}_3$, $x=10, 20, 35, 40$. Neutron diffraction (ND) experiments were performed on the PSD neutron diffractometer [1] ($\lambda_0=1.068 \text{ \AA}$) at the 10MW Budapest research reactor in the momentum transfer range $Q=0.5-10 \text{ \AA}^{-1}$. Data were corrected for detector efficiency, background scattering and absorption effects. The total structure factor, $S(Q)$ was calculated by local software packages. ND measurements indicate that the new compositions are stable glassy samples, no crystalline phase was detected, presented in Figure 1.

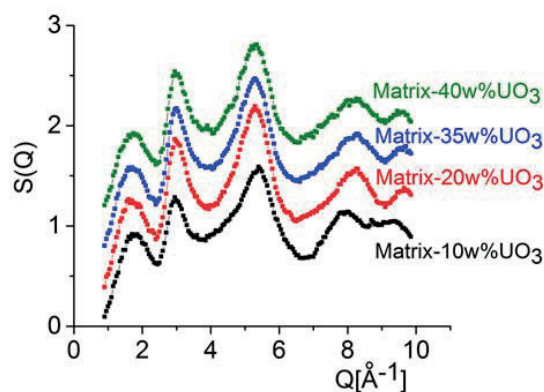


Figure 1. Neutron diffraction total structure factors for Matrix-U10(20,35,40w%).

It was established that the basic network structure of the matrix glasses and matrix glasses doped with uranium are similar. Preliminary results suggests that uranium doesn't change the basic network structure of the matrix glasses. For the doped glasses we have a stable basic network structure and uranium accommodates in both silicate and borate site. This may be the reason of the observed good glassy stability and incorporation ability of the ions.

For the high-concentration uranium samples we have established that the studied Matrix can incorporate maximum 40 w% UO_3 . Samples containing 45 w% UO_3 became crystalline.

The evaluation of the chemical-physical glass properties and the leachability tests are in progress.

References

[1] E. Svab, Gy. Meszaros, F. Deak *Mater. Sci. Forum* 228 (1996) 247; <http://www.bnc.hu/>

<h1 style="margin: 0;">BNC</h1> <p style="margin: 0;">Experimental Report</p>	<i>Experiment title</i> Neutron diffraction study of the proton conducting BCY15	<i>Instrument.</i> PSD_11 <i>Local contact</i> E. Sváb
	<i>Principal proposer:</i> Krezhov Kiril <i>Experimental team:</i> M. Fábrián, E. Sváb, K. Krezhov	<i>Experiment Number</i> BRR_450 <i>Date:</i> November 2015

Objectives

Solid oxide fuel cells (SOFCs) offer a promising green technology of direct conversion of chemical energy of fuel into electricity. The advancement of highly efficient ion conducting materials is essential to the development of SOFC and other electrochemical devices. The quest is on solid oxide materials with high ionic conductivity while preserving structural stability at high temperatures. The oxygen-deficient ceramics of oxides with perovskite structure $A^{2+}B^{4+}O_{3-\delta}$, ($A^{2+} = \text{Ba, Sr, etc.}; B^{4+} = \text{Zr, Ce, Ti, Nb, etc.}$) are recognized among the most efficient materials that can be used as electrolytes or electrodes (metal-ceramic electrode structures) in SOFCs. We propose a powder neutron diffraction study of $\text{BaCe}_{0.85}\text{Y}_{0.15}\text{O}_{3-\delta}$ (BCY15), which we used recently in a new design of SOFC.

Results

Neutron diffraction data were collected in the diffractometer PSD [1] of the Budapest Neutron Centre ($\lambda = 1.069 \text{ \AA}$, $3.60\text{-}114.0^\circ$ in scattering angle 2θ , angular step size 0.1°). The measurement was performed at 295 K on a powdered sample loaded in a thin-walled vanadium container. The diffraction data were analysed using the FULLPROF suite by applying profile matching mode followed by full profile Rietveld refinement of the structural model. The tabulated coherent scattering lengths b_{coh} for Ba, Ce, Y and O were used: 5.07, 4.84, 7.75 and 5.803 fm, respectively. A pseudo-Voigt function was used for the simulation of the Bragg peaks profile and a fifth-degree polynomial function was applied for the fitting of the background.

Careful inspection of the NPD patterns shown in Fig. 1 did not reveal any indications of difference in crystallographic symmetry of the particular samples. The patterns could be indexed in rhombohedral space group R-3c and monoclinic symmetry space group I2/m. We have also checked for a mixture of two perovskite phases of R-3c and I2/m symmetry as recommended for this composition. However, in all the cases the structure refinements did not produce better agreement factors than in Pnma.

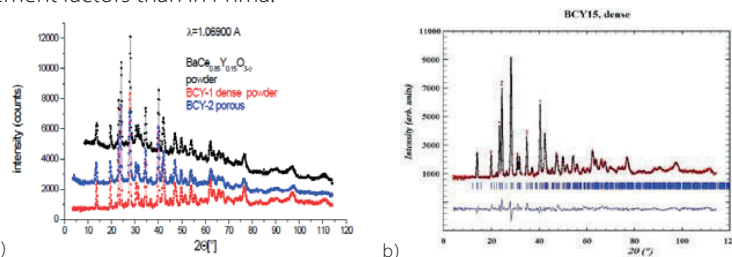


Figure 1. (a) NPD patterns of $\text{BaCe}_{0.85}\text{Y}_{0.15}\text{O}_{3-\delta}$ based samples at 295 K. The upper curve is from the sample denoted as powder and kept for three days in moist air.; (b) Observed (crosses), calculated (continuous line), and difference (bottom) Rietveld NPD profiles of powdered dense BCY15 based material at 295 K. The row of tick marks gives the positions of Bragg reflections.

The multi-pattern mode of the FullProf program was used to refine the structure and to determine the lattice parameters, atomic positions and thermal factors. We considered the undoped BaCeO_3 crystal structure as the starting structural model, with orthorhombic symmetry and space group Pnma; all the Bragg peaks of the diagram could be thus indexed. Yttrium atoms were introduced at random at 4b positions together with Ce, and the complementary occupancy factors were refined, constrained to a full occupancy. In the final refinement, the Ce/Y occupancy factors were unconstrained, indicating a slight deviation from the nominal 0.85:0.15 stoichiometry. Fig. 1b) shows on the example of a powdered “dense” material the agreement between the observed and calculated NPD curves in the final multi-pattern Rietveld fit. The results on powder, dense and porous samples of BCY15 used recently in a new monolithic design of SOFC indicate that with the protonation the interatomic M-M (where $M = \text{Ba, Ce, Y}$) distances vary only slightly but the Debye-Waller factors become strongly affected.

References: [1] E. Svab, Gy. Meszaros, F. Deak *Mater. Sci. Forum* 228 (1996) 247; <http://www.bnc.hu/>

<h1 style="margin: 0;">B N C</h1> <p style="margin: 0;">Experimental Report</p>	<i>Experiment title</i> NAA and PGAA study of synthetic and natural iron bacteria products	<i>Proposal No. BRR_398</i> <i>Instrument: INAA and Gamma-spectrometry, PGAA</i> <i>Local contact: Ibolya Sziklai-László</i>
	<i>Principal proposer:</i> Kiril Krezhov, Institute for Nuclear Research and Nuclear Energy, Bulgarian Academy of Sciences, Sofia, Bulgaria, <i>Ibolya Sziklai-László, HAS Centre for Energy Research,</i> <i>Experimental team:</i> Ibolya Sziklai-László, HAS CER, Dénes Párkányi, HAS CER, Ralica Angelova, Faculty of Biology, University of Sofia, Zsolt Révay, FRM-II, Munich	<i>Date of experiment:</i> 2014.10. 01. <i>Date of report:</i> 2016.02.27.

Objectives

The Fe(II)-oxidizing bacteria (FeOB) and Fe(III)-reducing bacteria (FeRB) were among the first groups of microorganisms to be recognized for carrying out a fundamental geological process - the bacterial iron redox cycling. The aim of our study was to determine the concentrations of elements in these products and the relative amounts of biogenic iron oxides/(oxy) hydroxides resulting from the bacterial metabolism.

Results

The samples studied were prepared in the laboratory of University of Sofia, Faculty of Biology. The natural biomass (reference sample) was isolated from freshwater wetland surface sediments in Vitosha Mountain. Biogenic nanostructured materials were obtained after growing the genus *Leptothrix* in the silicon-iron-glucose-peptone (SIGP) and Adler's nutrient medium (AD). Two types of bacterial cultivation – static and dynamic were carried out. Neutron activation analysis (NAA) and prompt gamma activation analysis (PGAA) were applied for the determinations of the concentrations of major and trace elements. Irradiations of the samples were carried out at the BRR and FRM-II (Munich). The concentrations of the elements in bacteria samples cultivated in different nutrient media were compared to those found in reference sample. Table 1 presents some selected NAA/PGAA data.

Sample/ Element	Fe g/kg	Mn g/kg	Cr mg/kg	Co mg/kg	As mg/kg	Ca g/kg	K mg/kg	Na mg/kg	Si w,%	P w,%	S w,%
Reference (Vitosha)	93 ±4	1.28 ±0.1	18.0 ±1.2	7.6 ±0.4	18.3 ±0.9	9.4 ±2.3	3080 ±204	4633 ±27	n.a.	n.a.	n.a.
SIGP	453 ±16	4.61 ±0.2	160 ±30	54.8 ±4.3	0.67 ±0.1	1.12 ±0.1	334 ±28	213 ±11	0.13 ±0.1	1.2 ±0.2	0.13 ±0.01
AM	415 ±16	2.53± 0.1	170 ±14	21.8 ±2.9	-	1.10 ±0.1	500 ±30	420 ±27	0.22 ±0.03	0.88 ±0.07	0.08 ±0.01

Table 1 NAA/PGAA results for the SIGP and AM samples as compared to the reference

The amounts of Fe, Mn, Cr and Co in the artificial culture medium increased markedly in comparison with the reference (product of nature). The strong increase in the iron content in the biogenic material resulting from bacterial growth is manifested clearly; it depends on the culture medium and is superior in the SIGP medium where the enrichment reached a factor close to 5. Three iron oxide phases were found after cultivation in Adler's medium: lepidocrocite (γ -FeOOH), non-stoichiometric magnetite ($\text{Fe}_3\text{-xO}_4$) and goethite (α -FeOOH). The cultivation in the SIGP medium yielded a single phase bacterial product-lepidocrocite of poor crystallinity.

References

R. Angelova, V. Groudeva, L. Slavov, M. Iliev, I. Nedkov, I. Sziklai-László and K. Krezhov (2015) Investigation of iron-containing products from natural and laboratory cultivated *Sphaerotilus-Leptothrix* bacteria. *J. Biol. Phys.*, (2015), **41**, issue 4, pp. 367-375.
 K. Krezhov, R. Angelova and I. Sziklai-László (2015) Study of products from neutrophilic iron bacteria by Prompt Gamma/Neutron Activation Analysis and X-Ray Diffraction. Extended Abstract 8th Congress of the Balkan Geophysical Society, 5-8 October 2015, Chania, Greece. DOI:10.3997/2214-4609.201414140.

<h1 style="margin: 0;">BNC</h1> <p style="margin: 0;">Experimental Report</p>	<i>Experiment title</i> Upgrade of the Budapest Neutron Activation Analysis laboratory	<i>Instrument.</i> NAA <i>Local contact</i> László Szentmiklósi
	<i>Principal proposer:</i> L. Szentmiklósi – MTA EK <i>Experimental team:</i> D. Párkányi, I. Sziklai-László, J. Janik, Cs. Katona – MTA EK	<i>Experiment Number</i> <i>Date</i> 2014-2016

Objectives:

upgrade of the NAA laboratory in order to benefit from the synergetic use of PGAA and NAA

Results

An infrastructure upgrade initiative of the Academy grant made it possible to modernize the equipment of the NAA laboratory. The fast pneumatic rabbit system was refurbished and the Sender/Receiver Station (#1 in Fig. 1) was redesigned to improve the reliability of the facility. The control software written in LabView was also extended and several bugs were fixed.

By setting up a new counting station (see Fig.2), now three high-purity Ge detectors (two *p*-type and one *n*-type), each with a 30-l liquid nitrogen Dewar are at our disposal. The 55 and 36 % detectors are connected to a dual-input ORTEC DSPEC 502 spectrometer, whereas the 13 % HPGe is coupled to an ORTEC DSPEC Plus unit. All spectrometers are operated by the ORTEC Maestro 7 software. The spectra, taken with 2×16 k channel instead of the 2×8 k, are recorded with the zero-dead time (ZDT) option enabled. The energy resolution and the count-rate tolerance were much improved over the old analog signal processing chain. New dosimeters and microbalance were also purchased. Hyperlab 2013 and Kayzero for Windows software became part of the renewed analysis protocol. This was validated with standard reference materials and round robin exercises.

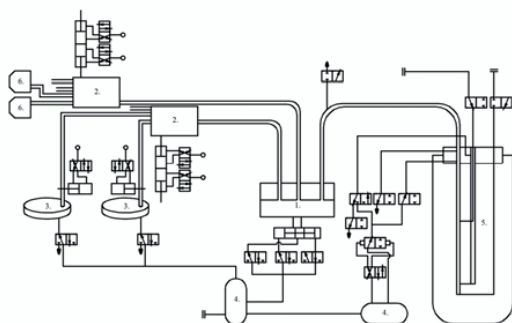


Fig. 1. the block scheme of the fast rabbit system with the redesigned sender-receiver station

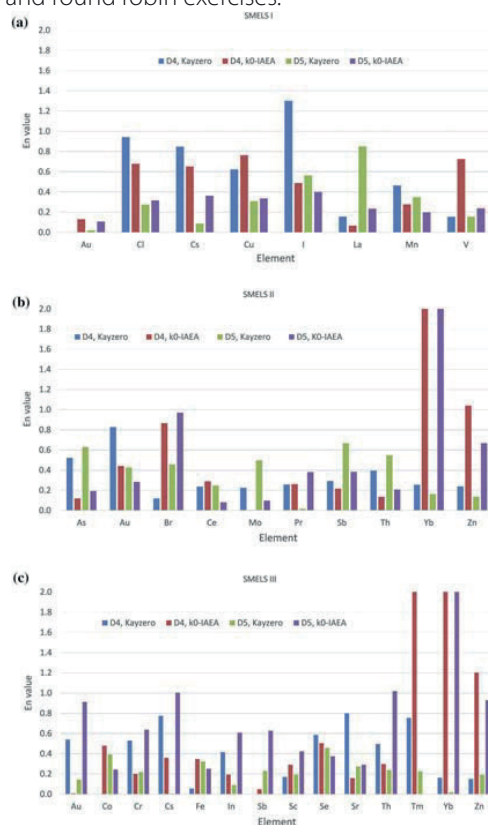


Fig. 2. the new counting station D3 with the ORTEC DSPEC 502 digital gamma spectrometer

Fig. 3 (right) the validation of the new analysis protocol on SMELS I-III standards (a-c) and the comparison of two analysis software (k0-IAEA and Kayzero for Windows 3). E_n values lower than one indicate adequate analytical performance

Reference

L. Szentmiklósi, D. Párkányi, I. Sziklai-László, Upgrade of the Budapest Neutron Activation Analysis laboratory, J. Radioanal. Nucl. Chem. (2016) **309** 91–99 DOI: 10.1007/s10967-016-4776-7



B N C Experimental Report	<i>Experiment title</i> Production of Mo-99 from natMo at Research Reactors: IAEA Inter-laboratory Comparison (Round Robin) 2014-2015	<i>Instrument.</i> NAA <i>Local contact</i> Dénes Párkányi
	<i>Principal proposer:</i> Menno Blaauw –TU Delft <i>Experimental team:</i> D.Párkányi, L. Szentmiklósi- MTA EK	<i>Experiment Number</i> <i>Date</i> 2015

Objectives

The purpose of the intercomparison described in this report is to improve sustainable utilization of research reactors by investigating their application for Mo-99 production for local needs. Mo-99 production issues were discussed in detail during a recent regional project coordination meeting of RER1007 "Enhancing Use and Safety of Research Reactors through Networking, Coalitions and Shared Best Practices" (Europe). It was concluded that regional/international activity should start in this context to evaluate local production capabilities at different RR facilities. This intercomparison study will provide estimates for the local production capacity of Mo-99, based on experimental results and supported by model predictions. The IAEA sent 3 molybdenum samples to each participant in the exercise: approx. 1 g of Mo₂O₃ in a polyethylene capsule (9 mm internal diameter x 9 mm height), and two rectangular pieces of Mo metal of 10 x 10 x 1 mm and 50 x 10 x 1 mm, weighing about 1 g and 5 g, respectively.

Results

Sample	Sample code	Activation rates (s ⁻¹)	Unc %
"5g Mo metal"	Mo 1.	3.58×10 ⁻¹¹	7.1
"1g Mo metal"	Mo 2.	3.57×10 ⁻¹¹	7.1
"1g MoO ₃ "	Mo 3.	4.00×10 ⁻¹¹	7.3

Table 1: Measured activation rate at Budapest Research Reactor

The specific saturation activity for the ⁹⁸Mo(n,γ)⁹⁹Mo reaction in natural molybdenum can be estimated with good accuracy, i.e. better than 10 %, if the epithermal activation contribution is taken into account and the epithermal neutron self-shielding is corrected for.

In-core irradiation facilities where the epithermal neutrons are strongly present are to be favoured over more thermalized facilities when the goal is to produce as much Mo-99 as possible. Metallic molybdenum exhibits more neutron self-shielding than molybdenum oxide, leading to a higher specific saturation activity in the molybdenum itself. On the other hand, due to the lower density, less material can be introduced in the irradiation facility. Finally, post-irradiation processing capabilities will determine which material is to be favored in practice.

References

M. Blaauw, D. Ridikas, S. Baytelesov, P. S. Bedregal Salas, Y. Chakrova, Cho Eun-Ha, R. Dahalan, X.O. Errazu, A.H. Fortunato, R. Jacimovic, A.Kling, Y. Mahlers, N.M.A. Mohamed, T. Singh, D. Parkanyi, Van Dong Duong, Estimation of ⁹⁹Mo production rates from natural molybdenum in research reactors, J. Radioanal. Nucl. Chem, submitted

<h1 style="margin: 0;">BNC</h1> <p style="margin: 0;">Experimental Report</p>	<i>Experiment title</i> NAA Proficiency Tests and workshop Performed in 2015	<i>Instrument.</i> NAA <i>Local contact</i> Dénes Párkányi
	<i>Principal proposer:</i> Danas Ridikas – IAEA Division of Physical & Chemical Sciences <i>Experimental team:</i> Dénes Párkányi, Ibolya Sziklai-László – MTA EK	<i>Experiment Number</i> <i>Date</i> 2015

Objectives

Enhancement of low and medium power research reactor utilization is often pursued by increasing the neutron activation analysis activities, and this analytical technique in principle is available in more than half of the 246 operational RRs world-wide. Whereas the markets for NAA laboratories may have been identified, an underestimated problem remains the quality assurance and quality control (QA & QC), which tremendously limits the commercial routine application of this powerful technique. In this context, a project to evaluate the level of performance of a great number of NAA laboratories has been conducted by the IAEA since 2010. An accredited company specializing in the organization of proficiency tests, Wageningen Evaluating Programs for Analytical Laboratories (WEPAL) of Wageningen University, Netherlands, prepared and distributed samples and received test results, while an independent expert was contracted to evaluate laboratory performance. The inter-laboratory comparison rounds were related to the determination of (trace) elements in soil (ISE) and plant (IPE) samples. With the Normal Distribution Approximation (NDA) model mean and standard deviation are calculated. The results provided by the individual laboratories have been evaluated on basis of z-scores (interlaboratory difference, corrected for the spread in the results) and on the bias, relative to the mean value of the measurand and reported by the WEPAL. Satisfactory performance is attained for $|z|$ -scores ≤ 3 and bias values $\leq 20\%$.

Results

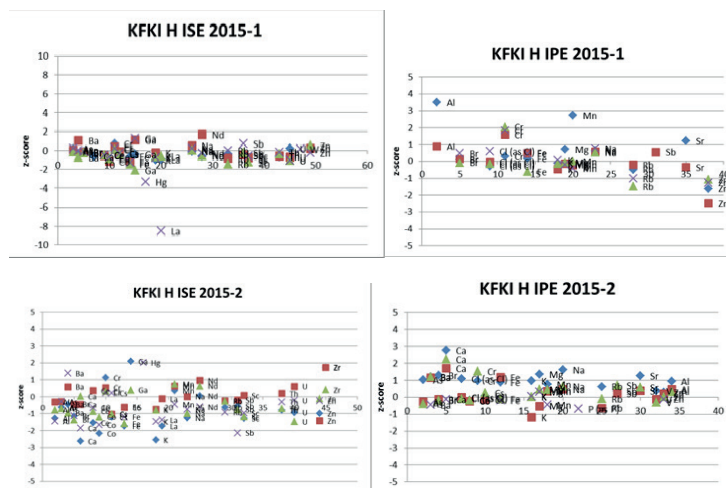


Figure 1: z-scores of the SOIL (ISE) and plant (IPE) samples in 2015

Figure 1 shows our NAA results based on the k_0 -standardization method. They agreed very well with the reported values only a few outliers were found.

References

Workshop on Inter-comparison feedback of Proficiency Tests performed in 2015 for NAA and other Analytical Techniques, Report of a Workshop under regional TC projects RAF4022, RAS1018, RER1007 and RLA0037, Working document

<h1 style="margin: 0;">BNC</h1> <p style="margin: 0;">Experimental Report</p>	<i>Experiment title</i> DÖME – a low-background counting chamber and developing a radon-tight sample holder	<i>Instrument</i> DÖME <i>Local contact</i> Kis Zoltán
	<i>Principal proposer:</i> Zoltán Kis – Centre for Energy Research <i>Experimental team:</i> Zoltán Kis – Centre for Energy Research	<i>Experiment Number</i> <i>Date</i> 2011.05.03-2011.10.27 2013.02.13-2013.03.01 2014.06.11-2014.06.13 2015.02.23-2015.03.25

Objectives: to revitalize a low-background counting chamber (DÖME) and to develop a radon-tight sample holder for gamma-ray spectroscopy measurements

Results

There was an emerging need at the Nuclear Analysis and Radiography Department to be able to perform low level radioactivity measurements of various samples from in-beam activation and from environmental studies. Low-level radioactivity measurements began in 2011. Important aspects of reusing the low-background chamber called DÖME, which had been unused for some years, were the development of an easily reusable radon-tight sample container and the setup of a measurement system capable of counting extended samples in close-in geometry.

There is usually a need to measure different nuclides in the natural radioactive decay chains, which quickly poses the problem of having a radon-leakage-free container. As a result of our efforts a special sample container made of HDPE (High-density Polyethylene) was developed. Several saturation curves for the activity concentration in a sealed container were measured, and the radon-escape was tested by comparing the measured decay constant of the daughters to the literature value of the ²²²Rn decay constant. It was proved that the probability of a radon loss larger than the 2% of its radioactive decay constant is less than 95%.

Preliminary measurements showed that the radioactivity level of the samples is usually rather low, and therefore close sample–detector geometry is advantageous to maximize the counting rates. Due to the lack of reference samples, containing the same radionuclides as the unknown sample, the absolute method of measuring the activity concentration of nuclides in the sample had to be applied, which implied the reliable determination of the full-energy peak efficiency. The absolute FEP efficiency values had to be determined at various energies for extended sources in close sample–detector geometry. A method called efficiency transfer combined with the correction for true coincidence summing effects is proven to be providing appropriate results and applied.



Fig. 1. (a) Photo of the low-background counting chamber (DÖME); (b) a special sample container made of HDPE; (c) saturation curves for the activity concentration in a sealed container.

References

Kis, Z., Völgyesi, P., Szabó Zs. DÖME: revitalizing a low-background counting chamber and developing a radon-tight sample holder for gamma-ray spectroscopy measurements, *J Radioanal Nucl Chem.* 298 (2013) 2029–2035.

<h1 style="margin: 0;">BNC</h1> <p style="margin: 0;">Experimental Report</p>	<p><i>Experiment title</i></p> <p>Study of secular equilibrium state between ^{226}Ra and ^{238}U in Hungarian coal slag samples</p>	<p><i>Instrument</i></p> <p>DÖME</p> <p><i>Local contact</i></p> <p>Kis Zoltán</p>
	<p><i>Principal proposer:</i></p> <p>Völgyesi Péter – Eötvös Loránd University</p> <p><i>Experimental team:</i></p> <p>Zoltán Kis – Centre for Energy Research</p>	<p><i>Experiment Number</i></p>

Objectives

to study the secular equilibrium state between ^{226}Ra and ^{238}U in Hungarian coal slag samples

Results

The ^{226}Ra is a prominent radionuclide in the ^{238}U decay chain, therefore the precise gamma spectroscopic determination is indispensable for radiological qualifications. Several scientific papers report that the equilibrium state between the ^{238}U and ^{226}Ra isotopes cannot be found in coal slags. It is important to note that certain Hungarian coals, from which the coal slag was formed, have elevated uranium and radium content.

Our main aim was to examine the equilibrium state in 12 coal slag samples from Budapest and Ajka city using the gamma peaks of different isotopes in the ^{238}U decay chain. The suitable experimental setup was established and the measurements were done by HPGe detector in a low background chamber. As a noble gas the ^{222}Rn isotope easily can escape from the closed sample container, therefore the progenies cannot be in equilibrium. The usage of a reliable experimental setup (i.e. escape-proof sample container, low background) can solve the aforementioned problems. A special sample container made of HDPE (High-density Polyethylene) was developed. The low background was ensured by a measurement chamber made of iron which was made before the atmospheric nuclear explosions. The evaluation of the ^{238}U and ^{226}Ra activity concentration values was done by using some peaks at characteristic energies. The measurement conditions allowed using some peaks which could not be used before. The ^{226}Ra activity concentration was measured based on the radon decay products and also the ^{226}Ra peak at 186 keV. Secular equilibrium existed in eight samples, whereas one sample showed a slight disequilibrium. The direct and fast measurement using only the 186 keV peak was validated which can be used after measuring the uranium isotopic ratio and verifying the ^{238}U - ^{226}Ra secular equilibrium. This method can be used to measure the ^{226}Ra content of high number of samples from the same geochemical background. Our results show that the activity-concentration values valid for ^{238}U and ^{226}Ra match within uncertainties.

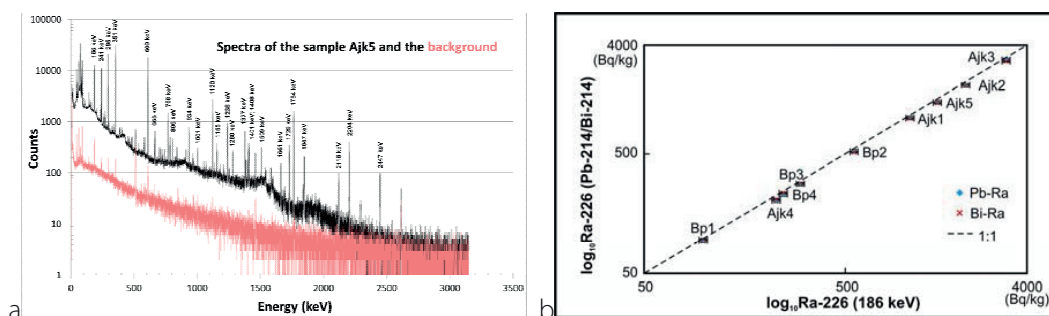


Fig. 1. (a) Spectrum of the sample Ajk5 together with the background spectrum. The 25 peaks used for the calculations are labeled according to their energy; (b) ^{226}Ra activity concentration measured by its own peak at 186 keV vs. ^{226}Ra activity concentration measured by the peaks of radon daughters. Dashed line is 1:1 line.

References

Völgyesi, P., Kis, Z., Szabó, Zs., Szabó, Cs. Using the 186-keV peak for ^{226}Ra activity concentration determination in Hungarian coal-slag samples by gamma-ray spectroscopy, *J Radioanal Nucl Chem.* 302 (2014) 375–383.

<h1 style="margin: 0;">BNC</h1> <p style="margin: 0;">Experimental Report</p>	<i>Experiment title</i> First survey of radioactivity levels in Angolan adobe determined by gamma spectrometry	<i>Instrument</i> DÖME <i>Local contact</i> Kis Zoltán
	<i>Principal proposer:</i> Judith Pena Dembo, Völgyesi Péter – Eötvös Loránd University <i>Experimental team:</i> Zoltán Kis – Centre for Energy Research	<i>Experiment Number</i> <i>Date</i> 2014.12.08-2016.02.13

Objectives

to systematically study the radioactivity levels in Angolan adobe samples

Results

Measurement of the environmental radioactivity in Angola is a novelty in spite of noticing a growing interest from all-over the world. This study therefore aimed to investigate systematically the radioactivity of adobe, a widely used building material in Angola. Sixty samples have been collected from three remote areas of the country with different geological background and climate. These were Cabinda in the North, Huambo in the central part and Menongue in the South. Activity concentrations for Ra-226 (assumed in secular equilibrium with U-238) and Th-232 as natural decay chain members and for K-40 have been determined by gamma spectrometry analysis. For this purpose a HPGe-detector-based acquisition system installed permanently in a low background chamber was used.

The activity concentration results obtained for the separate areas are as follows (mean and sample range in Bq kg⁻¹): in *Cabinda* 32 (26-45) for Ra-226, 40 (36-49) for Th-232 and 50 (36-83) for K-40; in *Huambo* 69 (53-78) for Ra-226, 67 (39-84) for Th-232 and 80 (56-96) for K-40; in *Menongue* 25 (15-42) for Ra-226, 27 (21-32) for Th-232 and 52 (25-73) for K-40. According to the UNSCEAR 2000 Report² the average values in soil for radionuclides U-238, Th-232 and K-40 are 35, 30 and 400 Bq kg⁻¹, respectively. A comparison shows that the activity concentration of Ra-226 in Huambo is higher than the average; similarly, the value for Th-232 is also higher in both Huambo and Cabinda; whereas the value for K-40 is lower in all areas. A comparison of the calculated and measured annual effective dose rates of the studied areas shows some underestimation for the calculated values because the gamma ray background in Angola need to be still considered. Based on the calculation of hazard indices (Ra_{eq}, I) the adobe is not a hazardous building material.

The importance of this survey comes from the fact that more than 30% of the Angolan population use adobe as building material. Therefore, results may have a social interest beside its scientific aspects and they will serve as reference for further studies.

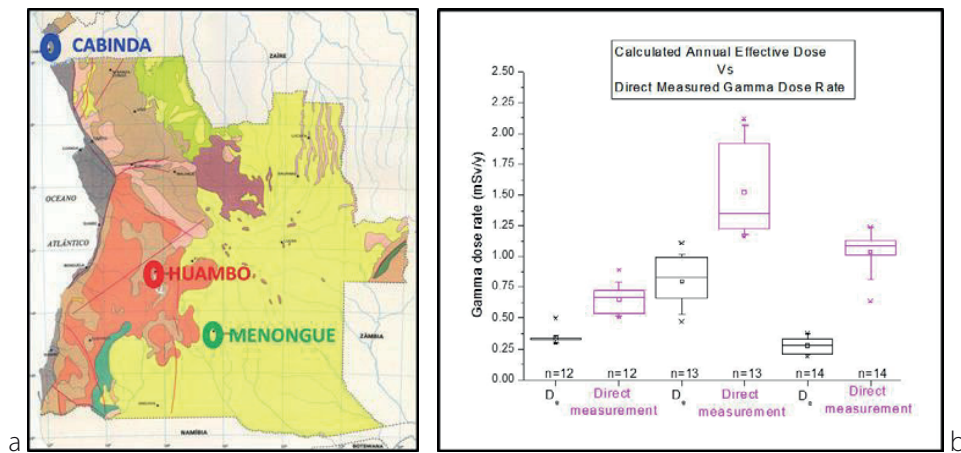


Fig. 1. (a) In this study three areas with different geological background, were chosen: Cabinda in the North, Huambo in the central part and Menongue in the South of Angola; (b) A comparison of the calculated and measured annual effective dose rates of the studied areas shows some underestimation for the calculated values.

<h1 style="margin: 0;">BNC</h1> <p style="margin: 0;">Experimental Report</p>	<i>Experiment title</i> A method for the standardization of PGAI spatial resolution measurements	<i>Instrument</i> NIPS-NORMA <i>Local contact</i> Kis Zoltán
	<i>Principal proposer:</i> Zoltan Kis – Centre for Energy Research <i>Experimental team:</i> Zoltán Kis, Gábor Benyács – Centre for Energy Research	<i>Experiment Number</i> <i>Date</i> 2013.09.04-2013.09.25 2014.11.05-2014.11.10 2015.02.27-2015.03.03

Objectives

to provide a method for the standardization of PGAI spatial resolution measurements

Results

Pilot experiments with home-designed and home-made etalon objects were carried out to provide a method for the standardization of PGAI spatial resolution measurements. The principle of these etalon objects is based on how the modulation transfer function (MTF) is measured in (neutron) imaging. The squeezing bar period of the imaging device has a spatial frequency limit, which could still give enough contrast to be visible by neutron radiography. At this level the value of the MTF function is about 10%. This method provides a fast measuring tool to assess and control the spatial resolution of the imaging system. For PGAI the contrast could be defined as the ratio between the counting rates of a gamma-ray detector.

The etalon objects for the PGAI spatial resolution measurements (see Fig. 1a) were made of high neutron absorption materials as Cd, B or Cu rods ($1 \times 1 \text{ mm}^2$ cross section), where the distances between two adjacent rods were well known (i.e. 4, 3, 2, 1, 0.5 and 0.25 mm). As an example, the neutron radiography of a Cd-rod device is shown in Fig. 1b. The spectra of the neutron radiography-driven PGAI during the vertical movement of the device in steps of 0.05 mm (200-400 spectra, 500-1000 sec/spectrum) were collected, and evaluated for the most characteristic peaks of the element. The neutron collimator was set to be $1 \times 3 \text{ mm}^2$.

The normalized counting rate of the 558 keV peak of the Cd can be seen in Fig. 1c. According to the Rayleigh criterion we measured the ratio between the max. amplitude and the (max.-Cd) amplitude. As long as the difference is greater than 27% the MTF is greater than 10% showing a good spatial resolution. In our case this resulted in a spatial resolution is about 0.25 mm for the specific setup.

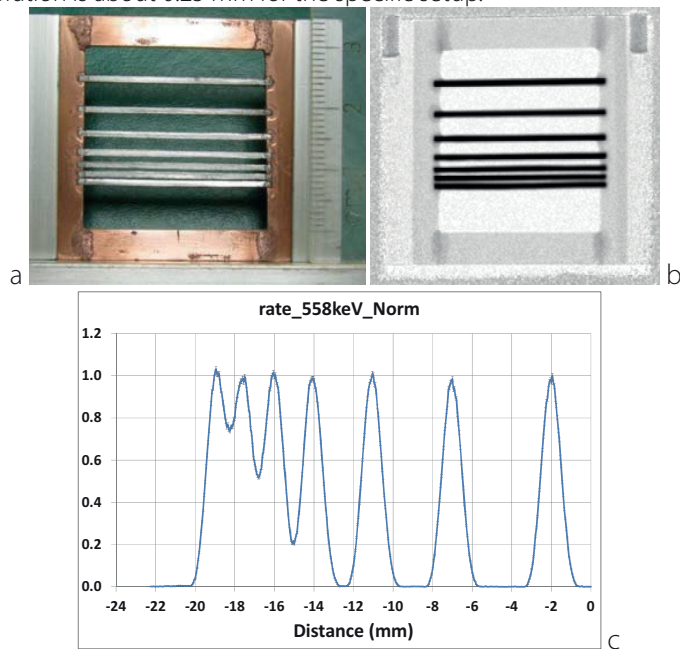


Figure 1: (a) Photo of an MTF object made of Cd. (b) The neutron radiography of an MTF object made of Cd. (c) PGAI results: profile of normalized count rates for the 558 keV peak of Cd.

<h1 style="margin: 0;">BNC</h1> <p style="margin: 0;">Experimental Report</p>	<i>Experiment title</i> Distribution of H/Zr ratio in a damaged Zr fuel rod cladding	<i>Instrument</i> NIPS-NORMA <i>Local contact</i> Kis Zoltán
	<i>Principal proposer:</i> Zoltán Hózer – Centre for Energy Research <i>Experimental team:</i> Zoltán Kis – Centre for Energy Research	<i>Experiment Number</i> <i>Date</i> 2013.03.20-2013.04.08 2015.06.05-2015.06.11

Objectives

to measure the longitudinal distribution of the H/Zr ratio in a damaged Zr fuel rod cladding using neutron imaging and position-sensitive element analysis

Results

Secondary hydriding can take place during a LOCA (loss of coolant accident) event after the ballooning and burst of Zr cladding. The oxidation and hydrogen uptake in the ballooned section can produce the weakest segment of the rod. When ballooning and then cladding breakup occurs at hot spots, the steam could penetrate through the burst opening into the gap between fuel pellets and inner cladding surface. The objective of the present work was the investigation of the effect of secondary hydriding in VVER reactors with E110 and E110G alloys.

In this study we used the position-sensitive NR/NT-driven PGAI method at NIPS-NORMA facility to analyse the longitudinal distribution of an element along an object. The element ratios can be determined with this technique, based on the precise evaluation of a pair of prompt-gamma peaks. In particular, the method was applied to determine the spatial distribution of the H/Zr atomic ratio along the longitudinal axis of a Zr clad fuel rod from Paks Nuclear Power Plant following secondary hydriding.

It was shown that the embrittlement of the Zr-alloy found during the mechanical testing is closely related to the local quantity of the hydrogen absorbed in the metal. The maximum of the axial distribution of the H-content was not in the middle part of the ballooned section but far from it as can be seen in Fig. 1. The imaging technique was indispensable to link the measured concentrations to the visual features of the item. The results of PGAI and hot extraction methods were in good agreement with each other.

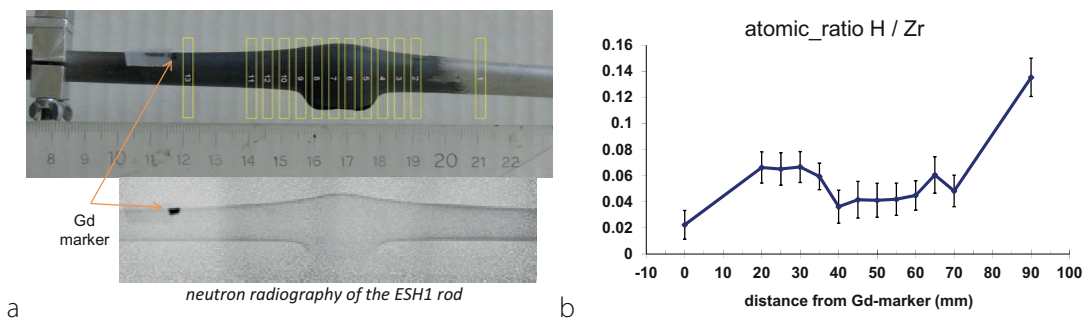


Figure 1: (a) The irradiated parts of the ESH1 rod cladding are shown in the photo. One can see the ballooning on the top edge and the bursting on the bottom edge of the rod cladding, respectively. The neutron radiographic image of the rod cladding is a merge of four overlapping tile-like images. There is no colorscale shown because radiographic images were used only for setting up PGAI. A Gd marker shown on both images was used to help positioning. (b) The spatial distribution of the H/Zr atomic ratio along the longitudinal axis of the cladding rod.

References

- Kis, Z., Szentmiklósi, L., Belgya, T., Balaskó, M., Horváth, L.Z., and Maróti, B., 2015. Neutron Based Imaging and Element-mapping at the Budapest Neutron Centre. *Physics Procedia*, 69, 40–47.
- Kis, Z., 2015. *Report on H/Zr distribution of GSH1M and GSH2M Zr claddings, following secondary hydriding*. Budapest: MTA Energetatudományi Kutatóközpont, Kutatási jelentés No. MTA EK-NAL-2015-441-1-1-M0.
- Novotny, T., Perezné Feró, E., Kis, Z., Szentmiklósi, L., Vimi, A., Nagy, I., Kunstár, M., and Hózer, Z., 2013. *Hidrogéntartalom a szekunder hidridizációs E110 és E110G mintákban*. Budapest: MTA Energetatudományi Kutatóközpont, Kutatási jelentés No. EK-FRL-2013-759-01/05-M1.

<h1 style="margin: 0;">BNC</h1> <p style="margin: 0;">Experimental Report</p>	<i>Experiment title</i> Characterization of radioactive or nuclear material in a sealed container of unknown origin	<i>Instrument</i> NIPS-NORMA <i>Local contact</i> Szentmiklósi László
	<i>Principal proposer:</i> HAEA – Hungarian Atomic Energy Authority <i>Experimental team:</i> Szentmiklósi László, Zoltán Kis – Centre for Energy Research	<i>Experiment Number</i> <i>Date</i> 2013.03.20-2013.04.08 2015.06.05-2015.06.11

Objectives

to develop a methodology for the characterization of radioactive or nuclear material in a sealed container of unknown origin using neutron imaging and position-sensitive element analysis

Results

One of the missions of the Centre for Energy Research is to develop methodology for the characterization of any illicit radioactive or nuclear material seized by the authorities. If a sealed object of unknown origin is confiscated, a preliminary screening is required to decide if a container is safe to open. Lead shield successfully attenuate gamma rays of 100-300 keV from uranium, so passive gamma counting outside of the container for radionuclide identification may be infeasible in such cases. PGAA (Prompt Gamma Activation Analysis) with a standard beam size (~cm), however, provided just the average composition of the irradiated volume. An alternative method is the combination of prompt gamma activation analysis and neutron imaging. The method is presented on a nuclear forensics application, and compared to the results from Monte Carlo calculations.

In Fig. 1a, the positions of the irradiation spots are overlaid on the radiographic image, and labels indicate their correspondences with the prompt gamma-spectra. The positions were defined to maximize the selectivity, and avoid the unwanted irradiation of the neighboring objects. The raw prompt-gamma spectra taken at the marked spots are good enough for a qualitative assessment. This quick screening can be achieved within a couple of hours, as rapid reporting time is an important requirement for a forensic method. Note the evenly rising baseline of the farthest prompt-gamma spectrum, as a first-glance evidence for the presence of fissile materials. For uranium, even the enrichment of the material can also be given from the ratios of peaks at 4060 and 6395 keV gamma energies. During the analysis it was possible to identify the characteristic peaks of the expected element in the spectra, while very little contribution (less than 1%) of other objects was found.

In order to determine the correspondence between the measured peak areas and the amounts of the items, Monte Carlo calculations were completed with MCNP 5/MCNP X codes. The masses of the items in the container, the composition and density of the objects may have to be iteratively adjusted to reproduce the measured count rates of characteristic peaks. As the compositions of the items are determined by PGAA, the densities can be estimated from the observed neutron attenuation coefficients in the tomographic slices. The total masses can be calculated by scaling up to the volume of the item, which can be estimated from the structural data.

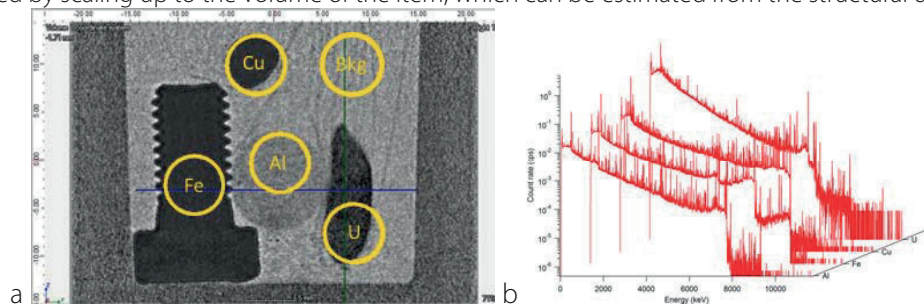


Figure 1: (a) The positions of the collimated beam overlaid on the radiography images and (b) the spectra measured at each spot, after background correction (from front to back: Al, Fe, Cu and U).

References: Szentmiklósi, L. and Kis, Z., 2015. Characterizing nuclear materials hidden in lead containers by neutron-tomography-driven prompt gamma activation imaging (PGAI-NT). *Anal. Methods*, 7 (7), 3157–3163.

<h1 style="margin: 0;">B N C</h1> <p style="margin: 0;">Experimental Report</p>	<i>Experiment title</i> Investigation of a XVIIIth Dynasty Egyptian sealed Pottery by cold Neutron Tomography	<i>Instrument.</i> NIPS-NORMA <i>Local contact</i> Zsolt Kasztovszky
	<i>Principal proposer:</i> Emmanuel Abraham - LOMA, CNRS UMR 5798, University of Bordeaux, France; Marie-Christine Hervé - Museum of Aquitaine, Bordeaux, France <i>Experimental team:</i> Zs. Kasztovszky, L. Szentmiklósi, Z. Kis – MTA EK	<i>Experiment Number</i> BRR_316_CH <i>Date</i> 08-10 April 2013

Objectives

The project was aimed to probe a sealed Egyptian pottery (15th c. B.C., Museum of Aquitaine, Bordeaux) at the Budapest Neutron Centre using the Neutron Induced Prompt Gamma Spectrometer (NIPS), equipped with "NORMA" neutron radiography and tomography system. Previous investigations (X-ray and Terahertz radiation) revealed the presence of an unidentified content inside the object. The main objectives of the present project are: (a) analysis of the jar itself using neutron tomography (presence of cracks, composition of the seal) and (b) analysis of the content using neutron tomography and Neutron Induced Prompt gamma Spectroscopy (NIPS).

Results

The main result was the precise identification of the cork stopper hidden by a clay cork. 3D neutron imaging clearly revealed that this stopper was made of a ball of linen or any other string-like organic material. This observation was not possible with both X-rays and THz radiation owing to insufficient spatial resolution and contrast. Neutron imaging also confirmed the presence of cracks in the wall of the pottery bottle, as already discovered with X-rays. 3D neutron imaging also provides some representations of the mobile content which is constituted of inhomogeneous dried materials. By semi-quantitative analysis of the (n,γ) spectra taken at NIPS, we concluded that the jar content is mainly composed of H, C, N, S and Cl elements, which supports the assumption about its organic nature. Without certitude, we can assume that this content could consist of germinated seeds of any other dried organic material.

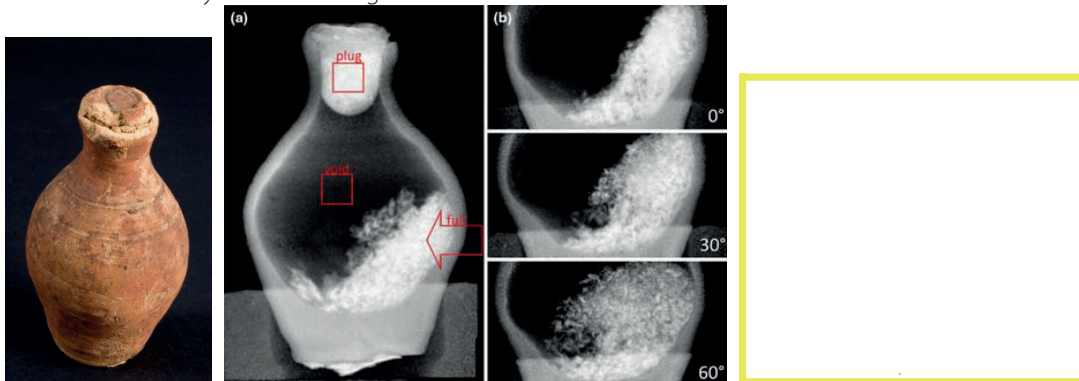


Fig. 1: Photograph of the Egyptian pottery (Museum of Aquitaine, inv. nr 8608)

Fig. 2: Neutron Radiography at NIPS-NORMA station. **(a)** Global front view obtained from a set of nine partial front views. Red markers indicate the illumination areas PGAI, **(b)** Front views in the region of the mobile content for three positions of the pottery: rotation by 0°, 30° and 60° around the vertical axis.

Fig 3: Neutron tomography at the NIPS-NORMA station. 3D representation of the cork obtained with a volume rendering software.

Reference

E. Abraham, M. Bessou, A. Ziégli, M.-C. Hervé, L. Szentmiklósi, Zs. Kasztovszky, Z. Kis, M. Menu, Terahertz, X-ray and neutron computed tomography of an Eighteenth Dynasty Egyptian sealed pottery, *Appl. Phys. A* (2014) 963-972.

<h1 style="margin: 0;">BNC</h1> <p style="margin: 0;">Experimental Report</p>	<i>Experiment title</i> Neutron tomography driven PGAI of a bronze object	<i>Instrument</i> NIPS-NORMA <i>Local contact</i> Kis Zoltán
	<i>Principal proposer:</i> Ibolya Gerelyes – Hungarian National Museum <i>Experimental team:</i> Zoltán Kis, Boglárka Maróti – Centre for Energy Research	<i>Experiment Number</i> <i>Date</i> 2013.11.17-2013.11.21

Objectives

to characterize the inner structure and elemental composition of Ottoman balance weights using non-destructive neutron imaging and element analysis

Results

The available literature does not provide enough information about the inner structure and elemental composition of Ottoman balance weights. This knowledge could be useful to distinguish them from the Roman weights. It is particularly uncertain how to classify the pear-shaped weights.

For a more comprehensive understanding, a pilot study using X-rays and cold neutrons was initiated at the BNC. The Turkish Collection of the Hungarian National Museum owns a proven Turkish origin balance weight from Ócsa (see Fig. 1a). The object is pear-shaped, with a lead filling inside the bronze mantle. Based on the archaeological context it is dated to the 16th century.

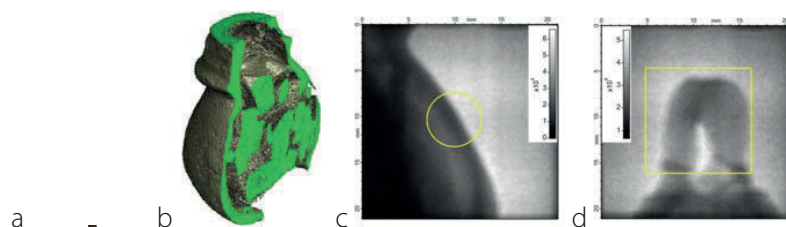


Fig. 1. Photography (a) and 3D tomography (b) image of a Turkish-Ottoman balance weight (catalog number: 92.57.2.B). Radiography images (c and d) show the exact positions of the PGAI measurements.

Non-destructive XRF measurements were carried out on several surface spots of the object with handheld equipment. The XRF results were, however, not consistent for the bronze alloy composition, presumably as a consequence of the previous restoration work and surface treatment processes. Therefore, a non-destructive bulk analytical method, the NR/NT driven PGAI technique was chosen for further position-sensitive analysis of the alloy composition.

To obtain detailed structural information neutron tomography was performed. After the 3D reconstruction several various sized chunks probably of bronze were discovered, which had been placed inside the filling material (Fig. 1.b). Based on the grayscale values the attenuation coefficient for these chunks and the mantle are similar. Their presumable role was to set the accurate weight.

PGAI measurements were carried out by irradiating the mantle and the top of the weight (Fig. 1c-d) to mitigate the effect of both neutron self-absorption and gamma-ray self-attenuation. Such kinds of attenuation corrections were beyond the scope of the present pilot study because of their extreme complexity. For elemental ratio comparisons only the peak areas from higher energy gammas were used to further mitigate attenuation effects.

The results show that the Sn/Cu ratios for the mantle ($\text{Sn}(1171 \text{ keV})/\text{Cu}(7636 \text{ keV}) = 0.042 \pm 18\%$) and the top ($\text{Sn}(1171 \text{ keV})/\text{Cu}(7636 \text{ keV}) = 0.049 \pm 9.3\%$) agree within the statistical uncertainty. This means that these two parts of the object were probably made from the same material. If, however, we consider the Fe/Cu ratio it turns out that the ratios for the mantle ($\text{Fe}(7645 \text{ keV})/\text{Cu}(7636 \text{ keV}) = 0.18 \pm 3.7\%$) and for the top ($\text{Fe}(7645 \text{ keV})/\text{Cu}(7636 \text{ keV}) = 0.008 \pm 16\%$) do not agree within the statistical uncertainty. The reason for this could be some elevated iron content of the filling material, which was irradiated together with mantle. These preliminary results are promising enough to encourage a wider study among the available Turkish and Roman weights.

References: Kis, Z., Szentmiklósi, L., Belgya, T., Balaskó, M., Horváth, L.Z., and Maróti, B., 2015. Neutron Based Imaging and Element-mapping at the Budapest Neutron Centre. *Physics Procedia*, 69, 40–47.

<h1 style="margin: 0;">B N C</h1> <p style="margin: 0;">Experimental Report</p>	<i>Experiment title</i> Prompt Gamma Activation Analysis of the Nyírlugos obsidian core depot find	<i>Instrument.</i> NIPS-NORMA <i>Local contact</i> Zsolt Kasztovszky
	<i>Principal proposer:</i> Katalin T. Biró – Hungarian National Museum <i>Experimental team:</i> Zs. Kasztovszky, Z. Kis – MTA EK	<i>Experiment Number</i> <i>Date</i> 12-14 March 2013

Objectives

The Nyírlugos obsidian core depot find is one of the most important lithic assemblages in the collection of the Hungarian National Museum (HNM). The original set comprised 12 giant obsidian cores, of which 11 are currently on the permanent archaeological exhibition of the HNM. The size and beauty of the exceptional pieces exclude any invasive analysis. Using Prompt Gamma Activation Analysis (PGAA), we can measure major chemical components and some key trace elements of stone artefacts with adequate accuracy to successfully determine provenance of obsidian.

Results

Based on non-invasive PGAA, the Nyírlugos hoard could be identified clearly as belonging to Carpathian 1 (Slovakian) sources, most probably from the Viničky sub-group (C1b). The study of the hoard as a batch is an important contribution to the assessment of prehistoric trade and allows us to know more about the Carpathian sources, especially the Carpathian 1 (Slovakian) source region. It also allows us to suppose underground mining activity in the territory of the Carpathian source area connected with large-scale exploitation of obsidian, probably in the Middle Neolithic (= LBC and derivatives) period.



Fig. 1. An obsidian core in the sample holder of the Budapest NIPS-NORMA station

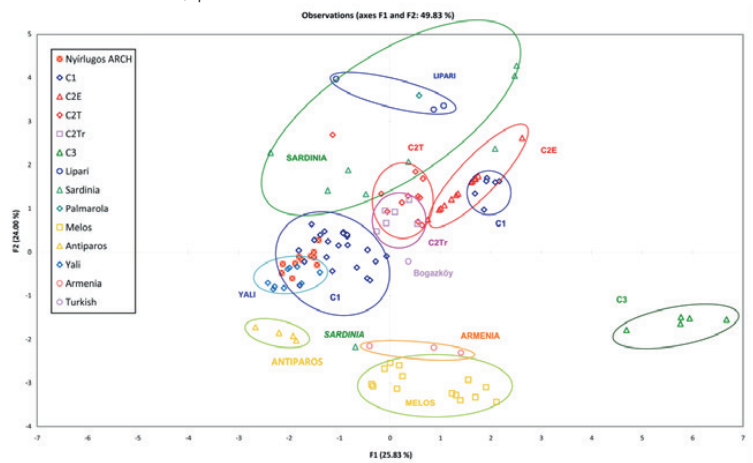


Fig. 2: Separation of obsidian source regions on the basis of Factors 1 and 2 of Principal Component Analysis of geochemical data, plotting the Nyírlugos hoard on the graph.

Reference

Kasztovszky, Zs., Biró, K. T., Kis, Z.: Prompt Gamma Activation Analysis of the Nyírlugos obsidian core depot find, *Journal of Lithic Studies* (2014) vol.1, nr. 1, p. 151-163.

B N C Experimental Report	<i>Experiment title</i> Material analysis of a metal statuette representing Egyptian goddess	<i>Instrument.</i> NIPS-NORMA <i>Local contact</i> Zoltán Kis
	<i>Principal proposer:</i> Éva Liptay – Museum of Fine Arts <i>Experimental team:</i> Zoltán Kis, Boglárka Maróti, László Szentmiklósi – Centre for Energy Research, HAS	<i>Experiment Number</i> BRR-370 <i>Date</i> 2013.09.25-26 2014.01.26-28

Objectives: to characterize the elemental composition of the different structural parts of the sculpture group in order to specify how the structural pieces were attached to each other. Confirm or disprove the meteoritic origin of the iron containing material filled in the palm stubs.

Results

Complementary neutron-based element analysis and imaging methods, i.e. prompt-gamma activation imaging and neutron tomography (PGAI-NT), were applied on a bronze statuette of assumed Egyptian origin. Based on the visual information obtained from the neutron radiography and tomography, different parts of the sculpture group were pin-pointed for localized elemental analysis (e.g. monkey head and the goddess leg for the characterization of the alloy composition; the lower parts of the palm stubs and the presumably iron containing upper parts were also analysed. In the latter case our aim was - besides the elemental composition - to confirm or disprove the meteoritic origin of its raw material. See Fig. 1a.)

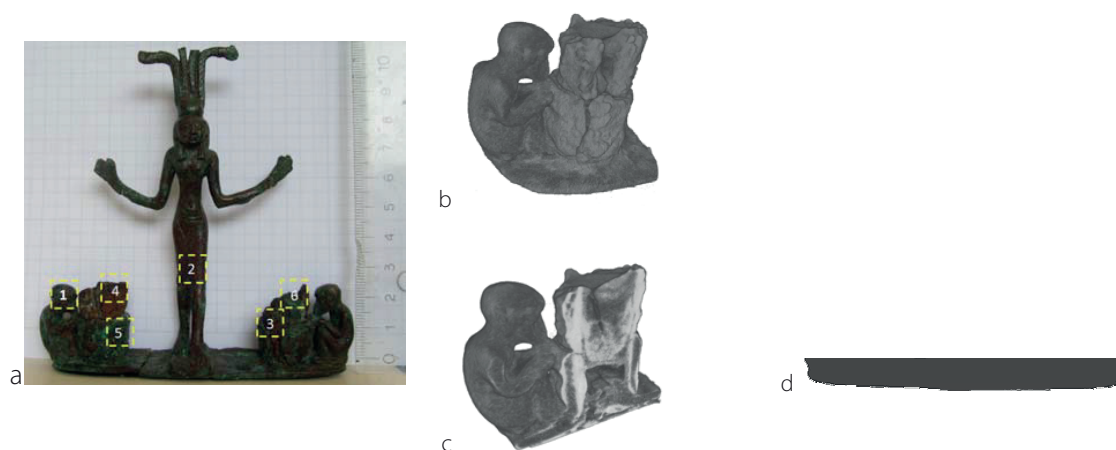


Fig. 1. a) Photography of the goddess sculpture with the selected parts for elemental analysis. b) cold neutron tomography reconstruction image of the left side monkey and the palm stub. c) vertical cross section of the 3-D reconstruction image. d)

With the combination of neutron imaging and prompt-gamma spectroscopy the elemental composition and structural information could be determined in a completely non-destructive way. The bronze object we presented as an example in this study, was found to contain 86 wt% Cu and 14 wt% Sn. Thanks to the neutron tomography, the 3-D dispersion of the different neutron absorption properties parts could be visualized (see Fig. 1b and 1c). Based on the elemental composition and visual information, it was concluded that the bearing, the goddess, the monkeys and the hollow mounts of the palms are all share the above composition (Fig. 1d). The different parts of the sculpture bear no traces of soldering or riveting, thus they were probably manufactured in one single casting process. Considering the missing Ni and Co signatures it can be confidently stated that the palm stubs were made of non-meteoritic iron.

References

B. Maróti et al: Characterization of an Egyptian bronze statuette using position-sensitive prompt-gamma activation analysis and neutron imaging, to be submitted to J. Radioanal. Nucl. Chem.

<h1 style="margin: 0;">B N C</h1> <p style="margin: 0;">Experimental Report</p>	<i>Experiment title</i> Standardized procedure to set the isocentre of the NIPS-NORMA station for PGAI experiments	<i>Instrument</i> NIPS-NORMA <i>Local contact</i> Kis Zoltán
	<i>Principal proposer:</i> Zoltán Kis – Centre for Energy Research <i>Experimental team:</i> Zoltán Kis – Centre for Energy Research	<i>Experiment Number</i> <i>Date</i> 2015.02.20-2015.02.24 2015.03.19-2015.03.20

Objectives

to provide a standard procedure for the setup of the isocentre of NIPS-NORMA facility for PGAI measurements

Results

If both the neutron beam and the gamma detector are highly collimated, the intersection of the neutron beam and the solid angle of the collimated gamma-detector define a spatially fixed probed volume, the so-called isovolume, usually much smaller than the sample. Its middle point is called isocentre, of which position plays a crucial role in PGAI measurements because it determines to which part of the object will be assigned the actually measured element composition.

We developed a method to determine the isocentre's coordinates as the midpoint of the FWHM (full width at half maximum) of the gamma-ray transmission of the actually applied lead collimator as a function of energy. Point-like radioactive source (e.g. Eu-152) is positioned in the vicinity of the isocentre, and then it is moved around it both vertically and horizontally (see Fig. 1a). During the movement several gamma-ray spectra are collected, and the intensities at the different energies are linked to the actual position in motor coordinates.

The midpoint of the FWHM of transmission curves can be determined with an accuracy of a hundredth of a millimetre for a 2x20 mm² lead collimator for lower energy gamma-rays (for some hundreds of keV). In Fig.1b and Fig. 1c one can see the effect of 0.51 mm offset of the isocentre coordinate measured by the horizontal movement of a Eu-152 point source in 0.2 mm steps. During the measurement 81 gamma-ray spectra were acquired with an acquisition time of 2844 s each.

By adjusting the zero point of the sample stage the coordinate of the isocentre along the neutron beam can be set where the transmission of the gamma collimator is optimal. By mechanically adjusting the height of the gamma collimator the vertical coordinate of the isocentre could be positioned to match the middle of the neutron beam. The third coordinate of the isocentre (i.e. perpendicular to the beam) could be set up by neutron imaging.

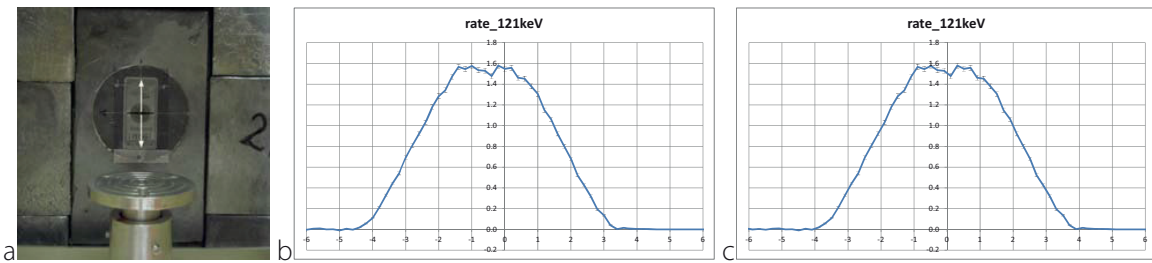


Figure 1. (a) Point-like radioactive source is positioned in front of the lead collimator, and by moving it up and down or vertically and horizontally the transmission curves of the gamma-ray spectrometer at different energies were measured. (b) The transmission function showing a shifted midpoint of the FWHM. (c) The transmission function where the isocentre was shifted by 0.51 mm to the right direction.

References

Kis, Z., Szentmiklósi, L., and Belgya, T., 2015. NIPS-NORMA station - A combined facility for neutron-based nondestructive element analysis and imaging at the Budapest Neutron Centre. *Nuclear Instruments and Methods in Physics Research, Section A: Accelerators, Spectrometers, Detectors and Associated Equipment*, 779, 116–123.

<h1 style="margin: 0;">BNC</h1> <p style="margin: 0;">Experimental Report</p>	<i>Experiment title</i> Characterization of electronic waste by nuclear analytical and imaging techniques	<i>Instrument</i> PGAA, NIPS-NORMA, RAD, NAA <i>Local contact</i> László Szentmiklósi
	<i>Principal proposer:</i> L. Szentmiklósi – MTA EK <i>Experimental team:</i> M. Papp, Z. Kis, B. Maróti, D. Párkányi – MTA EK	<i>Experiment Number</i> <i>Date</i> Nov 2015

Objectives

to characterize electronic waste by nuclear analytical and imaging techniques

Results

Elemental compositions of historical e-waste (various computer accessories) were determined with PGAA. Samples and analysis spots were selected based on our a priori knowledge where the presence of valuable or toxic elements was expected. During the study, in addition to the main components, In, Sm, Gd, Nd, W, Ag, Pt and Au were positively identified. With PGAI, the spatial distribution of the elements within a computer memory card could be directly studied. In the slices at an IC elevated concentrations of hydrogen, silicon, nickel and iron were observed, whereas high Ti and Sm content was found in the resistors in-between the chips. The levels of B, Ca, Cl, Br and Cu were found to be rather constant along the long axis of the memory card, so most likely they are part of the base composite plastic. Three samples were studied with in-beam neutron activation analysis by irradiation at horizontal channel No 2. (RAD). The NAA spectra of the activated samples often provided more reliable identification of elements that were at the margin of detectability with PGAA. With neutron and X-ray imaging the heterogeneity of the samples could be visualized, and the spatial distribution of certain components could be determined.

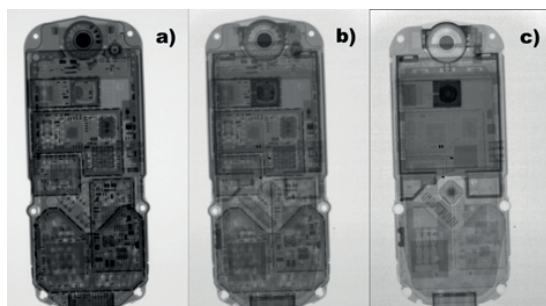


Fig.1. X-ray (left), composite (middle) and neutron (right) image of a SIEMENS cell phone

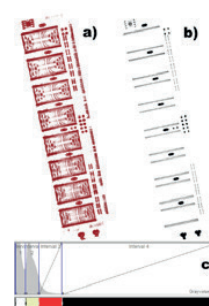


Fig.2. image segmentation of a computer memory card (a: chips, b: pins, c: histogram)

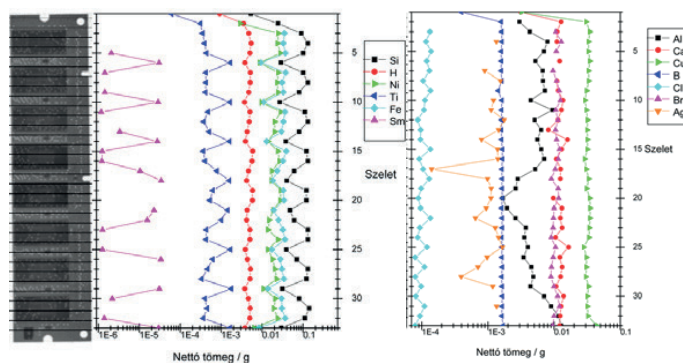


Fig.3. variation of the elemental compositions through the PGAI slices of the memory card

Reference

Papp M., Elektronikai hulladékok vizsgálata nukleáris analitikai és képalkotó módszerekkel, Eötvös Loránd Tudományegyetem, Természettudományi Kar, Vegyész Mester szakos diplomamunka, 2016

<h1 style="margin: 0;">BNC</h1> <p style="margin: 0;">Experimental Report</p>	<i>Experiment title</i> Studying the propagation of water and salt ions in porous construction materials by PGAI	<i>Instrument</i> NORMA <i>Local contact</i> Kis Zoltán
	<i>Principal proposer:</i> Francesca Sciarretta – University of Venice, Italy <i>Experimental team:</i> Zoltán Kis, László Szentmiklósi – Centre for Energy Research	<i>Experiment Number</i> BRR_433 <i>Date</i> 2015.05.06-2015.05.14

Objectives

to study the propagation of water and salt ions in the porous medium with cultural heritage significance from Venice, Italy

Results

As the H content of the water and the Cl content of a NaCl solution are well measurable in usual stone matrices by PGAI technique the mobilization of salt ions was studied with the analysis of pairs of prompt-gamma peaks in successively-recorded spectra. The concentration of Cl ions in the solution was set to a level, which will give approximately the same count rates at the 1163 keV doublet peak of Cl and at the 2223 keV peak of H. The Cl and H content at a specific position in the stone (at 47.9 mm above the bottom) were not spatially but temporarily resolved.

The result of PGAI experiments carried out for a Vicenza calcareous rock (V) is shown in Fig. 1. The front propagation for the NaCl solution was similar to that of the water solution. The difference we have experienced was that the NaCl solution front appeared later at the same height of the stone. As one can see from Fig. 1, the front reached the irradiated area at 47.9 mm above the bottom after ~5-6 h after starting the imbibition. The slower transport could be explained by the higher density and viscosity of the NaCl solution compared to that of the pure water.

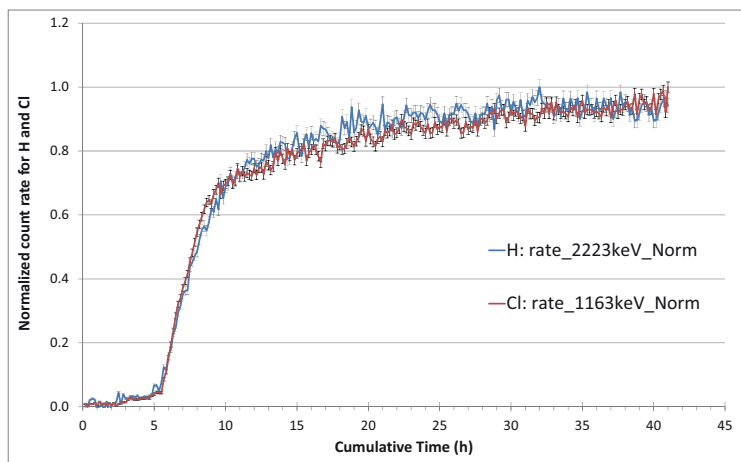


Figure 1: The time dependence of the normalized count rates of the gamma-ray peaks of Cl and H (1163 keV peak of Cl, 2223 keV peak of H) in the collected spectra. A position at 47.9 mm above the bottom of the stone was chosen where the water front appeared after ~5-6 hours after starting the imbibition with NaCl solution. The irradiated sample was a Vicenza calcareous rock (V2) and a $V \times H = 2 \times 43 \text{ mm}^2$ cross section neutron beam was applied. At the sample position the height of the irradiated area on the stone was 2.8 mm due to the divergent neutron beam. The vertical bars show the 1σ uncertainty range of the normalized count rates.

A further notable thing is that the Cl-ions were not trapped in the mineral phase of the stone during the diffusion and capillary rise of the solution. It can be concluded from the fact that the time dependence of their normalized count rate follows the same shape as that of the H in Fig. 1.

References

Kis, Z., 2015. Report on water uptake experiments carried out for various stones from Venice by neutron imaging and PGAI methods. Budapest: MTA Energetikai Kutatóközpont, Kutatási jelentés No. MTA EK-NAL-2015-441-1-2-M0.

BNC Experimental Report	<i>Experiment title</i> Neutron tomography of water in porous construction materials from Venice, Italy	<i>Instrument</i> NORMA <i>Local contact</i> Kis Zoltán
	<i>Principal proposer:</i> Francesca Sciarretta – University of Venice, Italy <i>Experimental team:</i> Zoltán Kis, László Szentmiklósi – Centre for Energy Research	<i>Experiment Number</i> <i>Date</i> 2015.05.06- 2015.05.14

Objectives

to assess the capabilities of neutron-based imaging techniques for detecting the distribution of water in porous construction materials of cultural heritage significance from Venice, Italy

Results

Four types of stone samples, having high, medium, low and negligible porosity, were tested, and the results were compared in order to better understand the effect of the hydraulic conductivity. The four porous stone samples were studied, identified as Vicenza calcareous rock (V), Trachite volcanic rock (T), Istria limestone (I), and Carrara marble (C). They were cut to similar dimensions of L(ength)×W(idth)×T(hickness) = 100×35×10 mm³. For the tomography of an object a series with 601 projections was acquired with 0.03° angular increments over 180°. Tomographic imaging was carried out in dry and wet conditions. Before the “wet” tomography the stones were soaked in MilliQ water to reach full saturation.

The results of tomographic imaging are shown in Fig. 1.a-d mirroring our expectations as for the quantity of water uptake. As it was expected the water content of a stone obeyed the magnitude of its porosity: the stone type with the highest value (T1) contained the most water and the stone type with the lowest one (C1) contained the less water.

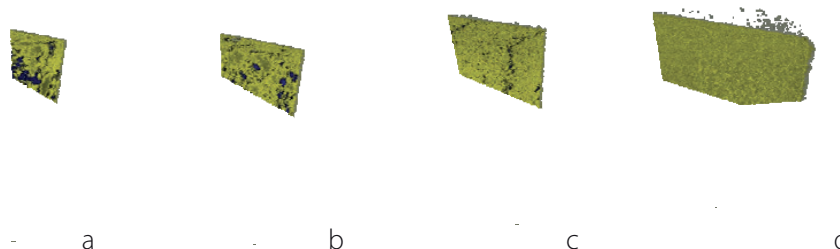


Figure 1: The tomographic images of the four types of the investigated stone samples: a, Vicenza calcareous rock (V); b, Trachite volcanic rock (T); c, Istria limestone (I) and d, Carrara marble (C). The yellowish colors refer to the solid mineral part, while the bluish colors refer to the water containing part of a stone. The clipping box visualization technique of VG Studio 2.1 is applied to the images to show inner plane cuts.

As the spatial resolution of the images limited the smallest pore size to be visualized the distribution of the water in the bulk of a stone could be seen in 3-D. For both Vicenza calcareous rock (V) and Trachite volcanic rock (T) one can see that the water is contained in bulky reservoirs between the mineral parts of the stones (Fig. 1.a-b). These reservoirs are likely being formed as a cluster via interconnections of pores, voids or fractures. The degree of the interconnection is different for the two types determining the maximum quantity of the water that can be taken up. The interconnections formed a completely different structure in Istria limestone (I). In this stone type water conduction channels are seen (Fig. 1.c), which could pipe the water flow along a specified direction through the object. Although the water content of the stone itself is rather low this water could nonetheless be transported effectively between distant parts. In the case of Carrara marble (C) there are no water reservoirs in the stone therefore its water content is negligible (Fig. 1.d). Moreover, the lack of water conducting channels excludes an effective water transport too.

References: Kis, Z., 2015. *Report on water uptake experiments carried out for various stones from Venice by neutron imaging and PGAI methods*. Budapest: MTA Energiatudományi Kutatóközpont, Kutatási jelentés No. MTA EK-NAL-2015-441-1-2-M0.

<h1 style="margin: 0;">BNC</h1> <p style="margin: 0;">Experimental Report</p>	<i>Experiment title</i> Elemental compositions of two historical bronze objects	<i>Instrument</i> NIPS-NORMA <i>Local contact</i> Kis Zoltán
	<i>Principal proposer:</i> Gábor Tarbay – Hungarian National Museum <i>Experimental team:</i> Zoltán Kis, Boglárka Maróti – Centre for Energy Research	<i>Experiment Number</i> BRR_456 <i>Date</i> 2015.04.20-2015.04.20

Objectives

to determine the elemental compositions of two historical bronze objects (a casting cake and a Copper Age axe) from the Hungarian National Museum (HNM)

Results

There was a request from HNM to determine the elemental compositions of a casting cake and a Copper Age axe, found in a Late Bronze Age depot from Nagyrábé by a joint application of PGAA and neutron radiography (NR).

The **casting cake** (Inv. nr. 17.1949.2) was irradiated as it can be seen in Fig. 1a. The main component is copper (96 wt%). Besides copper it contains small amount of iron (1.59 wt%) and sulphur (1 wt%), and additional traces of cobalt, nickel, hydrogen and chlorine. Hydrogen, chlorine and sulphur can be attributed to a contamination from the soil, conservation material or corrosion. The cobalt and nickel are probably surrogate elements of copper that might be characteristic to the provenance. This object is a suitable candidate of further investigations to detect possible composition differences at its various parts.

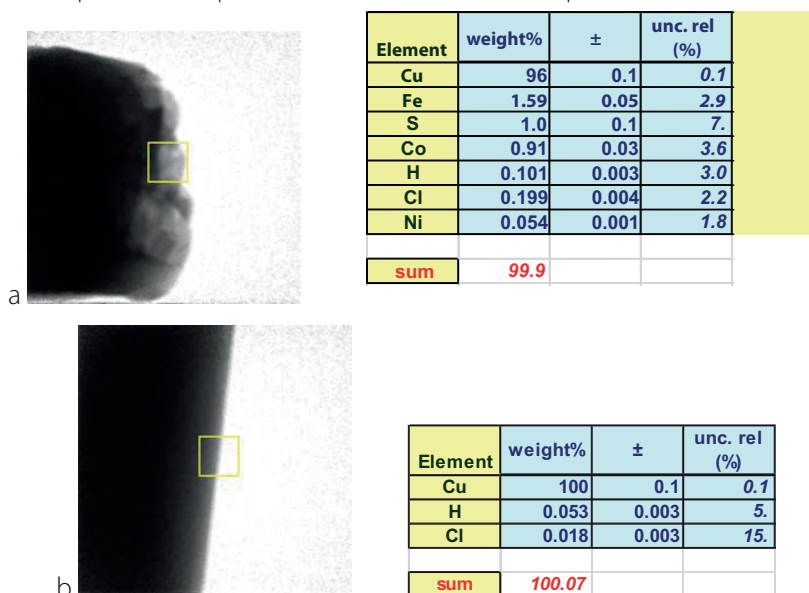


Figure 1: (a) Irradiated part of the casting cake with the elemental composition of the irradiated part of it. (b) Irradiated part of the Copper Age axe with the elemental composition of the irradiated part of it.

The **Copper Age axe** (Inv. nr. 17.1949.3) was irradiated as it can be seen in Fig. 1b. It is made of pure copper (100%). The identified traces of hydrogen and chlorine are possible corrosion products, or remaining of surface treatment. There was an indication for the presence of tin; however, the signal was well below the limit of quantitation. In the case of such copper matrix the limit is about 3%. For this reason, we do not give quantitative value for tin.

References: Kis, Z. and Maróti, B., 2015. *Report on the pilot PGAA and NR measurements of selected bronze objects from the Hungarian National Museum*. Budapest: MTA Energetikai Kutatóközpont, Kutatási jelentés No. MTA EK-NAL-2015-141-1-1-M0.

<h1 style="margin: 0;">BNC</h1> <p style="margin: 0;">Experimental Report</p>	<i>Experiment title</i> The first volcanic borate in the Carpathian region (Nagylóc-Zsunyuszta, Cserhát mts.)	<i>Instrument.</i> NIPS-NORMA <i>Local contact</i> Zsolt Kasztovszky
	<i>Principal proposer:</i> Sándor Szakáll – University of Miskolc, Institute of Mineralogy and Geology, Hungary <i>Experimental team:</i> Zsolt Kasztovszky, Boglárka Maróti, Katalin Gméling – MTA EK	<i>Experiment Number</i> Date 23-24 June 2015

Objectives

Borate occurs frequently in post-volcanic processes. It is extremely frequent in high K-content vulcanite material, in the region of Campania and Latium. The andesite in the Nagylóc-Zsunyuszta region, Cserhát mts. was first described in the 1890s by Schafarzik, later in 1973 by Puskás. Based on the descriptions, the authors presumably met borate in the Cserhát. We aimed to prove the presence of borate using neutron-based techniques, namely PGAA and neutron radiography.

Results

Three different samples were analyzed by PGAA. „Cserhát1”, „Cserhát2” and „Cserhát3” were supposed to be borate, andesite and feldspar, respectively. The boron content of them found to be 159 ppm, 17 ppm and 73 ppm. On the neutron radiography image of the „Cserhát1”, high contrast caused by pin-like crystals is clearly visible. During the repeated PGAA with a narrowed beam to the region of interest, extremely high B-content (630 ppm) was determined (Cserhát 1*)

	Cserhát 1		Cserhát 2		Cserhát 3		Cserhát 1*			Cserhát 1		Cserhát 2		Cserhát 3		Cserhát 1*	
	andesite, borate(?)		andesite		feldspar		5X5 mm2 collimator			andesite, borate(?)		andesite		feldspar		5X5 mm2 collimator	
El	Major / wt%	Rel. Unc. %	Major / wt%	Rel. Unc. %	Major / wt%	Rel. Unc. %	Major / wt%	Rel. Unc. %	El	Trace / ppm	Rel. Unc. %	Trace / ppm	Rel. Unc. %	Trace / ppm	Rel. Unc. %	Trace / ppm	Rel. Unc. %
SiO2	56.1	0.9	55.3	0.9	57.4	0.8	59.6	1.0	B	159	1.1	17	1.1	73	1.1	631	0.7
TiO2	1.30	2.3	1.28	2.5	1.25	2.4	1.28	2.5	Cl	36	29.	52	29.	36	21.	23	22.
Al2O3	16.7	1.6	17.5	1.5	15.6	1.6	14.6	2.1	Sc			48	13.	12	9.		
Fe2O3	8.11	2.5	9.06	2.2	8.19	2.4	7.78	2.4	V	255	5.	250	6.	19	9.	222	6.
MnO	0.119	2.2	0.140	3.1	0.121	3.1	0.107	6.	Ba	586	12.					439	18.
MgO	2.68	6.	2.60	10.	3.02	7.	2.82	7.	Nd	34	9.	24	9.	37	10.	38	9.
CaO	6.44	2.6	6.96	2.6	6.83	2.6	4.25	3.7	Sm	5.3	2.5	4.9	1.9	5.2	2.1	5.9	2.4
K2O	2.56	1.8	2.41	2.7	2.91	1.8	3.74	2.0	Gd	6.5	6.	6.1	6.	6.8	10.	6.9	9.
Na2O	3.04	2.5	2.92	3.0	3.19	2.7	2.77	3.5									
H2O	2.80	1.1	1.67	1.3	1.38	1.3	2.74	1.7									

Table 1: Composition of the Cserhát samples, measured by PGAA

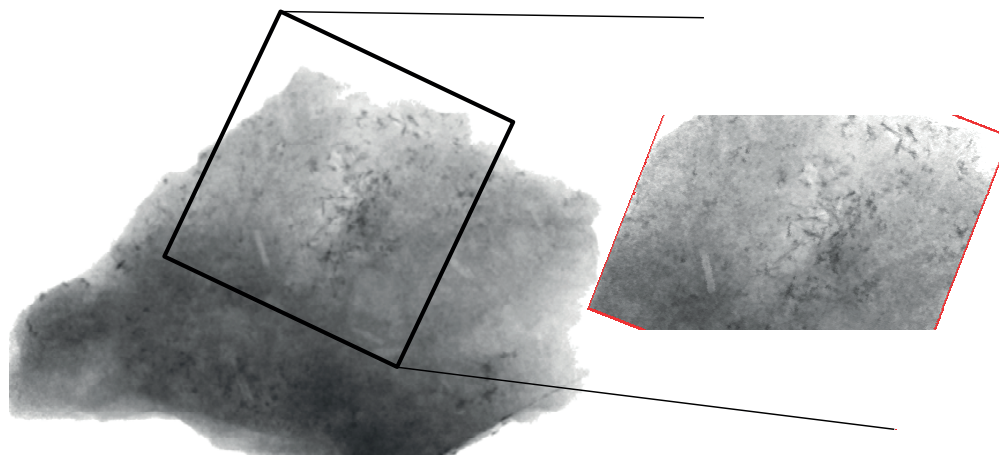


Fig.1. Neutron radiography image of the „Cserhát1” sample, done on the NIPS-NORMA station

Reference: Szakáll Sándor, Kristály Ferenc, Kasztovszky Zsolt, Maróti Boglárka: Vulkanéri eredetű borátásvány a Cserhátból (poster, in Hungarian), General Assembly of Hungarian Geologists, Ópálos, 10-12. Sept. 2015.

<h1 style="margin: 0;">B N C</h1> <p style="margin: 0;">Experimental Report</p>	<i>Experiment title</i> Neutron absorbing properties of pure metal sheets	<i>Instrument</i> NIPS-NORMA <i>Local contact</i> Boglárka Maróti
	<i>Principal proposer:</i> Boglárka Maróti <i>Experimental team:</i> Boglárka Maróti, László Szentmihályi, Zoltán Kis – Centre for Energy Research	<i>Experiment Number</i> <i>Date</i> 2015.

Objectives

to determine the experimental linear neutron attenuation coefficient values of different pure metal samples

Results

Our goal was to compare the neutron absorption properties of different pure metals at the cold neutron beam of the NIPS-NORMA facility. If we have prior information about the examined samples neutron imaging techniques can be indirectly used to estimate the compositional differences in a heterogeneous object. In order to examine the effect of the neutron scattering, the metal sheets were placed both to the iso-centre of the NIPS sample chamber (cca. 109 mm distance from the screen), and to the neutron screen in close-geometry. The radiography images were corrected by the open beam images and the closed beam images using Igor Pro software, and an average of higher amount grey values were estimated using ImageJ software. We concluded that minimum of 1 mm thickness is necessary to achieve sufficiently precise data. Pure metal sheets with different neutron absorption characteristics could be reliably distinguished (Fig. 1 a).

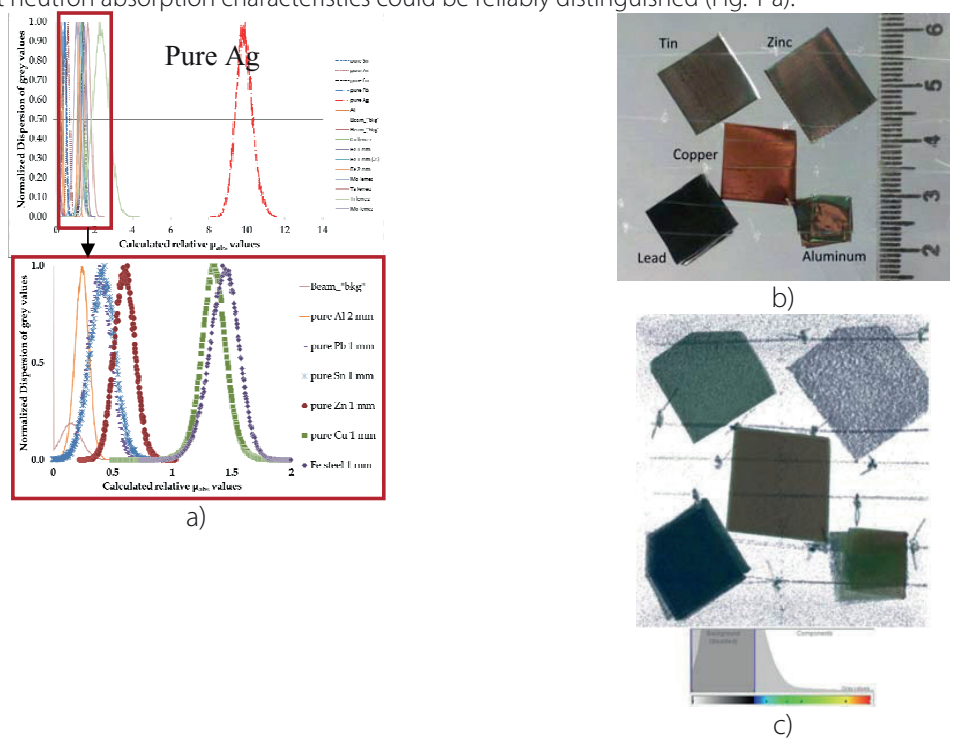


Figure 1: a) apparent linear absorption coefficient (μ_{abs}) values of several pure metals (Sn, Zn, Cu, Pb, Ag, Al, Fe, Mo, Ta, Ti) at the NORMA beamline, b) photography and c) cold neutron tomography reconstruction of pure Sn, Zn, Cu, Pb and Al sheets.

Another attempt to decrease the disturbing scattering and edge effects was the neutron imaging by rotating the samples and later 3-D reconstruction (see Fig 1/b-c). Further experiments were performed at the RAD facility. The interpretation of the neutron tomography and RAD experiments is in progress

<h1 style="margin: 0;">B N C</h1> <p style="margin: 0;">Experimental Report</p>	<i>Experiment title</i> Measuring the water content of porous medium in unsaturated condition by neutron imaging	<i>Instrument</i> NORMA <i>Local contact</i> Kis Zoltán
	<i>Principal proposer:</i> Zoltán Kis – Centre for Energy Research <i>Experimental team:</i> Zoltán Kis – Centre for Energy Research	<i>Experiment Number</i> <i>Date</i> 2015.05.15-2015.05.15

Objectives

to provide quantitative results for the water content of the medium using a water thickness calibration in neutron imaging

Results

Infiltration experiments were carried out using stones where the bottom part of the stones was immersed in the soaking water for hours and days long. In order to follow the water-front propagation during the imbibition experiments several series of radiographic images were taken in likely unsaturated conditions. The grayscale values of this image's pixels give the exponent part of the attenuation equation from pixel to pixel (i,j) (where μ_{eff} is a set-up specific effective linear attenuation coefficient and d is the thickness of the medium):

$$-\ln\left(\frac{I_{tr}}{I_0}\right)_{i,j} = \int_{beam\ path} \mu^{tot}(x,y) ds = \mu_{eff} \times d ,$$

We tested the use of the water thickness calibration curve to estimate the magnitude and the spatial distribution of the water content in a supposedly unsaturated condition. The last image of this 45-images-long series (3.75 hours after starting the experiment) was chosen for this quantitative testing of the water content (see Fig. 1a). Then a supposedly unsaturated part of the stone was chosen using the ROI Manager plugin of the FIJI code as one can see the rectangular shape area in Fig. 1a. The second order polynomial fitted to the measured data points of the calibration curve has the following coefficients: $a = -0.0281 \text{ cm}^2/\text{px}^2$, $b = 0.2430 \text{ cm}/\text{px}$ and $c = -0.0403 \text{ cm}$.

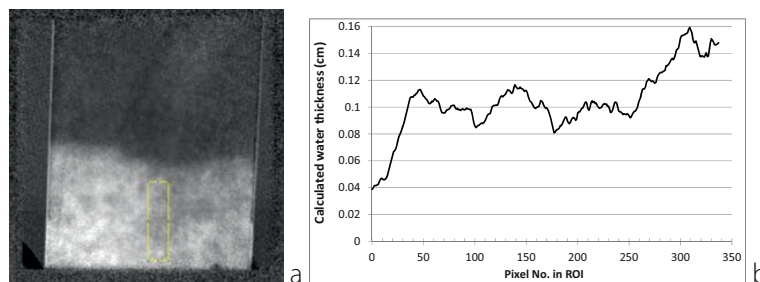


Figure 1: (a) An unsaturated part of the stone V2 was chosen using the ROI Manager plugin of the FIJI code as one can see the rectangular shape area to test the use of the calibration curve. (b) The calculated water thicknesses for the ROI area in the unsaturated part of stone V2. The first pixel refers to the top of the rectangular ROI (pay attention that lighter color means thicker water layer).

Based on the evaluation of the water content of the various stones after their preparatory soaking for tomographic imaging it was known that a V-type stones can take up ca. $7.28 \text{ g} \approx 7.28 \text{ cm}^3$ water in its $35 \text{ cm}^3 (= 10 \times 3.5 \times 1 \text{ cm}^3)$ volume as a maximum. This means that the average open (or effective) porosity of the stone is about $7.28/35 = 0.208$. For a volume, of which thickness is 1 cm along the neutron beam the number value of the calculated water thickness is the same as the open porosity value of the medium. Therefore the results in Fig. 1b show that the assumption of the unsaturated condition for this part of the stone is well supported because the thickness of the water was everywhere less than the average open porosity value.

References: Kis, Z., 2015. *Report on water uptake experiments carried out for various stones from Venice by neutron imaging and PGAI methods*. Budapest: MTA Energiatudományi Kutatóközpont, Kutatási jelentés No. MTA EK-NAL-2015-441-1-2-M0.

<h1 style="margin: 0;">BNC</h1> <p style="margin: 0;">Experimental Report</p>	<i>Experiment title</i> Providing quantitative results for the water content of the medium using a water phantom in neutron imaging	<i>Instrument</i> NORMA <i>Local contact</i> Kis Zoltán
	<i>Principal proposer:</i> Zoltán Kis – Centre for Energy Research <i>Experimental team:</i> Zoltán Kis – Centre for Energy Research	<i>Experiment Number</i> <i>Date</i> 2015.05.15-2015.05.15

Objectives

to provide calibration curve for the water content of the medium using a water phantom for water thickness calibration in neutron imaging

Results

There are several approaches developed until now to provide quantitative results for the water content of the medium, however, permanent difficulties arise using polychromatic neutron beams for imaging. First, the neutron beam is subject to a so called beam hardening effect, and as a consequence the effective attenuation coefficient for the beam will be different at different parts of the sample. Second, the incoherent scattering(s) (mainly on the hydrogen) can form paths for neutrons scattered already out of the beam, that such a neutron can still reach the scintillation screen. It will mimic a higher transmission of the neutrons, and lead to a less water content estimation.

To overcome these difficulties a wedge-like water calibration phantom was designed and fabricated of thin Al-sheets for a water thickness range of 0-4 mm. Using this method a facility specific empirical equation for water thickness calibration can be produced. The attenuation image of the water phantom showing the exponent part ($\mu_{eff} \times d$) of the attenuation equation from pixel to pixel can be seen in Fig. 1a. The calibrating function for the water thickness can be seen in Fig. 1b. This function is valid only for the cold neutron beam at NIPS-NORMA facility of the BRR for a specific set-up, in which the sample-to-screen distance is 63.4 mm. As one can see the shape of the function is not linear in the water thickness range of 0.05-0.31 mm. A second order polynomial was fitted to the measured data points of the calibration curve resulting in the following coefficients: $a = -0.0281 \text{ cm}^2/\text{px}^2$, $b = 0.2430 \text{ cm}/\text{px}$ and $c = -0.0403 \text{ cm}$.

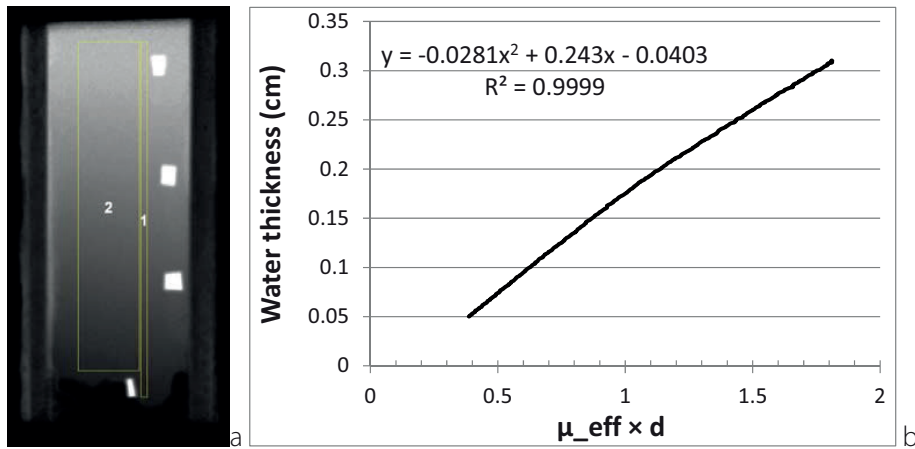


Figure 1: (a) The attenuation image of the water phantom showing the exponent part ($\mu_{eff} \times d$) of the attenuation equation from pixel to pixel. The white rectangles in the image show the position of the Gd markers. The two yellow rectangles are two ROI's created by the ROI (Region Of Interest) Manager plugin of the FIJI code. (b) The calibrating function between the exponent of the attenuation equation and the water thickness. This function is valid only for the cold neutron beam at NIPS-NORMA facility when the sample-to-screen distance is 63.4 mm.

References

Kis, Z., 2015. Report on water uptake experiments carried out for various stones from Venice by neutron imaging and PGAI methods. Budapest: MTA Energiatudományi Kutatóközpont, Kutatási jelentés No. MTA EK-NAL-2015-441-1-2-M0.

<h1 style="margin: 0;">B N C</h1> <p style="margin: 0;">Experimental Report</p>	<p><i>Experiment title</i> Iceland's early crucible metallurgy: a new investigation into Viking Age technology</p>	<p><i>Instrument.</i> PGAA <i>Local contact</i> Zsolt Kasztovszky</p>
	<p><i>Principal proposer:</i> Thomas Birch - University of Aberdeen, UK</p> <p><i>Experimental team:</i> Thomas Birch - University of Aberdeen; Zsolt Kasztovszky, Boglárka Maróti – MTA EK; Zoltán-Szőkefalvi-Nagy, Imre Kovács – MTA Wigner RCP</p>	<p><i>Experiment Number</i> BRR_353_CH</p> <p><i>Date</i> 18-21 November 2013</p>

Objectives

This project was the first comprehensive study of crucible metallurgy in Iceland. To date, very little is understood about Iceland's early metallurgy. The goal of this project was to empirically reconstruct and understand crucible technology in early Iceland. Scholars have generally assumed that it was simply an extension of that practised in the Scandinavian homelands. But was it? The results of the PGAA and PIXE analysis hoped to develop our knowledge about the ecology (resource procurement) and economy (metals) in early Iceland. The results were aimed to enable us to make substantiated interpretations about technological practice and its development.

Results

A careful desktop study of the crucibles revealed them to be similar in size and shape to contemporaneous examples from other The results from PGAA and PIXE analyses confirmed an industry of non-ferrous metalworking and recycling, which although previously hypothesised (for an island with no apparent copper ore deposits), has only now been confirmed empirically. The PIXE surface analysis and PGAA bulk analysis also brought to light evidence for precious metalworking or recycling, which appear associated with samples deriving from important religious centres. Neutron Radiography at the NIPS-NORMA instrument also highlighted differences in manufacture, as well as internal layering of the fabrics, most likely resulting from their usage.

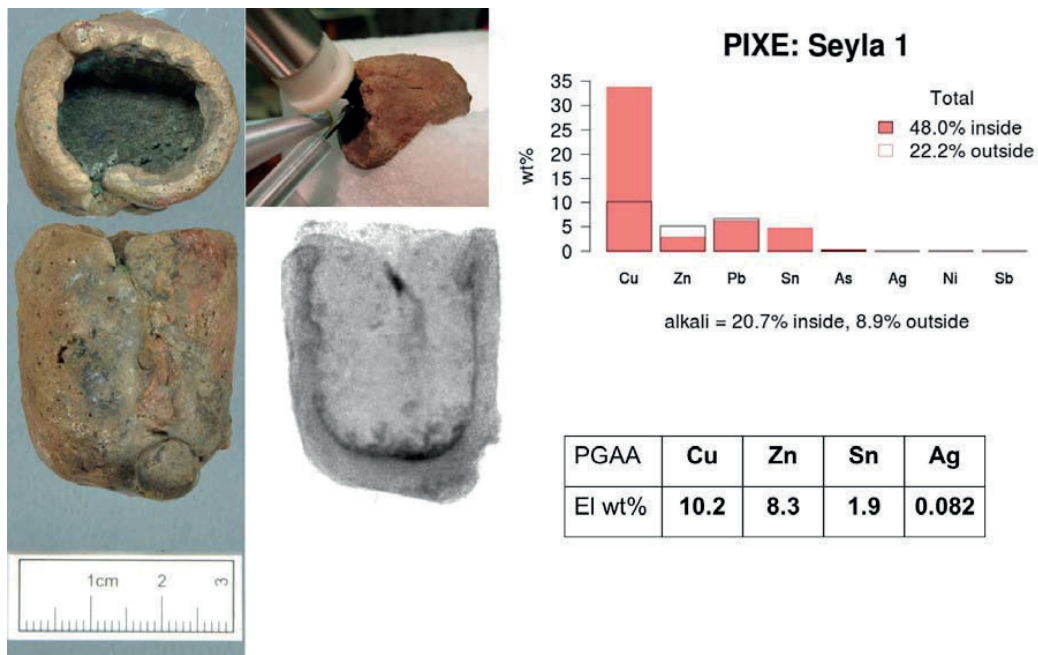


Figure 1: Image of the crucible from Seyla showing the crucible from two perspectives (side and aerial) alongside a neutron radiograph from the PGAA-NIPS facility, an action shot of the PIXE analysis, as well as the results from both PIXE and PGAA analyses.

BNC Experimental Report	<i>Experiment title</i> Characterization of radiolarites from the Northern Calcareous Alps and the Carpathian Basin in an archaeological context	<i>Instrument.</i> NIPS-NORMA <i>Local contact</i> Zsolt Kasztovszky
	<i>Principal proposer:</i> Michael Brandl - Institute for Oriental and European Archaeology, Austrian Academy of Sciences <i>Experimental team:</i> Michael Brandl - Institute for Oriental and European Archaeology, Austrian Academy of Sciences; Boglárka Maróti, Zsolt Kasztovszky – MTA EK	<i>Experiment Number</i> BRR_342_CH <i>Date</i> 08-23 May 2013

Objectives

The main objective of this project is the characterisation of selected radiolarite sources, from the Northern Calcareous Alps (Austria), the Carpathian Mountains (Slovakia, Poland) and the Bakony Mountains (Hungary), used for the production of chipped stone tools. We expect a higher resolution of our already existing geochemical database applying LA-ICP-MS by including PGAA investigations on chert and radiolarite. Specific trace elements determined by PGAA analysis hold the promise for supporting and refining our previous results. The impact would be the completion of the proposed “Multi Layered Approach” developed in Austria and will help to improve international chert source provenance studies on a transdisciplinary scale.

Results

The application of PGAA analysis on radiolarite samples successfully produced results which can be compared to results from previous chert sourcing studies. For archaeometry, compatibility of results has to be considered one of the principal goals. It was possible to measure oxides as well as trace elements, e.g., boron (B) and chlorine (Cl). However, vanadium (V), cobalt (Co) and nickel (Ni) are situated below the detection limit. Comparisons with data gathered by LA-ICP-MS from the identical samples show divergences between 10% and up to 50% error. This is due to the inherent differences between the methods, however, results obtained by PGAA will be incorporated into the datasets created by our Hungarian colleagues, completing their analytical database affording direct comparison between their previous results. The major advantage of PGAA analysis is the pure non-destructive character of the method, which certainly will increase the importance and use of this analytical technique in the future. In combination with other methods, PGAA can be considered one of the most promising archaeometric techniques to be further employed for chert sourcing studies.

The evaluation of the results, and the comparison with our previous radiolarite analytical data will require further work.

B N C Experimental Report	<i>Experiment title</i> PGAA measurements on bimetallic Ag-Au/SiO₂ catalysts	<i>Instrument</i> PGAA <i>Local contact</i> Boglárka Maróti
	<i>Principal proposer:</i> Tímea Benkó <i>Experimental team:</i> Boglárka Maróti, László Szentmiklósi – Centre for Energy Research	<i>Experiment Number</i> BRR-xxx <i>Date</i> 2013.11.17-20.

Objectives

to determine the Ag and Au content in SiO₂ supported bimetallic catalysts

Results

SiO₂ supported Ag-Au bimetallic catalysts were prepared by sol adsorption method with 10/90, 20/80, 33/67, and 50/50 Ag/Au molar ratios. Reduction of HAuCl₄ in Ag sol resulted in alloyed Ag-Au colloid particles and that structure remained after calcination and reduction treatment. The alloy structure of the catalysts was confirmed by UV-visible spectroscopy and high resolution transmission electron microscopy. The Au-Ag bimetallic effect and its dependence on the Ag/Au molar ratio was studied in glucose oxidation where synergistic activity increase was observed compared to the Au/SiO₂ reference sample in case of the bimetallic samples with less than Ag/Au=50/50 molar ratio. The Ag/SiO₂ was inactive at the same conditions. The Ag/Au surface atomic ratios – calculated by X-ray photoelectron spectroscopy (XPS) – were slightly higher than in the bulk – determined by prompt gamma activation analysis (PGAA). The higher activity of the bimetallic samples is suggested to be caused by the improved O₂ activating ability provided by Ag sites. The further increase of Ag loading above the optimal concentration may dilute the Au to such an extent that the population of extended active sites of gold necessary for glucose activation decreases deteriorating the activity.

References

Benkó T, Beck A, Frey K, Srankó DF, Geszti O, Sáfrán Gy, Maróti B, and Schay Z. "Bimetallic Ag–Au/SiO₂ Catalysts: Formation, Structure and Synergistic Activity in Glucose Oxidation." APPLIED CATALYSIS A-GENERAL 479 (2014): 103–11.

<h1 style="margin: 0;">BNC</h1> <p style="margin: 0;">Experimental Report</p>	<i>Experiment title</i> Characterization of Celtic coins from northern Italy and contemporary Roman coinage	<i>Instrument.</i> NIPS-NORMA <i>Local contact</i> Zsolt Kasztovszky
	<i>Principal proposer:</i> Jacopo Corsi - University of Torino <i>Experimental team:</i> Jacopo Corsi - University of Torino; László Szentmiklósi, Boglárka Maróti, Zsolt Kasztovszky – MTA EK	<i>Experiment Number</i> BRR_375_CH <i>Date</i> 02-04 July 2013

Objectives

The project intended to provide new data for the study of Celtic coinage from northern Italy, through a compositional characterization of the main emissions of drachmas (minted between IV and I century B.C.). The aims of the measurements at the BNC were to detect similarities or differences in the silver content in various series, and to understand if a silver debasement was present between the first and the last emissions. The possibility to analyse the Celtic coins collection from the Hungarian National Museum has been a great chance, because of the richness of the collection and the presence of several typologies. Finally, the analysis of some Roman coins, already characterized with different techniques, has been important to understand the relationship and the ratio between contemporary Roman and Celtic issues.

Results

With the PGAA technique, we analyzed forty Celtic coins from the Hungarian National Museum and some Roman coins already characterized with other techniques. The results show very clearly the presence of a general silver debasement in the Celtic coinage. Moreover, a significant loss of silver content is detected also within some series: for instance, the "scorpion-lion" drachma shows a fall from an average of 80%, to 70% and finally to 45%, as seen in some previous measurements on similar coins from the Archaeological Museum of Turin. These compositional differences confirm also the diverse stylistic issues. On the other hand, the analysis of five coins coming from a same hoard and stylistically very close one to each other, show very different results (see Fig. 1) in the silver content: this particular feature is probably due not to a devaluation process, but to the structure of the blanks: these coins are probably made of a core containing a low content of silver and a silver-rich upper level, sometimes with an irregular depth profile and sometimes eroded.

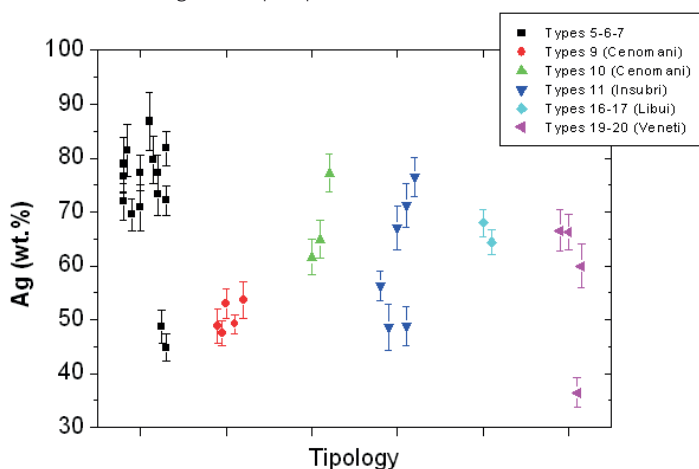


Fig.1: Silver content in different typologies of drachmas attributed to several Celtic tribes (in brackets)

Reference: Corsi J, Maroti B, Re A, Kasztovszky Z, Szentmiklosi L, Torbagyi M, Agostino A, Angelici D, Allegretti S Compositional analysis of a historical collection of Cisalpine Gaul's coins kept at the Hungarian National Museum *Journal Of Analytical Atomic Spectrometry* 30:(3) pp. 730-737. (2015)

<h1 style="margin: 0;">BNC</h1> <p style="margin: 0;">Experimental Report</p>	<i>Experiment title</i> Determination of organic textile fibre origin by trace element analysis	<i>Instrument.</i> PGAA <i>Local contact</i> László Szentmiklósi
	<i>Principal proposer:</i> R.B. Firestone, S. Basunia – Lawrence Berkeley National Laboratory, USA <i>Experimental team:</i> L. Szentmiklósi, B. Maróti – MTA EK	<i>Experiment Number</i> <i>Date</i> 25-27 June 2013 11-12 Dec 2013

Objectives:

to determine the radiative neutron capture spectrum of U-238

Results

A metal foil of 99.96% U-238 of 0.624 g was measured at PGAA and DÖME stations to characterize the (n, γ) spectrum of the U-238 and determine the partial capture cross-sections. After taking room background, the decay counting of the unirradiated sample took place at both facilities. This was followed by a neutron irradiation for 13500 sec. After shutting off the beam, the peaks of the short-lived decay products were recorded. After about 10 minutes, the sample was relocated to the DÖME chamber and counted for 165x1000 sec. After a few days cooling, another series of decay spectra was recorded in DÖME for 37x1000 sec. Finally, the sample was co-irradiated with a gold foil backing (Goodfellow gold foil, LS316994, 99.95%, 25 um thickness, 16x16 mm), and counted together in the DÖME, to relate the cross-section to that of the gold. As U-238 emits lower energy lines than Au-198, to minimize the gamma-attenuation, U-238 was placed towards the detector and gold was farther. Here 68 spectra were taken.

In a second run, the (n, γ) spectrum was also measured with a Low-energy Germanium detector (LEGe), in order to better resolve the low-lying multiplets.

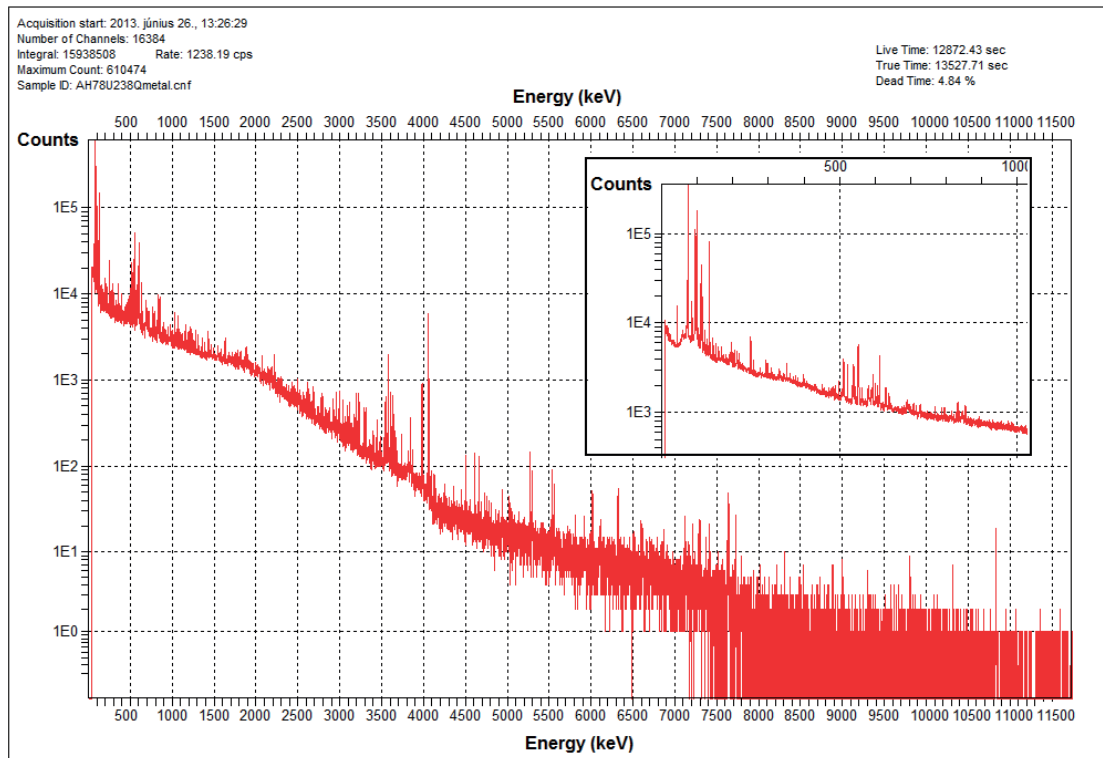


Fig.1. The (n, γ) spectrum of U-238. The inset shows the low-energy region using the LEGe setup.

The data analysis is still in progress, the results are expected to be published in a scientific paper, and will become part of evaluated nuclear data files, such as EGAF.

<h1 style="margin: 0;">BNC</h1> <p style="margin: 0;">Experimental Report</p>	<i>Experiment title</i> Determination of organic textile fibre origin by trace element analysis	<i>Instrument.</i> PGAA <i>Local contact</i> László Szentmiklósi
	<i>Principal proposer:</i> Chris Franklyn – NECSA, South Africa <i>Experimental team:</i> L. Szentmiklósi – MTA EK	<i>Experiment Number</i> <i>Date</i> 7-10 May 2013

Objectives

to provenance South-African wool based on their elemental compositions

Results

Eight wool samples were measured for 40-50 000 sec at the PGAA station with $1.2 \times 10^8 \text{ cm}^{-2} \text{ s}^{-1}$ neutron flux and using a $2 \times 2 \text{ cm}^2$ neutron collimator.

The major components (H, C, N, O, S, Ca) were found to be rather similar, differences were found only in K, Cl. Some elements (Ti, Sc, Mn, Fe, Br, Ag, Cd, were found only in one or two samples that might reflect some local environmental effect or specific treatment of the wool.

El	AF04		AH09		AH10		AH13		AH14		AH15		AH16		AH17	
	c% el/el	unc %	c% el/el	unc %	c% el/el	unc %	c% el/el	unc %	c% el/el	unc %	c% el/el	unc %	c% el/el	unc %	c% el/el	unc %
H	6.60	3.0	6.60	4.0	6.5	5.	6.60	3.5	6.51	6.	6.66	3.3	6.51	7.	6.15	2.9
B	1.58 ppm	3.0	0.74 ppm	5.	2.47 ppm	5.	0.67 ppm	4.			0.53 ppm	4.	1.25 ppm	7.	1.20 ppm	3.0
C	47	3.0	49	4.0	45	5.	49	3.5	49	7.	48	3.4	48	7.	50	3.0
N	15.0	3.4	16.4	4.	3.5	5.	16.6	3.7	16.1	7.	16.9	3.7	16.1	7.	15.5	3.3
O	27	7.	25	11.	44	6.	24	10.	25	19.	25	9.	26	19.	25	7.
Na									0.17	8.						
Al	0.39	3.8							0.53	8.						
Si	300 ppm	20.														
S	3.1	3.5	3.4	4.	0.77	5.	3.3	3.9	2.98	7.	3.2	3.8	3.4	7.	3.5	3.4
Cl	200 ppm	29.	40 ppm	28.	110 ppm	20.	0.07	33.	400 ppm	29.	220 ppm	21.	150 ppm	22.	0.16	13.
K	140 ppm	8.	140 ppm	12.	0.098	5.			70 ppm	22.					0.091	5.
Ca	0.06	10.	500 ppm	16.	0.07	12.	0.06	11.	0.12	11.	0.06	10.			0.050	9.
Sc			17 ppm	13.												
Ti	0.3 ppm	27.													19 ppm	5.
Mn	15 ppm	10.														
Fe	0.078	5.			0.13	8.										
Zn															90 ppm	19.
Br			0.05	14.												
Ag			19 ppm	13.												
Cd	0.38 ppm	4.													0.04 ppm	14.
Eu			38 ppm	4.												

Table 1. The components identified in the eight wool samples

Unfortunately the user did not finish the interpretation of the results and did not draw any conclusions from the provided analytical results. For future studies, the instrumental neutron activation analysis would be a more favorable tool.

<h1 style="margin: 0;">BNC</h1> <p style="margin: 0;">Experimental Report</p>	<p><i>Experiment title</i></p> <p>Obsidian Least Destructive Analysis Provenancing System</p>	<p><i>Instrument.</i></p> <p>PGAA</p> <p><i>Local contact</i></p> <p>Zsolt Kasztovszky</p>
	<p><i>Principal proposer:</i></p> <p>Attila Nándor Hágó - Satu-Mare County Museum, Romania</p> <p><i>Experimental team:</i></p> <p>Attila Nándor Hágó - Satu-Mare County Museum, Romania; Boglárka Maróti, Zsolt Kasztovszky – MTA EK</p>	<p><i>Experiment Number</i></p> <p>BRR_350_CH</p> <p><i>Date</i></p> <p>23-26 2013</p>

Objectives

By non-destructive analytical method of PGAA we can separate identify source regions, social, technological, economical relationship between different prehistoric (in that case Middle Neolithic) communities in EW Hungary and NW Romania. The aim of our project is to compare the PGAA results of new objects with previous PGAA data, with petrographic studies and with the existing information available in different databases. Finally we aim to reveal provenance of the tools' raw material, their trading routes and to create a map with the spread of this raw materials and lithic tools.

Results

Thanks to the non-destructive PGAA of Middle Neolithic obsidians and silex from Northern-western part of Romania, we have obtained information about their chemical compositions, which helped to identify the sources of this raw material and. We have investigated 19 pieces of obsidians, silexes and other lithic tool artefacts. Most of the objects are valuable pieces from the collection of Carei Museum, on which no analytical investigations have been done before.

From the PGAA results, we are quite certain that the provenance region of the objects is in the Tokaj-Eperjes zone, and their raw material is a very characteristic the Carpathian 1 type obsidian, more specifically Vinicky or Mala Bara types obsidians.

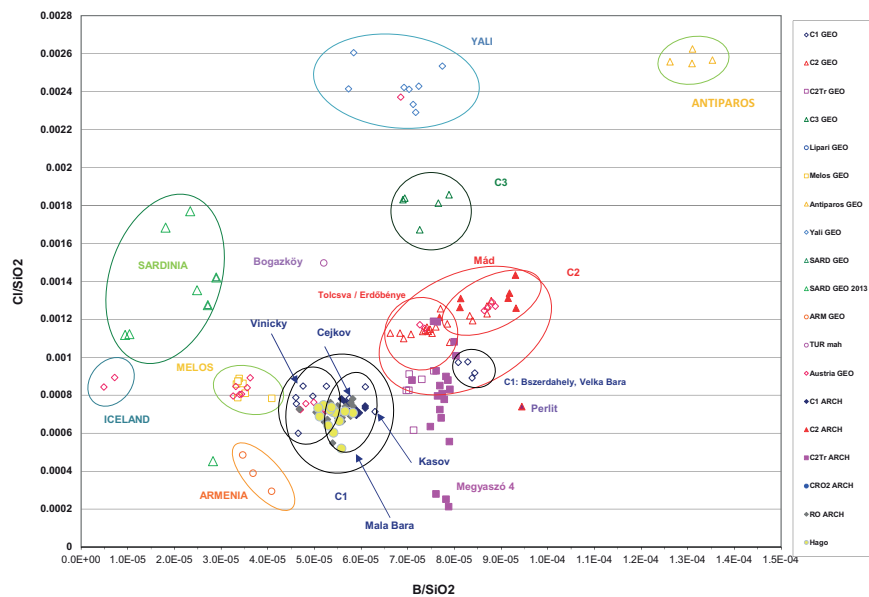


Fig 1: Provenance of archaeological obsidian from NW Romania, based on PGAA

<h1 style="margin: 0;">BNC</h1> <p style="margin: 0;">Experimental Report</p>	<i>Experiment title</i> Occurrences and provenances of prehistorichornfels polished stone tools in Hungary	<i>Instrument.</i> PGAA <i>Local contact</i> Zsolt Kasztovszky
	<i>Principal proposer:</i> György Szakmány - Department of Petrology and Geochemistry, Eötvös Loránd University <i>Experimental team:</i> Zsolt Kasztovszky, Szandra Szilágyi, Ildikó Harsányi – MTA EK	<i>Experiment Number</i> <i>Date</i> February 2013 - June 2016

Objectives

Hornfels is a fine grained contact metamorphic rock commonly used in the Carpathian Basin and its surroundings as raw material for polished stone artefacts, starting from the Early Neolithic onwards. Although hornfels stone tools are distributed on the whole territory of the Carpathian Basin, they dominate within the archaeological polished stone assemblages especially in its eastern part, with an increasing amount of occurrences toward the SE part of the Great Hungarian Plain. It was aimed at characterizing the raw materials of the artefacts on the base of their petrological and geochemical properties with scientific methods. Its challenging objective was to determine/localize the geological source and the exact provenance(s) of their raw materials combining archaeometricanalyses and geological field survey. Besides Magnetic Susceptibility (MS) measurements, SEM-EDS and PGAA were applied to determine their chemical composition.

Results

Hornfels artefacts have high CaO (13–23 m/m%) and relatively high Al₂O₃ content (13–16 m/m%), the alkalis (Na₂O+K₂O) occur only in small amount (1–5 m/m%). The geological source of hornfels was previously unknown. We could localize two areas where hornfels occur: in the Rusca Mts. and the South Apuseni Mts. In both territories hornfels formed on the contact zone of sub-volcanic intermediate-acidicrocks (so called Banatite) and high Ca-content clayish Cretaceous Gosau-facies sediments (possible marl). The wider compositional range of the geological samples of hornfels and a narrower one showed by the artefacts suggests that prehistoric people carefully selected the polished stone tools' raw materials.

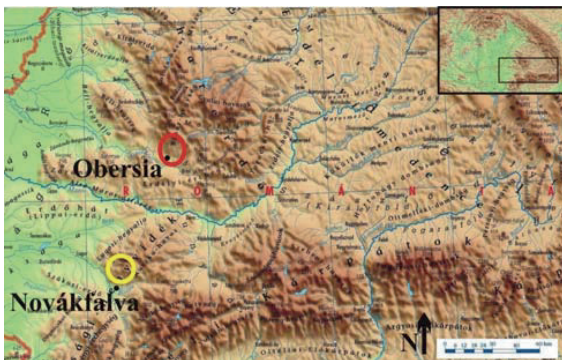


Fig. 1: Map of the surveyed area in SE Carpathians and S Apuseni Mts.

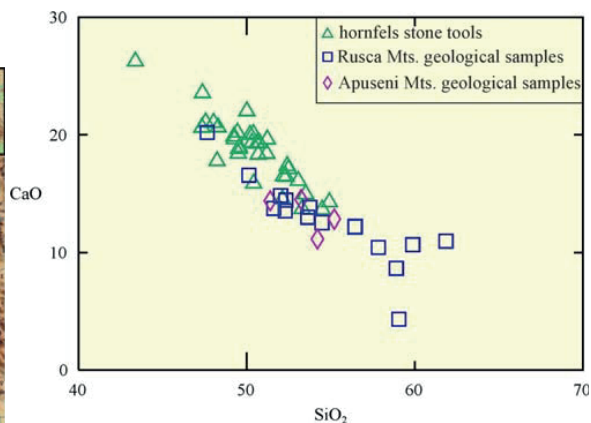


Fig. 2: Chemical composition of hornfels rock samples and Neolithic polished tools

Reference

G. Szakmány, Z. Bendő, S. Józsa, Z. Kasztovszky, E. Starnini and F. Horváth: Occurrences and provenances of Prehistoric hornfels polished stone tools in Hungary, *41st International Symposium On Archaeometry*, May 15-21, 2016 Kalamata, Greece

<h1 style="margin: 0;">BNC</h1> <p style="margin: 0;">Experimental Report</p>	<i>Experiment title</i> Analysis of Late Bronze Age glass beads from Western Hungary	<i>Instrument.</i> PGAA <i>Local contact</i> Zsolt Kasztovszky
	<i>Principal proposer:</i> Gábor Ilon - H-9730 Kőszeg Várkör 18. <i>Experimental team:</i> Zsolt Kasztovszky, Boglárka Maróti – MTA EK	<i>Experiment Number</i> <i>Date</i> Nov 2013 - Dec 2013

Objectives

The previous semi-quantitative analysis of the chemical composition of Late Bronze Age glass beads from various sites in the Bakony mts. identified these artefacts as made of soda-glass, comparable to alkaline glasses in Western Europe on the basis of their high potassium content. The beads represented the Late Tumulus–Early Urnfield culture (Bz C2–Ha A1) at the sites of Bakonyjákó (1988), Németbánya, and Ugod (1994), beads from the tumulus at Jánosháza (Vas County) have also been included. The aim of the non-destructive PGAA was to identify their raw materials and to find plausible similarities among contemporary HMG glass from Mycenae, Egypt or Mesopotamia.

Results

PGAA results showed that on the basis of their main components (Na_2O , K_2O and MgO) the Bakony beads are made of HMG glass, very similar to those found in Mycenae. Trace elements (B, Cl) on the other hand show that they are unlikely to have originated from the same source as their Mycenaean counterparts (Fig. 3). Theoretically it is possible that the raw material originated from different areas within the same geographical region. Meanwhile glass beads of Egyptian and Mesopotamian origins have been identified among finds from Denmark. Thus it is possible that such high status items imported to Mycenae from the Eastern Mediterranean (e.g. Uluburun) strayed into transit areas such as the East Alpine Foreland along the Amber Route. They may also have ended up in the hands of the wealthy in this area as war booty or the spoils of robbery.

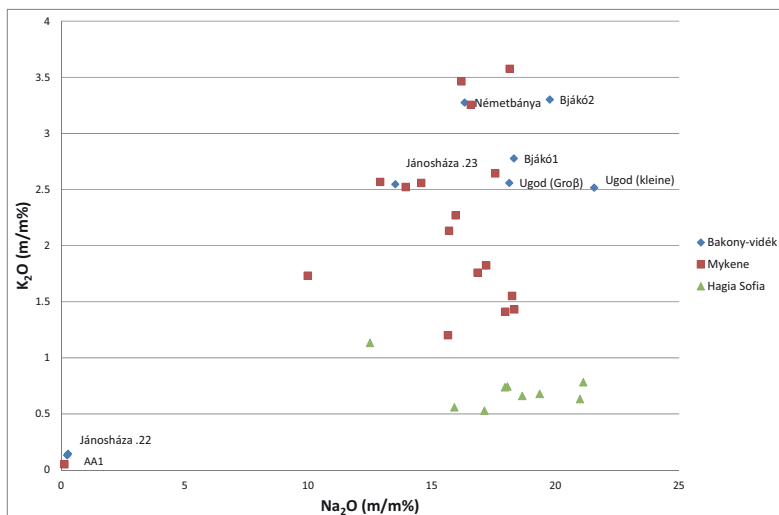


Fig. 1: Classification of LBA glass finds from the Bakony-region, Mycenae and the Byzantium



Fig. 2: Photo of LBA glass beads from Bakonyjákó, Hungary

Reference

Gábor Ilon, Zsolt Kasztovszky, Untersuchung Spätbronzezeitlicher Glasperlen aus West-Ungarn (in German), *Archeometria* Műhely 2016/XIII./1, 55-68.

<h1 style="margin: 0;">BNC</h1> <p style="margin: 0;">Experimental Report</p>	<i>Experiment title</i> Nephrite artefacts in Hungary – the present state of knowledge	<i>Instrument.</i> PGAA <i>Local contact</i> Zsolt Kasztovszky
	<i>Principal proposer:</i> Bálint Péterdi - Geological and Geophysical Institute of Hungary <i>Experimental team:</i> Zsolt Kasztovszky, Szandra Szilágyi, Ildikó Harsányi – MTA EK	<i>Experiment Number</i> <i>Date</i> April 2013 - February 2015

Objectives

Nephrite is mainly known in prehistoric context as raw material for polished stone tools. It is present among archaeological finds in Hungary only in a few numbers. The general aim of our investigations is the detailed petrographic and geochemical examination of the nephrite artefacts found on Hungarian sites, and locating the origin of the raw materials. The material was investigated by non-destructive methods (PGAA, non-destructive SEM-EDX). We have already built a database of the possible nephrite raw material sources of Europe

Results

Based on their chemical composition, most of the artefacts measured so far belong to the serpentinite-related nephrite deposits. On the basis of their microscopic and mineral-chemical features, the artefacts investigated so far can be divided into five raw material types: (1) almost pure tremolite-nephrite with only a few fine grained magnetite or ilmenite grains and some pseudomorphs after pyroxenes; (2) almost pure actinolite-nephrite with only a few very fine grained magnetite or ilmenite grains; (3) almost pure tremolite-nephrite with a few chlorite and some pseudomorphs after pyroxenes; (4) actinolite-nephrite, with chlorite, relict clinopyroxenes (diopside), pseudomorphs after pyroxenes, spinels and garnets. Magnetite, limonite, apatite and titanite also occur. There is a typical association of chromite spinel and grossular garnet in this type; (5) actinolite-nephrite – sometimes also tremolite - with chlorite, relict clinopyroxenes and spinel (chromite), but garnet is missing.

On the basis of our investigations the most probable raw-material sources are the following: type (1) and (3) belongs to Jordanów, Poland. The provenance of the other types are not so clear, but we have candidates from the Swiss Alps.

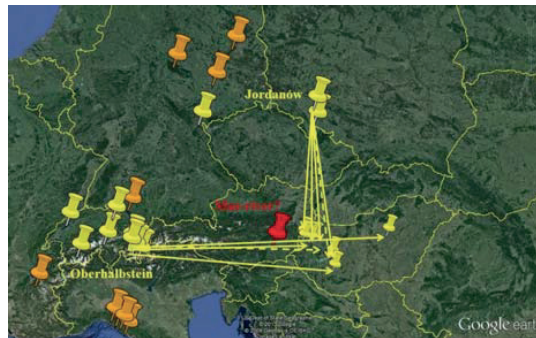
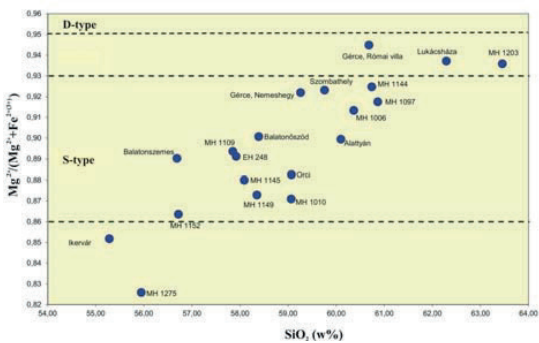


Fig. 1: Classification of the objects, based on PGAA. MH – Mihály Collection, Laczkó Dezső Museum, Veszprém; EH – Ebenhöch Collection, Hungarian National Museum, Budapest

Fig. 2: The most likely raw material sources of the studied artefacts

Reference

B. Péterdi, Z.Bendő, G.Szakmány, Z. Kasztovszky, K.T. Biró and G. Gil, Nephrite artefacts in Hungary – the present state of knowledge, *41st International Symposium On Archaeometry*, May 15-21, 2016 Kalamata, Greece

<p style="text-align: center;">B N C</p> <p style="text-align: center;">Experimental Report</p>	<p><i>Experiment title</i></p> <p>A comparative study of medieval silver coins from Poland and Central Europe</p>	<p><i>Instrument.</i> NIPS-NORMA</p> <p><i>Local contact</i> Zsolt Kasztovszky</p>
<p><i>Principal proposer:</i> Ewa Pańczyk - Institute of Nuclear Chemistry & Technology, Warsaw, Poland</p> <p><i>Experimental team:</i> Ewa Pańczyk - Institute of Nuclear Chemistry & Technology, Warsaw, Poland; L. Szentmiklósi, B. Maróti, Zs. Kasztovszky – MTA EK; Z. Szőkefalvi-Nagy, I. Kovács – MTA Wigner RCP</p>	<p><i>Experiment Number</i> BRR_345_CH</p> <p><i>Date</i> 25-26 June 2013</p>	

Objectives

The Sachsenpfenning struck from the mid tenth century till the end of the eleventh century were selected for the examination. Moreover, the Saxon coins, so called the Otto and Adelheid denarii as well as the Polish ones, the Władysław Herman and Bolesław Śmiały coins were examined as a comparative material. Prompt Gamma Activation Analysis and milli-beam PIXE were chosen as the analytical method on the basis of ready application as non-destructive methods which can be used to study a large number of samples. An overall aim was to determine the provenance and dating of a few groups of the early medieval Central Europe coins.

Results

Totally, 56 coins were studied by means of PGGGA method and 62 coins by PIXE method. Using these methods the concentration of Ag, Cu, Au, Bi, Zn, Hg, Pb, Fe, Mn, As, Se and Sn in investigated coins was determined. The Ag/Cu ratio was measured for the detection of debasement and falsifications.

The evaluation of the results is still in progress. Interpretation of the results of the statistical methods was allowed to differentiate the artefacts in relation to the various production centers, various recipes as well as various raw materials and methods of their purification used. Unique documentation and database for different types of coins is result of these studies.

The obtained results are of a crucial significance for our knowledge of the history of central European coinage and especially of Polish coinage. Various specialists and professionals from the areas of nuclear technique methods, materials research and technology, analytical chemistry and archaeology have involved in this interdisciplinary project.

<h1 style="margin: 0;">BNC</h1> <p style="margin: 0;">Experimental Report</p>	<i>Experiment title</i> A comparative study of non-destructive PGAA and XRF used for provenancing archaeological obsidian	<i>Instrument.</i> PGAA, NAA <i>Local contact</i> Zsolt Kasztovszky
	<i>Principal proposer:</i> Zsolt Kasztovszky – MTA EK <i>Experimental team:</i> Zsolt Kasztovszky, Boglárka Maróti, Szandra Szilágyi, Ildikó Harsányi, Dénes Párkányi – MTA EK	<i>Experiment Number</i> <i>Date</i> February 2013 - June 2015

Objectives

In this study, we have compared the applicability of PGAA and portable XRF equipment in provenance study of obsidians on a selected collection of 81 geological reference samples that belong to the Lithotheca of the Hungarian National Museum. The selection was made in such a way to be representative for the major European-Mediterranean sources. On a limited set of **17** geological reference samples, the performance of Instrumental Neutron Activation Analysis has been tested on the upgraded INAA system of the Budapest Neutron Centre.

Results

PGAA and NAA showed good agreements with the nominal concentration values of JR1 and JR2 geological reference samples. Although only PGAA and NAA provide the real bulk composition of obsidians, and only PGAA and pXRF are non-destructive, all the 3 methods themselves can be effectively and self-consistently used for classification of the samples of different origin. Based on B-, Cl- and Ti-contents, PGAA is even more effective in identification of various types, notably, it can differentiate between the two *Melos*-types (*Adamas* and *Demenegaki*) as well as between *Sardinian A, B* and *C* types.

Interestingly, combination of PGAA and pXRF results does not improve the efficiency of clustering when using AHC.

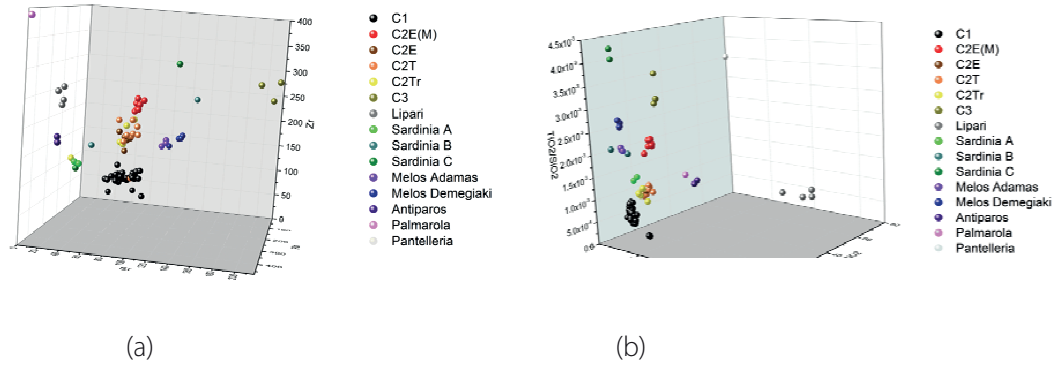


Fig.1. 3D discrimination diagrams of 81 geological obsidians based on (a) XRF – Sr, Rb, Zr and (b) PGAA – Ti, Cl, B

The data analysis is still in progress, the results are expected to be published in a scientific paper.

Reference

Zs. Kasztovszky, B. Maróti, I. Harsányi, D. Párkányi, V. Szilágyi, K. T. Biró, A. Markó, A comparative study of non-destructive PGAA and XRF used for provenancing archaeological obsidian (poster), *International Obsidian Conference*, 1-3 June 2016, Lipari.

<h1 style="margin: 0;">BNC</h1> <p style="margin: 0;">Experimental Report</p>	<p><i>Experiment title</i> PGAA, INAA and luminescence to trace the “history” of “The Panoramic View of Lisbon”: Lisbon before the earthquake of 1755 in painted tiles</p>	<p><i>Instrument.</i> PGAA <i>Local contact</i> Zsolt Kasztovszky</p>
	<p><i>Principal proposer:</i> Maria Isabel Dias, Maria Isabel Prudencio - Centro de Ciências e Tecnologias Nucleares, Lisbon, Portugal</p> <p><i>Experimental team:</i> Maria Isabel Dias, Maria Isabel Prudencio - Centro de Ciências e Tecnologias Nucleares, Lisbon, Portugal; Zsolt Kasztovszky, Boglárka Maróti – MTA EK</p>	<p><i>Experiment Number</i> BRR_344_CH</p> <p><i>Date</i> 02-04 July 2013</p>

Objectives

“The Panoramic View of Lisbon” is a unique masterpiece of Portuguese glazed tiles which depicts the city before the earthquake of 1755. Compositional analysis by PGAA, INAA (at the Portuguese Research Reactor) and XRD, as well as luminescence dating was made for the identification of the raw materials used and the production technology to make the ceramic bodies; and also for a better establishment of the manufacture date of the panel and for the assignment of the artist

Results

The PGAA, INAA, and XRD indicate that the tiles may have been made of carbonated clays from Lisbon region. Gehlenite and wollastonite are the high temperatures phases found in the tiles pointing to firing temperatures around 1000–1100 °C. The luminescence results also indicate a careful production technology at higher temperatures. Reconstruction of the history of radiation exposure of the pieces was accomplished by combining historical records, field, and laboratory analyses. The dating results obtained so far (late 17th, early 18th centuries) are within uncertainties of the expected period for manufacture of the “Vista”, and agree with Jose´ Mecowho for stylistic reasons has attributed the panel to the Spanish tile painter Gabriel del Barco (1648–1703?).

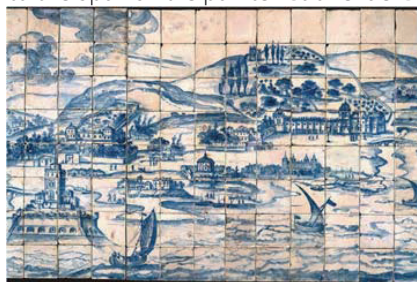


Fig 1: Partial view of “The Panoramic View of Lisbon” panel exhibited in the MNAz (Lisbon, Portugal)

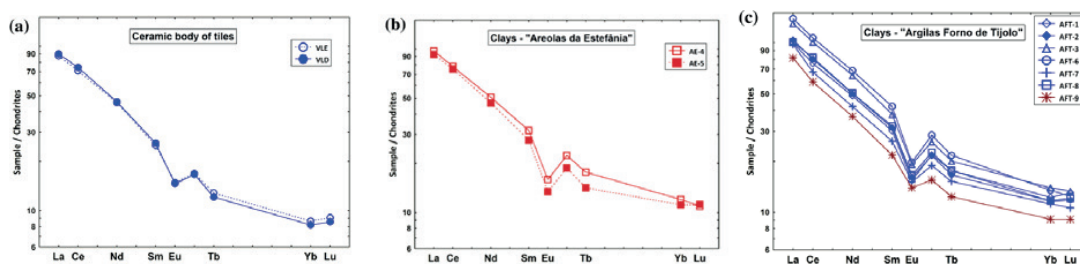


Fig.2: Chondrites-normalized REE patterns of the ceramic body of (a) the two tiles of the panel “The Panoramic View of Lisbon” – VLE and VLD; (b) clays from Lisbon region, “Areolas da Estefânia” formation, and (c) from “Argilas do Forno de Tijolo” formation – measured at the CTN

Reference: Prudencio MI, Dias MI, Burbidge CI, Kasztovszky Zs, Marques R, Marques JG, Cardoso GJO, Trindade MJ, Maróti B, Ruiz F, Esteves L, Matos MA, Pais A, *Journal Of Radioanalytical And Nuclear Chemistry* 307 (2016) 541-547

<p>B N C Experimental Report</p>	<p><i>Experiment title</i> Obsidian Least Destructive Analysis Provenancing System</p>	<p><i>Instrument.</i> PGAA <i>Local contact</i> Zsolt Kasztovszky</p>
<p><i>Principal proposer:</i> Johannes Sterba - Vienna University of Technology, Atominstitut, Austria</p> <p><i>Experimental team:</i> Johannes Sterba, Fabienne Eder - Vienna University of Technology, Atominstitut, Austria; Boglárka Maróti, Zsolt Kasztovszky – MTA EK</p>	<p><i>Experiment Number</i> BRR_346_CH</p> <p><i>Date</i> 19-22 March 2013</p>	

Objectives

The dataset of Obsidian samples from Europe available in Austria was measured with INAA, LA-ICP-MS, PIXE and PIGE. It is aimed to extend the data by the application of PGAA measurements. Especially yet unmeasured elements like H, B and Cl could potentially greatly contribute to the overall chemical fingerprint of the samples and allow easier distinction of closely related obsidian sources, e.g. Demenegakion and Agia Nychia from the Greek island of Melos. With the re-measurement of already known elements, a basis for the intercomparison of the different methods applied will be facilitated.

Results

The expected extension of the dataset was achieved. Good agreement between already measured data and data collected by PGAA was found, so the additional values were accepted into the database. In fact, the additional data made it possible to establish the origin of several samples from a museum collection that were previously all assumed to be from the same source. Those samples could be assigned to several subtypes that have already been identified in the literature. In this way, some ambiguities could be cleared up, strongly enhancing the database.

<h1 style="margin: 0;">BNC</h1> <p style="margin: 0;">Experimental Report</p>	<p><i>Experiment title</i></p> <p>Technology and Provenance Studies of Byzantine Glazed Pottery from Corinth, Greece</p>	<p><i>Instrument.</i></p> <p>PGAA</p> <p><i>Local contact</i></p> <p>Zsolt Kasztovszky</p>
	<p><i>Principal proposer:</i></p> <p>N. Zacharias - University of the Peloponnese</p> <p><i>Experimental team:</i></p> <p>N. Zacharias, M. Xanthopoulou - University of the Peloponnese; Zs. Kasztovszky, B. Maróti – MTA EK</p>	<p><i>Experiment Number</i></p> <p>BRR_352_CH</p> <p><i>Date</i></p> <p>13-15 November 2013</p>

Objectives

The present study makes use of glazed pottery sherds of the Byzantine Era, excavated at Corinth during very recent excavations (2006-2010), in an attempt to tackle technological and provenance questions related to that Era that refer to the ceramic production (4-15th c A.D.) and trade through the Eastern Mediterranean (Italy, Greece, Turkey). Corinth being a major city (by Byzantine standards), it produced and imported a great variety of pottery wares. Archaeological Science/Archaeometry scholars are particularly interested in understanding the technology involved for the production of these glazed pottery, the technology transfer between East and West (Byzantine vs Ottoman) technological practices and, moreover, to provide absolute answers to provenance questions (cf. below) regarding the excavated material.

Results

The analysis of whiteware revealed a uniform production. The vast majority of whitewares were made by the same raw materials (clay Group I), though their provenance has not yet been identified. A lead compound by itself was used for the production of the high-lead glaze, which was applied on unfired ceramic bodies. Only two whiteware samples differ forming a distinct group, taking into consideration both the different clay fabric (Group II) and the different glaze technique (frit).

On the contrary, the redware samples have a high variation in terms of fabrics, glaze composition and manufacturing techniques. Three main fabrics are identified: Group A is an import from Chalkis, Group C is likely another import with a yet unidentified origin and Group B most probably corresponds to the local Corinthian production. The use of each fabric is highly specialised to specific classes of pottery. The political fragmentation of the 13th c. AD caused significant changes in the pottery production: the predominance of few specialized workshops seized and the trade among cities was minimized. In their place, smaller regional workshops flourished, using local raw material of lower quality in order to cover the local needs.

The glazes of the redware samples were produced using a suspension of lead with silica, which was applied either on unfired or biscuit-fired bodies. The glaze firing temperature is estimated at approximately 750 °C. The introduction of technological novelties in the glazing process, which occurred at the early 13th c. AD, resulted to a better control of the firing conditions and therefore the production of homogenous glazes of improved quality.

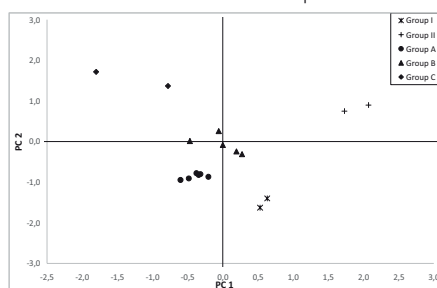


Fig 1: PCA of the ceramic bodies based on PGGA data

Reference: E. Palmara et al., Technology issues of Byzantine glazed pottery from Corinth, Greece, *Microchemical Journal* 129 (2016) 137–150

<h1 style="margin: 0;">BNC</h1> <p style="margin: 0;">Experimental Report</p>	<i>Experiment title</i> Provenance analysis of lapis lazuli	<i>Instrument.</i> PGAA <i>Local contact</i> Zsolt Kasztovszky
	<i>Principal proposer:</i> Judit Zöldföldi - University of Stuttgart, Institute of Materials Testing <i>Experimental team:</i> Judit Zöldföldi, Renate Nöller - University of Stuttgart, Zsolt Kasztovszky – MTA EK, György Káli – MTA Wigner RCP	<i>Experiment Number</i> BRR_321_CH <i>Date</i> 22-27 May 2013

Objectives

In this study, we aimed to extend the existing database of the PGAA and external PIXE measurements on lapis lazuli with samples from occurrences like Tadjikistan, Uzbekistan, Turkistan, Pakistan and Pamir, which were not analysed yet. Additionally, we studied the question of the inhomogeneity within one piece of lapis lazuli. Furthermore, we focused on TOF-ND analyses in order to determine the mineralogical composition non-destructively.

Results

Based on the present experiments, the data base of lapis lazuli samples has grown tremendously. Altogether, we have ca. 90 measurements of lapis lazuli samples from various sources over the world. The results have made it possible, to elaborate further details that can lead to a decision in question: "Where lapis lazuli comes from?".

Because of the fact that PGAA is a bulk analyses, it is particularly suitable to investigate the very inhomogeneous lapis lazuli material, especially in case of archaeological samples: the weathered layer can not be removed from the surface of the high valuable objects, nonetheless, the determination of the chemical composition of the whole object is possible. During the evaluation, we were working with ratios of the determined concentration of the elements, so it was possible to avoid the influence of the inhomogeneity of the raw material to the discrimination of the provenance. The best way to differentiate the lapis lazuli occurrences is to use the ratios Cl/SiO_2 vs. SO_3/Fe_2O_3 .

We also started the investigations of lapis lazuli by TOF-ND. The main difficulties in this area is, that the comparative database is not so extended like in the case of other methods on the one hand and the main mineral of lapis lazuli is a mixed crystal on the other hand, that which complicates the interpretation of the measurements.

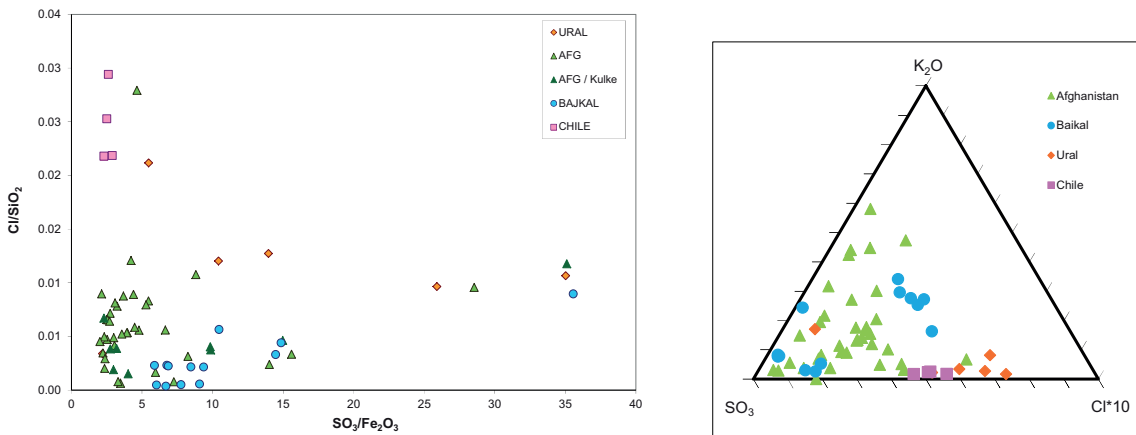


Fig. 1a and 1b: Classification of geological reference lapis lazuli, based on PGAA measurements

<h1 style="margin: 0;">BNC</h1> <p style="margin: 0;">Experimental Report</p>	<i>Experiment title</i> Neutron and X-ray based non-invasive analysis of Pre-historical stone artefacts	<i>Instrument.</i> PGAA Local contact Zsolt Kasztovszky
	<i>Principal proposer:</i> Maria Isabel Dias, Maria Isabel Prudencio - Centro de Ciências e Tecnologias Nucleares, Lisbon, Portugal <i>Experimental team:</i> Zsolt Kasztovszky, Boglárka Maróti, Ildikó Harsányi, Zoltán Kis – MTA EK; Zoltán Szőkefalvi-Nagy, Imre Kovács – MTA Wigner RCP	<i>Experiment Number</i> BRR_376_CH <i>Date</i> 10-14 February 2014

Objectives

This study aims to contribute to provenance issues, by means of compositional studies of both artefacts and potential raw materials (regional and trans-regional). In the case of carbonate rich idols, we are aware that marbles and carbonated rocks deriving from the metamorphic evolution of previous carbonates are difficult to identify, especially when only non-invasive analysis was possible. Elemental composition was obtained by Prompt Gamma Activation Analysis (PGAA) and External Beam PIXE (particle induced X-ray emission); homogeneity of the stone idol and the presence/absence of internal fractures were obtained by neutron radiography.

Results

Obtained results are very promising and useful in general assessments of provenance. The stone artefacts at Perdigões show signs of both nearby and long distance procurement, as well as of unknown attribution, like it was already found for the ceramic materials. Furthermore, different raw material provenances seem to be associated with different contexts and rituals, deepening the contrasts that we can see between these funerary features in Perdigões. No stone idols (between the 13 analysed) from the contexts with cremated remains is related to the Estremadura or Algarve analysed sources. The majority are from the nearby area of Estremoz-Borba-Vila Viçosa, some 30-40 km North of Perdigões, and the rest are from unknown sources. These results support that imported foreign materials were used in parallel with regional available materials.



Fig.1: Stone idols and stone vessels from Perdigões Pre-historic archaeological site. studied at the BNC

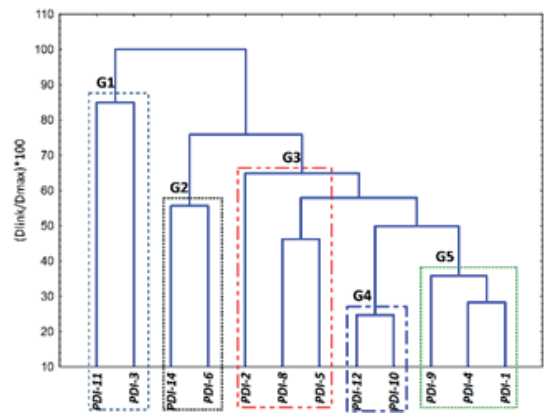


Fig.2: Tree clustering diagram by using the unweighted pair-group average as amalgamation linkage rule and the Euclidean distances as distance measure

<h1 style="margin: 0;">BNC</h1> <p style="margin: 0;">Experimental Report</p>	<i>Experiment title</i> Characterization of bare HPGe gamma spectrometers by <i>geant4</i> Monte Carlo simulations	<i>Instrument.</i> PGAA <i>Local contact</i> László Szentmiklósi
	<i>Principal proposer:</i> L. Szentmiklósi – MTA EK <i>Experimental team:</i> L. Szentmiklósi, B. Maróti – MTA EK	<i>Experiment Number</i> <i>Date</i> 2013

Objectives

to determine the response functions of bare HPGe detectors

Results

The spectrum of a HPGe detector is complex, even if exposed to a mono-energetic gamma radiation. This spectrum, called the detector response function, is a consequence of energy-dependent interaction probabilities of the basic physical processes, the photoelectric effect, the Compton-scattering and the pair production. Our ultimate objective is to accurately determine the response function of a detector at arbitrary energy and geometry, as the real spectrum could be approximated by the weighted sum of these contributions.



Fig.1. the X-ray image and *geant4* implementation of the three HPGe detectors

To achieve this goal, two coaxial and a low-energy HPGe detector were characterized with Monte-Carlo simulations, using the *geant4* toolkit. The geometry of the detectors, including the dimensions of the crystal and the internal structural parts, were initially taken from the factory specifications and from X-ray radiographies, and were later fine-tuned. The detector response functions, with special emphasis on the absolute full-energy peak efficiencies and peak-to-total ratios, were calculated and compared to experimental data taken at different measurement geometries. Between 150 keV and 11 MeV an agreement within 1-2 standard deviation has been achieved, whereas systematic deviations were experienced at lower energies.

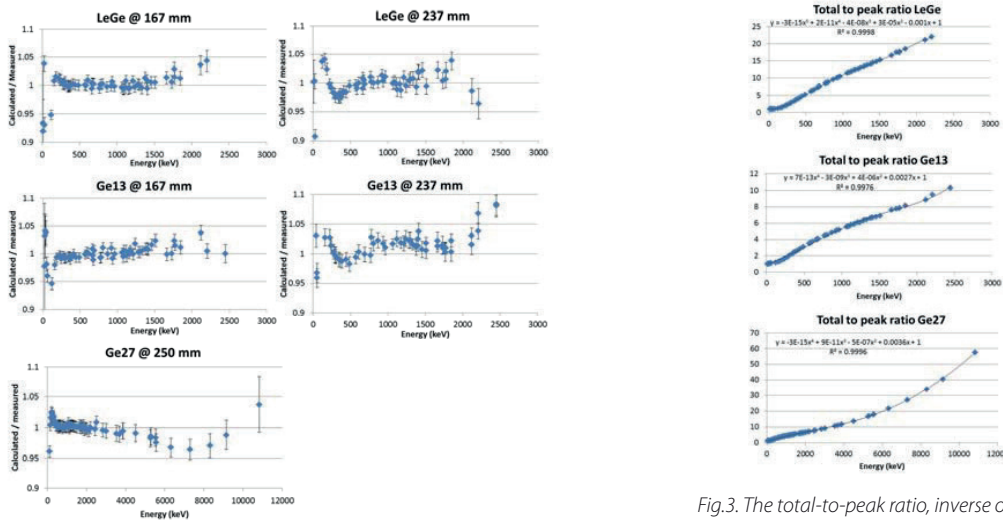


Fig.2. The ratio of calculated over measured full-energy-peak efficiency for the three tested detector

Fig.3. The total-to-peak ratio, inverse of the peak-to-total ratio, can be better interpolated with a 4-5 order polynomial

Reference: L. Szentmiklósi, T. Belgya, B. Maróti, Z. Kis, J Radioanal Nucl Chem (2014) **300** 553–558 DOI 10.1007/s10967-014-2976-6

<h1 style="margin: 0;">BNC</h1> <p style="margin: 0;">Experimental Report</p>	<i>Experiment title</i> Determination of the effective sample thickness via radiative capture	<i>Instrument</i> PGAA <i>Local contact</i> László Szentmiklósi
	<i>Principal proposer:</i> A.M. Hurst – Lawrence Berkeley National Laboratory, USA <i>Experimental team:</i> L. Szentmiklósi – MTA EK	<i>Experiment Number</i> <i>Date</i> 2014

Objectives

to adequately correct for self-absorption of samples during PGAA experiments

Results

For accurate nuclear-data measurements, targets with well defined geometries, thicknesses, homogeneities and compositions (e.g. thin metal foils and pellets) are generally preferred. In many cases, however, this ideal case cannot be achieved. For irradiated powders in particular, the material will need to be held in a sample holder such as a Teflon bag. Consequently, the sample mass is unlikely to distribute itself into a regular shape with a uniform surface; measuring the areal density and thickness, or the average pile density, of these non-uniform samples then becomes extremely challenging.

To solve this issue, a procedure for determining an *effective* thickness of non-uniform irregular-shaped samples via radiative capture is worked out. For the low-energy transitions, the measured cross sections are apparently lower than their standard values due to significant photoelectric absorption of the γ rays within the bulk-sample volume itself. Using standard theoretical techniques, the amount of γ -ray self absorption and neutron self shielding can then be calculated by iteratively varying the sample thickness until the observed cross sections converge with the known standards.

The amount of overall attenuation, therefore, provides a measure of the apparent, effective, thickness of the sample volume illuminated by the neutron beam. In general, this measured effective thickness is likely to be somewhat less than the true thickness represented by the entirety of the bulk sample material, and the amount of absorption and self shielding from an integration over the true thickness may constitute an over estimate of the correction factor. Furthermore, γ -ray transmission through samples with high neutron-capture cross sections, or low- γ materials, is far less likely to be impeded to a measurable extent.

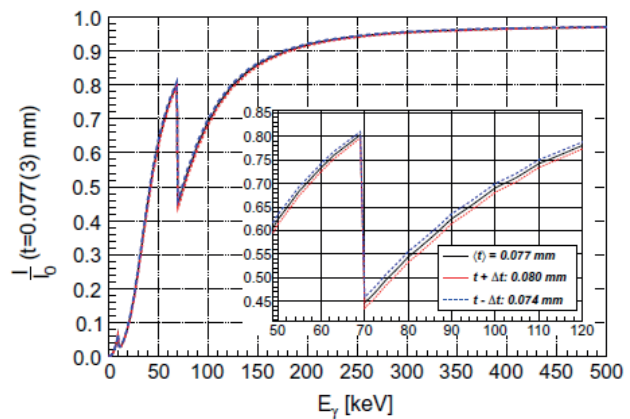
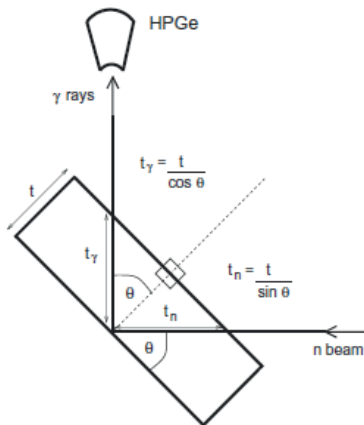


Fig.1. The sketch of the PGAA geometry. Fig. 2. attenuation factor, for the ^{186}W sample assuming $t = 0.077(3)$ mm thickness

Reference: A.M. Hurst, N.C. Summers, L. Szentmiklósi, R.B. Firestone, M.S. Basunia, J.E. Escher, B.W. Sleaford, Determination of the effective sample thickness via radiative capture, Nuclear Instruments and Methods in Physics Research B 362 (2015) 38–44

<h1 style="margin: 0;">BNC</h1> <p style="margin: 0;">Experimental Report</p>	<i>Experiment title</i> Composition determination of sol-gel derived SiO₂-CaO bioactive glasses	<i>Instrument</i> PGAA <i>Local contact</i> Ildikó Harsányi
	<i>Principal proposer:</i> Pál Jóvári - Wigner RCP of HAS <i>Experimental team:</i> Boglárka Maróti, Ildikó Harsányi – Centre for Energy Research	<i>Experiment Number</i> <i>Date</i> 2014.09.19-2014.09.25

Objectives

to understand the microscopic origin of bioactivity and the functional differences between conventional (melt quenched) and sol-gel derived glasses. To determine the bulk elemental composition of sol-gel derived CaO-SiO₂ glasses and in particular their hydrogen content by PGAA technique

Results

Sol-gel derived glasses exhibit appreciable differences compared to bulk (melt-quenched glasses) at the microstructure as well as at the morphological or textural (porosity, etc.) properties. Calcium and phosphorus containing silicate glasses exhibit bioactivity, which pertains to the ability of the material to form bonds to living tissues in vivo. The previous attempts to model the structure of sol-gel derived CaO-SiO₂ glasses by fitting neutron and X-ray diffraction data was not yet successful due to the poor quality of fits. Neutron diffraction measurements indicated the presence of large amount (> few atomic%) ¹H in our samples, indicating that sample compositions significantly deviate from the nominal values. The elemental compositions including the hydrogen contents were successfully determined. PGAA results verified the high hydrogen content in the samples. Knowing the composition of the material reliable structural models can be set up. The interpretation of the results is under way.

AM39 SiO ₂ -40Ca(F) - oxygen calculated								AM21 SiO ₂ -40Mg(F) - oxygen calculated							
Elem	Atom %	unc %	abs unc	Weight %	Ox. state	unc %	abs unc	Elem	Atom %	unc %	abs unc	Weight %	Ox. state	unc %	abs unc
H	34.9	1.0	0.3	0.853	1	0.8	0.007	H	48.0	1.2	0.6	1.536	1	1.0	0.015
B	167 ppm	1.0	1.7 ppm	43.9 ppm	3	0.8	0.4 ppm	B	159 ppm	1.3	2.0 ppm	54.5 ppm	3	1.1	0.6 ppm
Si	41	1.2	0.5	28	4	1.4	0.4	Mg	21	3.9	0.8	16	2	4	0.6
Cl	50 ppm	5	2.5 ppm	43 ppm	-1	5	4.3 ppm	Si	31	1.9	0.6	28	4	1.8	0.5
Ca	24	2.0	0.5	23	2	1.9	0.4	Gd	0.19 ppm	7	0.01 ppm	1.0 ppm	3	7	0.07 ppm
O (spectr.)								O (spectr.)							
O calc.				48	-2			O calc.				55	-2		
Σ	99.9			99.9				Σ	100.0			100.5			
Si/Ca	1.71	2.3	0.04	1.22		2.4	0.03	Si/Mg	1.48	4.3	0.06	1.75		4.4	0.08
AM24 SiO ₂ -30Ca(F) - oxygen directly from spectrum								AM50 SiO ₂ -30Ca(N) - oxygen calculated							
Elem	Atom %	unc %	abs unc	Weight %	Ox. state	unc %	abs unc	Elem	Atom %	unc %	abs unc	Weight %	Ox. state	unc %	abs unc
H	37.4	1.1	0.4	0.963	1	1.0	0.010	H	31.3	1.4	0.4	0.728	1	1.0	0.007
B	127 ppm	1.3	1.7 ppm	34.3 ppm	3	1.0	0.3 ppm	B	24.5 ppm	1.4	0.3 ppm	6.12 ppm	3	1.1	0.07 ppm
Si	45	1.3	0.6	31	4	1.6	0.5	Si	49	1.4	0.7	32	4	1.8	0.6
Cl	20 ppm	16	3 ppm	18 ppm	-1	16	3 ppm	Cl	13 ppm	8	1 ppm	10 ppm	-1	8	0.8 ppm
Ca	18.0	2.4	0.4	18	2	2.3	0.4	Ca	20	2.5	0.5	19	2	2.4	0.5
Gd	0.47 ppm	6	0.03 ppm	1.9 ppm	3	6	0.1 ppm	O (spectr.)							
O (spectr.)								O calc.				49	-2		
O calc.				50	-2			Σ	100.3			100.7			
Σ	100.4			99.9				Si/Ca	2.45	2.9	0.07	1.68		3.0	0.05
Si/Ca	2.50	2.7	0.07	1.73		2.8	0.05								

AM19 Bonalive							
Elem	Atom %	unc %	abs unc	Weight %	Ox. state	unc %	abs unc
H	0.46	3.0	0.01	95 ppm	1	2.9	2.8 ppm
B	5.1 ppm	1.7	0.09 ppm	1.12 ppm	3	1.4	0.02 ppm
Na	36	1.7	0.6	17.1	1	2	0.3
Si	44	1.5	0.7	25	4	1.7	0.4
P	3.0	5	0.1	1.9	5	5	0.1
Ca	16.5	2.4	0.4	13.5	2	2.3	0.3
O (spectr.)							
O calc.				42	-2		
Σ	100.0			99.5			
Si/Na	1.22	2.2	0.03	1.46		2.5	0.04
Si/P	14.7	5.1	0.8	13.2		5.1	0.7
Si/Ca	2.67	2.9	0.08	1.85		2.9	0.05

Table 1. the obtained compositions of the five samples.

<h1 style="margin: 0;">BNC</h1> <p style="margin: 0;">Experimental Report</p>	<i>Experiment title</i> Re-determination the boron content in the NIST SRM 57b certified reference material	<i>Instrument.</i> PGAA <i>Local contact</i> László Szentmiklósi
	<i>Principal proposer:</i> J.R. Sieber – NIST Chemical Sciences Division, Gaithersburg, USA <i>Experimental team:</i> B. Maróti, L. Szentmiklósi – MTA EK	<i>Experiment Number</i> <i>Date</i> 2014

Objectives

to re-determine the boron content of the NIST SRM 57b certified reference material

Results

In a recent paper by P. Galler (J. Anal. At. Spectrom., 2014 **29** 614-622 DOI: 10.1039/C3JA50383F) discrepancy arose regarding the boron content of the NIST SRM 57b [1] certified reference material. The reference B value of 12.5 ± 2.1 ppm came out as an average of an earlier PGAA result (14.3 ± 0.2 ppm) and an apparently biased ICP-OES data (10.6 ± 0.4 ppm) that were not in agreement [2]. Following the discussions with J.R. Sieber of NIST, the coordinator of this CRM, it was decided to measure this material at the Budapest PGAA facility, at NIST and elsewhere, and reconsider the certificate.

New measurements were performed by E.A. Mackey, A.F. Marlow, R.L. Paul, and J.R. Sieber of the NIST Chemical Sciences Division. Additional measurements were performed by R. Martin, Globe Metallurgical, Inc. (Beverly, Ohio); P. Galler, K. Blandhol, A. Storesund, A.S. Elkem, and M. Grønn, Technology Central Analytical Laboratory (Kristiansand, Norway); A. Raab, S. Freitag, and J. Feldmann, University of Aberdeen (Aberdeen, Scotland); and here at the BNC by L. Szentmiklósi and B. Maróti. Statistical consultation for this SRM was provided by D.D. Leber and A.N. Heckert of the NIST Statistical Engineering Division.

Z	El	M	m meas	unc %	m Bkg	unc %	m net	c% atom	unc %	c% el/el	unc %
1	H	1.00794	1.97E-4	2.5	2.07E-5	1.9	1.76E-4	0.32	3.4	115 ppm	3.5
5	B	10.811	2.33E-5	0.8	4.77E-8	1.5	2.32E-5	39.2 ppm	2.2	15.1 ppm	2.2
14	Si	28.0855	1.53	2.1		0.0	1.53	99	0.01	100	0.01
22	Ti	47.867	5.44E-4	2.7		0.0	5.44E-4	210 ppm	3.4	350 ppm	3.4
23	V	50.9415	4.28E-5	12.		0.0	4.28E-5	15 ppm	11.	28 ppm	11.
25	Mn	54.93805	1.19E-4	3.2	6.03E-6	6.	1.13E-4	38 ppm	4.0	74 ppm	4.0
26	Fe	55.845	5.14E-3	2.5	1.28E-4	4.	5.02E-3	0.164	3.3	0.33	3.3
27	Co	58.9332	2.70E-5	4.		0.0	2.70E-5	8.4 ppm	5.	18 ppm	5.
64	Gd	157.25	1.06E-6	6.		0.0	1.06E-6	0.12 ppm	6.	0.69 ppm	6.

Table.1. The analysis results at the Budapest PGAA facility for NIST SRM 57b

During revision, our data for hydrogen, boron, cobalt, and vanadium were considered and evaluated along with the data by other parties and the NIST itself. As a result an updated boron data 14.43 ± 0.27 ppm came out on 28 April 2015, replacing the original certificate issued on 07 November 2006. This exercise once again proved the accuracy of our laboratory.

Reference

1. NIST SRM 57B updated certificate, <https://www-s.nist.gov/srmors/certificates/57B.pdf>
2. John R. Sieber et al, Validation of an alkali reaction, borate fusion, X-ray fluorescence method for silicon metal, NIST Internal report.

<h1 style="margin: 0;">BNC</h1> <p style="margin: 0;">Experimental Report</p>	<i>Experiment title</i> Applicability of non-destructive neutron techniques to investigate archaeological silver – a pilot study	<i>Instrument.</i> PGAA, TOF-ND, NIPS-NORMA, NAA <i>Local contact</i> László Rosta
	<i>Principal proposer:</i> Zsolt Mráv – Hungarian National Museum <i>Experimental team:</i> Zsolt Kasztovszky, Boglárka Maróti, Zoltán Kis, Dénes Párkányi, János Osán – MTA EK; László Rosta, György Káli – MTA Wigner RCP	<i>Experiment Number</i> <i>Date</i> 12-13 February 2013 February and April 2015

Objectives

The aim of this pilot study was to investigate, how effectively can the available neutron-based techniques be applied to provide useful information for the research of the unique and high valued Seuso treasure, PGAA, neutron radiography, TOF-ND, in-beam NAA, and other non-destructive techniques (portable XRF, PIXE and micro-XRF) have been applied on contemporary (Roman) and modern objects.

Results

The major components (Ag, Cu and Au) were possible to determine with high accuracy using bulk- and surface methods. The results of different methods (PGAA, pXRF, PIXE) agree well. The phase composition and microstructural studies using TOF-ND revealed that the Roman objects (fibula and the part of the quadripus) are homogenous and isotropic casted silver, but the casting methods are slightly different. Neutron radiography provides a high resolution image of the “niello” on the foot of the fibula, suitable for further structural studies. Moreover, neutron imaging can be applied only in case of the objects with less than 5 mm.

Comparison of silver content (Cu balance)					
Ag*m/m%	PGAA	PIXE	XRF átlag	XRF	TOF ND
Csúszka	93.30	94.22	n.d.	93.02	94.70
Fibula	93.24	93.96	95.26	95.36	96.14

Table 1: Comparison of silver content of the Roman silver objects – determined by various methods

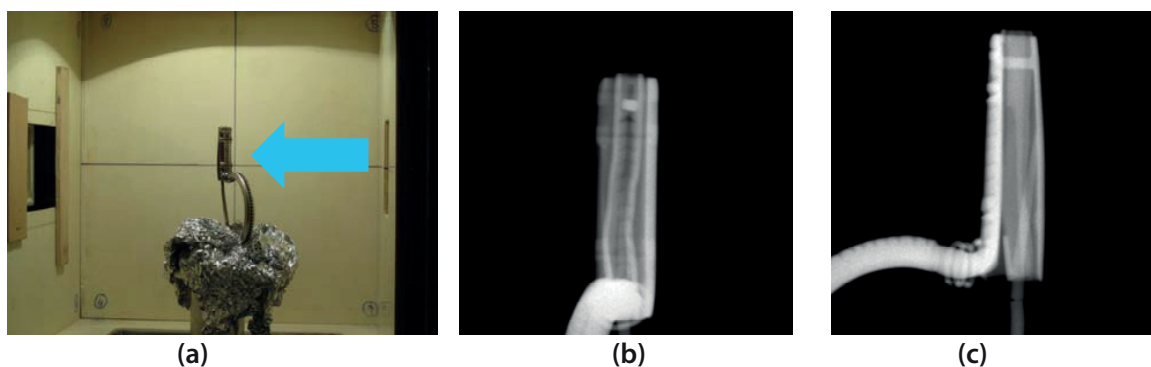


Fig.1: (a) Experimental set-up at the NIPS-NORMA station and (b) and (c) neutron radiography images of the Roman fibula

<h1 style="margin: 0;">B N C</h1> <p style="margin: 0;">Experimental Report</p>	<i>Experiment title</i> Nephrite artefacts in Hungary – the present state of knowledge	<i>Instrument.</i> PGAA <i>Local contact</i> Zsolt Kasztovszky
	<i>Principal proposer:</i> Sándor József Sztáncsuj - Muzeul Național Secuiesc, Sfântu Gheorghe, Romania <i>Experimental team:</i> Sándor József Sztáncsuj - Muzeul Național Secuiesc, Sfântu Gheorghe, Romania, Zsolt Kasztovszky, Ildikó Harsányi – MTA EK	<i>Experiment Number</i> BRR_378_CH <i>Date</i> 03-07 November 2014

Objectives

The Ariușd Culture is the western (Transylvanian) group of the Copper Age Ariușd-Cucuteni-Tripolje Cultural Complex (cca. 4500-3800 B.C.). Although its eponym settlement (Ariușd/Erősd-Tyiszk-hegy) is known in the archaeological literature from the beginning of the 20th century, the lithic material of the whole group has never been studied by petroarchaeological methods, until very recent times. The main objective of the present study was to provide information on the geochemical composition of the main raw material types identified on the most prominent archaeological sites of the Ariușd Culture. The selected samples are subjected to non-destructive Prompt Gamma Activation Analysis (PGAA) in the Budapest Neutron Centre. The data we will obtain by the analysis can help us to specify the individual raw material categories, and on the long run, to be able to identify the prehistoric raw material sources, used in the process of the manufacturing of stone tools.

Results

PGAA was applied for a number of 34 lithic material samples, most of them (27 pcs.) proving from the eponym settlement (Ariușd-Tyiszk-hegy). A smaller number of samples were collected from the archaeological material of our recent excavations on the contemporary site of Boroșneu Mic/Kisborosnyó-Borzvára (7 pcs.). The samples were chosen in order to represent the main suspected raw material types (*i.e.* Carpathian obsidian, Prut- and Volhynian flint, Balkan flint and several raw materials of local, Eastern Carpathian origin).

The evaluation of the experimental data is still in progress. The data obtained will be compared with the results on samples from Ariușd, Boroșneu Mic and Olteni/Oltsem-Vármege. Further analysis of samples collected from geological sources will hopefully indicate the closer provenience of these materials. As a conclusion we're already able to determine the main long-distance trade lithic materials used in the Copper Age Eastern Transylvania, which are the moldavian Prut flint and the Volhynian flint. Beside them, we can document the trade of the Carpathian obsidian, proving most probably from North-East Hungary (Tokaj-Eperjes Mts.) and some varieties of the Balkan and Banat flint.

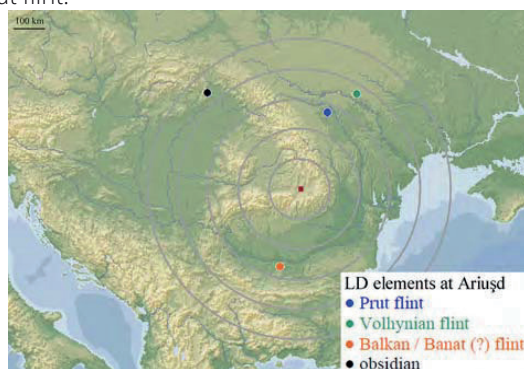


Fig.1: Long distance contacts of the Ariușd site on the basis of the petroarchaeological analysis results

Reference: S. J. Sztáncsuj, Katalin T. Biró, Zs. Kasztovszky, S. Józsa, K. Gméling, B. Maróti, Lithic Implements At Ariușd (Erősd) A Preliminary Report, Communications Archaeologiae Hungariae 2014, pp. 19-36.

<h1 style="margin: 0;">BNC</h1> <p style="margin: 0;">Experimental Report</p>	<i>Experiment title</i> Evaluation of prompt gamma-ray data and nuclear structure of Niobium-94 with statistical model calculations	<i>Instrument.</i> PGAA <i>Local contact</i> László Szentmiklósi
	<i>Principal proposer:</i> D. Turkoglu – Graduate School of the Ohio State University, USA <i>Experimental team:</i> L. Szentmiklósi, B. Maróti – MTA EK	<i>Experiment Number</i> <i>Date</i> 17-18 Sept 2014

Objectives

to determine the radiative neutron capture spectrum and level scheme of Nb-94

Results

Niobium alloys, such as niobium-bearing zirconium (Zr-1Nb), are used in nuclear reactors as fuel cladding material due to high corrosion and radiation resistance. Additionally, a novel, accident-tolerant fuel incorporates a high thermal conductivity material, such as niobium. The focus of this work is applying the methodology used for measuring and evaluating prompt γ -ray data for the EGAF to the niobium element. Gamma-ray transitions following neutron capture in ^{93}Nb have been studied at the cold-neutron beam PGAA facility at the Budapest Research Reactor. Measurements have been performed using a coaxial HPGe detector with Compton suppression. The Nb_2O_5 target had a mass of 0.47144 gram and 99.5% purity. The powder sample had approximate dimensions of 8 mm \times 24 mm, a thickness less than 1 mm and 4.47 g/cm³ theoretical density. It was irradiated for 23.9 hours with a 1.4% dead time. A 39.6-hour count of the background accompanied the measurement for identification of background γ -rays.

Partial γ -ray production capture cross sections have been deduced relative to that of the 255.9-keV transition after cold-neutron capture by ^{93}Nb . With a subsequent measurement of a NbCl_5 target that had a 0.2-gram mass, 6 mm \times 16 mm dimensions, 1.2-mm thickness, theoretical density of 2.75 g/cm³ and 99.995% purity for 15.6 hours at a 4.8% dead time, this partial cross section was internally standardized to the cross section for the 1951-keV transition after cold-neutron capture by ^{35}Cl . The resulting (0.1377 ± 0.0018) barn partial cross section produced a calibration factor that was 23% lower than previously measured for the EGAF database. The thermal-neutron cross sections were deduced for the $^{93}\text{Nb}(n,\gamma)^{94\text{m}}\text{Nb}$ and $^{93}\text{Nb}(n,\gamma)^{94\text{g}}\text{Nb}$ reactions by summing the experimentally measured partial γ -ray production cross sections associated with the ground-state transitions below the 396-keV level and combining that summation with the contribution to the ground state from the quasi-continuum above 396 keV, determined with Monte Carlo statistical model calculations using the DICEBOX computer code. These values, σ_m and σ_0 , were (0.83 ± 0.05) barn and (1.16 ± 0.11) barn, respectively, and found to be in agreement with literature values. Comparison of the modelled population and experimental depopulation of individual levels confirmed tentative spin assignments and suggested changes where imbalances existed.

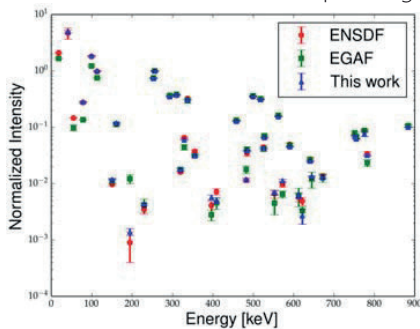


Fig.1. Comparison of intensities $\sigma_{\gamma}(1+\alpha)$ normalized to the 255.9-keV transition for ENDF, EGAF and this work.

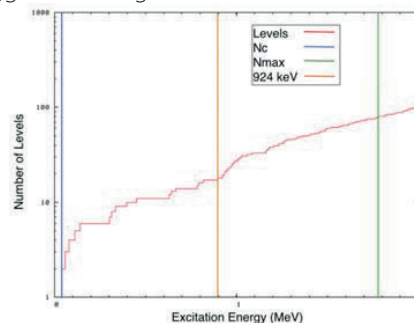


Fig.2. The cumulative plot of known ^{94}Nb discrete levels with increasing excitation energy

References

- D Turkoglu, S Basunia, A Hurst, R Firestone, L Szentmiklósi, L Cao: ^{93}Nb thermal neutron capture cross section from prompt γ -ray intensities, *Trans. Am. Nucl. Soc.* **111** 560-563 (2014)
 D Turkoglu, Evaluation of Prompt Gamma-Ray Data and Nuclear Structure of Niobium-94 with Statistical Model Calculations, Ph.D. dissertation, The Ohio State University 2014

<h1 style="margin: 0;">BNC</h1> <p style="margin: 0;">Experimental Report</p>	<i>Experiment title</i> Compositional analysis of certified standard copper alloys (BCR-691) using 27% coaxial HPGe detector, and high resolution LEGe detector	<i>Instrument</i> PGAA, NIPS <i>Local contact</i> László Szentmiklósi
	<i>Principal proposer:</i> Boglárka Maróti <i>Experimental team:</i> Boglárka Maróti, László Szentmiklósi, Tamás Belgya – Centre for Energy Research	<i>Experiment Number</i> BRR-xxx <i>Date</i> 2014-2015

Objectives

to determine the bulk elemental composition of standard copper alloys

Results

The five bronzes (Fig. 1/a) which were analysed in this study have a composition that is representative for the major copper alloys known in antiquity (Constantinides et al. 2001). Our goal was to quantitatively determine additional alloying components besides the certified elements (As, Sn, Pb and Zn). For the preparation of the alloys pure (purity > 99%) elemental powders were used, and were mechanically blended. The production procedure was described in more detail by Ingelbrecht et al. in 2001 (Report EUR 19778/1 EN). By the standard PGAA setup (27% HPGe) additional Fe, Mn and Ni content was determined, and with LEGe detector, Sb could be quantified, too (see Fig 1/c-d).

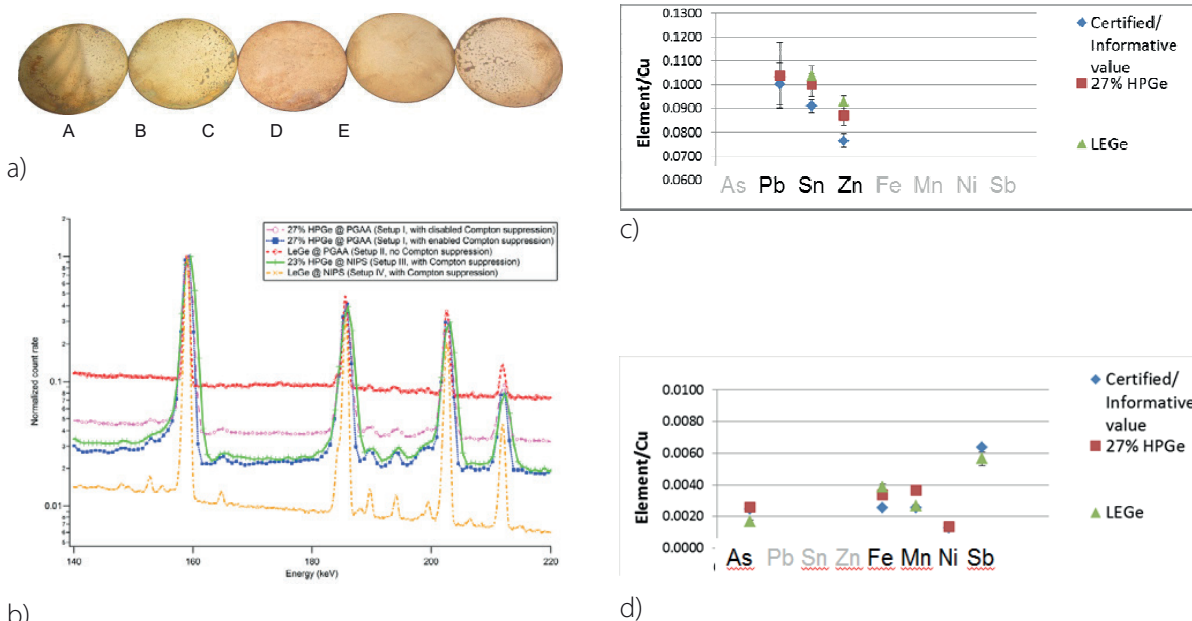


Figure 1. a) five pieces of the BCR-691 standard copper alloy series b) comparison of the BCR-691 A alloy spectra recorded by different Ge detectors c-d) comparison of elemental compositions (BCR-691 A) determined using 27% HPGe and LEGe detectors.

Better signal-to-background ratios were found in the case of Compton-suppressed LEGe than 27 % coaxial HPGe up to 0.5 MeV (see Fig 1/d). The S/B ratios of the two coaxial detector and Compton-suppressed LEGe were comparable between 1 and 2 MeV, while 27 % HPGe of Setup I had the best amplitude/background ratio above 2 MeV. The better energy resolution also opens the way to improve the partial gamma-ray production cross-section data of a few elements with highly-complicated spectra at low energies.

References:

Maróti B, Szentmiklósi L, Belgya T, Compton-suppressed low energy germanium (LEGe) detector for metal analysis by PGAA, Abstract at 25th Seminar on Activation Analysis and Gamma Spectroscopy (SAAGAS), 2015. 02. 23-25. Aachen, Germany
Maróti B, Szentmiklósi L, Belgya T, Comparison of low-energy and coaxial HPGe detectors for prompt gamma activation analysis of metallic samples. *Journal of Radioanalytical and Nuclear Chemistry*, online first, DOI 10.1007/s10967-016-4822-5
Maróti B. et al. (2016) to be submitted

BNC Experimental Report	<i>Experiment title</i> Elemental composition analysis of Pt, Ru and Ir containing Ti mesh monolith catalysts	<i>Instrument.</i> PGAA <i>Local contact</i> Boglárka Maróti
	<i>Principal proposer:</i> Erika Szabados <i>Experimental team:</i> Boglárka Maróti, Erika Szabados, Antal Tungler – Centre for Energy Research	<i>Experiment Number</i> xxxxxxx <i>Date</i> 2015.02.11-04.24

Objectives

to determine the precious metal content of the Ti mesh monolith catalysts in a completely non-destructive way

Results

The amount of platinum group element (such as Ru and Ir) content is one of the most important parameters of the monolith catalysts. Due to the properties of Ti, the analytical methods requiring the dissolution of relatively large catalyst samples in strong mineral acids at extreme conditions were excluded. Prompt gamma activation analysis (PGAA) was chosen for the sample can be placed into the neutron beam as received. Another advantage of this method could be that besides the metals, carbon content of the catalysts (if significant) can also be measured. However the error of C content measurement is rather high, as the sensibility of PGAA for carbon is low.

Ten samples cut from the catalyst mesh about 180–220 mg of each were analyzed using PGAA (see Fig. 1a and 1b). The commercial catalyst and its reduced version, before and after usage were characterized with PGAA method (besides TPR, SEM with EDX, XPS techniques). The precious metal content of the bulk Ti mesh monolith catalysts was successfully determined, however the carbon content was below the detection limit of the PGAA method. Catalytic wet oxidation of N,N-dimethylformamide was tested in designed experiments without and with Ru–Ir on Ti mesh monolith catalysts. During ~55 h usage the precious metal loss was insignificant.

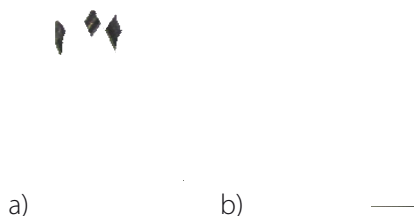


Fig. 1 a) Ti mesh monolith catalyst and b) the catalyst placed in the PGAA sample holder.

References

Szabados E , Srankó DF, Somodi F , Maróti B , Kemény S , Tungler A. Wet oxidation of dimethylformamide via designed experiments approach studied with Ru and Ir containing Ti mesh monolith catalysts *Journal Of Industrial And Engineering Chemistry* 34: pp. 405-414. (2016)

<h1 style="margin: 0;">BNC</h1> <p style="margin: 0;">Experimental Report</p>	<i>Experiment title</i> In situ PGAA studies of HBr oxidation over Deacon catalysts	<i>Instrument</i> PGAA <i>Local contact</i> László Szentmiklósi
	<i>Principal proposer:</i> J. Pérez-Ramírez – ETH Zürich, D. Teschner – Fritz-Haber Institute Berlin <i>Experimental team:</i> M. Moser, V. Paunovic, G. Zhen, L. Szentmiklósi	<i>Experiment Number</i> BRR_381 <i>Date</i> 2015.01.12-23

Objectives

To determine the Br and Cl uptake on the rutile-type catalysts during HBr and HCl oxidation

Results

The gas-phase oxidation of the hydrogen halides was studied in a quartz fixed-bed micro-reactor (8 mm internal diameter) at ambient pressure and in the temperature range of 413–713 K. The reactor was loaded with 0.5 g of RuO₂ or 0.23 g of TiO₂ catalyst (particle size = 0.4–0.6 mm) or 0.4 g of various ceria-zirconia mixed oxides and was placed inside a furnace in the path of the neutron beam (Fig. 1). A total volumetric flow of 250 cm³ STP min⁻¹ consisting of 10 vol.% HBr or HCl (Air Liquide, anhydrous) and 0–90 vol.% O₂ (Linde, purity 4.5) balanced in N₂ (Linde, purity 5.0) was continuously fed. Furthermore, 0–4 vol.% Br₂ (Acros, 99.8%) were added to the gas feed by passing a split of the N₂ flow through a saturator filled with liquid Br₂ at STP conditions. The halogen formation was quantified by iodometric titration. Br, Cl, Ru, Ti, Ce, and Zr were determined from the characteristic peak areas. The surface coverage was calculated as the amount of halogen per surface sites taking into account the surface area of the catalysts and the density of sites of the (110) and (101) facets weighted by their relative occurrence. The gas-phase signals of HBr, Br₂, HCl, and Cl₂ were subtracted, thus, all reported values corresponded only to the solid catalyst.

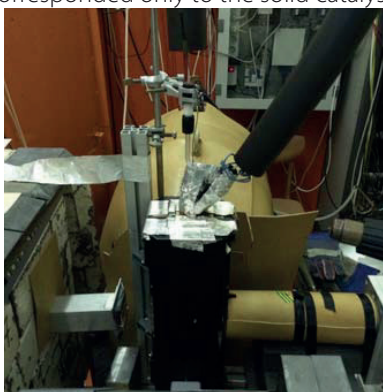


Fig.1. The PGAA setup with the micro-reactor and the furnace

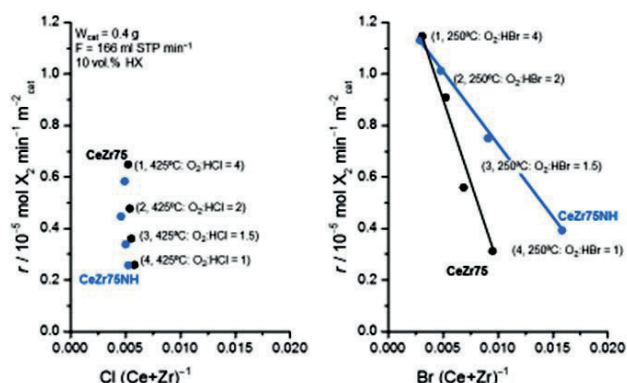


Fig.2. The Cl or Br content in homogeneous or non-homogeneous CeZr mixed oxides. Note the difference in tendencies between chlorination and bromination

In an attempt to enhance the stability of CeO₂, it has been shown that the use of ZrO₂ as a carrier could significantly promote the performance of ceria compared to Al₂O₃ and TiO₂ and exhibited lower chlorine uptake during reaction compared to CeO₂/Al₂O₃. By comparing the homogeneous and non-homogeneous CeZr-oxides (e.g. CeZr75 and CeZr75NH) it was found that Cl content and rate are very similar at the surface, in contrast to the Br content, where the non-homogeneous particles tend to brominate stronger than the homogeneous materials, thus the homogeneous Ce-Zr sample is preferred for bromination (Fig. 2).

References

1. M. Moser, V. Paunovic, G. Zhen, L. Szentmiklósi, M. Hevia, M. Higham, N. Lopez, D. Teschner, J. Perez-Ramirez, Chemical Science (2016) **7** 2996–3005
2. M. Moser, G. Vilé, S. Colussi, F. Krumeich, D. Teschner, L. Szentmiklósi, A. Trovarelli, J. Pérez-Ramírez, J. Catal. **331** 128–137 (2015)
3. M. Moser: Bridging HCl and HBr Oxidation over Heterogeneous Catalysts for Halogen Production, Ph.D. thesis, ETH Zürich, ETH-Zürich, 2016, No. 23186

<h1 style="margin: 0;">BNC</h1> <p style="margin: 0;">Experimental Report</p>	<i>Experiment title</i> Compositional Analyses of Bioactive Glass	<i>Instrument.</i> PGAA <i>Local contact</i> László Szentmiklósi
	<i>Principal proposer:</i> G. Chass – Queen Mary University of London <i>Experimental team:</i> L. Szentmiklósi, B. Maróti – MTA EK	<i>Experiment Number</i> BRR_406 <i>Date</i> 12-14 Dec 2013 06 July 2015 12-14 Dec 2015

Objectives

to follow the time-evolution of cementation bioactive cements

Results

At ISIS, the cementation of multiple bioactive cements is extensively studied. As a complementary technique, PGAA was attempted to reveal potential changes in the peak count rates of major components during the setting of the bioactive cements, potentially attributed to evaporation or dilatation. The raw materials with brand names CHEMFLEX, KETAC, ESPE and FUJU IX were measured for elemental compositions. Subsequently the two constituents were mixed and the time-dependent data collection was immediately started. Only the hydrogen signal showed significant change with time, the count rates of other components were found to be stationary.

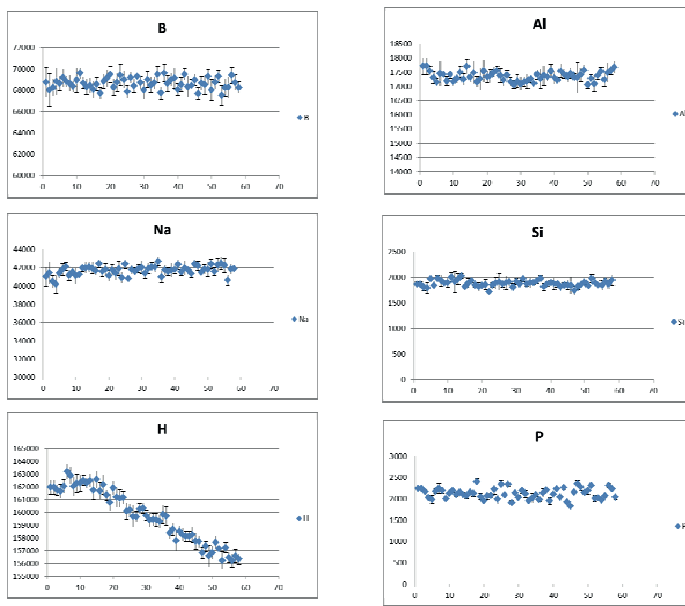


Fig. 1. Time evolution of the setting cement sample over 60 × 1200 sec time slices

Special attention was paid to the shape-parameter of the boron peak that has to some extent dependence on the matrix composition or local density. Unfortunately no clear variation beyond the statistical uncertainty could be observed.

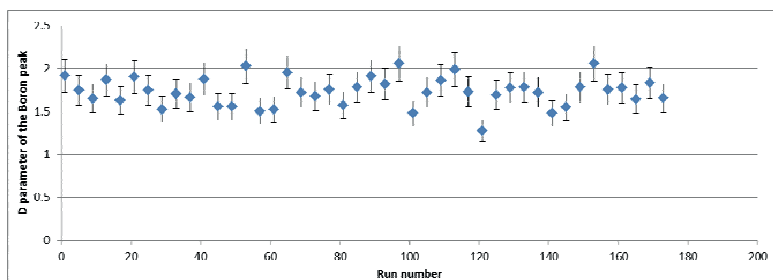


Fig. 2. The time series of the D peak shape parameter of the Boron peak during setting.

<h1 style="margin: 0;">BNC</h1> <p style="margin: 0;">Experimental Report</p>	<i>Experiment title</i> Jade and related HP greenstone polished stone implements from Hungary	<i>Instrument.</i> PGAA <i>Local contact</i> Zsolt Kasztovszky
	<i>Principal proposer:</i> György Szakmány - Department of Petrology and Geochemistry, Eötvös Loránd University <i>Experimental team:</i> Zsolt Kasztovszky, Boglárka Maróti, Ildikó Harsányi – MTA EK	<i>Experiment Number</i> <i>Date</i> February 2015 - September 2015

Objectives

Good quality high pressure (HP) metaophiolite rock types suitable for making stone implements, like jade and eclogite, are absent from the geological formations of Carpathian Basin and its surroundings. Therefore, this raw material type was unknown among Hungarian findings for a long time, and henceforward this is one of the rarest raw materials of polished stone implements in Hungary. The nearest geological locality where these raw materials can be found is over 1000 kms away. The specific form and integrity of these stone implements indicate that they were transported as complete artefacts. Non-destructive PGAA and SEM-EDS were applied to determine the possible sources of the raw material.

Results

Based on these data stone implements were divided into raw material type groups. Our results are corresponding to results on HP metaophiolites of North-western Italy, obtained both on geological and archaeological samples. Based upon these facts, the HP metaophiolite stone implements in Hungary probably originated from the same raw material sources as Italian (and other Western European) HP metaophiolite stone tools. According to technical literature, these primary sources can be the Monviso, the Voltri Massif and secondary in the resedimented Oligocene conglomerates in Quaternary of River Po, Staffora and Curone equally.

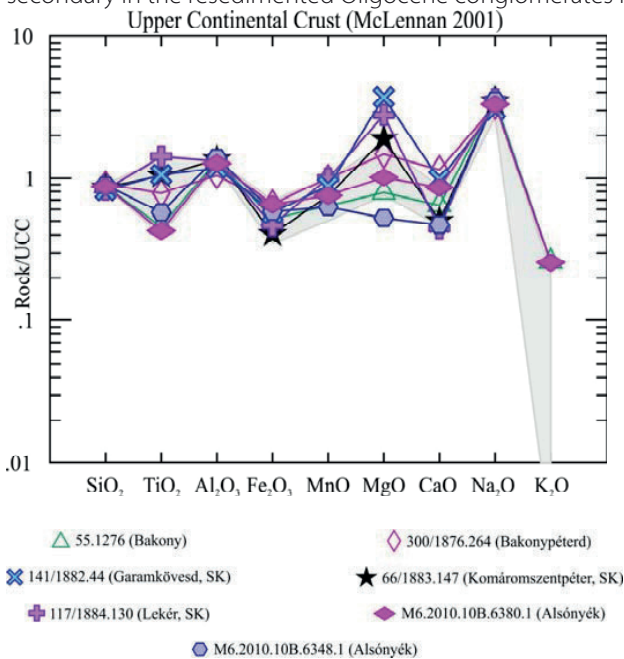


Fig.1: Bulk rock chemistry of jadeitites, measured by PGAA



Fig. 2: Possible origin of jadeitite and other „green stone” raw materials

Reference: Bendő et al., Jades and related HP greenstone polished stone implements from Hungary, *Raw materials exploitation in Prehistory*, 10-12 March 2016, Faro, Portugal

<h1 style="margin: 0;">BNC</h1> <p style="margin: 0;">Experimental Report</p>	<i>Experiment title</i> Investigation of ^{186}Re via radiative thermal-neutron capture on ^{185}Re	<i>Instrument.</i> PGAA <i>Local contact</i> László Szentmiklósi
	<i>Principal proposer:</i> J.J. Carrol – U.S. Army Research Laboratory, USA <i>Experimental team:</i> L. Szentmiklósi – MTA EK; D.A. Matters – Air Force Institute of Technology, USA	<i>Experiment Number</i> <i>Date</i> 12-19.05.2015

Objectives

to determine the radiative neutron capture spectrum and level scheme of ^{186}Re

Results

Partial γ -ray production cross sections and the total radiative thermal-neutron capture cross section for the $^{185}\text{Re}(n,\gamma)^{186}\text{Re}$ and the $^{187}\text{Re}(n,\gamma)^{188}\text{Re}$ reactions were measured at PGAA with an enriched ^{185}Re target (96.74% ^{185}Re and 3.26% ^{187}Re , $m = 0.15076$ g) and ^{187}Re target (99.52% ^{187}Re , $m = 0.07386$ g). The Re cross sections were standardized using well-known $^{35}\text{Cl}(n,\gamma)^{36}\text{Cl}$ cross sections from irradiation of a stoichiometric $^{\text{nat}}\text{ReCl}_3$ target.

The resulting cross sections for transitions feeding the ^{186}Re ground state from low-lying levels below a cutoff energy of $E_c = 746$ keV were combined with a modeled probability of ground-state feeding from levels above E_c to arrive at a total cross section of $\sigma_0 = 111(6)$ barn for radiative thermal-neutron capture on ^{185}Re . A comparison of modeled discrete level populations with measured transition intensities led to proposed revisions for seven tentative spin-parity assignments in the adopted level scheme for ^{186}Re . Additionally, 102 primary γ rays were measured, including 50 previously unknown. A neutron-separation energy of $S_n = 6179.59(5)$ keV was determined from a global least-squares fit of the measured γ -ray energies to the known ^{186}Re decay scheme. The total capture cross section and separation energy results are comparable to earlier measurements of these values.

The analysis of the ^{188}Re prompt gammas and the DICEBOX simulation of its level scheme are still in progress.

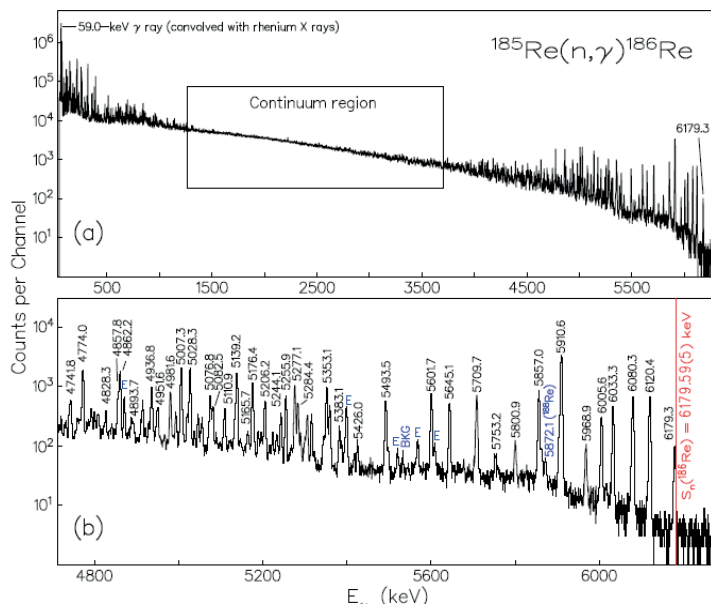


Fig.1. The prompt γ -ray spectrum from the $^{185}\text{Re}(n,\gamma)^{186}\text{Re}$ reaction. S_n denotes the neutron binding energy

Reference: D.A. Matters, A.G. Lerch, A.M. Hurst, **L. Szentmiklósi**, J.J. Carroll, B. Detwiler, Zs. Révay, J.W. McClory, S.R. McHale, R.B. Firestone, B.W. Sleaford, M. Krčička, T. Belgya, Investigation of ^{186}Re via radiative thermal-neutron capture on ^{185}Re , Phys. Rev. C 93, 054319 (2016), DOI: 10.1103/PhysRevC.93.054319

<h1 style="margin: 0;">BNC</h1> <p style="margin: 0;">Experimental Report</p>	<i>Experiment title</i> Novel investigations on the mineralogy of Carpathian mahogany obsidian	<i>Instrument.</i> PGAA <i>Local contact</i> Károly Lázár
	<i>Principal proposer:</i> Katalin T. Biró, András Markó – Hungarian National Museum <i>Experimental team:</i> Károly Lázár, Viktória Kovács Kis, Zsolt Kasztovszky – MTA EK, Adél Len – MTA Wigner RCP	<i>Experiment Number</i> <i>Date</i> June 2015

Objectives

The occurrence of red (or mahogany-coloured) obsidian from the vicinity of Tolcsva was reported in the 19th century. In the archaeological collections the first piece of mahogany obsidian was spotted among the finds of the Arka Upper Palaeolithic settlement. In 2005, it was possible to re-identify the primary source of mahogany obsidian near Tolcsva. The surroundings supplied, nevertheless, mainly the common black C2T type black obsidian. The aim of this study to identify the mineralogical / geochemical difference between the mahogany and the black obsidian both collected from the Szokolya hill near Tolcsva – based on PGAA, TEM and Mössbauer-spectroscopy measurements.

Results

The chemical composition of the amorphous matrix of the mahogany obsidian was compared with that of the grey sample, based on TEM studies. Both obsidians proved to be aluminosilicate glasses, however, the mahogany sample contains more alkali elements (**Na** and **K**) than the grey sample. The grey sample contained **0.18-0.3 at%** Fe, while the iron content of the mahogany sample was one order of magnitude less ($\ll 0.1$ at%). Thus, the iron content of the parent lava in case of the mahogany sample seems to differentiate during cooling which lead to the formation of the hematite nanocrystals. The Mössbauer spectrum of the dark gray sample is dominated by the contributions of ferrous ions. It can easily be decomposed to two Fe(II) doublets, as reported for several other samples collected from various locations. The mahogany sample exhibits a distinctly different spectrum. The decomposition attests for the dominance of ferric components.

To summarize, the bulk chemical composition of the mahogany and grey obsidians from the same locality does not differ significantly. However, the iron content of the glassy phase is significantly lower in the mahogany obsidian than in the grey one. Furthermore, a certain amount of Fe is dominant in different phases, in case of mahogany and grey obsidians. The differences between the red and grey variants could be also explained by the different oxidation states of the Fe-ions (Fe(III)).

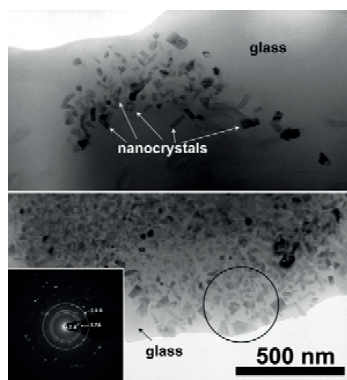


Fig. 1: Bright field images and SAED of the mahogany sample

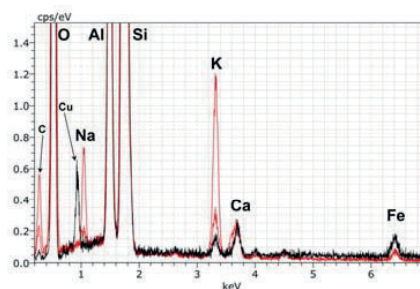


Fig. 2: TEM-EDS of the grey (black line) and mahogany samples (red lines) from Tolcsva.

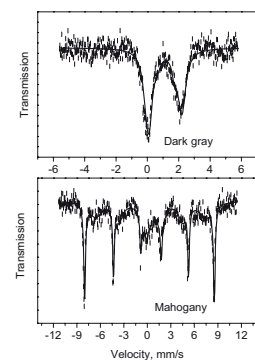


Fig. 3 Mössbauer spectra of dark grey and mahogany obsidians from Tolcsva

Reference: K. Lázár, V. Kovács Kis, A. Len, Zs. Kasztovszky, A. Markó, K. T. Biró, Novel investigations on the mineralogy of Carpathian mahogany obsidian (poster), *International Obsidian Conference*, 1-3 June 2016, Lipari.

<h1 style="margin: 0;">B N C</h1> <p style="margin: 0;">Experimental Report</p>	<i>Experiment title</i> Experimental search for the bound state singlet deuteron in the radiative $n - p$ capture	<i>Instrument.</i> PGAA <i>Local contact</i> Tamás Belgya
	<i>Principal proposer:</i> Yu.N. Pokotilovski – Joint Institute for Nuclear Research, Dubna, Russia M. Jentschel – Institut Laue-Langevin, Grenoble, France <i>Experimental team:</i> T. Belgya, L. Szentmiklósi, B. Maróti – MTA EK	<i>Experiment Number</i> BRR_423 <i>Date</i> 24-31 March .2015

Objectives

to search for an indication about the postulated existence of singlet deuteron

Results

Singlet deuteron is usually considered as not bound, but as a virtually bound state with binding energy $B < 0$ indicating unstable configuration. Recently claims appeared in the literature that the binding energy of the n-p pair in the singlet state might be positive, and singlet deuteron is stable in respect to decay to neutron and proton. We performed an experimental search for the bound state singlet deuteron predicted by such microscopic calculations. The predicted energy of this metastable level is in vicinity of the deuteron disintegration threshold. This state should manifest itself in two-photon transition following thermal neutron capture by protons.

To confirm or dismiss this speculation, (n, γ) experiments were carried out using Milli-Q water, pieces of polyethylene and plexiglass as targets. The gamma radiation was observed with the Compton-suppressed PGAA as well as an unsuppressed LeGe detector. The experiment aimed at finding a second gamma-ray in a possible cascade through a high-statistics gamma measurement of cold neutron capture on hydrogen nuclei.

The main difficulty in interpretation of this experiment is that one has to confidently rule out all other sources of peaks, including the background of gamma-rays generated in the target and in material surrounding the target and detectors. Numerous peaks from neutron capture by different isotopes of Ge, Cl, ^{56}Fe , ^{27}Al , ^{12}C , ^{14}N , etc. have been observed. We detected >250 peaks in the total spectrum up to 10 MeV. To scrutinize the scattered-neutron background, a block of carbon was also measured in addition to the beam background. It was proven that the signal-to-background ratio of the Budapest PGAA system is superior to those of the FRM II and ILL neutron capture facilities.

The region 2152-2164 keV attracted a special interest, as it contains double peak with energies 2156.3 and 2158.8 keV, for which there was found no positive identification yet, neither in the prompt, nor in the radioactive gamma-ray databases (Fig 1).

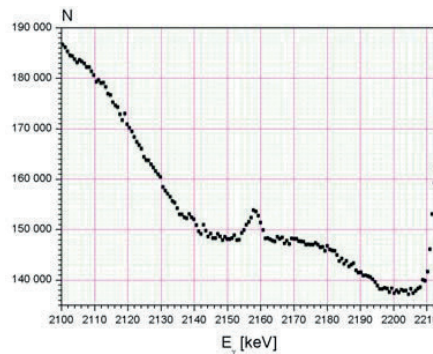


Fig.1 The spectrum region between 2152-2164 keV using the Milli-Q water target

As a tentative result, a constraint for the peak area ratio of the searched peak corresponding to transition $^3S_1 - S_0$ vs. the main transition $^3S_1 - S_1$ with the energy 2223 keV was deduced, giving $R < 6 \times 10^{-6}$. This means, that the cross-section of such reaction is less than $2b$ (two standard deviations). These results require independent confirmation before publication.

<h1 style="margin: 0;">BNC</h1> <p style="margin: 0;">Experimental Report</p>	<i>Experiment title</i> Contribution to the petroarchaeological study of radiolarites in the Carpathian Basin	<i>Instrument.</i> PGAA <i>Local contact</i> Zsolt Kasztovszky
	<i>Principal proposer:</i> Katalin T. Biró – Hungarian National Museum <i>Experimental team:</i> Zsolt Kasztovszky, Ildikó Harsányi – MTA EK	<i>Experiment Number</i> <i>Date</i> September 2015

Objectives

Radiolarites are deep-sea sedimentary siliceous rocks, composed mainly of skeletal elements of Radiolaria. By the parallel investigation of source-collected and archaeological chipped stone assemblages, certain „phenotypes” could be separated among the lithic raw materials. By the accumulation of petroarchaeological data it became evident that possibly interacting „phenotypes” should be also considered. On the southernmost regions of Hungary, especially in early Neolithic lithic assemblages, raw materials similar to Szentgál and Úrkút-Eplény radiolarite variants were located in much higher number than „rational” for the distance from the sources and the general pattern of distribution encountered. The problem for us was the lack of information on the potential raw material sources.

Results

Most of the radiolarite samples contain over 90% silica. The quantities of SiO₂ and CaO are complementary and characterise the quality of the siliceous rocks rather than its provenance. Both the cluster diagram and the PCA show (Fig 1) that the data are weakly sorted. Some categories like Bakony radiolarites and Bosnian Jurassic radiolarites tend to cluster together while Mecsek and Gerecse radiolarites occupy a much wider range. The bivariate plot (made on the basis of boron and chlorine concentrations) demonstrate similar pattern (Fig. 2). Certainly, the current data are not adequate to assign archaeological pieces unambiguously into source regions on the basis of the geochemical data.

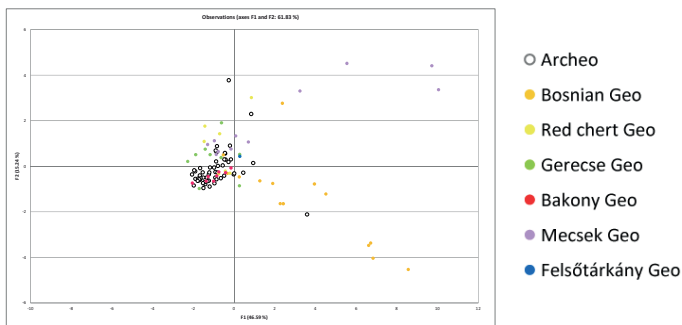


Fig. 1: PCA of the PGAA data

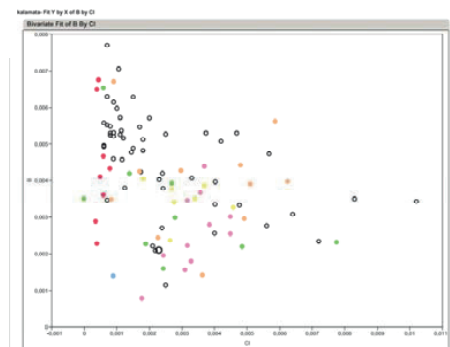


Fig 2: Bivariate plot of the PGAA data

References:

- K. T. Biró, V. Szilágyi, Zs. Kasztovszky, Új adatok a Kárpát-medence régészeti radiolarit forrásainak ismeretéhez, *Archeometriai Műhely* (2009) 6(3), pp. 25-44
- K.T. Biró, Z. Kasztovszky, S. Józsa, A. Markó, Contribution to the petroarchaeological study of radiolarites in the Carpathian Basin, *41st International Symposium On Archaeometry*, May 15-21, 2016 Kalamata, Greece

<h1 style="margin: 0;">BNC</h1> <p style="margin: 0;">Experimental Report</p>	<i>Experiment title</i> PGAA, SR-based FTIR and Raman spectroscopies investigation of XIX century A. D. decorated pottery fragments from Azerbaijan archaeological site	<i>Instrument.</i> PGAA <i>Local contact</i> Zsolt Kasztovszky
	<i>Principal proposer:</i> Valentina Venuti - Università degli Studi di Messina <i>Experimental team:</i> Valentina Venuti, Barbara Rossi - Università degli Studi di Messina; Zsolt Kasztovszky, Szandra Szilágyi – MTA EK	<i>Experiment Number</i> <i>Date</i> 01-03 July 2015

Objectives

The main goal of the present study is to introduce a combined methodological approach involving different spatial regimes, based on PGAA, SR-FTIR and SR-Raman spectroscopies, to define raw materials and pigments used for the potteries production, so achieving crucial information in order to clarify technological features and preparation processes typical of the local population. Up to now, these samples have not been investigated from an archaeometric point of view, and only preliminary measurements have been performed by SEM-EDS. Morphological analysis revealed the presence of three layers: ceramic body, decorated layer and probably alteration patina. For the ceramic body, the presence of the same raw materials for all the investigated samples has been evidenced, whereas the surface layers showed Cu, Pb and Fe.

Results

The glazed potteries coming from Agsu were distinguished in two main groups based on different petrographic and compositional features of the samples. It suggests the probably presence of different production technologies and raw materials explicable partly with the site position as crossroad of commercial routes. In particular, two types of clay were identified: a more heterogeneous clay rich in quartz, plagioclase, feldspar and hematite employed in Group 1; a more selected clay constituted essentially by quartz and plagioclase used in Group 2. XRD analysis suggested the reaching of similar firing temperatures higher than 850°C thanks to the “fingerprint” diopside in both groups. Group 1 shows compositional features close to the Chinese production.

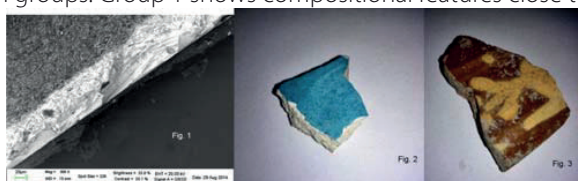


Fig. 1-3: Microscopic and normal photos of some objects

Spectr. Nr.	AS86		AS87		AS88		AS89		AS90		AS91		AS92		AS93	
Code	BR3		BR4		BR2		BR7		BR8		BR1		BR5		BR6	
Description	ceramics		ceramics		ceramics		ceramics		ceramics		ceramics		ceramics		ceramics	
	c% el/ox	Rel. unc %	c% el/ox	Rel. unc %	c% el/ox	Rel. unc %	c% el/ox	Rel. unc %	c% el/ox	Rel. unc %	c% el/ox	Rel. unc %	c% el/ox	Rel. unc %	c% el/ox	Rel. unc %
El																
H	0.18	1.2	0.12	1.4	0.27	1.1	0.15	1.4	0.05	1.4	0.09	1.4	0.14	1.3	0.05	1.4
B	0.00851	1.2	0.00692	1.3	0.00756	1.1	0.00844	1.3	0.05374	1.4	0.03651	1.4	0.00748	1.3	0.04191	1.4
Na	1.68	2.4	0.84	2.9	1.51	2.9	0.72	3.4	5.35	2.0	4.87	2.3	1.06	2.5	5.00	2.1
Mg	1.8	6.	1.5	6.	1.3	7.	1.5	7.	0.9	6.	0.7	7.	1.2	6.	1.6	5.
Al	7.8	1.6	9.3	1.6	7.6	1.9	9.4	2.4	6.1	1.9	7.1	1.8	8.9	1.7	6.4	1.9
Si	27.0	0.9	28.7	0.9	27.1	0.8	28.6	0.9	33.8	0.6	34.3	0.6	29.0	0.8	32.8	0.6
S	0.11	7.			0.10	6.			0.15	3.1	0.10	4.		0.27	3.1	
Cl	0.092	1.7			0.107	1.8	0.001	18.	0.073	1.9	0.144	1.7	0.004	4.	0.181	1.6
K	2.30	1.7	2.82	1.8	2.30	1.7	2.95	1.8	1.30	1.9	1.02	2.2	2.65	1.8	1.42	1.9
Ca	7.3	2.2	1.6	4.	7.6	2.2	1.8	3.9	1.8	2.9	1.2	3.2	0.8	3.8	2.8	2.5
Sc	0.0012	10.	0.0017	8.	0.0021	12.	0.0017	8.								
Ti	0.427	2.6	0.774	2.6	0.426	2.5	0.786	2.6	0.071	3.0	0.062	2.9	0.495	2.9	0.099	2.7
V	0.021	6.	0.014	6.	0.018	6.	0.016	6.	0.001	20.	0.001	15.	0.015	6.	0.005	10.
Mn	0.114	2.7	0.097	2.8	0.117	3.2	0.090	2.7	0.024	2.8	0.015	3.4	0.091	1.9	0.026	3.2
Fe	4.32	2.2	5.31	2.4	4.50	2.3	5.33	2.6	0.56	2.9	0.52	3.1	4.79	2.2	0.65	2.8
Co															0.026	2.1
Cu									1.0	3.0	0.34	2.9				
Nd	0.0033	7.	0.0060	7.	0.0026	9.	0.0055	7.	0.0030	9.	0.0016	8.	0.0043	8.	0.0020	7.
Sm	0.00036	2.6	0.00058	2.0	0.000395	1.9	0.000567	2.0	0.000151	2.4	0.000133	5.	0.000515	1.8	0.000155	5.
Gd	0.00045	9.	0.00068	6.	0.00048	9.	0.00070	6.	0.00015	15.	0.00014	10.	0.00062	6.	0.00018	5.
Pb			1.5	18.			1.0	18.						4.0	6.	
SUM w/o O	53.23		52.57		52.94		52.38		51.26		50.49		53.17		51.42	
O (calc)	46.8		47.4		47.1		47.6		48.7		49.5		46.8		48.6	

Table 1: Composition of the ceramic fragments, measured by PGAA

B N C Experimental Report	<i>Experiment title</i> Comparative PGAA and NAA measurements on reference materials	<i>Instrument.</i> PGAA, NAA <i>Local contact</i> Katalin Gméling, Ibolya Sziklai, Dénes Párkányi
	<i>Principal proposer:</i> MTA EK NAL and also in the framework of IAEA-WEPPAL round measurement and proficiency test (2013) <i>Experimental team:</i> Katalin Gméling, Dénes Párkányi, Ibolya Sziklai-László– MTA EK	<i>Experiment Number</i> Date 2013.04.10. 2013.06.27. 2013.09.05.-09.12.

Objectives

Participation in inter-comparison tests has been a way to control the performance of laboratories. Our neutron activation analysis (NAA) laboratory participated in the IAEA TC projects RAF4022, RER1007 and RLA0037 in the previous years (2015-2011), organized by the WAGENINGEN Evaluating Programs for Analytical Laboratories (WEPPAL). In 2013 our prompt gamma activation analysis (PGAA) laboratory joined our NAA lab to participate in the round measurements.^[1] The scopes were not only to prove the good performance of the labs, but also to show: (1) the complementarity of NAA and PGAA methods, which allows nearly panoramic analysis of the samples, from light elements to the rear earth elements; (2) the good comparability of results due to the same nuclear physical basis of the methods. Next to WEPPAL soil samples, geological reference materials were determined by NAA and PGAA, both using the k_0 -standardization method. Results were introduced as an oral presentation on the 6th International k_0 -Users' Workshop (2013), and published in the Proceedings of the Workshop.^[2]

Results

PGAA gives precise results for major elements (Si, Ti, Al, Fe, Mn, Mg, Ca, Na, K and—as a unique method—for H), for some of the light trace elements as B and Cl, as well as for Sc, S, Cr, Co, Ni, Cd, Nd, Sm and Gd. NAA is sensitive for the rare earth elements, and for many major (Ti, Al, Fe, Mn, Mg, Ca, Na, K) and trace elements (e.g.: Sc, V, Cr, Co, Ni, Cu, Zn, As, Se, Rb, Sr, Zr, As, Sb, Ce, Ba, Hf, Ta, W). For most major elements the results obtained by the two methods show good agreement. The comparison of the results obtained for trace elements is not always possible, since PGAA is less sensitive and concentrations are often below its detection limits.

Obviously, NAA outperforms PGAA considering the number of elements analysed and the detection limits. NAA has the capability to provide the concentration value of more than forty elements. Since different nuclides of one element can be detected either simultaneously or via different protocols, NAA has a self-validation character. It is highly specific due to the individual characteristics of the induced radionuclide. However, Si, B, H and Cd, could only be measured by PGAA, and Cl and Gd results of PGAA are more reliable than the NAA values. Furthermore, PGAA is a real non-destructive method, does not require sample preparation, and its analysis turnaround time is much shorter than that of NAA. The statistical evaluation of the results and the use of reference materials are indispensable to keep the analysis under control.

From the experience of geochemical analysis, it can be stated that a single analytical method is not sufficient to form a comprehensive geological conclusion. PGAA and NAA procedures were found to be well suited for the characterization of geological samples. The two nuclear analytical methods complement each other in elemental coverage and provide independent results for the major and several trace elements.

References

[1] I Sziklai-László, K. Gméling (2013): Results of the k_0 -based instrumental neutron activation analysis (k_0 -INAA) for WEPPAL plant and soil IPE/ISE 2013 in Hungary. In *Annex on CD-ROM of IAEA TECDOC*. TECDOC and Annex connected to IAEA TC project RER1007: Workshop on inter-comparison feedback of NAA and other analytical techniques proficiency tests performed in 2012–2013.

[2] K. Gméling, A. Simonits, I. Sziklai László, D. Párkányi (2014): Comparative PGAA and NAA results of geological samples and standards. *J. Radioanal Nucl. Chem.* **300**. 507-516.

BNC Experimental Report	<i>Experiment title</i> Analysis of Titanium implants	<i>Instrument.</i> PGAA, NAA <i>Local contact</i> Boglárka Maróti Dénes Párkányi
	<i>Principal proposer:</i> Zsófia Szalmás <i>Experimental team:</i> Boglárka Maróti, Dénes Párkányi – Centre for Energy Research, Zsófia Szalmás – Semmelweis University	<i>Experiment Number</i> BRR-403 <i>Date</i> 2014.

Objectives

to determine the minor and trace elements in different Titanium dental implants

Results

The goal of the present research was the examination of the electrochemical behaviour of Titanium dental implants at neutral and acidic pH in artificial saliva solutions (e.g. Ringer- and Fusayama-Meyer – solution), with and without fluoride. Another aim was to examine the corrosion procedure of the implants at oral conditions, (e.g. when the implants are integrated in the jawbone and palate, and the consumed food, drink and gastric solution affects to its composition). The implants are standing from 2 parts, but the composition of the under – and upside is not the same.

Impurities can strongly affect the electrochemical properties of Ti implants. The aim of the PGAA and NAA measurements is to precisely characterize the bulk compositions of the samples, and to achieve more accurate data to support the electrochemical calculations.



Fig. 1 Titanium implants sealed in Teflon bags for the PGAA measurements.

With PGAA the main component (Ti) could be determined. In this matrix, the estimated detection limits for Ni, Cu, Fe and Co are 0.2, 0.1, 0.2 and 0.04 weight%, respectively.

Using NAA method, ten trace elements were determined. See Table 1.

Element	Concentration (mg/kg)	Relative uncertainty (%)
As	26.6	3.5
Au	1.2	3.5
Co	0.08	4.7
Cr	4.3	3.9
Fe	155	3.7
Hg	0.11	23
Mo	11.5	7.5
Sb	6.4	5.5
Sn	200	4.5
Ta	0.1	4.2

Table. 1 Impurities in the Titanium implants determined by NAA method.

<h1 style="margin: 0;">BNC</h1> <p style="margin: 0;">Experimental Report</p>	<i>Experiment title</i> Neutron and gamma dose rate and flux measurements at imaging station RAD	<i>Instrument</i> RAD <i>Local contact</i> Kis Zoltán
	<i>Principal proposer:</i> Zoltán Kis – Centre for Energy Research <i>Experimental team:</i> Zoltán Kis, László Horváth, Gábor Benyács – Centre for Energy Research	<i>Experiment Number</i> Date 2014.08.25-2014.11.06

Objectives

to measure the dose rate levels and neutron fluxes at various positions of the RAD imaging facility

Results

Measuring the dose rate levels and neutron fluxes at various positions of the RAD imaging facility is important to be able to assess the dose burden on the components. During these measurements there was no intention to measure the dose rate levels outside the biological shielding, where staff members and guests stay.

There are, practically, two interesting positions of the facility, where the measurements took part: at the sample positions in the beam in front of the scintillation screen (206 cm and 282 cm to the beam port), and at the position of the camera chip. The measurements in the beam were to determine the neutron fluxes for three energy ranges of the beam: thermal (sub-cadmium), epithermal and fast (above 2.9 MeV). The thermal and epithermal flux were measured using bare and Cd-covered Au foils, while for the fast part the Ni-58(n,p)Co-58 reaction was used. The gamma dose rate was measured by standard Fricke solution, and Gaf and Sunna films. At chip position (about 70 cm far from the beam perpendicularly) a Bonner sphere and a Geiger-Müller counter were used for neutron and gamma dose rate measurements, respectively.

The thermal neutron fluxes at the two sample positions are $4.64 \times 10^7 \text{ cm}^{-2}\text{s}^{-1}$ and $3.38 \times 10^7 \text{ cm}^{-2}\text{s}^{-1}$, respectively. The beam has a neutron to gamma ratio of $1.72 \times 10^5 \text{ cm}^2\text{mR}^{-1}$ and a cadmium ratio of 3.3. The thermal to epithermal flux measured by the cadmium covered and bare gold monitor method is about 51. The beam diameter is adjustable up to a maximum of 230 mm. The gamma-ray intensity in the neutron beam measured with thermoluminescence dosimetry is about 8.5 Gy/h. The ambient dose rate from neutrons and gamma-rays at the position of the digital camera chip were 20 mSv/h and 4 mSv/h. As a consequence beam filtering might be advantageous to shield the camera and avoid the bright spots in the images.

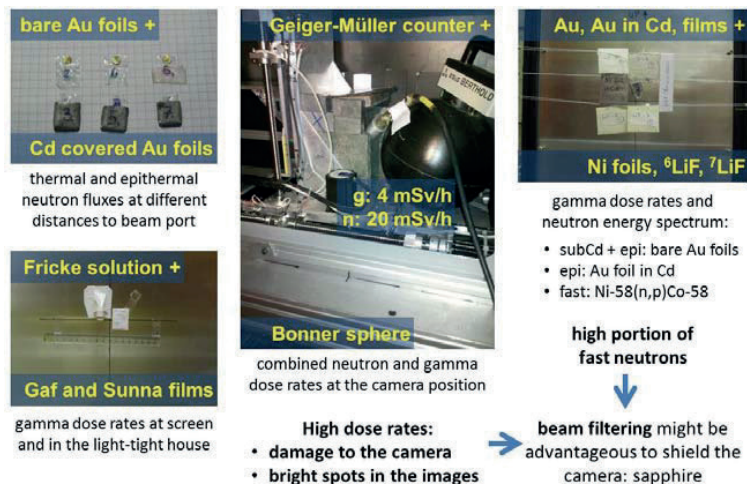


Figure 1: (a) Measuring the dose rate levels and neutron fluxes at various positions of the RAD imaging facility.

References

Z. Kis, L. Szentmiklósi, T. Belgya, M. Balaskó, L. Z. Horváth, B. Maróti: Neutron based imaging and element-mapping at the Budapest Neutron Centre, Physics Procedia **69**, 40-47 (2015)

<h1 style="margin: 0;">B N C</h1> <p style="margin: 0;">Experimental Report</p>	<i>Experiment title</i> Improvement of the neutron and X-ray imaging station, RAD at channel No. 2 of Budapest Research Reactor in 2014	<i>Instrument</i> RAD <i>Local contact</i> Kis Zoltán
	<i>Principal proposer:</i> Zoltán Kis – Centre for Energy Research <i>Experimental team:</i> Zoltán Kis, László Szentmihályi, László Horváth, Gábor Benyács – Centre for Energy Research	<i>Experiment Number</i> <i>Date</i> 2014.08.25-2014.11.06

Objectives

to develop neutron imaging instrumentation and methodology at channel No. 2 of Budapest Research Reactor

Results

The imaging station (RAD) at the thermal neutron beamline gives a possibility to study objects by thermal neutron- and X-ray imaging, and to benefit from the complementary features of the different radiations. The station has been receiving a significant upgrade (digital imaging and tomographic capabilities) in 2014. In addition to the old analog system, new imaging equipment was built around a state-of-the-art digital camera. The static radiography and tomography images are acquired by a new, large area sCMOS camera (Andor Neo 5.5 sCMOS 2560x2160 px, 16-bit), whereas the dynamic radiography is accomplished by a low-light-level TV camera and a frame grabber card. The image detection is based on suitable converter screens. The available screens are as follows: for neutron radiography, ZnS/LiF and Gadox scintillation screens with resolution of 50-200 μm ; for X-ray radiography a Gadox-based screen with resolution of 200 μm . To better fulfil demands from users there is a possibility to apply larger or smaller fields of view with lower and higher spatial resolution, respectively. Here altogether three different optical systems can be setup using the available lenses with 50 mm, 105 mm and 300 mm fixed focal lengths interchangeably coupled to the digital camera, as one can see in Fig. 1. The dynamic radiography will be done by a low-light-level TV camera (640x480 px) with a light sensitivity of 10^{-4} lux. The imaging cycle of this camera is 40 msec, making possible real-time imaging. A zoom optics coupled to this camera gives a variable field of view. The two cameras can be used interchangeably in the light-tight camera box equipped with a rail system providing the necessary optical path length.

The basic parameters of the facility have been measured. It has two measurement positions along the neutron beam with the calculated L/D ratios of 170 and 195, respectively. The thermal neutron fluxes at the two sample positions are $4.64 \times 10^7 \text{ cm}^{-2}\text{s}^{-1}$ and $3.38 \times 10^7 \text{ cm}^{-2}\text{s}^{-1}$, respectively. The beam has a neutron to gamma ratio of $1.72 \times 10^5 \text{ cm}^{-2}\text{mR}^{-1}$ and a cadmium ratio of 3.3. The thermal to epithermal flux measured by the cadmium covered and bare gold monitor method is about 51. The beam diameter is adjustable up to a maximum of 230 mm. The gamma-ray intensity in the neutron beam measured with thermoluminescence dosimetry is about 8.5 Gy/h. The ambient dose rate from neutrons at the position of the digital camera chip (20 mSv/h) was found still too high to be able to use the new digital camera continuously.

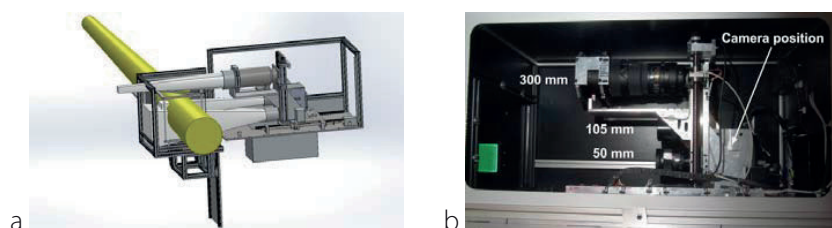


Figure 1: (a) The structural layout of the new RAD facility with the neutron beam and the three lenses used for static imaging. The system is to accomplish dynamic radiography using a low-light-level TV camera coupled to a zoom optics which is placed at the camera position. (b) The side view photo of the light-tight camera house showing the three lenses interchangeably coupled to the digital camera. Lenses with 50 mm, 105 mm and 300 mm fixed focal lengths are used for 3-step magnification to match the image to the chip size of the camera.

References: Z. Kis, L. Szentmihályi, T. Belgya, M. Balaskó, L. Z. Horváth, B. Maróti: *Neutron based imaging and element-mapping at the Budapest Neutron Centre*, Physics Procedia **69**, 40-47 (2015)

BNC Experimental Report	<i>Experiment title</i> Neutron and X-ray imaging of a ceramic pottery	<i>Instrument</i> RAD <i>Local contact</i> Kis Zoltán
	<i>Principal proposer:</i> Katalin Bajnok – Wigner Research Centre for Physics <i>Experimental team:</i> Zoltán Kis – Centre for Energy Research	<i>Experiment Number</i> <i>Date</i> 2015.12.12-2015.12.14

Objectives

to perform neutron and X-ray imaging of a ceramic pot from Budakalász, Hungary from the 7th century AD.

Results

There was a request to perform neutron and X-ray imaging of an ancient ceramic pottery to find out the possible joint application of neutron (NR) and X-ray tomography (XR).

As an example from the results, the neutron transmission tomographic image can be seen in Fig. 1a. The object is made up of original ceramic shreds and a contemporary complementary material (gypsum) for the lacking parts. As one can see the different parts of the pottery can easily be separated based on their grayscale values. During the rendering of the 3-D dataset there is a possibility to show just that range of the grayscale values which is interesting for the researcher. For example, in Fig. 1b parts with higher neutron attenuation values are visualized. This image shows the gluing material between the fragments, the tiny grain-like material in the body of the clay and some gypsum.

A vertical cut of the X-ray transmission image of the pottery can be seen in Fig. 1c. This image shows the different structures of the original clay and the contemporary gypsum. In Fig. 1d only the higher attenuation value parts of the materials are shown. The gluing materials cannot be visible because it is a high H-containing matter, which gives negligible contrast for X-rays. The more dense parts, however, are more or less clearly seen.

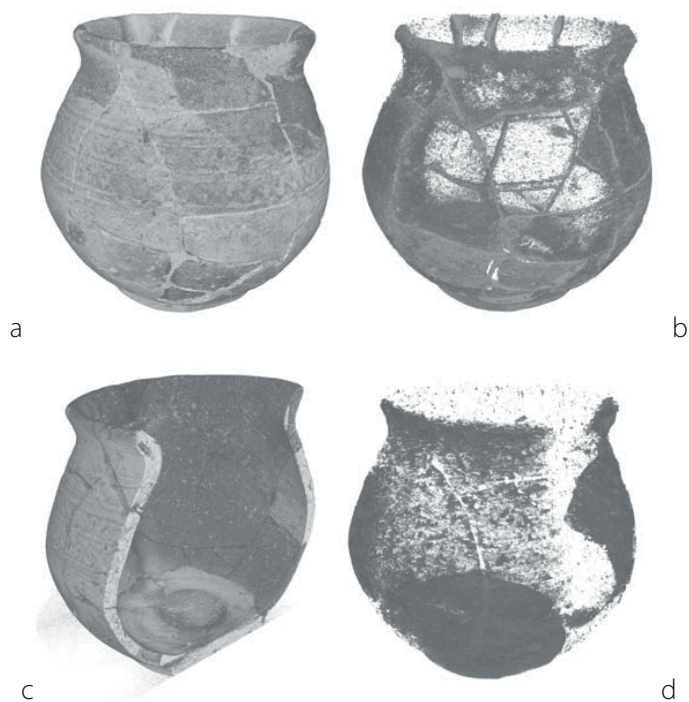


Figure 1: (a-b) The neutron and (c-d) X-ray transmission tomographic images of the ceramic pottery

BNC Experimental Report	<i>Experiment title</i> Quality assurance of boron containing paint of neutron choppers	<i>Instrument</i> RAD <i>Local contact</i> Kis Zoltán
	<i>Principal proposer:</i> Alex Szakál – Wigner Research Centre for Physics <i>Experimental team:</i> Zoltán Kis – Centre for Energy Research	<i>Experiment Number</i> <i>Date</i> 2015.07.02

Objectives

to provide quality assurance tool for boron containing paint of neutron choppers

Results

Neutron choppers use Al disks covered by e.g. boron containing paint to cut out selectively a part of the neutron energy spectrum. The attenuation capabilities of the disks strongly depend on the thickness and homogeneity of the covering material. These characteristics are hard to detect with X-rays, instead, neutron imaging is a suitable tool.

The boron containing paint of the disks produced by a local company could have been removed in large fragments from its supporting Al plate. It meant that the attenuation pattern of the covering material was not disturbed by its Al support during the neutron radiography. The transmission images of two of the six fragments can be seen in Fig. 1a-b. One can see that there are a lot of tiny dark spots, which could be attributed to higher boron-level-containing grain-like particles. Moreover, as one can easily see the quality of the covering of the fragments are not the same. The fragment in Fig. 1a has a more homogeneously distributed paint layer; while the homogeneity of the covering layer of the other fragments is rather poor (Fig. 1b). A surface averaged transmission value can be calculated for the fragments. For the layer in Fig 1a this value is about 0.073 ± 0.005 . For the layer in Fig 1b there are two characteristic values: for the darker part it is about 0.087 ± 0.004 , while for the lighter part it is about 0.056 ± 0.002 .

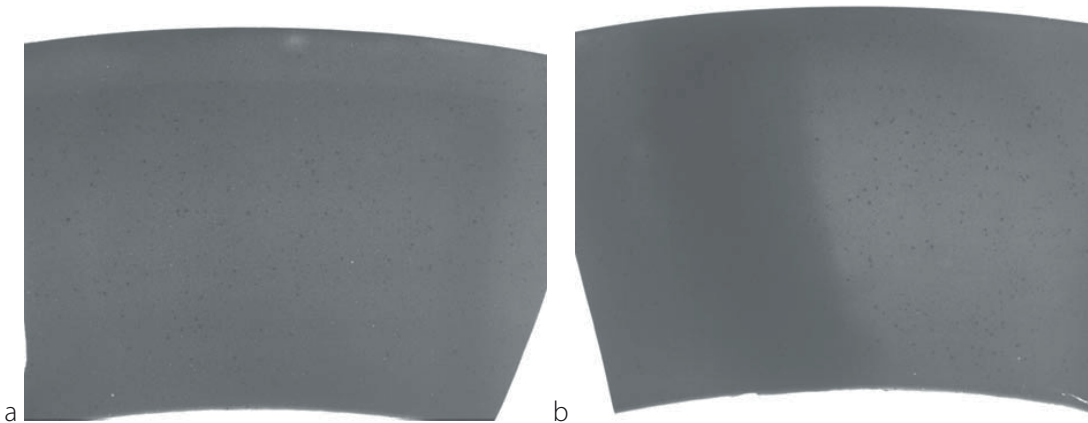


Figure 1: (a) A more homogeneous covering, and (b) a less homogeneous covering of the same Al disk.

BNC Experimental Report	<i>Experiment title</i> Quality assurance of boron carbide containing nuclear reactor control rods	<i>Instrument</i> RAD <i>Local contact</i> Kis Zoltán
	<i>Principal proposer:</i> József Janik – Centre for Energy Research <i>Experimental team:</i> Zoltán Kis, László Horváth, Gábor Benyács – Centre for Energy Research	<i>Experiment Number</i> <i>Date</i> 2015.04.17

Objectives

to provide quality assurance tool for boron carbide containing nuclear reactor control rods

Results

Boron carbide containing rods are used to control the operation of Budapest Research Reactor. These are key safety components in nuclear reactors therefore their quality have to be assessed regularly. Neutron and X-ray imaging can play a vital role in the quality assurance due to the complementary features of the two imaging modalities. The attenuation capabilities of the rods strongly depend on the thickness, integrity and homogeneity of their constituents. These characteristics can be detected only with the joint apply of X-ray and neutron imaging.

The result of the measurement for one of the newly fabricated rods can be seen in Fig. 1. The neutron image (Fig. 1a) shows the quite homogeneous boron carbide filling of the rod. Some boron carbide can be found at both ends of the void part as a consequence of the fabrication process. The X-ray image (Fig. 1b) shows the structure of the aluminum cladding. It proofs the good quality of the weld seams and the lack of ruptures. Both images show the integrity and the constant thickness of the walls. These findings contributed to the evaluation process of the rods and the permission of the use.

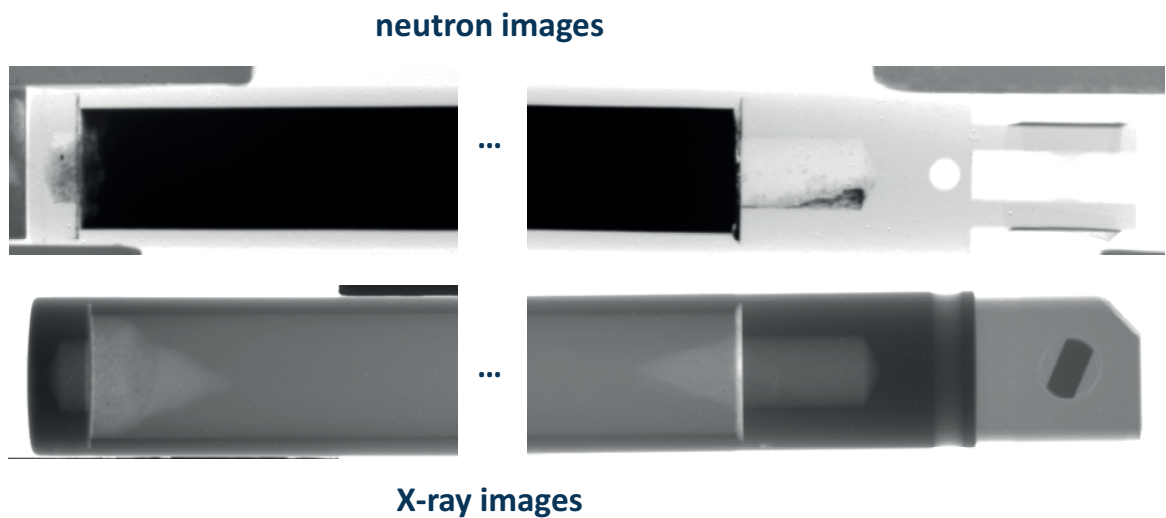


Figure 1: The neutron and the X-ray radiography images of the control rod.

<h1 style="text-align: center;">B N C</h1> <p style="text-align: center;">Experimental Report</p>	<i>Experiment title</i> Neutron imaging of the ANCARA supercritical loop at RAD	<i>Instrument</i> RAD <i>Local contact</i> Kis Zoltán
	<i>Principal proposer:</i> Attila Kiss – Budapest University of Technology and Economics <i>Experimental team:</i> Zoltán Kis, László Horváth, Gábor Benyács – Centre for Energy Research	<i>Experiment Number</i> <i>Date</i> 2015.02.20-2015.04.02 2015.09.07-2015.09.10

Objectives

to exploit the capabilities of the digital imaging in supercritical pressure water measurements

Results

The upgraded RAD station made it possible to carry out digital neutron imaging on the ANCARA loop for supercritical pressure water (SCW) measurements. The application of NR simultaneously with conventional measurements seems a very powerful tool for both to validate the CFD calculations and discover more details of the thermal hydraulics of SCW.

The imaging was carried out in “wet” and “dry” conditions for the area around a thermocouple. “Wet” condition means that the loop was filled up with water during the heating process; “dry” condition means that the loop was heated in its empty state, without water. Subtracting the belonging dry image from the wet one creates theoretically an image showing (apart from some scattering effects) the water only. Before doing the subtraction the wet and dry images have been aligned to each other to account for some small movements of the system (e.g. due to thermal expansion). In order to facilitate the alignment process images were cropped to an area containing the environment of the tp8 thermocouple only. The changes in the grayscale values due to the changing conditions (e.g. temperature, pressure) at an interesting spot of the object can be followed quantitatively.

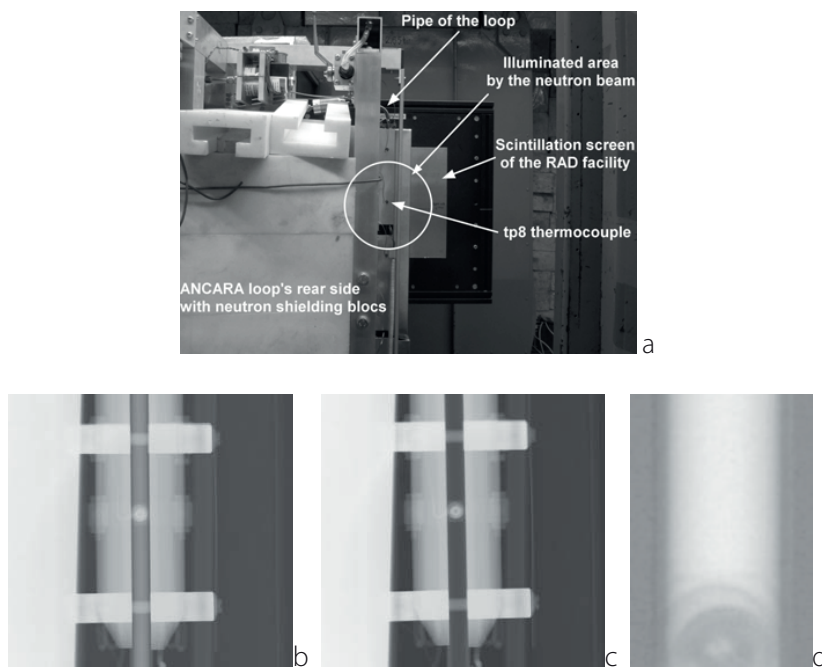


Figure 1: (a) The rear side of the ANCARA loop facing the beam (Beam's Eye View (BEV)); (b-d) Neutron radiography attenuation images of the loop around the tp8 thermocouple at the temperature of 300°C and pressure of 255 bar. (b) The image of the loop filled with water (wet image). (c) The image of the loop without water (dry image). (d) The resulted image after the subtraction of the belonging dry image from the wet one (it shows the water only)..

<h1 style="margin: 0;">BNC</h1> <p style="margin: 0;">Experimental Report</p>	<i>Experiment title</i> Improvement of the neutron and X-ray imaging station, RAD at channel No. 2 of Budapest Research Reactor in 2015	<i>Instrument</i> RAD <i>Local contact</i> Kis Zoltán
	<i>Principal proposer:</i> Zoltán Kis – Centre for Energy Research <i>Experimental team:</i> Zoltán Kis, László Szentmiklósi, László Horváth, Gábor Benyács – Centre for Energy Research	<i>Experiment Number</i> <i>Date</i> 2015.01.14-2015.11.03

Objectives

to develop neutron and X-ray imaging instrumentation and methodology at channel No. 2 of Budapest Research Reactor

Results

In 2015 the RAD station has been upgraded by a *portable X-ray unit*. The new unit together with the older ones makes it possible to cover a wider voltage range (5-300 kV) than before. That is important for delicate imaging, e.g. thin materials as paintings, electronic parts, etc. *Reference samples* were imaged by neutrons at both RAD and NORMA stations to be able to compare the effects of the different neutron energy spectra. The completion of measurements with *two modalities* in delicate imaging was accomplished by fulfilling the requests from Hungarian National Museum to perform neutron and X-ray imaging of historical bronze objects (spearheads, a round shield). For the *ANCARA supercritical loop* neutron imaging was carried out in “wet” and “dry” conditions for the area around a thermocouple. “Wet” condition means that the loop was filled up with water during the heating process; “dry” condition means that the loop was heated in its empty state, without water. Subtracting the belonging dry image from the wet one creates theoretically an image showing (apart from some scattering effects) the water only.

The basic parameters of the *new X-ray unit* have been measured. Moreover, the necessary *configuration setups* for the various imaging conditions (for the available screens with different optical and electronic setup of the RAD) were elaborated and standardized. The *reference samples’* investigations (Fig. 1) show that different materials (plexi, Pb, Al, Fe) have different thickness ranges and scattering effects for neutron and X-rays at the RAD station. As a result from the *two-modality imaging*, the neutron image of a *spearhead* revealed that the hollow in the head is filled with different materials not seen in the X-ray images (Fig. 1). It means that all of them should be some kind of organic material, an important knowledge for the archeologist.

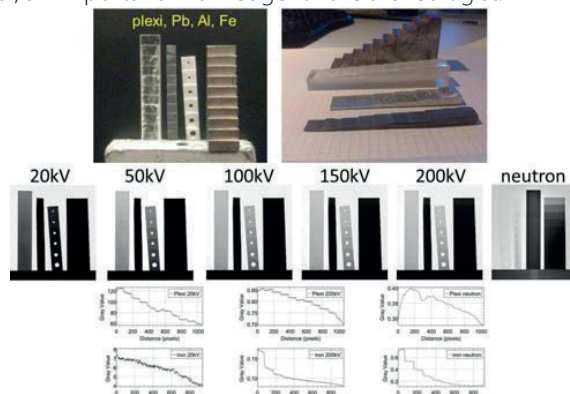


Figure 1: The neutron and X-ray (kV) transmission images of the reference wedges showing the thickness range and scattering effects of the different materials used frequently (plexi, Pb, Al, Fe).

References:

- Z. Kis, L. Szentmiklósi, T. Belgya, M. Balaskó, L. Z. Horváth, B. Maróti: *Neutron based imaging and element-mapping at the Budapest Neutron Centre*, Physics Procedia **69**, 40-47 (2015)
- Z. Kis, B. Maróti: *Report on the pilot PGAA and NR measurements of selected bronze objects from the Hungarian National Museum*, Kutatási jelentés, MTA EK-NAL-2015-141-1-1-M0 (2015)
- Z. Kis, B. Maróti: *Report on the Pilot XRF and NR Measurements of a Selected Bronze Shield from the Hungarian National Museum*, Kutatási jelentés, MTA EK-NAL-2015-141-1-2-M0 (2015)

<h1 style="margin: 0;">B N C</h1> <p style="margin: 0;">Experimental Report</p>	<i>Experiment title</i> Neutron and X-ray imaging of bronze spearheads from Hungarian National Museum	<i>Instrument</i> RAD <i>Local contact</i> Kis Zoltán
	<i>Principal proposer:</i> Gábor Tarbay – Hungarian National Museum <i>Experimental team:</i> Zoltán Kis – Centre for Energy Research	<i>Experiment Number</i> <i>Date</i> 2015.04.22-2015.04.28

Objectives

to perform neutron and X-ray imaging of two bronze spearheads from the Hungarian National Museum (HNM)

Results

There was a request from HNM to perform neutron and X-ray imaging of a fragment of a bronze spearhead as a stray find and a bronze spearhead in better condition from Szarvas by a joint application of neutron (NR) and X-ray radiography (XR).

The **bronze spearhead** (Inv. nr.: 52.29.716) was exposed to neutrons and X-ray as it can be seen in Fig. 1.a-b. The neutron image reveals a tube-like inner structural material with layers (red arrows in Fig. 1.a). It fills the hollow in the bronze; however, it could hardly be seen in the X-ray image (red arrow in Fig. 1.b). This indicates a presence of a presumably organic material, which is most probably a piece of wood. It could have layers; however, a 3D tomography could better answer this hypothesis. The X-ray image compared to the neutron one better reveals the fragmented structure of the bronze material.

The **bronze spearhead** (Inv. nr.: 75.1893.1200) was exposed by neutrons and X-ray as it can be seen in Fig. 1.c-d. The neutron image stitched from two overlapping parts reveals that the hollow in the head is filled with different materials. All of them should be some kind of organic ones because those could not be seen in the X-ray images. From top to bottom in Fig. 1.c there is a small fibrous-like (1) material, then a sharp, long and slim wand (2), next to it a similar but thicker wand (3), and around the bottom of wands perhaps a filling material again made of fibrous-like (4) substance. In the X-ray image (b) the grayscale is adjusted so that the hollow of the head could be better seen. This object is a suitable candidate for further investigations to determine the elemental composition of e.g. the fibrous-like (1) material by PGAA measurements.

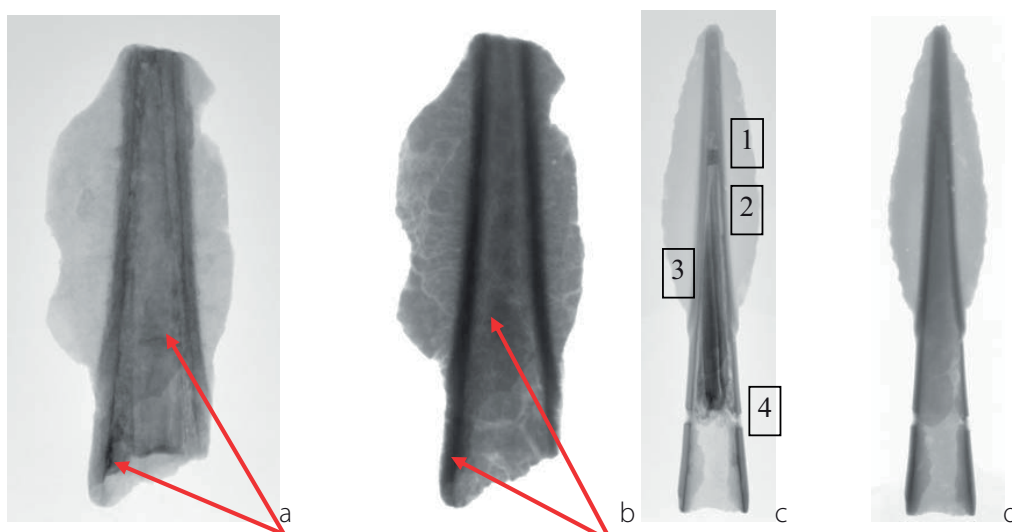


Figure 1: (a) The neutron (a) and X-ray (b) attenuation images of the bronze spearhead. (b) The neutron (c) and X-ray (d) attenuation images of the bronze spearhead.

References: Kis, Z. and Maróti, B., 2015. *Report on the pilot PGAA and NR measurements of selected bronze objects from the Hungarian National Museum*. Budapest: MTA Energiatudományi Kutatóközpont, Kutatási jelentés No. MTA EK-NAL-2015-141-1-1-MO.

BNC Experimental Report	<i>Experiment title</i> Neutron and X-ray imaging of an Early Iron Age bronze shield from Hungarian National Museum	<i>Instrument</i> RAD <i>Local contact</i> Kis Zoltán
	<i>Principal proposer:</i> Gábor Tarbay – Hungarian National Museum <i>Experimental team:</i> Zoltán Kis – Centre for Energy Research	<i>Experiment Number</i> Date 2015.09.02-2015.09.03

Objectives

to perform neutron and X-ray imaging of an Early Iron Age bronze shield from the Hungarian National Museum (HNM)

Results

There was a request from HNM to perform neutron and X-ray imaging of an Early Iron Age bronze shield found amongst other confiscated objects originating supposedly from the territory of Balkan by a joint application of neutron (NR) and X-ray radiography (XR).

As an example from the results, an interesting part of the shield can be seen in Fig. 1. A part of the shield, e.g. where the rim and the adjacent layer is held together, could contain from outside invisible materials, which are different compared to the shield's own material. There are darker spots, which give contrast in both the X-ray and the neutron images (arrows labeled by 1 in Fig. 1). These are presumably the broken-down parts of the rivets. There are darker spots, which give contrast in the X-ray image, without giving contrast in the neutron image (arrows labeled by 2 in Fig. 1). These could be materials with higher atomic number (e.g. lead), which have high and low attenuation for X-rays and neutrons, respectively. There is a darker spot, which gives contrast in the neutron image, without giving contrast in the X-ray image (arrow labeled by 3 in Fig. 1). This could be an organic material.

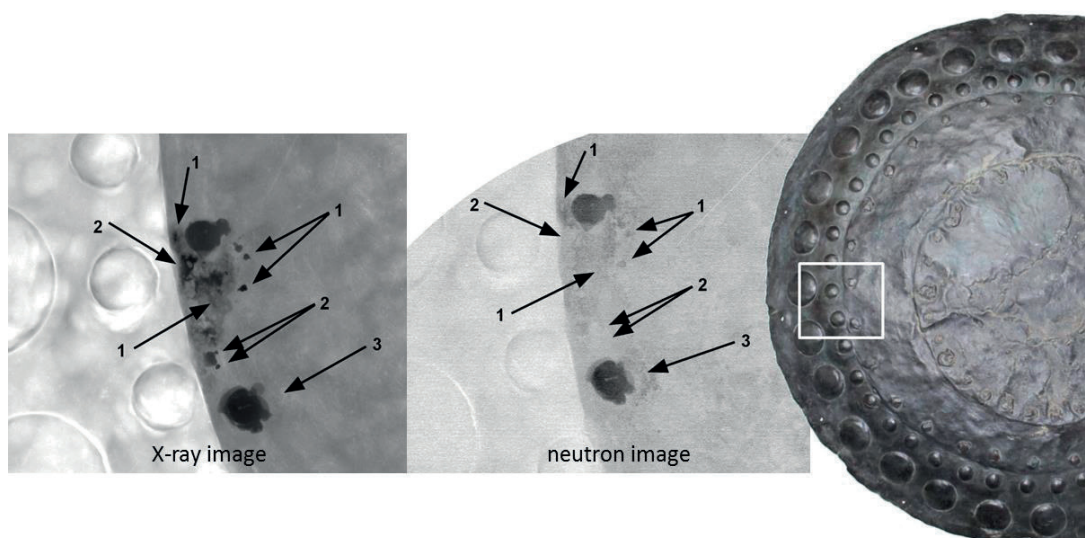


Figure 1: (a) The neutron and X-ray transmission images of the bronze shield showing materials invisible from outside.

References

Z. Kis, B. Maróti: *Report on the Pilot XRF and NR Measurements of a Selected Bronze Shield from the Hungarian National Museum*, Kutatási jelentés, MTA EK-NAL-2015-141-1-2-M0 (2015)

<h1 style="margin: 0;">B N C</h1> <p style="margin: 0;">Experimental Report</p>	<i>Experiment title</i> Neutron imaging of a reference sample at the RAD and NORMA stations	<i>Instrument</i> RAD <i>Local contact</i> Kis Zoltán
	<i>Principal proposer:</i> Zoltán Kis – Centre for Energy Research <i>Experimental team:</i> Zoltán Kis – Centre for Energy Research	<i>Experiment Number</i> <i>Date</i> 2015.12.14-2015.12.15

Objectives

to image reference sample by neutrons at both RAD and NORMA stations to be able to compare the effects of the different neutron energy spectra

Results

A reference sample designed for the evaluation of contrast of neutron tomography in the framework of a round robin (RR) exercise organized by IAEA and Paul Scherrer Institute (PSI) was imaged at both RAD and NORMA stations to be able to compare the effects of the different neutron energy spectra. The sample contained the following materials: sample body, Al, and insets rods of Pb, Ti, Fe, Ni, Al, and Cu. The sample dimensions are 30mm diameter of the sample body and the insets have a diameter of 6mm and are placed equidistantly on an 18 mm ring.

The resulting cold and thermal beam NT images are shown in Fig. 1a-c and Fig. 1d-f, respectively. Fig. 1c shows both the linear and the logarithmic histogram of the grayscale values of the contrast sample taken at NORMA station by cold neutrons. From this histogram it can be seen that there are only three large “bumps” in the attenuation values, which figure is less than the number of the different materials in the sample. It means that there are materials of which attenuation coefficient values are quite similar, and cannot be resolved in a cold neutron beam. The Fig. 1f shows both the linear and the logarithmic histogram of the grayscale values of the contrast sample taken at RAD station. From this histogram it can be seen that there are six large “bumps” in the attenuation values according to the number of different materials used to fabricate the sample. Here the energy spectrum of the thermal beam makes it possible to distinguish between the different materials according to their attenuation values.

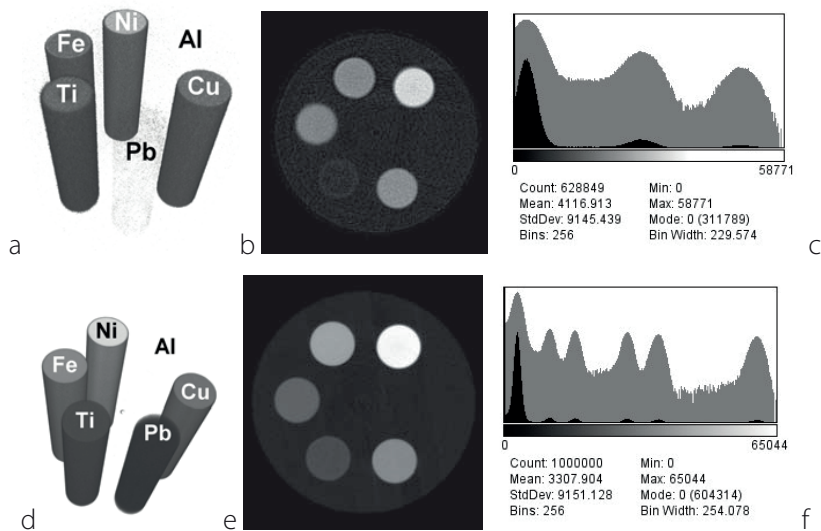


Figure 1: The Li100N NT image, a slice and the histogram of the grayscale values of the contrast sample taken at the NORMA (a-c) and the RAD (d-f) station. The histograms show both the linear and the logarithm of the values.

References: Z. Kis: Report on pilot NT measurements on test objects intended for the evaluation of the performance of neutron computed tomography installations, Kutatási jelentés, MTA EK-NAL-2016-141-1-1-M0 (2016)

<h1 style="margin: 0;">BNC</h1> <p style="margin: 0;">Experimental Report</p>	<p><i>Experiment title</i></p> <p>PGAA measurements on volcanic rocks from the Deception Island, Antarctica</p>	<p><i>Instrument</i></p> <p>PGAA</p> <p><i>Local contact</i></p> <p>Katalin Gméling</p>
	<p><i>Principal proposer:</i></p> <p>Zoltán Pécskay Krzysztof Birkenmajer– ATOMKI, Debrecen, Hungary; Institute of Geological Sciences, Polish Academy of Sciences, Krakow, Poland</p> <p><i>Experimental team:</i></p> <p>Katalin Gméling, Boglárka Maróti, Ildikó Harsányi – MTA EK</p>	<p><i>Experiment Number</i></p> <p>Date</p> <p>2013.03.14-04.04.</p> <p>2015.04.16-04.22.</p>

Objectives

Volcanic rock samples from Deception Island, and King George Island, Antarctic Peninsula (Fig. 1) were measured by PGAA to examine the geochemical composition of the volcanic rock samples. The Antarctic Peninsula is an excellent example of ocean-continent collision resulting in subduction. Deception Island is a very young (< 4 Ma) basalt-andesite volcano (a 9 km diameter caldera flooded by the sea) at the northern end of the Antarctic Peninsula. The caldera formed following the largest-known Antarctic eruption, while the post-caldera activity comprised numerous small pyroclastic cones. All the samples from pre- and post-caldera formations were collected by volcanologist to examine any cyclicity in geochemical character of successive eruptions, and to check the vertical differentiation of geochemical signatures, from the bottom to the top of the succession. King George Island is almost entirely composed of igneous rocks; four volcanic episodes and one intrusive phase are represented. The oldest volcanics form a calc-alkaline suite with an andesite-rhyolite association. Geochemical character of these samples was also interesting to compare with those from Deception Island.

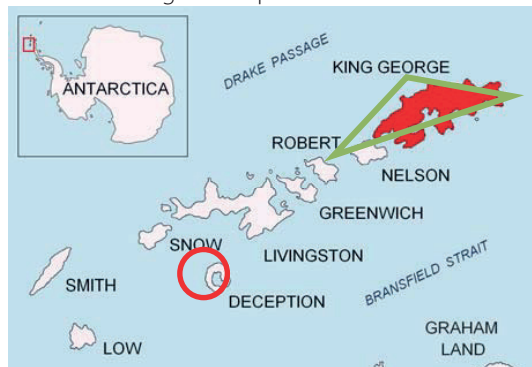


Fig. 1. Location of Deception and King George Islands at Antarctica

Results

Most of the examined samples are basalt and basaltic andesite, only few samples from the Deception Island are rhyolite by their geochemical character. The andesite samples fall in the medium-K field. The boron content of the samples are low (below 10 mg/g), typical of alkaline basalt rocks, although low-B in subduction related area refers to low influx of subducted sediments, or exhausted slab. Nuclear analytical measurements on the samples set from Antarctica are still in progress.

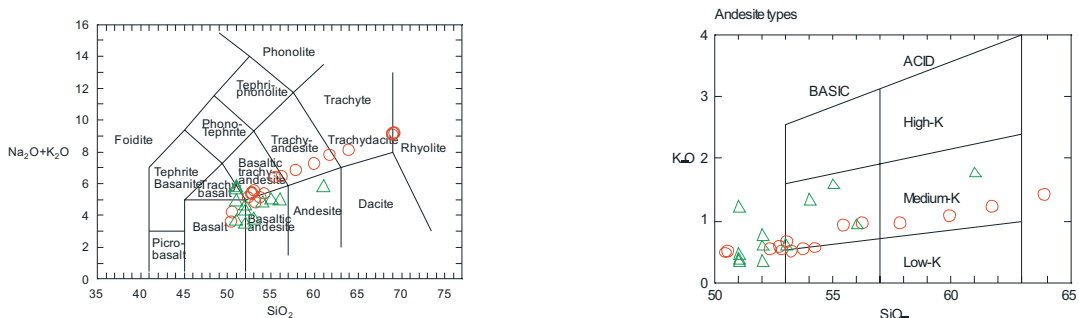


Fig. 2. Geochemical character of the examined samples of Deception (red circle) and King George Islands (green triangle).

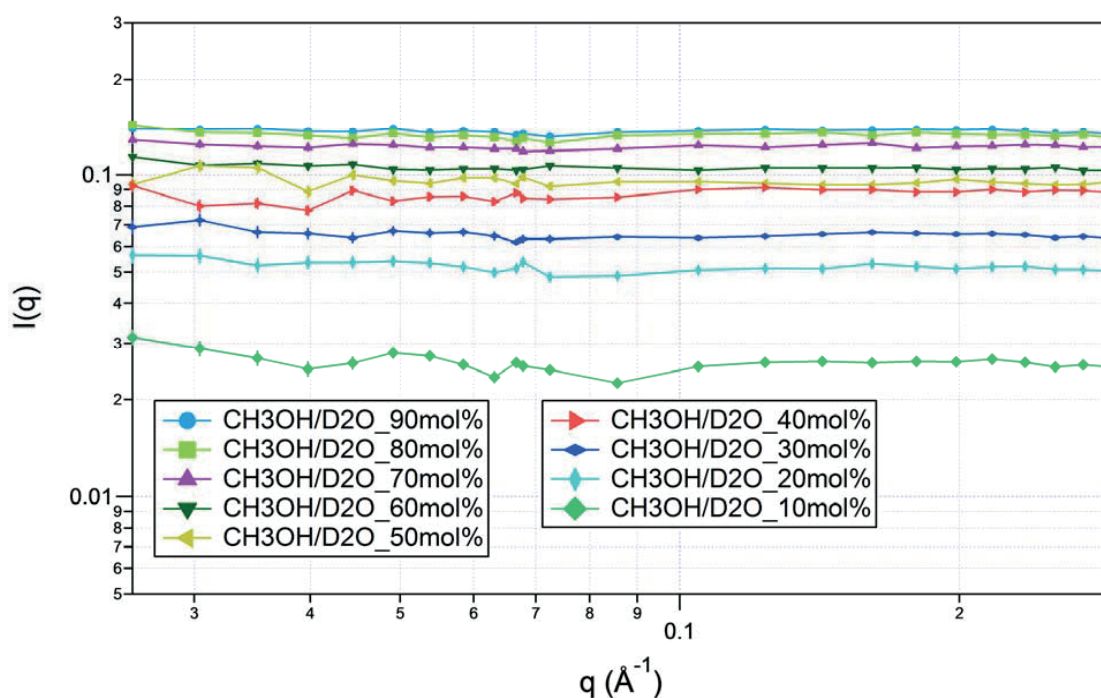
<h1 style="margin: 0;">BNC</h1> <p style="margin: 0;">Experimental Report</p>	<i>Experiment title</i> Small angle neutron scattering signal from methanol-water mixtures	<i>Instrument:</i> SANS <i>Local contact:</i> LEN, Adél
	<i>Principal proposer:</i> PUSZTAI, László <i>Experimental team:</i> PUSZTAI, László; LEN, Adél	<i>Experiment Number:</i> <i>Date:</i> February 2015

Objectives

For more than a decade, the concept of ‘micro-heterogeneities’ has been known, in conjunction with the structure of alcohol-water and in particular, methanol-water liquid mixtures. The idea is that the hydrophobic methyl groups would form these nanosize aggregates. From wide angle neutron diffraction, the existence of such ‘micro-heterogeneities’ was found (or rather, speculated) in the methanol-rich region. In order to provide experimental evidence, pro or contra, we have proposed SANS experiments on mixtures of CD₃OD and H₂O, as well of CH₃OH and D₂O, so that there would be contrast between the CH₃/CD₃ groups and the hydrophilic parts - provided that there really are ‘micro-heterogeneities’ in these mixtures.

Results

The figure below summarizes the SANS curves for most of the methanol-water liquid mixtures. As it is well visible, no small angle scattering could be observed, suggesting that the aggregates most probably do not exist in the form thought before.



<h1 style="margin: 0;">BNC</h1> <p style="margin: 0;">Experimental Report</p>	<p><i>Experiment title</i></p> <p>SANS analysis for acid catalyzed silica xerogels and sonogels synthesized with butyl-4-methylpyridinium tetrafluoroborate ionic liquid</p>	<p><i>Proposal No.</i></p> <p>BRR_414</p>
	<p><i>Principal proposer:</i> Ana-Maria Putz</p> <p><i>Experimental team:</i> Ana-Maria Putz, Adél Len, László Almásy</p>	<p><i>Local contact</i></p> <p>László Almásy</p>

Objectives

This study addressed the structure formation in new materials, nanostructured xerogels and sonogels, prepared by using butyl-4-methylpyridinium tetrafluoroborate (BMPyBF₄) ionic liquid (IL) as co-solvent, in various IL/Si molar ratios. As silicon precursors: trimethoxymethylsilane and tetramethylorthosilicat were used.

Results

We have measured two different set of samples: the samples denoted by X were prepared by classical synthesis; the samples denoted by S were prepared under ultrasound. The scattering intensity curves (Figure 1) are characteristic for a material with inhomogeneities having a characteristic size, as seen by the broad plateau with decay starting at higher q values. These can be attributed to the primary particles that form in the initial phase of the condensation reaction. Compact particles with rough, surface can be modelled by equation $I(q) = \frac{K}{(1+q^2\xi^2)^p} + bg$, where K is a

scale factor, ξ is a characteristic length related to the particle size and p is related to the surface roughness. The bg term contains the incoherent background. The radius of gyration R_g and the correlation length ξ can be considered as an approximate measure of the size of the scattering entity. Interparticle interference effects are not included in this model, as in the given q -range there is no visible decrease or increase of the scattering intensity toward low q values.

The scattering data show that the primary particle size in the xerogels and sonogels is about 2 nm, while at higher ionic liquid content they grow to 4-6 nm (Figure 2). No appreciable difference could be seen between the structure of sonogels and xerogels.

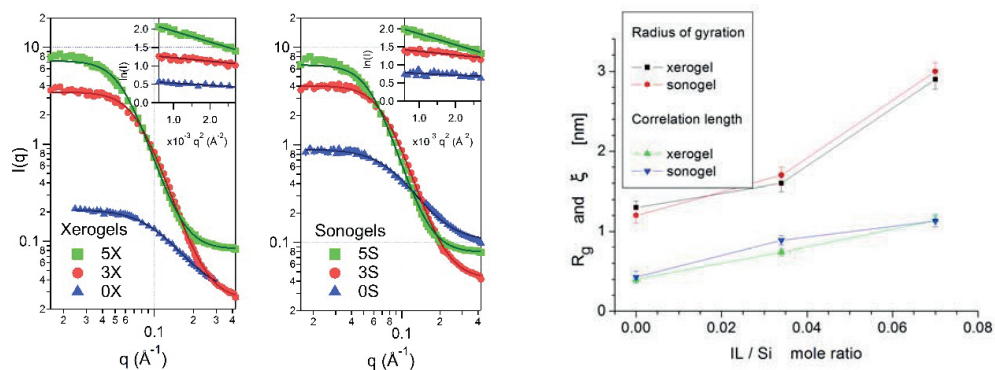


Figure 2. SANS scattering curves of xerogels (left) and sonogels (right); and the gyration radii and correlation lengths, obtained from the SANS data.

In general, sonication applied during synthesis does not affect the size of monomer particles but influences their secondary aggregation. SANS data did not reveal any influence of ultrasonication on the level of the primary particle formation. The primary particle sizes do not differ significantly upon applying ultrasound, but the addition of IL slows down the polycondensation and produces particles of larger size.

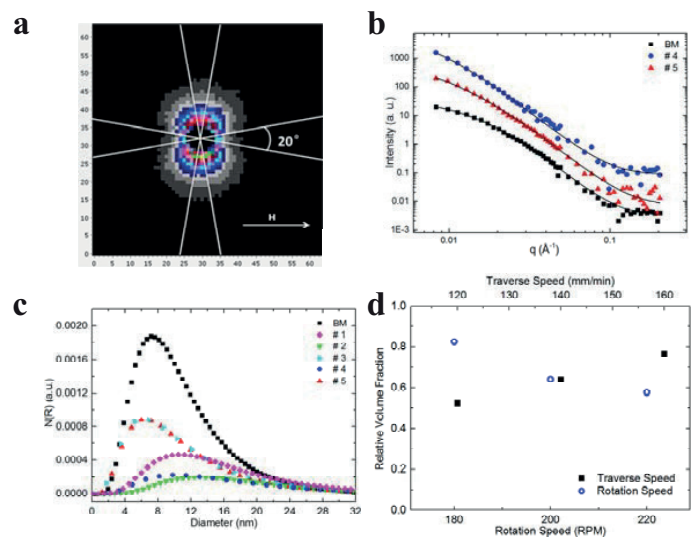
A.M. Putz, A. Len, C. Ianăși, C. Savii, L. Almásy (2016) Ultrasound assisted preparation of mesoporous silica using N-butyl-3-methylpyridinium tetrafluoroborate, Korean J. Chem. Eng., 33, 749.

<h1 style="margin: 0;">BNC</h1> <p style="margin: 0;">Experimental Report</p>	<i>Experiment title</i> The effect of Friction Stir Welding on the size distribution of nanoparticles in the ODS steel MA956	<i>Instrument:</i> SANS <i>Local contact:</i> László Almásy
	<i>Principal proposer:</i> Huw Dawson <i>Experimental team:</i> Huw Dawson, Enrique Jimenez-Melero	<i>Experiment Number:</i> BRR-422 <i>Date:</i> 2015

Objectives

Friction stir welding can change the distribution of the essential nano-oxide particles in oxide dispersion strengthened (ODS) steels. Due to the mechanical mixing and heat generated through the process the dispersion can change through a combination of agglomeration, dissolution and coarsening. The objective was to use small angle neutron scattering to observe changes to the size distribution and number density of nano-particles compared to that of the base material for 5 welded samples which used different welding parameters – the rotation speeds and the traverse speeds were varied.

Results



It was possible to produce particle size distribution curves (PSD) for the welds from the SANS data. This can be seen in c). The PSD for the base material agrees well with literature and PSDs produced by TEM. The data shows that following welding the volume fraction of measured particles has decreased. d) shows the volume fraction of nano-particles relative to the base material as a function of the welding parameters. The volume fraction decreases with increasing RPM and decreasing traverse speed. There are two main reasons for this. Increased RPM and decreased traverse speed will increase the amount of mixing, shear and/or temperature during welding. This will increase the amount of agglomeration of the particles during welding. Some of the agglomerates can become larger than the detection range of the SANS setup and therefore the measured volume fraction will decrease. This will occur more often for lower traverse speeds and higher RPM. The other cause for the decrease in volume fraction arises from dissolution of the particles. Higher RPM and lower traverse speed will create a greater temperature and therefore more particles, particularly the smaller particles, will dissolve. c) shows that the smallest population of particles, 1-4 nm, has completely dissolved for the three hottest welds but seems mostly unaffected for the two coldest welds. This agrees with TEM observations. Therefore we can identify the parameters close to which dissolution starts to occur.

It was also found that the volume fraction of particles in the welded samples correlates well with the grain sizes measured, implying that the number density of particles strongly affects the grain size due to pinning of the grain boundaries.

<h1 style="margin: 0;">BNC</h1> <p style="margin: 0;">Experimental Report</p>	<i>Experiment title</i> Experiment SANS for analysis of CTAB template mesoporous silica based materials	<i>Proposal No.</i> BRR_424
	<i>Principal proposer:</i> Ana-Maria Putz <i>Experimental team:</i> Ana-Maria Putz, Adél Len, László Almásy	<i>Local contact</i> Adél Len <i>Date(s) of Exper.</i> November 26-27, 2015 <i>Date of Report</i> March 21, 2016

Objectives

Mesoporous silica particles were synthesised by sol-gel methods from tetraethoxysilane (tetraethylorthosilicate, TEOS) and methyltriethoxysilane (MTES) precursors, by changing the molar ratio of the silica precursors. Ammonia was used as catalyst cetyltrimethylammonium bromide (CTAB) as the structure directing agent. The effects of TEOS/MTES molar ratios on gel structures and pore morphologies were explored. Materials with low MTES content showed hydrophobic properties, also having the specific properties for MCM-41 type of materials as well, like: ordered structures, big specific surface areas and pore volumes, suitable for selective uptake of guest species in drug loading applications. Therefore, the objectives were to evaluate the properties and structures of mesoporous materials varying based on the choice of different molar ratio of the two precursors in the synthesis condition.

Results

Small-angle scattering allows to study the structure of the materials at length scales 1-100 nm, providing a volume-average of the inner structure of the materials. SANS scattering curves of the xerogel silica gels are shown in Figure 1a and for the calcinated materials, Figure 1b. There is one peak visible in each sample, which is the same as the first XRD peak at about 2.2 degrees.

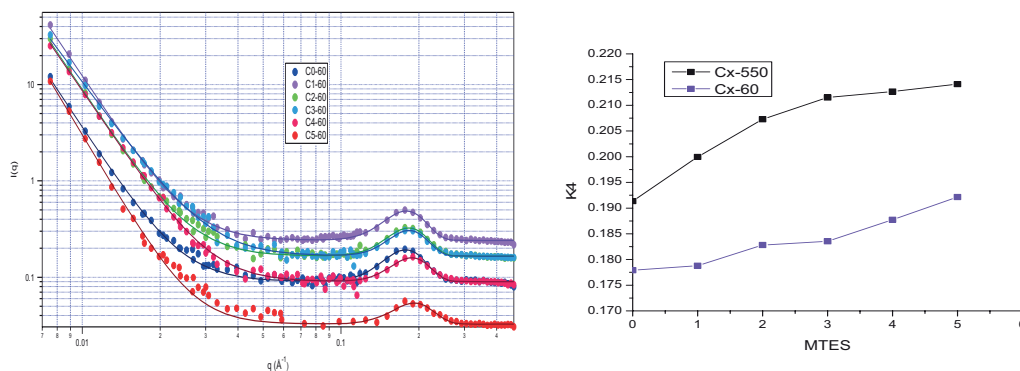


Figure 1 The scattering curves, and the peak position as a function of MTES content.

Scattering curves, and variation of the periodicity as a function of MTES content is shown in Figure 1. SANS and XRD analyses proved that the main specific peak around 2.2 degrees (CuK α), was visible in all samples. The second and the third diffraction peaks of the obtained spherical material (indexed as (110) and (200), respectively) overlap, in good agreement with other literature studies for mesoporous silica synthesis using in the reaction mixture a molar ratio TEOS: EtOH = 1:58. With the increase of MTES content in Cx-550 series of samples a comparative evolution was observed for the structural parameters as well; therefore the main diffraction peak shifted to higher values, and the surface areas, pore diameters and pore volumes, were slightly decreasing. The resulting materials have enhanced surface hydrophobicity which is retarding the leaching of a possible cargo, while (when small amounts of MTES are added in the reaction mixture) the mesostructural integrity and the large pore dimensions are retained.

<h1 style="margin: 0;">BNC</h1> <p style="margin: 0;">Experimental Report</p>	<i>Experiment title</i> Impact of polyethylene glycol on aqueous micellar solutions of sodium oleate	<i>Proposal No.</i> BRR_430 <i>Local contact</i> L.Almasy
	<i>Principal proposer</i> V.I.Petrenko, FLNP, Joint Institute for Nuclear Research, Dubna, Russia <i>Experimental team</i> M.V.Avdeev, L.A.Bulavin, V.M.Garamus, P.Kopcansky	<i>Date of Experiment</i> May 2015 <i>Date of Report</i>

Objectives

The goal of the experiment was to reveal by means of SANS the structure and interaction in complex aqueous micellar solutions of surfactant (Sodium Oleate (SO)) with polymer (Poly(ethylene glycol) (PEG)) of different molecular weights in an interval of 400 – 20000. Surfactant/polymer systems exhibit different properties in comparison with pure surfactant or polymer solutions and have prospects in various applications. Particularly SO/PEG solutions are used for stabilization of biocompatible ferrofluids. The influence of PEG on SO micelles was checked out by changes in the SANS curve of mixed SO+PEG solution at comparing with solutions of pure SO in D₂O. The obtained results are important specifically for understanding the synthesis procedure of highly stable magnetic fluids with controllable properties for biomedical applications with addition of biocompatible polymer PEG.

Results

The obtained experimental SANS curves for the SO micelle solutions with addition of various molecular mass PEG are compared in Fig.1. For the mixed SO/PEG solutions shift of the micelle interaction peak towards higher q -values takes place together with some changes in its width as well as the variations of the forward scattered intensity, which is proportional to isothermal solution compressibility. Also effect of PEG on SO was checked by surface tension measurements.

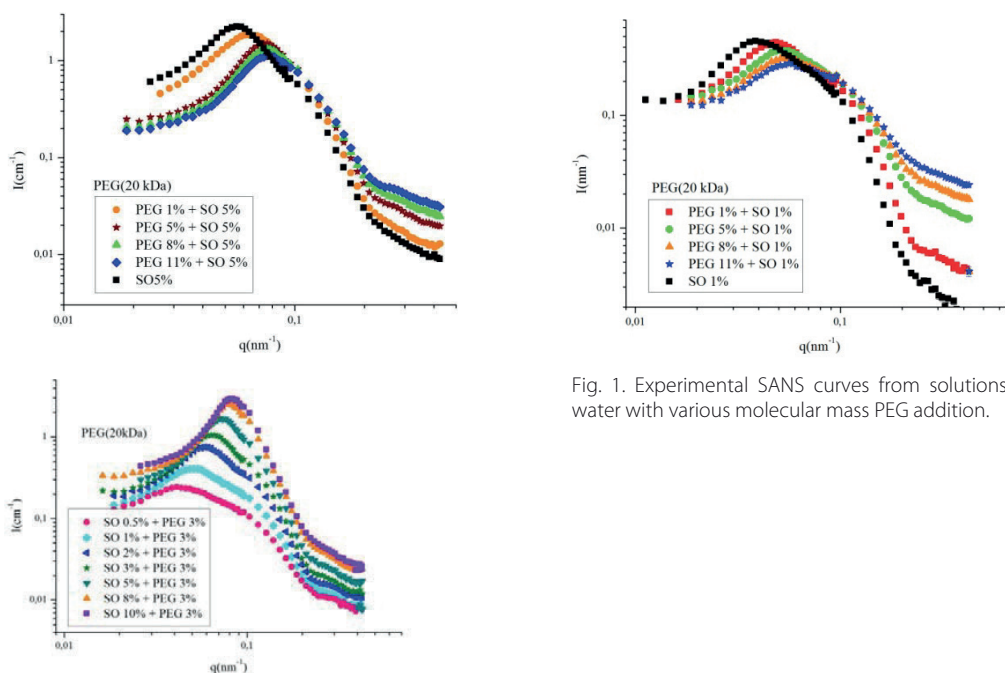


Fig. 1. Experimental SANS curves from solutions of SO in d-water with various molecular mass PEG addition.

Further fit of SANS curves by model of interacting spheres/ellipsoids will be done to obtain structure and interaction characteristics.

B N C Experimental Report	<i>Experiment title</i> Mn doping influence on structure and magnetism of FePt-based nanocomposite alloys	<i>Instrument:</i> SANS diffractometer <i>Local contact:</i> Dr. Adel Len
	<i>Principal proposer:</i> Dr. Ovidiu Crisan, NIMP, Bucharest <i>Experimental team:</i> Dr. Aurel Leca, Dr. Ovidiu Crisan, NIMP Bucharest	<i>Experiment Number:</i> CERIC - 20147028 <i>Date:</i> 21-24/04/2015

Objectives

The objective is to characterize and evidence novel phenomena in rare-earth (RE) free nanocomposite magnets derived from the FePt and MnAl binary alloy system. Compared with either Nd-Fe-B or Sm-Co permanent magnets (PM), these PM exhibit superior corrosion resistance and can operate at significant higher temperatures due to their higher Curie point. The promising FePt and MnAl systems can provide nanocomposite magnets with good magnetic properties, especially in the high temperature and corrosion-resistant applications. The hard magnetic L1₀ FePt phase has high coercivity, high magnetocrystalline anisotropy and its Curie temperature is around 500°C. Equiatomic FePt is usually first obtained in its soft magnetic A1 fcc structure and until recently, high temperature annealing (500°C) was thought that is needed in order to promote formation of the hard magnetic ordered L1₀ phase. Our group has proven that it is even possible to achieve the hard magnetic phase without post-synthesis annealing [1]. A major step forward is related to the addition of Mn. It has been shown that FeMnPt promotes easier than FePt the L1₀ hard magnetic phase [2]. On the other hand MnAl system also exhibit formation of hard magnetic L1₀ phase via a two-step reaction process during annealing of as-cast samples. In this proposal, FeMnPt and MnAlFe, and also iron oxides are to be studied. The alloys are obtained in form of melt spun ribbons by rapid solidification (RS) or by mechanical alloying. Previous magnetic investigations hints to a possible AFM/FM magnetic transition in FeMnPt and MnAlFe, never reported before in granular alloys, possible to document using SANS. The interplay of structure and magnetic properties is most finely characterized using synchrotron XRD and neutron diffraction studies. Recent preliminary results of synchrotron XRD studies on FePtNbB alloys [3] showed the co-existence of hard and soft magnetic phases during crystallization of the amorphous precursor. These results prompts us to further structural investigations using the combined protocol of synchrotron XRD and neutron scattering in order to monitor the magnetic exchange coupling mechanisms dynamically, during the disorder-order phase transformation process. By this, optimization of the alloy performances can be achieved. The SANS measurements are aiming to evidence a possible AFM/FM magnetic transition in Fe/Fe oxides and FeMnPt and to probe the exchange coupling mechanisms at the interfaces between hard and soft magnetic regions.

Results

A number of 6 samples have been investigated at SANS – BNC. The samples investigated are depicted in Table 1.

Mn ₄₅ Al ₄₅ Fe ₁₀	3955.04
Mn ₄₅ Al ₄₅ Fe ₁₀ +MAGNET	3975.04
Fe-magnetite 4/6	3967.04
Fe-magnetite 4/6+MAGNET	3974.04
Fe-magnetite 8/2	3968.04
Fe-magnetite 8/2+MAGNET	3973.04
FeMnPt P7	NO good scattering
FeMnPt P7+ MAGNET	NO good scattering
LFO	3906.004
LFO+MAGNET	3914.004
SFMO	3912.004
SFMO+MAGNET	3913.004

The scans have been performed for each sample firstly in regular setup and then under an applied magnetic field of 0.5 – 0.8 Tesla. The SANS scans, recorded in transmission mode, have revealed for all but two samples relatively good signal. The exception was for the bulk sample Fe₅₇Mn₈Pt₃₅. In that case, the scattering was not observed, possibly due to the high amount of Pt. The effect of the applied magnetic field has been well pointed out. Figures 1 and 2 present the 2D pictures of scattered intensity for powder samples Fe/Fe₃O₄, with the relative concentration ratio 4/6 and 8/2 respectively, with and without applied magnetic field.

<h1 style="margin: 0;">BNC</h1> <p style="margin: 0;">Experimental Report</p>	<i>Experiment title</i> Structure and Toxicity of Aqueous Fullerene C60 Solutions	<i>Proposal No.</i> SANS <i>Local contact</i> L.Almasy
	<i>Principal proposer</i> O.A.Kyzyma, FLNP, Joint Institute for Nuclear Research, Dubna, Russia <i>Experimental team</i> M.V.Korobov, M.V.Avdeev, L.A.Bulavin, V.I.Petrenko,	<i>Date of Experiment</i> May 2015 <i>Date of Report</i>

Objectives

Modern carbon nanomaterials (fullerenes, nanodiamonds, nanotubes, etc.) are increasingly being tested in the development of systems for drug delivery, as well as a basis for anticancer, antibacterial, and other pharmaceutical preparations. In this regard, various methods for preparing aqueous solutions of carbon nanostructures, including fullerene, have attracted much interest. Solutions of fullerene C60, including both solutions of modified C60 (solubilization, complexes with polymers) and those prepared without stabilizers (condensation, solvent-exchange method), are among the most prospective. The issue of the toxicity of such systems has not been completely studied.

Results

In this work we have investigated an aqueous solution of fullerene C60 (VDF60), prepared by the solvent exchange method, and a solution of C60/H₂O(NMP) with a low content of NMP. The structure of VDF60 at the nanoscale level (up to 100 nm) was analyzed by small-angle neutron scattering (SANS) (fig.1) and compared with published data on similar systems and mixed solutions of C60/H₂O(NMP). In order to assess the prospects of using these solutions in biology, we investigated their toxicity to Chinese hamster V79 cells; among other things, the effect of the NMP concentration in mixed solutions on their toxicity is studied. The ultimate goal was to determine whether the size of fullerene clusters in the solution affects the level of its toxicity.

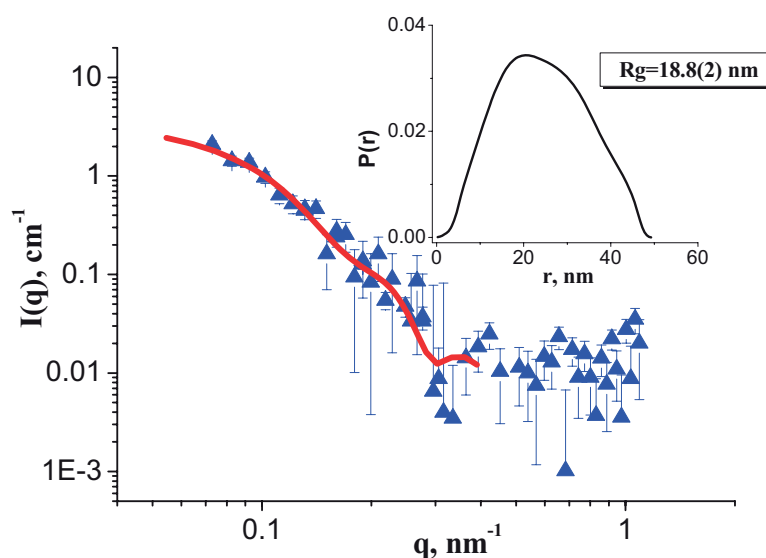


Fig. 1. SANS curves for the system of VDF60; the concentration of C60, 0.03 mg/mL; (solid line) the model curve obtained by the indirect Fourier transform. The inset shows the distribution function of the pair distances as a result of processing of the curve by the indirect Fourier transform.

Structural studies of fullerene solutions prepared by different methods showed a double difference in the fullerene cluster size. The radius of gyration for a solution of VDF60 is 18.8 ± 0.2 nm, compared to 8 ± 1 nm for a solution of C60/H₂O(NMP). Regardless of the method of preparation and size of clusters in a solution of C60 in water, both the investigated systems of C60/H₂O(NMP) and VDF60 showed no toxicity in in vitro experiments on Chinese hamster V79 cells in the investigated concentration range of C60 of 0.05–5 μ g/mL.

<h1 style="margin: 0;">BNC</h1> <p style="margin: 0;">Experimental Report</p>	<i>Experiment title</i> IMPACT OF SURFACTANTS ON THE STRUCTURE OF AQUEOUS FERROFLUIDS	<i>Proposal No.</i> SANS <i>Local contact</i> L.Almasy
	<i>Principal proposer</i> V.I.Petrenko, FLNP, Joint Institute for Nuclear Research, Dubna, Russia <i>Experimental team</i> M.V.Avdeev, L.A.Bulavin, V.M.Garamus, P.Kopcansky	<i>Date of Experiment</i> May 2015 <i>Date of Report</i>

Objectives

Nowadays structure investigations of ferrofluids have both fundamental and applied interest. It should be mentioned that synthesis of highly stable aqueous ferrofluids with pre-defined properties is quite big problem for the moment. Aggregation stability of such systems depends on used surfactants and its amount in the ferrofluids. Possibilities of various surfactants for stabilization of aqueous ferrofluids were checked previously by us. The aim of the given work was to study structure of aqueous ferrofluids stabilized by various surfactants and to find out correlation between behavior of surfactant in the solutions and final structure of water-based MFs. Behavior of surfactants molecules in aqueous solutions with and without MNPs were compared in the given work according to small-angle neutron scattering data. Critical micelle concentration and some other characteristics were obtained by surface tension measurements.

Results

Impact of surfactant on structure organization of magnetic fluids was concluded from SANS data, namely different size and type of magnetic nanoparticles (MNPs) aggregates was observed in case of stabilization by sodium oleate (SO) or dodecylbenzene sulfonic acid (DBSA) - quite small and compact MNPs aggregates are observed in case of SO stabilization and large and developed fractal type aggregates in water based MF is found in DBSA case. Behaviour of surfactants molecules in aqueous solutions with and without MNPs was studied in the SANS experiment. Critical micelles concentration was obtained from surface tension experiments for SO and DBSA aqueous solutions. Structure and interaction parameters of micelles (micelles aggregation number, fractional charge, charge per micelle and surface potential, etc.) in aqueous surfactants solutions were derived from SANS analysis. Correlation between ferrofluids structure and behaviour of surfactant in aqueous solution is discussed.

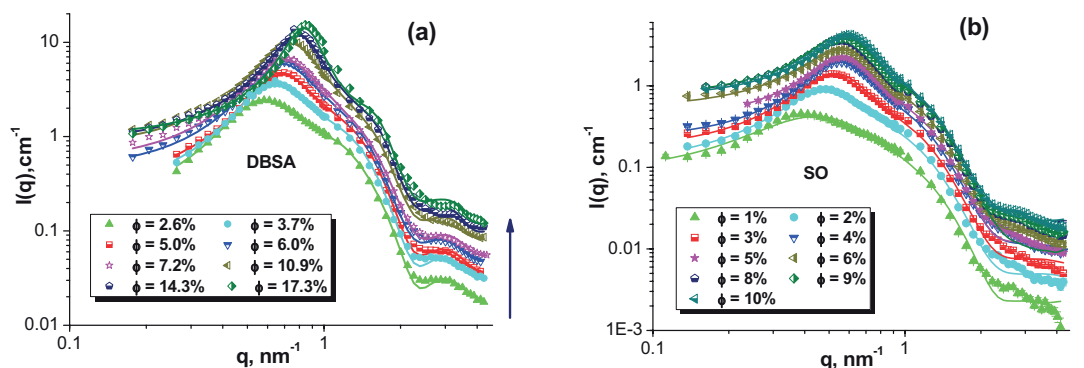


Fig. 1. Experimental SANS curves from solutions of DBSA (a) and SO (b) in d-water with various surfactants content. Arrow shows concentration growth. Solid lines represent best fitting curves.

The determined dependences micelles structure and interaction parameters as a function of the surfactant concentration in aqueous solution can be used in the study of complex systems with DBSA and SO, where potential presence of micelles takes a strong effect on the properties and synthesis of such systems. Particularly, the micelle size is comparable with the size of surfactant aggregates in water-based ferrofluids with double stabilization.

<h1 style="margin: 0;">BNC</h1> <p style="margin: 0;">Experimental Report</p>	<i>Experiment title</i> Structure characterization of perfluorosulfonic short side chain polymer membranes	<i>Proposal No.</i> BRR_420 <i>Local contact</i> Gy. Török.
	<i>Principal proposer</i> Kulvelis Yu. V. ^a V.T. Lebedev ^a , S. S. Ivanchev ^b , Gy. Török ^c <small>. PNPI^a, ^bInstitute of Catalysis of Siberian Branch of RAS. ^c SZFKI</small> <i>Experimental team:</i> Gy. Török (SzFKI) V. T. Lebedev ^a Kulvelis Yu.V. ^a (PNPI)	<i>Date(s) of Exp.</i> 2003 <i>Date of Report</i> 2005

Objectives *(Aim of the research in some sentences)*

The development of hydrogen power has initiated the studies of perfluorinated membranes with $-SO_3H$ groups for hydrogen fuel cells, based on copolymers with different side chain lengths. While earlier the attention was focused on almost only Nafionon® membranes, which were positioned as having the best structure and properties, the recent studies have a tendency to use the perfluorinated membranes with short side chains with sulfonic acid groups in fuel cells. To improve the functional properties of complicated porous membranes it was necessary to evaluate the protons diffusion paths and to determine their structure features by the small-angle neutron scattering studies which were carried out in the present experiments for new types of membranes with short side chains first synthesized at the Institute of Catalysis of RAS.

Results

Supramolecular structure of a new type of polymer membranes (Fig.1) for hydrogen fuel cells has been studied by small angle neutron scattering. These membranes were designed at the Institute of Catalysis SB RAS using a new effective aqueous emulsion method for synthesis. The membranes are based on fluorine-containing macromolecules with sulfonic acid groups and grafted with short side chains. Such new prospective materials for hydrogen fuel cells have advantages over long side chain Nafion-type membranes (foreign analogues) due to optimal chemical structure and a type of macromolecules' packaging that creates stable conduction channels for protons. The results of neutron experiments allowed discover the interrelation between the structural and functional properties of membranes by using physical modeling of membrane structure having a system of linear and branched diffusion channels with diameter of few nanometers and the walls covered with SO_3H -groups that provide proton hopping conductivity. The results are published [1]. The SANS-experiment on new original short side chain (SSC) perfluorinated membranes has discovered the parameters of their internal structure, dependent on polymer characteristics. The general structure elements are similar to those observed for long side chains (LSC) samples – cylindrical channels with diameter ~ 1 nm, regularly arranged and forming ordered structure – short-range order for neighbouring channels combined into bundles with gyration radius $R_g \sim 3-5$ nm and long-range order – correlations between different bundles at the distances > 20 nm. The difference of SSC and LSC membranes appears in thinner channels for SSC samples with diameter 20–50% less than for LSC. Neighbour channels are also closer to each other in SSC membranes.

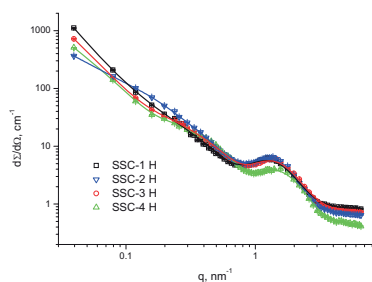


Fig.1. Scattering cross sections of membranes saturated with H_2O as dependent on momentum transfer. The samples SSC-1-4 have different equivalent weight per a SO_3H -group in polymer chain (752; 804; 807; 1021). Curves are the approximation functions used by modeling.

Future prospects *(Summary of the remaining problems to be solved, basis for the continuation of the work)*

The above data appears to be related to the different conditions of formation of physical state (conformation, molecular packing) of hydrophobic and hydrophilic parts of membranes. The continuation of neutron studies of new membranes will enable to improve the method of synthesis affects on the internal packaging of membrane and thus can influence on the proton conductivity and membrane performance. These problems require further neutron researches of nanostructural features of polymer membrane materials.

[1]. Yu. V. Kulvelis, S. S. Ivanchev, V. T. Lebedev, O. N. Primachenko, V. S. Likhomanov, Gy. Török. Structure characterization of perfluorosulfonic short side chain polymer membranes. // RSC Advances., 2015, 5, 73820-73826.

BNC Experimental Report	<i>Experiment title</i> NIPS, TOF-ND AND PIXE INVESTIGATION OF ROMAN METAL ARCHAEOLOGICAL OBJECTS FROM THE MUNICIPIUM TIFERNUM MATAURENSE AREA, ITALY	<i>Instrument:</i> PIXE
	<i>Principal proposer:</i> Massimo Rogante, Rogante Engineering Office <i>Experimental team:</i> Massimo Rogante, Imre Kovács	<i>Local contact:</i> I. Kovács <i>Experiment Number:</i> BRR_351 <i>Date:</i> 13.03.2014

Objectives

To obtain helpful information in order to verify composition, possible manufacture technologies, origin of the metals used and to understand the origin context of the investigated objects. The expected results compared with archaeological and contextual data could supply useful knowledge also of a more precise dating of the life phases of this interesting - but still little well-known - mountain centre of the Roman Italy. To enhance the modest regional database currently available, which is based essentially on the investigations in recent times performed, e.g., by PGAA on comparable Picenan objects coming in particular from Matelica and Fabriano necropolis. To obtain possible indications to create replicas of the major element compositions and in accordance with the supposed manufacturing process, and also to analyse that as a standard to compare with the original objects.

Results

Due to some unforeseen technical problems emerged at the Budapest Research Reactor, it was not possible to perform the neutron-based investigations (NIPS-NORMA and TOF-ND analyses).

Among the intended analyses only the PIXE measurements were carried out on the studied archaeological bronzes, since PIXE facility is not connected to the operation of the BRR. We investigated all the 6 objects listed in the Proposal description, obtaining in total 14 PIXE spectra: 4 spectra for the scapel (inv. 1061), which was investigated in two spots (clean and corroded) of the blade, one spot of the handle and one spot of the cross section blade-handle; 2 spectra for the capsella (inv. 1867), i.e. one dark spot of the main side and another spot of the reverse side; 2 spectra for the golden fragment of statue (inv. 1567), i.e. one spot of the gold plated part and another spot for the unplated part; 2 spectra for the carved lamina (inv. 1870), i.e. one dark spot and another gray spot; 2 spectra for the foot finger fragment (inv. 1570); 2 spectra for the coin (inv. 1594).

We were able to get information on the elemental composition of the base material for each investigated point, in particular detecting as main elements Cu, Zn, Pb, Ag, Sn, Au. As a preliminary statement, we can say that: objects inv. 1061 and 1870 are made of tin bronze; the object inv. 1867 shows Sn and Ag; the object inv. 1570 is a zinc bronze with Ag as added component; the object inv. 1594 is a tin bronze also with Ag as added component, and it does not show Zn; the object inv. 1567 does not show gold in the not plated part, which also shows less content of silver.

Concerning the neutron-based analyses, the BNC declared to be available to proceed these analyses as well, later, as soon as the technical conditions would have permitted it, and depending on the availability of the considered archaeological objects.

BNC Experimental Report	<i>Experiment title</i> SANS and TOF-ND Investigation of ancient and modern Linen cloths	<i>Instruments:</i> SANS diffractometer + PIXE <i>Local contacts:</i> A. Lén, I. Kovács
	<i>Principal proposer:</i> Massimo Rogante, Rogante Engineering Office <i>Experimental team:</i> Massimo Rogante, Matilde Borla, Adel Lén, László Rosta, Imre Kovács	<i>Experiment Number:</i> BRR_331 <i>Date:</i> 15.01.2014

Objectives

To carry out by SANS an investigation at micro- and nano-scale levels, in order to assess various parameters, properties and other important characteristics of the considered material. To achieve by Neutron Diffraction important information on the structural properties, so completing the data obtained by SANS in investigating the molecular structure, the hydrogen bonding system and the texture of the relevant textiles. To provide substantial new data to complement the analytical and crystallographic information, which are crucial to comprehend the structural basis for the chemical, physical, and biological properties of the considered material. To supply scientific contributions to the study of linen cloths, either considering each single sample, or making comparisons. To achieve, in general, a better understanding of characteristics and behaviour of the investigated materials.

Results

The SANS investigation was carried out comparing 9 ancient - mainly from pre-dinastic (3500-2000 B.C.) and Ptolemaic ages - and 5 modern linen samples. A relatively high small angle scattering of neutrons was observed in case of all (old and new) samples. In case of the old samples, no orientation was observed on the scattering pictures. This could be caused by the degradation of the samples and the destruction of cellulose fibrils or - with smaller probability - the dirt from the samples could shadow the scattering from the oriented fibrils. The new samples, on the other hand, showed anisotropy along the linen wire axis. The samples showed fractal like scattering. In the case of the old samples the fractal behavior can be caused by a destroyed fiber-structure that does not show any clearly distinguishable scattering object inside the samples; the scattering is coming from randomly oriented surfaces, arranged in multilevel structure. In the case of the new samples we could observe oriented scattering in two perpendicular directions, similar to the weaving of the fabric. We have treated the samples as they would be isotropic scatterers, because the two different orientations could not be well-separated, and the scattering was not coming from the cross section of the linen fibrils, but from its length. This allowed us to obtain fractal exponents to the new fabrics as well. New and old samples showed different fractal like behavior. The pleated and not pleated samples are not showing a characteristic difference in their nanostructure that could be visible by small angle neutron scattering.

It was not possible to carry out TOF-ND analyses. Instead, the ancient samples were investigated also by PIXE and their elemental composition was assessed.

B N C Experimental Report	<i>Experiment title</i> NIPS, TOF-ND and PIXE investigation of Roman-Picenum metal archaeological objects from the Academia Georgica Treiensis collection	<i>Instrument:</i> + PIXE <i>Local contact:</i> I. Kovács
	<i>Principal proposer:</i> Massimo Rogante, Rogante Engineering Office <i>Experimental team:</i> Massimo Rogante, László Rosta, György Káli, Zsolt Kasztovszky, Zoltán Kis, Imre Kovács, Boglárka Maróti, Zoltán Szőkefalvi-Nagy	<i>Experiment Number:</i> BRR_300 <i>Date:</i> 31.01.2013

Objectives

To obtain helpful information in order to verify composition, possible manufacture technologies and origin of the metals used. The analyses carried out by using NIPS were expected to supply considerable scientific contributions to understand the origin context of the Treia objects, contextually enhancing the modest local database currently available, which is based essentially on the investigations in recent times performed by PGAA on comparable Picenan objects coming in particular from Matelica and Fabriano necropolises. These works remarkably sustained the local source of the manufactured objects. These data are very useful to better interpret the possible geographical origins.

To obtain possible indications to create replicas of the major element compositions and in accordance with the supposed manufacturing process, and also to analyse that as a standard to compare with the original objects.

Results

Objects n. 1 (laminated bronze basin), n. 2 (*Oinochoe* with high vertical cone-shaped beak), n. 3 (winding-arch-shaped fibula), nn. 4 and 5 (swollen-arch-shaped fibulas with extended bracket), n. 6 (*olla* with varied applied plaques), n. 7 (metallic rod with two sliding inserts) and n. 8 (metallic polilichnes oil lamp with six radial nozzles of ogive-shape tip) were investigated. These objects have been investigated by using all the considered techniques. The evaluation results of PGAA spectra, with concentrations of all the identified elements and their absolute (+/-) and relative uncertainties, were obtained. Objects from n. 1 to n. 6 result made of tin-bronze (Cu+Sn) alloys, with Sn varying in the range 1.7-6.9 (wt %) and Ag as minor element varying in the range 0.03-0.09. Objects n. 2 and 6, in particular, show practically no minor element, and object n. 6 has a much lower content of Sn, compared to the others (objects n. 1 to n. 5). Object n. 7 results made of Cu-Zn-(Sn) alloy. Object n. 8 (the investigated polilichnes lamp with six radial nozzles) results made mainly of Zn (87.4), with Pb (7.8), Sn (4.0) and Cu (0.83). TOF-ND results have been obtained for all the objects. Concerning the object 8, in particular, The TOF-ND data pointed out that metallic zinc was melted and cast during the manufacturing process. No significant amount of other phases was measurable (neither other metals nor epsilon brass). By analysing the obtained PIXE data, the following considerations can be written. Object n. 1 results made of a tin-bronze (Cu+Sn) alloy (examination in a corroded area), with Fe and Pb as minor elements. Object n. 2 results made of a tin-bronze alloy (examinations in black areas). Object n. 3 as well results made of a tin-bronze alloy, with about 15-20 m/m% Sn and 1.5-2.3 m/m% Pb. All of them can be classified as high tin bronzes, presenting percentages above 14%. Moreover, Si and K are present on the surface. Object n. 4 results made of Cu (examination in a corroded area), with Fe and Pb as minor elements. Object n. 5 results made of Cu + minor and trace elements + light elements on the corroded surface. Object n. 6 results made of Cu (corroded) with Fe and As as minor elements. Object n. 7 results made of Cu-Zn-(Pb) alloy, with surface inhomogeneities. Object n. 8 results made mainly of Zn, while Pb has been detected only on some areas. The presence of elements other than the main alloy constituents (e.g., Pb), sometimes, appears relevant, being able to reach even values over 1%. The interpretation of the results by the historical-archaeological point of view is in progress.

<h1 style="margin: 0;">BNC</h1> <p style="margin: 0;">Experimental Report</p>	<i>Experiment title</i> Structure changes of casein micelle by microbial transglutaminase	<i>Proposal No.</i> BRR_392
	<i>Principal proposer:</i> Lívia Darnay <i>Experimental team:</i> Lívia Darnay, Adél Len	<i>Local contact</i> Adél Len

Objectives

Our research aim was to observe the cross-linking effects of MTG on casein micelle structure under the sol-gel transformation of lactic acid fermentation of model yogurt solutions to give an answer on the texture-modifying property of the enzyme in low-fat yogurts. Our further research was dedicated to identify the casein micelle structure changes due to enzyme treatment in low-fat yoghurt.

Results

Effect of mTG can be seen only after 1 hour of fermentation according to the obtained Porod exponents (p). The enzyme activity causes remarkable decrease in the p values, which refers to a tendency of compact micelle network structure development process (see on Fig. 1.). Due to the structure modifying property of the enzyme the structure of mTG treated sample becomes more and more compact, what increases the neutron scattering intensity. This structure can be modelled in a first approximation with the sum of a spherical model function and the model of a stabilized texture, described by a volume fractal characteristic exponential function (see on Fig. 2.). In this first approximation we have obtained sizes around 100 Å for the sphere's radii. For the first time we could follow in-situ the nanostructure changes in the fermentation process of the low-fat yoghurt.

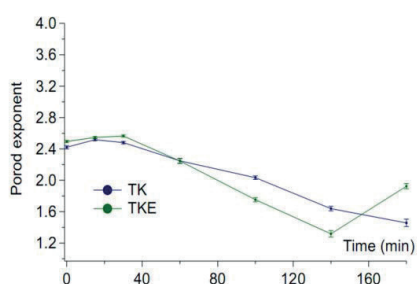


Fig. 1.: Porod exponents of control (TK) and enzyme treated (TKE) yogurt model solutions during fermentation

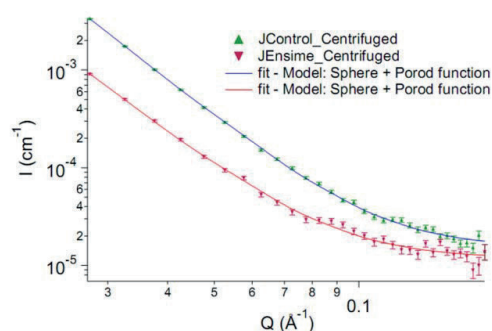


Fig. 2.: Size difference between control and enzyme treated low-fat yogurts

References

- De Kruijff, C.G., Huppertz, T., Urban, V.S., Petukhov, A.V. (2012) Casein micelles and their internal structure (Review) *Advances in Colloid and Interface Science*, 171-172, 36-52
- Huppertz, T., de Kruijff, C.G (2008): Structure and stability of nanogel particles prepared by internal cross-linking of casein micelles. *International Dairy Journal* 18, 5, 556-565

Future prospects

We would like to make new measurements with concentrated casein powder to analyse the structure of casein micelles individually using our own developed sample preparation method.

<h1 style="margin: 0;">BNC</h1> <p style="margin: 0;">Experimental Report</p>	<i>Experiment title</i> Residual stress measurements with a four point bending device at BNC	<i>Instrument:</i> ATHOS <i>Local contact:</i> Török Gyula
	<i>Principal proposer:</i> <i>Experimental team:</i> Gyula Török	<i>Experiment Number:</i> <i>Date:</i>

Neutron diffraction is a non-destructive method for determining residual stresses in crystalline materials. At the Budapest neutron center the ATHOS spectrometer is used to carry out this type of measurements. In our case the used wavelength 3.3 Å results in higher absorption in materials than the usually applied thermal beam (1-2 Å), the used geometry however, is more comfortable. The used 002 reflection of PG monochromator provides more broad angular distribution than for this task is optimal. Using the 004 reflection gives much less error bar and not substantial intensity loss. The mechanical positioning error was 0.1mm, so the displacement of gauge cube can cause this distortion.

We performed measurements using a four bending device and tested a 10mm thick 20mm x 200 mm steel plate. That was an additional proof of instrument setup and the bending device itself. The setup and serial of results are displayed on Figures 2a and 2b. The results fit well to the expected line. At the last point the gauge volume is partially out from material giving false result so the value is not taken into account.

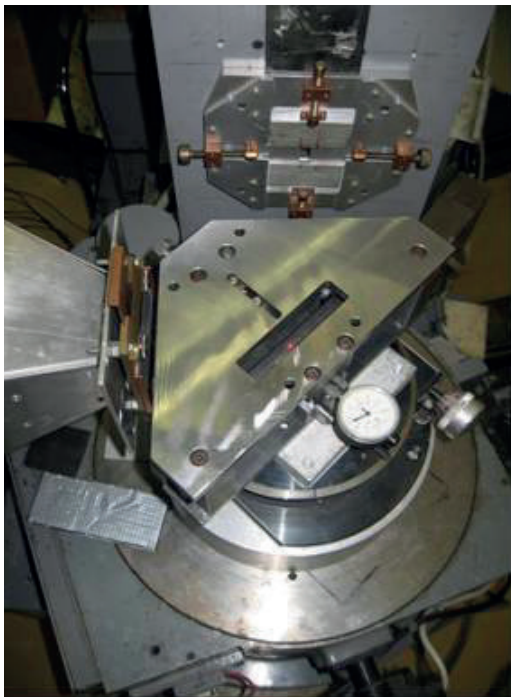


Fig. 1. The bending device in test position

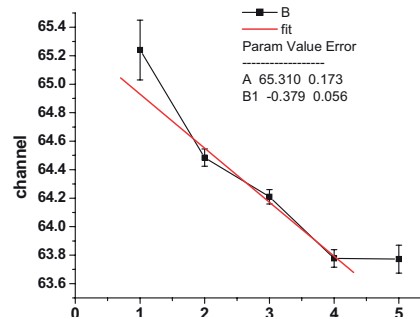
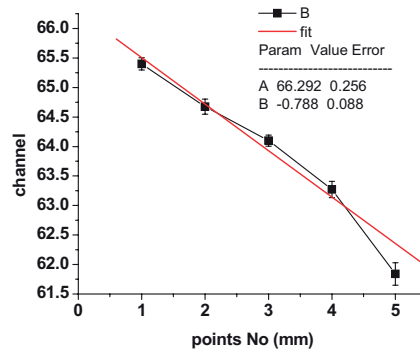


Fig.2. The resulted peak shifts parallel and perpendicular to the surface

References

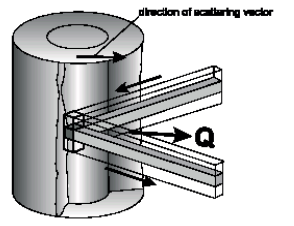
G.A. Webster, R.C. Wimpory Development of procedures for the measurement of residual stress by neutron diffraction Appl. Phys. A 74 [Suppl.], S1227–S1229 (2002).

<h1 style="margin: 0;">BNC</h1> <p style="margin: 0;">Experimental Report</p>	<i>Experiment title</i> Residual stress measurements at BNC on VAMAS round robin Al sample	<i>Instrument:</i> ATHOS <i>Local contact:</i> Török Gyula
	<i>Principal proposer:</i> <i>Experimental team:</i> Gyula Török	<i>Experiment Number:</i> <i>Date:</i>

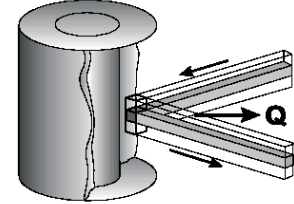
Neutron diffraction is a non-destructive method for determining residual stresses in crystalline materials. We have carried out on the ATHOS spectrometer at BNC measurements on a VAMAS standard round robin Al plug sample [1]. Following the recommended procedure the study was made with accuracy of 0.2 mm in position and 20 Mp in stress. This setup is to be used for investigation of real engineering components.

SAMPLE: VAMAS Aluminum Ring & Plug Set No.: 2

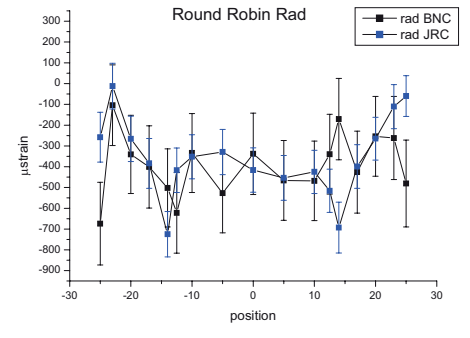
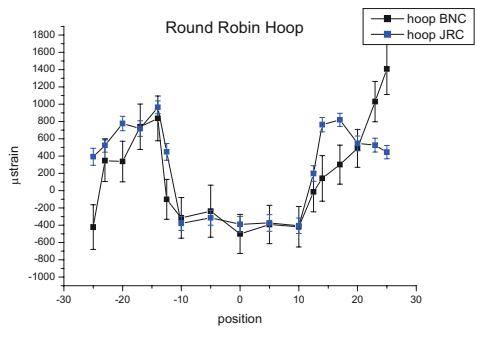
Measurement Direction:	Hoop	Radial	Axial
Reflection [hkl]:	111	111	111
Absolute or Nominal Wavelength [Å]:	3.3	3.3	3.3



c) hoop strain



b) radial strain



The comparison of hoop and radial strain result were made with measurements at JRC. The measured strains are in good agreement [2]. The figures show that the strain fits on the negative side of sample position, while on the positive side of sample position the fit is more poor.

References: [1] G.A. Webster et al. Appl. Phys. A 74 [Suppl.], S1227–S1229 (2002). [2] G.A. Webster ed.: VAMAS Rep. No. 38, January 2000) [ISSN 1016-2186]

<h1 style="margin: 0;">BNC</h1> <p style="margin: 0;">Experimental Report</p>	<i>Experiment title</i> Experiment Title: Structural study of magnetocaloric (Mn,Fe)₂(P,As) compounds around the first order phase transition	<i>Instrument:</i> MTEST <i>Local contact:</i> Laszlo Temleitner
	<i>Principal proposer:</i> Lukasz Hawelek, Institute of Non-Ferrous Metals, ul. Sowinskiego 5, 44-100 Gliwice, Poland <i>Experimental team:</i> Lukasz Hawelek, L. Temleitner	<i>Experiment Number:</i> BRR_448 <i>Date:</i> 17-27.11., 8-16.12.2015

Objectives

The project objective was to perform the temperature dependent neutron diffraction (ND) measurements for silicon doped two different Fe₂P-type magnetocaloric materials below and above their Curie temperatures (temperature of magnetic phase transformation) determined previously using magnetic measurements. The ND measurements should be done for further Rietveld-analysis using series of high-resolution, low-Q measurements (with 1.44 Å wavelength) and for real-space analysis, high-Q range (with 0.88 Å wavelength).

Results

During this beamtime the neutron diffraction experimental has been performed on two powder samples with chemical composition as follows: sample1 - Mn₁Fe₁P_{0.3}As_{0.5}Si_{0.2}, sample2 - Mn_{1.1}Fe_{0.9}P_{0.3}As_{0.5}Si_{0.2} with small difference in the Mn/Fe atomic ratio. To achieve the proposal objectives the measurements for sample 1 has been performed below and above Curie temperature e. g. at 300K and 410K respectively. To obtain the best relation of resolution and scattering vector Q range the measurements has been done using two monochromators Cu(111) and Cu(220) that allow to reach the different Q range: up to 7.7 Å⁻¹ and 12.7 Å⁻¹. Because of the 10 times lower intensity of the scattered neutrons for Cu(220) monochromator setup in comparison to Cu(111), the higher Q value measurements were time-consuming. The Cu(111) monochromator is giving the wavelength 1.45 Å whereas the Cu(220) the wavelength 0.89 Å. To obtain the correct sample intensity, the intensity of the vanadium empty can (8 mm in diameter) was subtracted from the measured intensity. Additionally for proper detector positioning in both monochromators setup the nickel powder as a pattern was measured. The measured data using both monochromators at 300K and 410K after correction and combining for sample1 is presented in Figure 1.

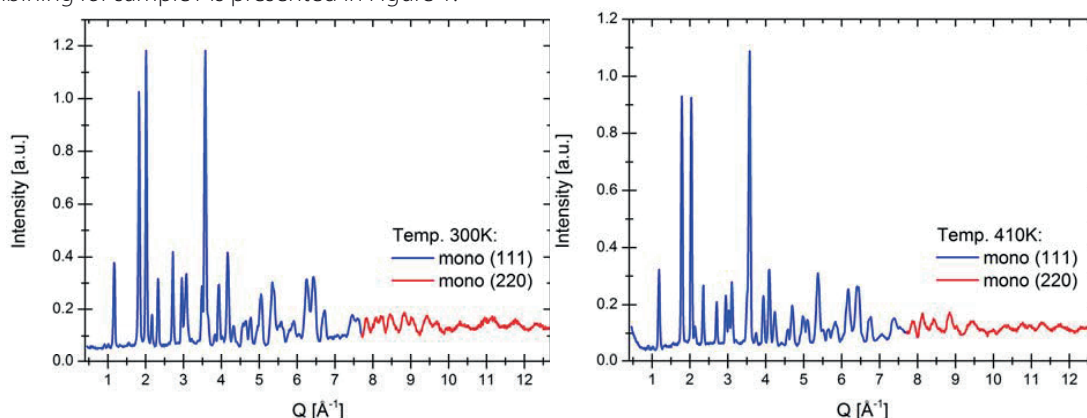


Figure 1. The Q-scale representation of the neutron diffraction intensity for sample 1 measured at 300K (left) and 410K (right) using Cu(111) and Cu(220) monochromators

In the next part of this beamtime the sample2 was measured at three different temperature below the Curie temperature 300K, above the Curie temperature 410K and 610K using also both monochromators to cover the maximum Q-scale range.

The successfully obtained results are suitable for further comparative analysis of temperature dependant atomic structure evolution around the magnetoelastic transformation that coexists in the giant magnetocaloric effect in Fe₂P-type compounds. The data evaluation and comparative analysis is still in progress.

Instruments | **6.**

6.1. PSD – NEUTRON POWDER DIFFRACTOMETER WITH POSITION SENSITIVE DETECTORS

Instrument scientist: Margit Fábrián^{1,2}, Erzsébet Sváb²

¹ Centre for Energy Research

² Wigner Research Centre for Physics

The PSD neutron diffractometer is suitable for atomic structure investigations of amorphous materials, liquids and crystalline materials where the resolution requirements are not high. It is a 2-axis diffractometer equipped with a linear position sensitive detector system. The detector assembly is mounted on the diffractometer arm and it spans a scattering angle range of 25° at a given detector position. The entire diffraction spectrum can be measured in five steps. During the year of 2002, the detector system of the PSD has been upgraded, a new system has been installed from Studsvik NFL (Sweden) with a digital electronics technology. The detector system is based on three ³He filled linear position sensitive Reuter-Stokes detectors (610 mm in length, 25 mm diameter). The three detectors are placed in the

scattering plane above each other. Data transfer and instrument control has been done by PC-AT (Master PC) with Eagle I/O card. A Windows based instrument software program package has been developed.

During the year of 2009, the interface electronics has been upgraded. A new dedicated electronic device has been constructed, which serves for the electronic control of the movements and data transfer of the diffractometer.

Recently have been developed a new sample environment. An in-situ cell have been designed and build up to the PSD diffractometer. The High Temperature and Pressure (HTP) cell may be operated at pressure ranging from ambient to about 300 bar and at high temperature from RT to 900°C.

Table 1. ▶
Characteristic features
of the PSD diffractometer for
two actual arrangements

Channel	thermal, 9T tangential
Primary collimation	Soller-type : 20'
Take-off monochromator angle facility	$-5^\circ < 2\Theta_M < 45^\circ$
Monochromator and mosaicity	Cu(111), 16'
Monochromatic wavelength	1.069 Å
Resolution, $\Delta d/d$	$1.2 \cdot 10^{-2}$
Flux at the sample position	$10^6 \text{ ncm}^{-2}\text{s}^{-1}$
Beam size at the specimen	10 mm×50 mm
Scattering angle, 2θ	$5^\circ < 2\theta < 110^\circ$
Momentum transfer interval, Q	$0.6\text{-}9.2 \text{ \AA}^{-1}$
Monitor counter	fission chamber
Detector system	3 linear position sensitive ³ He detectors - the detector assembly spans 25° scattering angle at a given position
Data collection	Xilinx pre-programmed unit
Data transfer and control	PC-AT with Eagle I/O card and a dedicated electronic device
Remote control and file transfer	Windows programme package

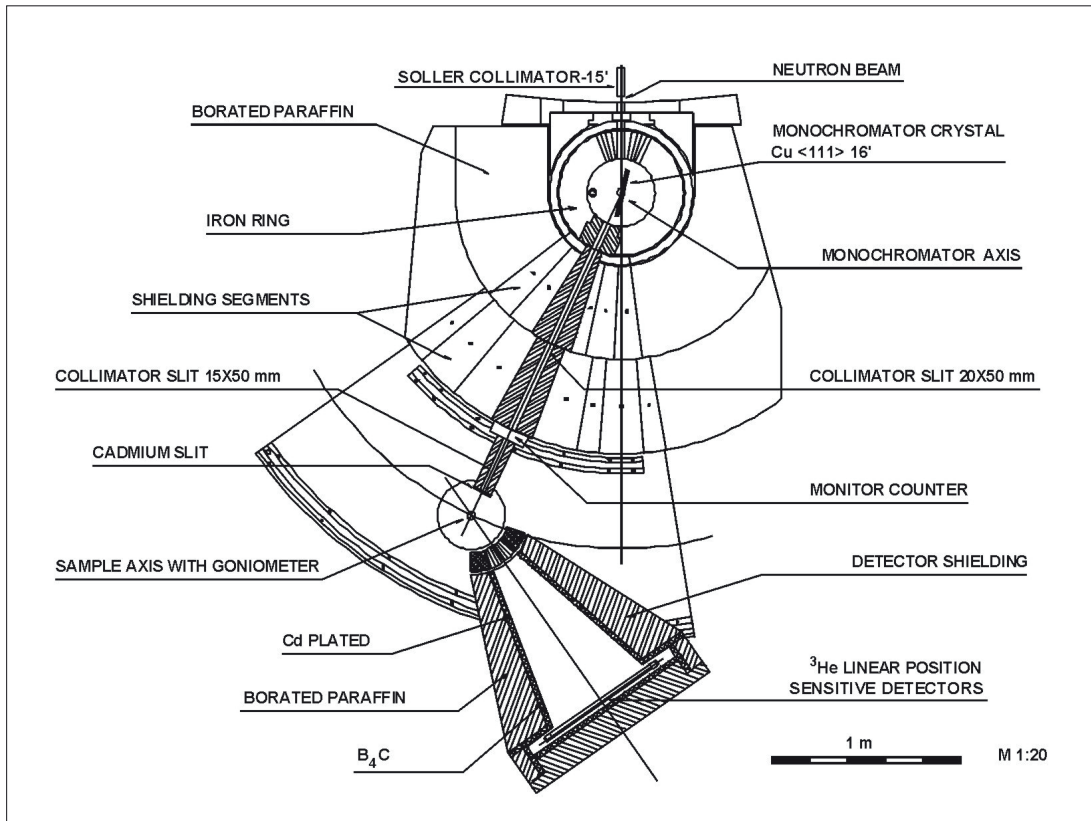


Figure 1. Schematic arrangement of the PSD neutron diffractometer

6.2. MTEST DIFFRACTOMETER

Instrument scientists: László Temleitner, László Kőszegi

Wigner Research Centre for Physics, Institute for Solid State Physics and Optics

The M(aterial) TEST neutron diffractometer is a general-purpose powder diffractometer: it covers the area of medium-resolution powder, liquid and amorphous total (Bragg and diffuse) scattering diffraction measurements, as well. The instrument obtains various sample environments allowing to perform studies on powder samples between 77K — 1273K and spinning, scanning or orienting (by Eulerian-craddle) the samples at room temperature.

The MTEST diffractometer is installed on the 6th axial thermal channel of the reactor. The maximum flux can be obtained at a wavelength of 0.144 nm. A sapphire single crystal is used, deep inside the beam shutter, to filter out epithermal neutrons. The neutron flux at the sample table is $2 \cdot 10^6$ neutron/($\text{cm}^2 \cdot \text{sec}$) at a wavelength of 0.133 nm. The standard size of the beam is 10 mm (width) x 40 mm (height), which can be adjusted by slits for the required size.

The instrument is equipped with a monochromator changer that uses 3 crystals: Ge(111), Cu(111) and Cu (220), allowing to tailor the beam for the required Q-range and resolution even during the measurement period of one sample (see Table 1).

A low efficiency fission chamber monitor and an Ordela position sensitive detector (with two sample/detector positions) serve data collections. The ultimate angular upper limit of the detector in “near position” is 141°, whereas 151° at “far position”. However, practically the pattern from 7° to 138° can be recorded by 5 positions in the “near” and from 6° 139° by 12 positions in the “far” positions. The current level of background in “near” position equals to the scattered intensity from a 6 mm diameter, 0.05 mm thick, 40 mm long vanadium sample holder.

To mount samples standard O-ring sealed vanadium cans (6 and 8 mm in diameter) are available for room temperature measurements.

Ancillary equipments:

- low background vanadium vacuum furnace (RT-1000°C)
- aluminium-shielded cryostat (77K-RT)
- X,Y scanning table for residual stress measurements

Our group is ready to help users, starting from measurements, through data evaluation, simulation and publication.

Table 1. ▶
Some typical setup

Setup	Monochromator	Wavelength [Å]	Q-range [Å ⁻¹]	Best resolution	Intensity
“Disordered crystal”	Cu(111)	1.45	0.45 - 8.1	0.6°	100%
“Medium resolution crystal”	Cu(220)	1.35	0.5 - 8.5	0.6°	40%
“Liquid/amorphous”	Cu(111)	1.11	0.65 - 10.6	1.2°	85%
“Medium-Q liquid/amorphous”	Cu(220)	0.89	1.0 - 13.1	1.0°	10%
“Low-Q liquid/amorphous”	Ge(111)	2.27	0.25 - 5.1	1.2°	6.5%

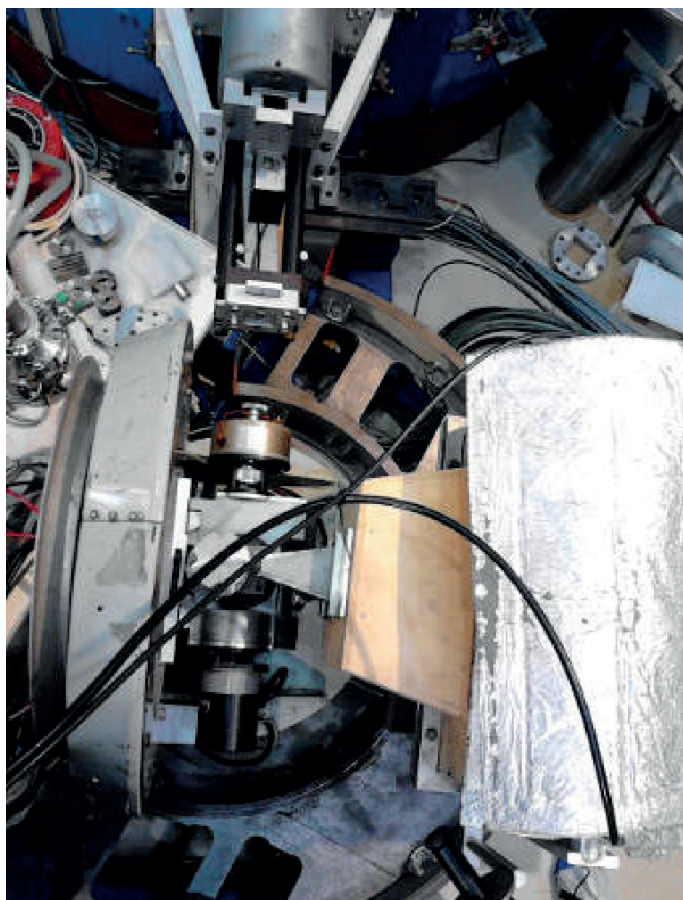


Figure 1.
MTEST overview: sample changer with the “near” position of the detector in the center and vacuum furnace on the left. The width of the dark foot at the left bottom corner corresponds to about 12 cm



Figure 2.
Side view of the sample changer RT setup

6.3. TOF – HIGH RESOLUTION TIME-OF-FLIGHT POWDER DIFFRACTOMETER

Instrument scientists: György Káli

Wigner Research Centre for Physics, Institute for Solid State Physics and Optics

The TOF is a general purpose high resolution time-of-flight powder diffractometer. It can cover a d -spacing range from 0.5 to 2.5 Å (2.5 to 12.5 Å⁻¹ in Q-range) at variable band-width and resolution ($\Delta d=0.0015$ -0.15 Å). It is applicable for structure determination and refinement, peak profile analyses, phase and texture analyses of crystalline materials and for liquid diffraction as well.

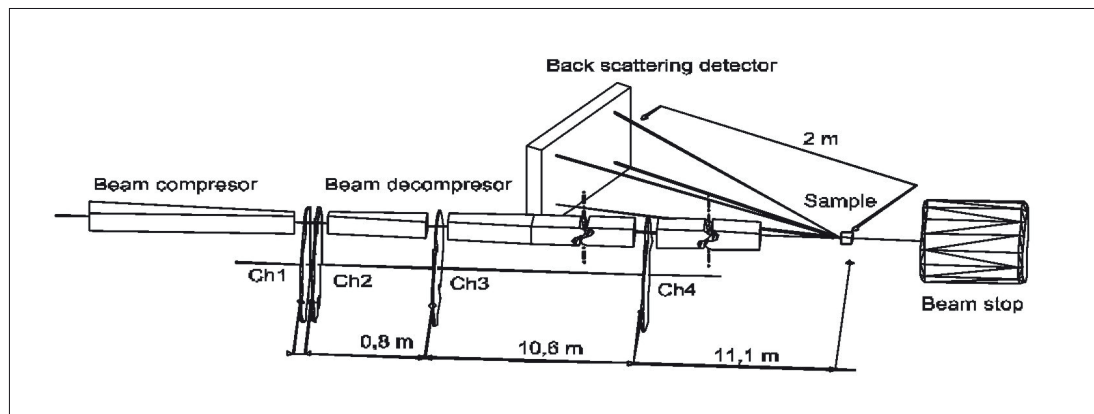
The instrument is installed to a radial thermal neutron beam and placed in a separated measuring hall. The monochromator system consists of a fast double and the two single choppers and a straight neutron guide with 2.5x10 cm² cross section at the end. The double chopper is designed for a maximum speed of 12000 rpm. While in high resolution mode the very short - 10 μs – neutron pulse and the 25m total flight path allows us to obtain a diffractogram with an accuracy of 1.5x10⁻³ Å (at back scattering mode) in a single measurement on polycrystalline materials, in low resolution mode liquid diffraction can be performed at good neutron intensity up to 12.5 Å⁻¹ scattering vector. The beam is filtered by single crystal silicon against fast neutrons. The double disk chopper (Ch1 and Ch2) has two windows: a 1.5°

opening for short pulses (10 μs) and a 15° window for long variable pulses (20–200 μs), They can be operate in parallel and counter rotating mode. The latter option is used to produce very short pulses at high speed. To minimize the opening time the neutron beam is reduced from 25 to 10 mm width at the position of the pulse choppers using a 4.5m compressor neutron guide section before and a same decompressor after them (see Figure 1). Ch3 limits crosstalk between different pulses and Ch4 prevents frame overlap.

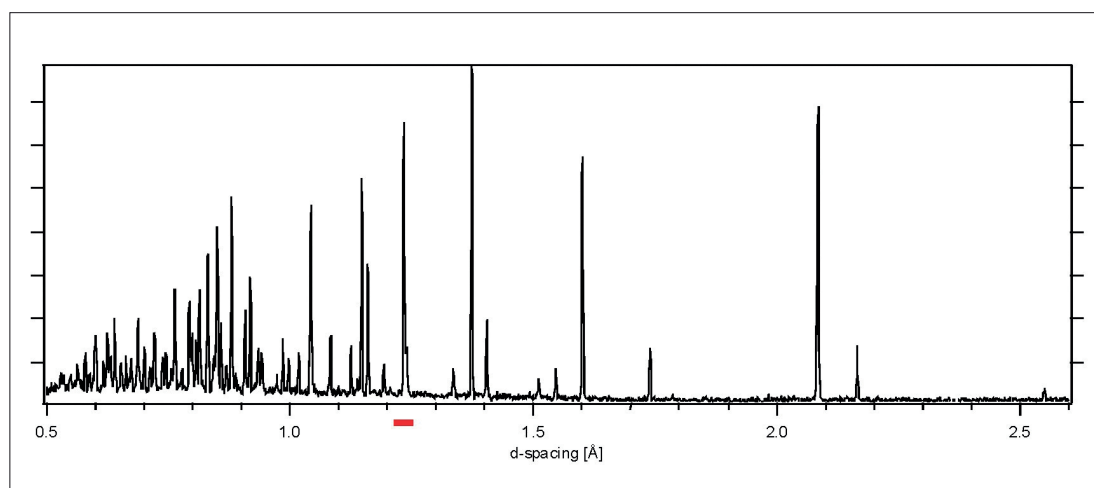
The instrument is recently equipped with a large surface back-scattering detector bank consist of 88 pieces of squashed ³He tube (Figure 3). It cover 20° scattering angle ($2\theta=145^\circ$ -165°). The data are acquired in so called "list" or "time stamping" mode: all the event on the detector, the chopper signals and optionally changes in the sample environment are registered with the time passed since the starting of the experiment. In this mode many uncertainties can be filtered out during the treatment and re-treatments and allows to perform time dependent in-situ experiment in a single measurement.

Table 1. 
Main parameters

Total flight path from chopper 1	L=25 m
Wavelength range	0.08-0.5 nm
Bandwidth in single experiment $\Delta\lambda$	from 0.4 nm to 0.08 nm (200 Hz)
Resolution $\Delta d/d$	1.5x10 ⁻³
Straight neutron guide cross section	25x100 mm ²
Coating	Supermirror NiTi, m=2
Beam flux at opened windows	4x10 ⁷ neutron/s/cm ²
Pulse length	10-1000 μs
Max. speed for the double chopper	12000 rpm



◀ **Figure 1.**
Instrument Layout



◀ **Figure 2.**
The medium resolution wide-band spectra from sintered alumina illustrates the d-spacing range available for high resolution at back scattering



◀ **Figure 3.**
Detector bank

6.4. YS-SANS – SMALL ANGLE NEUTRON SCATTERING INSTRUMENT YELLOW SUBMARINE

Instrument scientists: László Almásy, Adél Len, Renáta Ünne

Wigner Research Centre for Physics, Neutron Spectroscopy Department

The SANS diffractometer *Yellow Submarine* covers a Q-range from 0.003 to 0.7 Å⁻¹ allowing to probe structures at length scales from 5 Å to 1500 Å. It has a wide range of applications from studies of defects and precipitates in materials, surfactant and colloid solutions, ferromagnetics, magnetic correlations, alloy segregation, polymers, proteins, biological membranes. The instrument is installed on the curved neutron guide No.2, with 4x4 cm² cross-

section, made of (1.5 θ_c) supermirrors. The beam is monochromatized by a multidisc type velocity selector, (L. Rosta: Physica B 174 (1991) 562) the rotation speed can be tuned between 700 and 7000 rot/min (wavelengths between 3 and 12 Å). The width Δλ/λ of the transmitted wavelength distribution can be varied between 12% and 30% by changing the tilt angle between the selector axis and the direction of the neutron beam. The collimation distance is 5 m.

Sample environment

In most of the experiments an automatic sample changer with 6 positions is used. It can be thermostated from an external bath between 10°C and 90°C. An 11 position sample changer can be used for ambient temperature experiments. Liquid

nitrogen cryostat, or closed cycle refrigerator can be used (from 10K-300K). Electromagnets can also be mounted on the sample table (field 1.6T in the gap 25mm), with a vertical automatic sample holder with 9 sample positions.

Detector

The scattered neutrons are detected by a 64 x 64 pixels (1cm x 1cm pixel size) two dimensional

position sensitive LETI (Grenoble, France) detector filled with BF₃ gas.

Data acquisition

The control and data acquisition electronics has been made by Laboratoire Léon Brillouin, Saclay,

France, and ANTE Ltd., Budapest, Hungary, the data acquisition software was designed in our Lab.

Table 1. ▶
Main characteristics

Beam tube:	Cold neutron guide No. 2/1
Monochromator:	Multidisk velocity selector
Detector:	2D position sensitive, 64x64 cm ² , filled with BF ₃ gas
Collimation:	5 m
Flux at the guide exit:	5 x 10 ⁷ n/cm ² /sec
Sample-to-detector distance:	Continuously adjustable between 1 m and 5.5 m
Incident wavelength:	3 - 12 Å
Wavelength spread:	Adjustable between 12 - 30 %

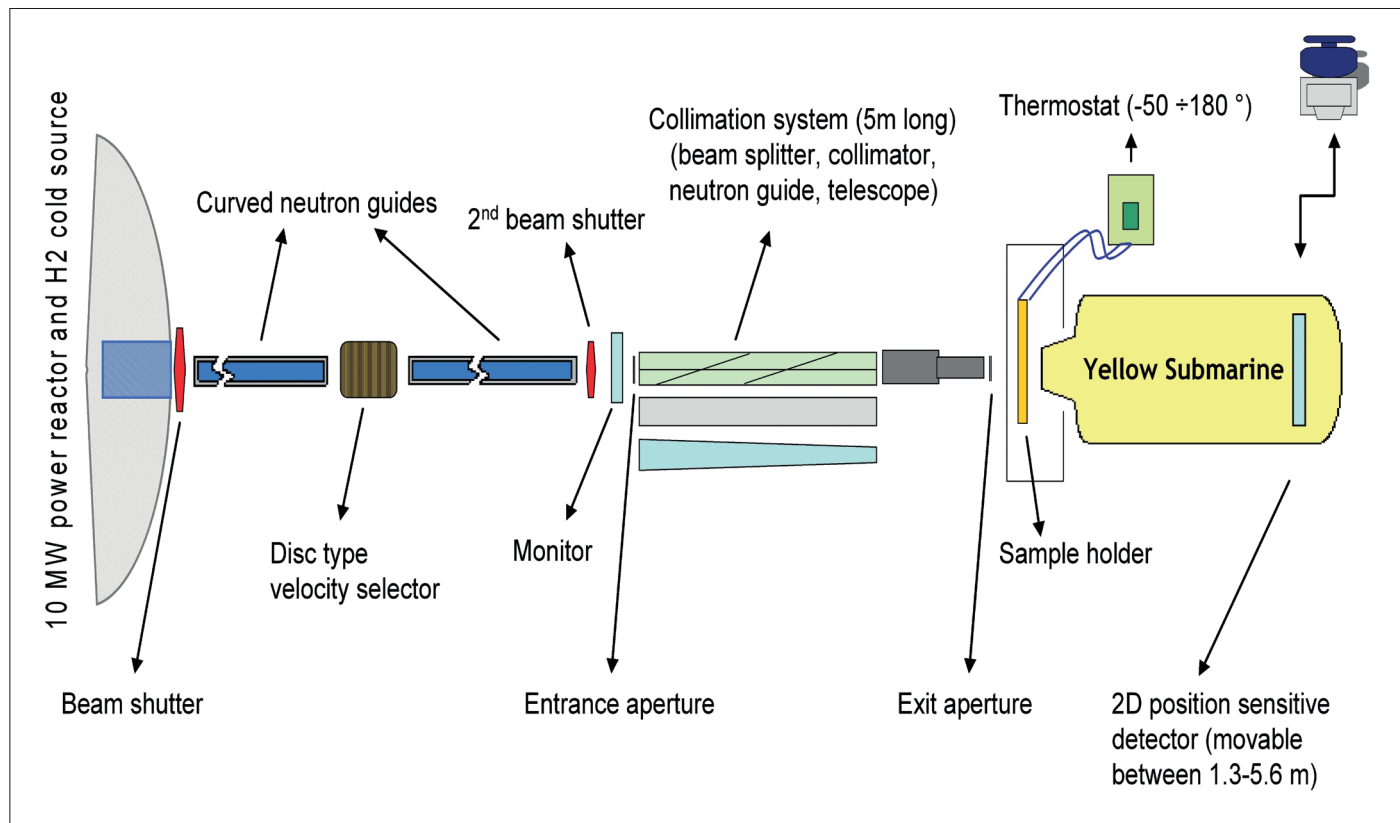


Figure 1. Scheme of the SANS diffractometer Yellow Submarine

6.5 FSANS – TIME OF FLIGHT SMALL ANGLE NEUTRON SCATTERING INSTRUMENT

Instrument scientists: János Füzi, Adél Len

Wigner Research Centre for Physics, Neutron Spectroscopy Department

The FSANS diffractometer covers a Q-range from 0.0003 to 0.03 Å⁻¹ and complementary to the Yellow Submarine SANS instrument allows to probe structures at length scales from 100 Å to 5000 Å. It has a wide range of applications from studies of defects and precipitates in materials, surfactant and colloid solutions, ferromagnetics, magnetic correlations, alloy segregation, polymers, proteins, biological membranes. The instrument is installed on the bottom section of the curved neutron guide No.3, made of $m = 2$ supermirrors.

The beam time structure is provided by 4 choppers: a counter-rotating pair of pulse definition choppers, one wavelength limiting and one frame overlap chopper. The available wavelength range is 2 - 16 Å. The width $\Delta\lambda$ of the wavelength uncertainty can be set by choosing the pulse definition chopper window to 0.3 Å with 8° opening (better resolution mode) or 0.75 Å with 20° opening (higher intensity mode) respectively. The collimation distance is 3.7 m, the sample to detector distance 4.3 m.

Sample environment

Samples from several millimetres to several tens of centimetres in diameter can be placed at the sample

position, the beam size can be varied from 4 (pinhole collimation mode) to 40 mm (focusing mode) in diameter.

Detector and Data acquisition

The scattered neutrons are detected by a 256 x 256 pixels (0.7 mm x 0.7 mm pixel size) two dimensional position sensitive detector filled with ³He gas. Data acquisition is performed in event

recording mode. Figure 2 displays an example of a small angle scattering measurement. Data were collected on both FSANS and Yellow Submarine instruments.

Table 1. ▶
Main characteristics

Beam tube:	Cold neutron guide No 3B
Monochromation:	Chopper system
Detector:	2D position sensitive, 200x200 mm ² , filled with ³ He gas
Collimation:	3.7 m
Sample-to-detector distance:	4.3 m
Flux at the guide exit:	5 x 10 ⁷ n/cm ² /sec
Incident wavelength range:	2 - 16 Å
Wavelength uncertainty:	0.3 – 0.74 Å
Scattering vector range:	0.0003 ... 0.03 Å ⁻¹
Scattering vector resolution:	0.00005 Å ⁻¹



◀ **Figure 1.**
 Post sample flight tube
 and detector positioning
 mechanism of the FSANS
 diffractometer.

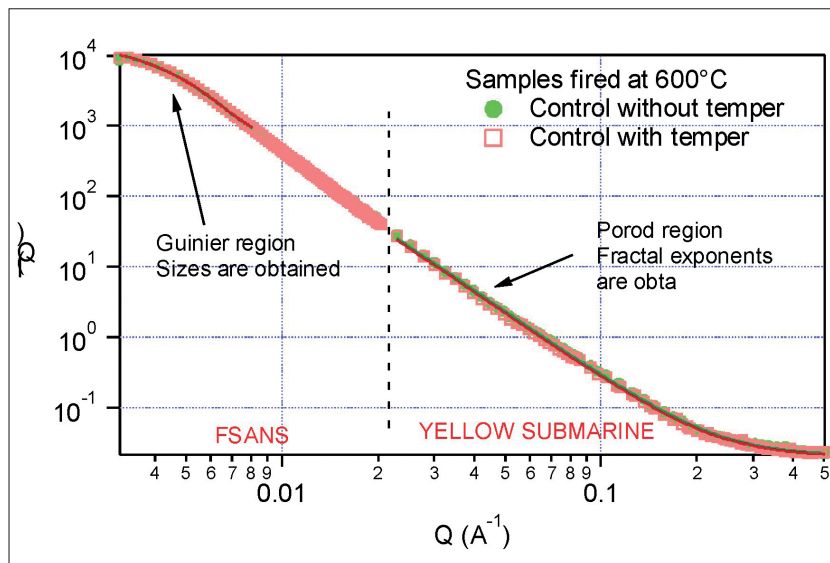
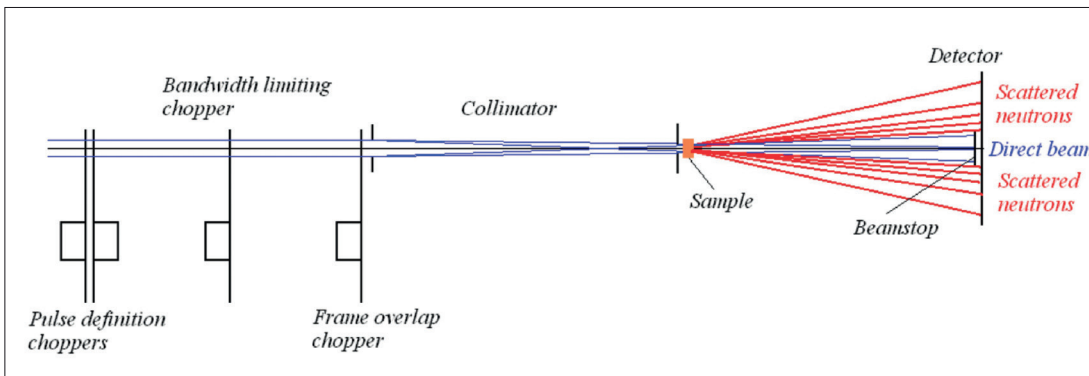
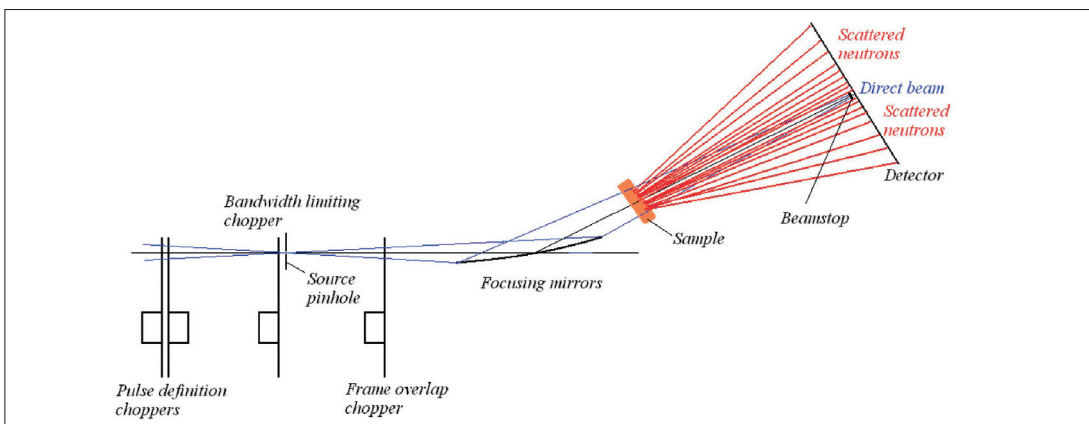


Figure 2. ▲
 Small angle scattering curve
 measured on pottery control
 samples on the FSANS (left
 side) and Yellow Submarine
 (right side) instruments



◀ **Figure 3.**
 Layout of the FSANS
 diffractometer with
 pinhole collimation



◀ **Figure 4.**
 Layout of the FSANS
 diffractometer with
 focusing collimation

6.6. REF – COLD NEUTRON REFLECTOMETER

Instrument scientists: Tamás Veres, László Cser

Wigner Research Centre for Physics, Neutron Spectroscopy Department

The neutron reflectometer (REF) located in the cold neutron hall, at guide 1 is under reconstruction. At present time reflectivity can be measured down to $5 \cdot 10^{-5}$ in the case of large samples. The instrument operates at constant wavelength $\lambda = 4.28 \text{ \AA}$. The schematic view of the reflectometer is shown in Fig. 1. below.

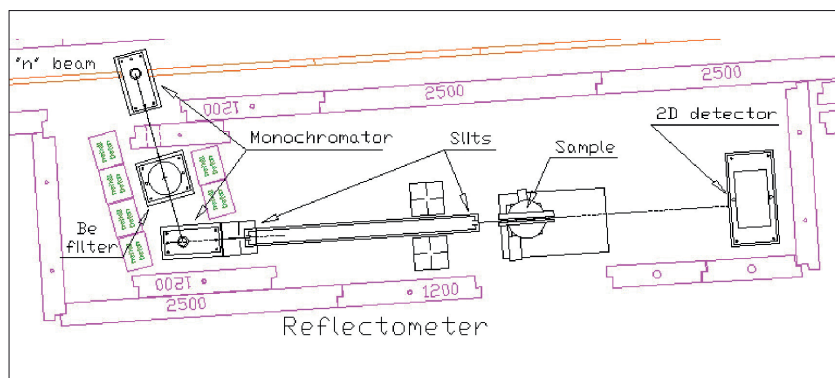


Figure 1.
The schematic view of the reflectometer (REF) at the guide No.1.

Due to the geometrical restrictions the neutron path had to be aligned parallel with the guide. A double PG crystal monochromator is used for this purpose. The elements of the focusing monochromators have mosaicity of 0.4° . The inner monochromator has

5x5 elements, the outer one consists of 5. The sketch of the focusing arrangement is displayed on Fig. 2. The relative intensity is about 3.7 times compared to the previous one. The height of the beam is 8 cm at the sample position, the middle part is the brightest. The higher harmonics of the $\lambda = 4.28 \text{ \AA}$ are filtered out using a Be filter positioned between the two monochromators. The Be filter can be cooled by liquid N_2 .

The usual slit width of the collimator is 1 mm, but it can be changed between 0.1 and 3 mm, the slit distance is 2 m.

The smallest possible angular step of the sample holder is 0.0055 grad .

The reflected neutrons are detected using a position sensitive ^3He detector, with active area $20 \times 20 \text{ cm}^2$. Our new measurement control software allows to save the 2D picture for every measurement point and to count only neutrons arrived to specular position.

The sample-detector distance is 160 cm, it gives the angular limit (according to the detector size) of the usual measurement, but by manual moving of the detector the angular limit can be increased.

Flux of the neutrons at sample position: $780 \text{ n/cm}^2 \text{ sec}$

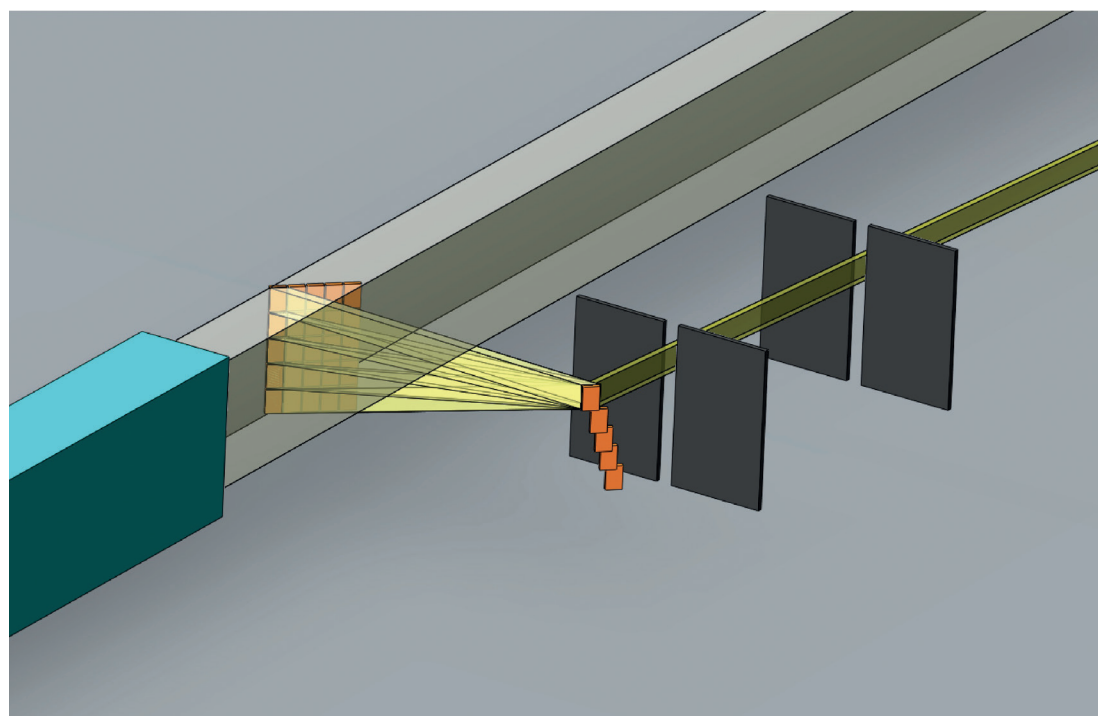


Figure 2.
The focusing arrangement of the new monochromators.

Typical measurements

In order to illustrate the ability of the instrument several typical measurements are displayed below.

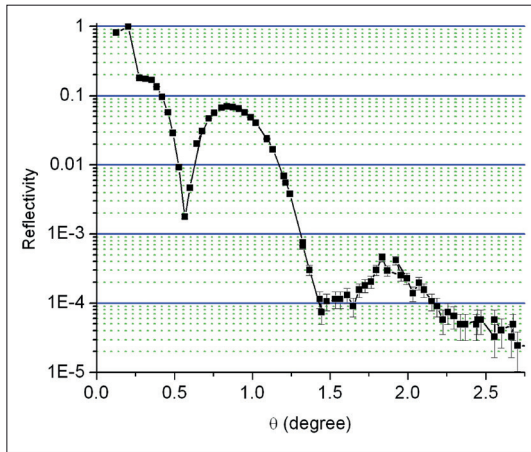


Figure 3. The reflectivity of two Ni-Ti bilayer ($d_{Ni}=84 \text{ \AA}$, $d_{Ti}=70 \text{ \AA}$) on glass substrate.

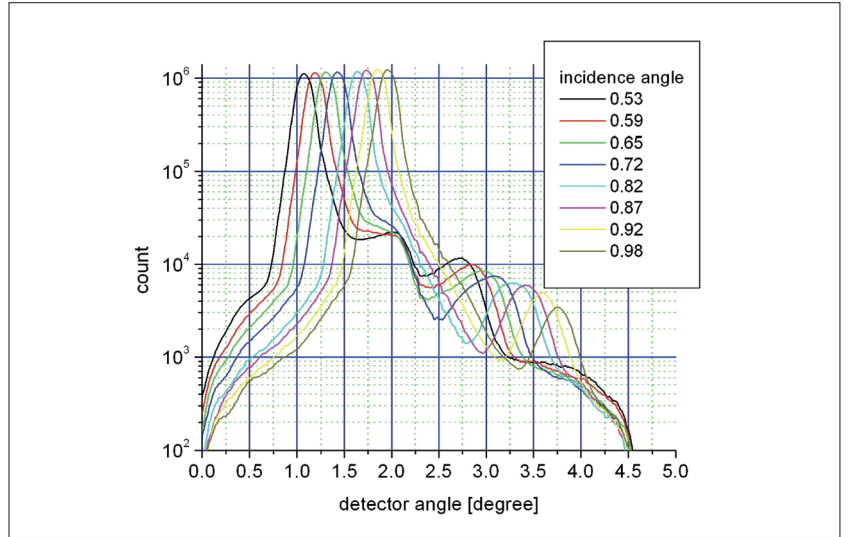


Figure 4. Off-specular neutron reflectograms of reverse layer sequence $m=2.5 \text{ SM}$ at different incidence angles. The first and second orders of Resonant Diffuse Scattering are observable beside the specular peak.

Necessary and recommended improvements

- It is essential to suppress the background. For that both the shielding of the guide No.1 and that of the reflectometer has to be essentially improved. It means that relatively large amount

- of shielding material (e.g. boron-carbide) has to be procured.
- It is important for the solid operation of the instrument to build new control electronics.

6.7. GINA - NEUTRON REFLECTOMETER WITH POLARIZATION OPTION

Instrument scientists: L. Bottyán, D.G. Merket, B. Nagy

Wigner Research Centre for Physics

Neutron reflectometry (NR) investigates the elemental/isotopic depth profile and lateral structure of thin films and nanostructures. The GINA neutron reflectometer (operated by the Functional Nanostructures research group of the Wigner Research Centre for Physics) is a constant-

energy angle-dispersive, vertical-sample instrument. Reflectivity ranges above four orders of magnitude have been measured in magnetic and non-magnetic sample environments. The setup and operation parameters are summarized in Figure 1 and Table 1, respectively.

GINA construction and sample environments

A focusing graphite monochromator (MONO in Figure 1) provides neutrons with wavelengths ranging 3.2 to 5.7 Å and $\Delta\lambda/\lambda \sim 2\%$. The present operation is ensured at $\lambda = 4.67$ Å. Unpolarized and polarized beams are available, which can be combined with different sample environment options. The unpolarized beam is provided using a cryocooled Be-filter (BF). Higher harmonics intensity is efficiently filtered by the Be block, the transmission of which is 41% and 87% for $\lambda = 4.67$ Å, without and with liquid N₂ cooling, respectively. The polarized neutron beam is produced by using a magnetized supermirror (P1) and an adiabatic radio-frequency (RF) spin flipper (SF1). The beam scattered by the sample may be spin analysed by an identical setup of a spin flipper and a spin analyzer (P2, polarized specular beam option), and finally it is detected by a 2D position sensitive detector (DET). The intensity is monitored by an intensity monitor (IM, efficiency $\sim 0.1\%$ at $\lambda = 4.67$ Å).

The central sample tower ST supports the various sample environment components (permanent-magnet sample stage for large samples, electromagnet, cryostat, Helmholtz coils, liquid cell, etc.). The incident angle on the sample surface is set by the Θ -goniometer of ST. The detector arm supports the slits S3, and S4 with optional flight tube (unpolarized beam option) or S3, spin flipper SF2, spin analyzer P2 (polarized beam option) and DET (both options) along with their electronics and dedicated control PC. The flight tube minimizes neutron scattering by air. The detector arm is moved

by a wheel running on the marble floor while the air pads are activated to levitate the arm.

Fine definition of the beam is maintained by the four slits of repetitive precision of 0.05 mm. With its optical elements the setup exhibits a relative Q-resolution of 10% to 2% for the Q-range of 0.005 to ~ 0.25 Å⁻¹. The MONO comprises five highly oriented pyrolytic graphite crystals on small motorized 2-circle cradles for horizontal alignment and vertical focusing. The latter doubles the intensity reflected by a 20x20 mm² sample at 0.7° incident angle as compared to the non-focused case.

Polarized neutrons are produced either by a single Fe-Co/Si magnetic SM in transmission (P1 in Figure 1) or by a 4-bounce SM polarizer in reflection geometry. Spin analysis of the specularly reflected beam is performed by devices (P2) of identical construction. The spin flippers are of adiabatic RF type [3]. The flipper coil is placed in a longitudinal gradient field of 20-40 mT/m, with a center field of 5.6 mT. The coil is part of a resonant circuit, with effective RF current and bandwidth of 4 A and 4.5 kHz at the resonance frequency of 166 kHz.

DET in Figure 1 is a delay line type multi-wire proportional chamber (with active area of 200x200 mm² and spatial resolution FWHM of 1.8 mm) encased in boron-containing shielding for background suppression. The detector is filled with a gas mixture of ³He and CF₄. A DASY TDC module (produced by ESRF, Grenoble) is installed in a slot of the dedicated detector PC.

GINA is dedicated to magnetic heterostructures for studies occasionally requiring low temperature and high external magnetic fields. Low temperature measurements are performed in a closed-cycle cryostat (20 to 340 K range) fitted with (cf. Figure

2) or without magnet. The electromagnet and the Helmholtz pair provide fields up to 0.55 T and 35 mT, resp. A vertical-sample liquid cell with thermostated bath is available to investigate Si-adhered soft matter surfaces.

Data evaluation

Specular reflectivity data (modeling the depth profile of the layer structure, i.e. thicknesses, scattering lengths, roughnesses can be evaluated in terms of the Parratt or the supermatrix algorithms, The method to extract the *lateral structure* of scatterers is the Distorted Wave Born Approximation (DWBA). Both specular and off-specular data can be evaluated by the locally developed fitting environment code, FitSuite, which is more than

a reflectometry evaluation program. It is capable of evaluating 14 different types of experiments (including specular neutron and x-ray reflectometry, off-specular neutron and x-ray reflectometry (by DWBA), transmission, emission, conversion-electron and synchrotron Mössbauer spectra, etc.) with extended on-line help and video demonstrations. The software is freely downloadable from <http://www.fs.kfki.hu>.

Preparation of thin films and multilayers for reflectometry

Most thin film and multilayer samples investigated on the GINA are prepared in the ultra-high vacuum Thin Film Technology Laboratory (Figure 3) of the research group. Serving local and external user projects the molecular beam epitaxy facility (<http://mffo.rmki.kfki.hu/molecular>) comprizes

13 atom sources in two e-guns and five effusion (Knudsen) cells for single and co-evaporation of even complex multilayer sequences without the need of venting the chamber. The laboratory offers the GINA users its sample preparation services.

Parameter	Range
Wavelength	3.9 ÷ 5.1 Å in 5 steps
Present operational wavelength	4.67 Å
Max. scattering angle	$>\Theta=35^\circ$
Angular resolution ($\Delta\Theta$)	0.003°
$\Delta\lambda/\lambda$	~2%
Background level	0.01 cps·cm ⁻²
Detector	2D PSD, 200x200 mm ²
Detector spatial resolution	1.8x1.8 mm ²
Neutron flux at the monochromator position	4x10 ⁵ n x cm ⁻² x s ⁻¹
Background reflectivity	< 7x10 ⁻⁵
Overall polarization efficiency	0.895(3) (single SM) 0.996(2) (4-bounce)

Table 1.

Operational parameters of the GINA neutron reflectometer

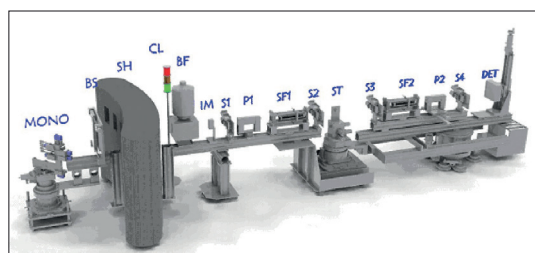


Figure 1. GINA neutron reflectometer layout (see text).



Figure 3. The Thin Film Technology (MBE) Laboratory of the Wigner Research Centre.

6.8. ATHOS - COLD NEUTRON TREE-AXIS SPECTROMETER

Instrument scientists: Gyula Török, Alex Szakál

Wigner Research Centre for Physics, Neutron Spectroscopy Department

The cold neutron three-axis spectrometer (TAS) at BNC is installed on the 17 m position of the first neutron guide (NG1). The beamline is a borofloat glass substrate NiTi coated supermirror ($m=2$) guide. This instrument was in extensive use on a thermal beam in the period of 1972-86. Since the reactor reconstruction and the cold source installation this instrument – with a major upgrade – has been relocated on this cold neutron guide and it was named ATHOS.

The ATHOS instrument provides moderate resolution (0.01-1.0 meV) with sufficient intensity for use in a wide range of problems. It is ideally suited for the study of phonon dispersion curves in single crystals, tunneling modes of energies greater than ≈ 0.025 meV, quasielastic scattering studies of rotational and non-local diffusion in the time regime of picoseconds, vibrations of surfaces or molecules adsorbed on surfaces and phonon density of states for that large class of materials which contain hydrogen. Specific mention of the applicability of neutron scattering to the study of hydrogenous materials should be emphasized here. The hydrogen nucleus has the largest cross section (scattering interaction) for neutron scattering and is predominantly incoherent. Hydrogen vibrations have been detected in samples containing as little as 0.01 mol. of total hydrogen in the sample. Because the instrument is energy sensitive, it can also be used to measure purely elastic scattering whether it be due to coherent (nuclear or magnetic) or incoherent events. Information on the time-averaged structure of the atomic and molecular constituents of the sample is therefore accessible. Finally, the ability of producing and analyzing polarized neutrons allows more detailed measurement of the magnetic properties of the sample. These magnetic properties can be static, i.e., a structural description of the magnetic moments, or dynamic such as magnons.

The range of energies (0.025-14 meV) of excitations accessible to this instruments is substantially larger (although with poorer resolution) than available with the spin-echo and backscattering spectrometers. Independent control of the momentum (Q) and energy transfer (E) is routine if required as opposed to the time of flight spectrometer in which Q and E are related by the instrumental configuration. The monochromatic beam is provided by a 90mm high focusing multi-blade ZYA grade pyrolytic graphite monochromator.

The movable part of the monochromatic shielding has a chain type construction. Changing the incident wavelength the whole chain is driven by the monochromator-sample arm. This construction automatically provides the most effective shielding near the detector area (see Fig.1). This enables very low background conditions (1 neutron/300s).

For higher order filtering in the incident monochromatic beam a multidisc neutron velocity selector can be installed in front of the sample goniometer, or Ge analyzer used. The beam divergence is determined by thin film Soller-type Mylar collimators coated with gadolinium-oxide paint. A 200x200 mm² two dimensional position sensitive ³He detector in medium resolution mode was installed in 1999. Using this detector the efficiency of data collection has been raised 40 times in quasielastic mode.

Although this tree-axis spectrometer has been designed for structural and dynamical studies of condensed matter – because of the limited number of other operational equipment – the instrument is extensively used in a multi purpose regime, e.g. for high-resolution diffractometry, strain analysis, reflectometry, quasielastic and inelastic scattering. This spectrometer has been served also for testing polarization setups, detectors, monitors, any other neutron beam components developed in our

Laboratory. For example a neutron spin-echo setup was also realized on this instrument (Fig.1). This “mini-spin-echo” can be used for training and methodical

development purposes (Török Gy, Lebedev VT, Nagy A, Gordeev GP, Zsigmond G, *Physica Status Solidi C* **1**, No 11, 3182 (2004).

Beam tube :	Cold neutron guide No.1/1
Monochromator :	pyrolitic graphite 90x80 mm (24min mosaicity)
Analyser :	pyrolitic graphite 50x90 mm (24min mosaicity), or Ge monocrystal (15min mosaicity)
Collimations :	interchangeable 45', 30', 15'
Range of monochromator angle:	$36^\circ < 2\Theta < 126^\circ$
Range of scattering angle :	$-120^\circ < 2\Phi < 70^\circ$
Range of analyser angle :	$-40^\circ < 2\Theta < 120^\circ$
Range of crystal orientation :	$0^\circ < 2\Theta < 360^\circ$
Angular resolution :	0.01°
Flux at specimen :	2×10^6 n/cm ² /.sec
Beam size :	25x90 mm ²
Momentum transfer :	0 – 2.7 Å ⁻¹
Energy transfer :	0 - 9 meV
Characteristic resolution at 3.3 Å	120-150 µeV
Sample enviroment :	Thermostate (-20°C - 100°C), cryostat (15 K) , magnet up to 2T (max scattering angle 100 deg) furnace up to 1000°C

❏ **Table 1.**
Main parameters of the spectrometer



❏ **Figure 1.**
Neutron spin-echo setup installed on the TAS

6.9. TAST/HOLO - THERMAL NEUTRON TREE-AXIS SPECTROMETER AND NEUTRON HOLOGRAPHIC INSTRUMENT

Instrument scientists: Alex Szakál, Gyula Török

Wigner Research Centre for Physics, Neutron Spectroscopy Department


The thermal neutron three-axis spectrometer (TAST) at BNC is installed on the thermal neutron channel No.8 at the Budapest Research Reactor. The instrument provides moderate resolution (~ 1.0 meV) with sufficient intensity for use in a wide range of problems. It is ideally suited for the study of phonon and magnon dispersion curves in single crystals, phonon density of states for that large class of materials which contain hydrogen. Independent control of the momentum (Q) and energy transfer (E) is routine if required as opposed to the time of flight spectrometer in which Q and E are related by the instrumental configuration. This triple axis spectrometer can also be used in a multipurpose regime, e.g. for high-resolution diffractometry, inelastic scattering as well as for thermal beam irradiation and transmission tests or tests of various kinds of neutron optical components.

The monochromatic beam is provided by a 90mm high and 150mm wide horizontally and vertically focusing Cu[002] monochromator. In order to suppress the intensity of fast neutrons, a 15 cm long

sapphire single crystal is inserted in the primary shutter. For higher order filtering in the incident monochromatic beam a Ge analyzer can be used. The beam divergence is determined by thin film Soller-type Mylar collimators coated with Gd_2O_3 .

A highly efficient (90% at 1 \AA) ^3He single counter of 1" diameter is applied as detector. A two dimensional position sensitive detector in medium resolution mode is also available. For energy analyzing a horizontally focusing pyrolytic graphite crystal assembly is used.

The spectrometer can be equipped by an Eulerian Cradle, or a tilt table that can hold various sample environment devices up to a weight of 100 kp. Since 2005 TAST can be used also as an instrument for atomic resolution neutron holography measurements both in neutron or gamma ray detection modes. A BGO gamma detector is available with a proper shielding to filter the rather high gamma background of the environment and detect the small inside detector holographic signal.

Table 1. 
Main parameters
of the spectrometer

Beam tube:	Channel No. 8. (radial channel with sapphire filter)
Monochromator	Cu[002], horizontally and vertically focusing
Analyzer	PG[002], horizontally focusing
Detector	^3He tube
Range of monochromator angle:	$14^\circ < 2\Theta_{\text{monochromator}} < 44^\circ$
Range of analyzer angle:	$-100^\circ < 2\Theta_{\text{monochromator}} < 100^\circ$
Angular precision	0.01°
Flux at sample at 1 \AA wavelength	$2 \times 10^6 \text{ n/cm}^2/\text{sec}$
Beam size	$50 \times 50 / 10 \times 15 \text{ mm}^2$ depending on focusing
Momentum transfer	$1.5 - 10 \text{ \AA}^{-1}$
Energy transfer	$1 - 60 \text{ meV}$

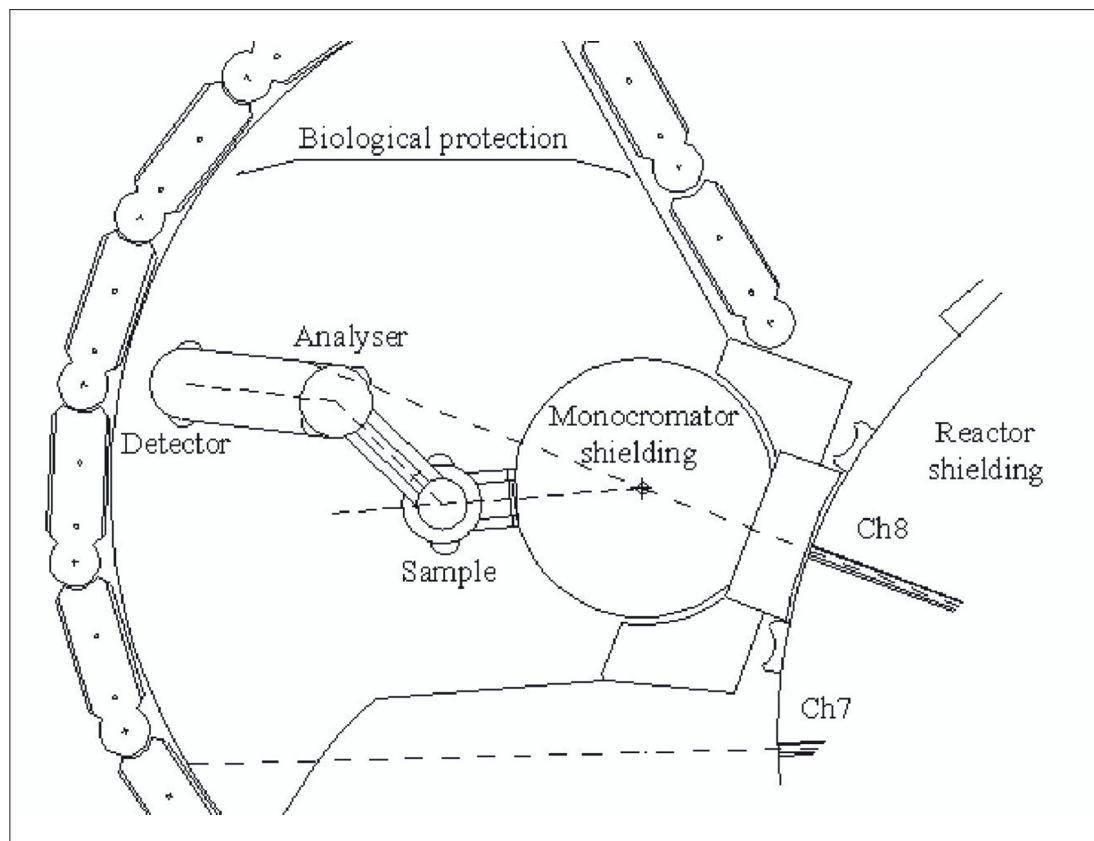


Figure 1. Layout of the Thermal triple axis spectrometer

6.10. RAD – STATIC/DYNAMIC THERMAL-NEUTRON AND X-RAY IMAGING STATION

Instrument responsible: Zoltán KIS, László Zoltán HORVÁTH, Gábor BENYÁCS

Centre for Energy Research, Nuclear Analysis and Radiography Department

Radiography utilizes transmission of photons or neutrons to obtain information on the structure and/or inner processes of a given object. The RAD thermal neutron imaging facility is served by an in-pile, Cd-covered pin-hole-type collimator for neutron and gamma radiation. The facility has two measurement positions along the neutron beam path with a beam diameter of ~200 mm, used for dynamic (DNR) and for static (SNR) imaging with a measured L/D ratio of ~250. There is a possibility to use beam filters made of boron-containing rubber and lead bricks, resulting in a significant modification of the beam energy distribution, giving a fast/thermal neutron flux ratio of 77 instead of 0.6. The RAD facility is also equipped with an optional Xray tube, allowing dual-modality imaging. Two motorized sample stages, one for small and one for large samples (with a maximum load up to 250 kg) are available to support the investigated objects. A sapphire-crystal-based filter is under installation to suppress fast neutrons.

The image detection of the RAD station now comprises new digital imaging equipment being able to carry out 2D and 3D imaging using suitable scintillation screens. The spatial resolutions of the available screens are as follows: scintillation screens for neutron radiography have resolutions between 70-250 μm ; intensifying screens for X-ray radiography are with a resolution of 100-200 μm . For better flexibility, there is a possibility to apply

larger or smaller fields of views (FOV) with lower and higher spatial resolutions, respectively. The static radiography and tomography is accomplished by a new, large area sCMOS camera. Here altogether three different optical systems can be setup using the available lenses with 50 mm, 105 mm and 300 mm fixed focal lengths, interchangeably coupled to the digital camera, giving the different FOVs.

For the manipulation, reconstruction and visualization of the 3D neutron and X-ray datasets (i.e. the tomographic images), the latest Fiji-ImageJ, Octopus 8.9 and VG Studio 2.1 software packages are used.

The dynamic radiography is performed by means of a low-light-level TV camera with a fast imaging cycle, making possible real-time imaging. A zoom optics coupled to this camera gives a variable field of view. The two cameras can be used interchangeably in the light-tight camera box equipped with a rail system providing the necessary optical path lengths.

In addition to the cameras, the photo-luminescent imaging plate (IP) technique is also available for high-resolution X-ray and neutron radiation detection with transfer method using In and Dy (100 μm) foils. The exposed IP-s are read out by a BAS 2500 image plate reader unit coupled to the AIDA image processing software.

Reference:

Z Kis, L Szentmiklósi, T Belgya, M Balaskó, LZ Horváth, B Maróti. (2015) Neutron based imaging and element-mapping at the Budapest Neutron Centre, Physics Procedia. **69** (2015) 40 – 47.

RAD – Static/dynamic thermal-neutron and X-ray imaging station >

Beam energy distribution:	radial thermal neutron channel
Thermal-equivalent flux at target:	<ul style="list-style-type: none"> • $4.64 \times 10^7 \cdot \text{cm}^{-2} \cdot \text{s}^{-1}$ at 209 cm (DNR) • $3.38 \times 10^7 \cdot \text{cm}^{-2} \cdot \text{s}^{-1}$ at 282 cm (SNR)
Thermal-to-epithermal flux ratio $\Phi_{\text{th}}/\Phi_{\text{epi}}$	51
Collimator ratio (L/D) :	250
Gamma dose rate:	8.5 Gy/h
X-ray sources:	5-300 keV; 5-10 mA
Field of view (useful):	41×34 mm ² , 110×93 mm ² or Ø200 mm
Scintillator screens (thickness):	<ul style="list-style-type: none"> • Li⁶F/ZnS (100, 200, 225 and 450 μm) • Gadox P43 (10 and 20 μm)
Mirror:	Al coated quartz mirror set in 45° to the beam
Optics:	<ul style="list-style-type: none"> • Sigma 50 mm f/1.4 DG HSM ART; • Nikon-Nikkor 105 mm f/1.8 • Nikon AF-S 300 mm f/2.8 G ED VR II
Imaging detectors :	<ul style="list-style-type: none"> • Andor Neo 5.5 sCMOS camera with 2560×2160 pixels and 16-bit pixel depth • low-light-level TV camera (640×480 px) with a light sensitivity of 10⁴ lux and imaging cycle of 40 msec • BAS 2500 image plate reader
Spatial resolution:	70250 μm depending on the FOV and scintillators
Exposure times:	<ul style="list-style-type: none"> • 1-35 s per image • 601 – 1001 projections for a tomogram • 25 fps for dynamic measurements
Sample stages:	<ul style="list-style-type: none"> • motorized sample manipulator for heavy objects up to 250 kg • ω turntable for 3D imaging up to 5 kg

Table 1.
Specifications of the
RAD facility

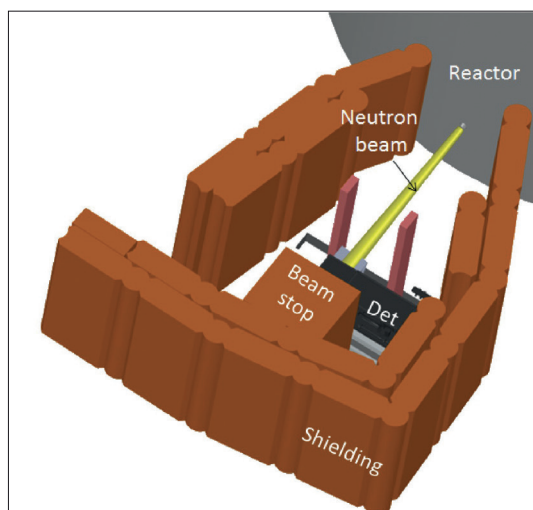


Figure 1.
a) The 3D view of the facility.
b) The light-tight optical assembly, ImageFrame hosting the scintillators, the mirror, the optics and the camera

6.11. NORMA - NEUTRON OPTICS AND RADIOGRAPHY FOR MATERIAL ANALYSIS

Instrument scientists: Zoltán Kis, László Szentmiklósi

Centre for Energy Research, Nuclear Analysis and Radiography Department

The NORMA facility is located at the end position of the neutron guide NG1 as a complementary part of the NIPS facility. It has been designed for neutron radiography (NR) and tomography (NT), and as a position feedback for imaging-driven Prompt Gamma Activation Imaging (PGAI). In this latter mode, the combination with the element information obtained with NIPS gamma spectroscopy detector makes possible to assign element analysis results to a well-defined volume of a large object.

The beam arrives through a flight tube of 45×45 mm² cross section into a sample chamber with dimensions of 200×200×200 mm³ for imaging and position-sensitive applications. The frame of the chamber is made of AlMgSi alloy, and lined from inside with ⁶Li-enriched polymer. By removing one or more side panels, larger objects (or at least parts of those) up to 5 kg weight could also be imaged (such as a sword, vase, stone, etc.). Samples can be loaded manually from the top, or placed onto an XYZw motorized sample stage with a travel distance of 200 mm and a guaranteed precision of 15 μm. The sample stage is introduced to the sample chamber from the bottom.

The imaging system of the NORMA setup consists of a 100 μm thick ⁶Li/ZnS scintillator, an Al coated quartz mirror and a cooled, black-and-white, back illuminated Andor iKon-M CCD camera with 1024×1024 pixels and 16-bit pixel depth, mounted in a light-tight aluminum housing. The custom optics projects a 48.6×48.6 mm² field of view

(in which the beam spot is about 40×40 mm²) onto the 13.3×13.3 mm² sensitive surface of the CCD chip. The spatial resolution of the imaging system changes linearly between 230660 μm, proportional to the 1.5100.5 mm distance from the scintillator screen. The measured L/D ratio, characteristic to the neutron beam's divergence, was found to be 233. An improvement of the L/D ratio to 2380 is under implementation by applying interchangeable primary apertures (together with a graphite scatterer) at the end of the neutron guide. The specifications of the facility are listed in Table 1. The spatial distribution of the beam intensity is illustrated in Fig. 1a; the energy distribution of the neutrons, measured by time-of-flight technique is shown in Fig. 1b.

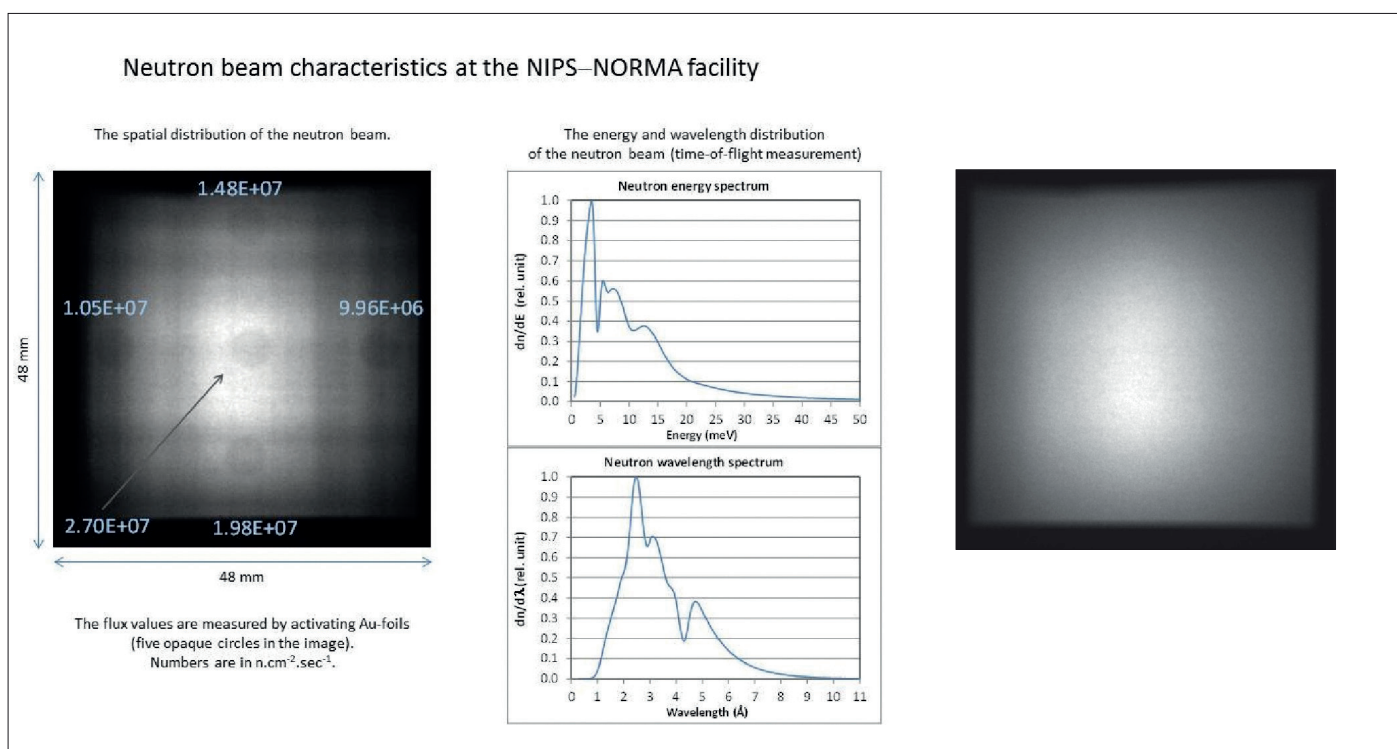
The radiography images taken at NORMA require several steps of data treatment. The spatial inhomogeneity of the beam and the thermal noise of the camera should be removed. These are called 'beam image or flat-field correction' and 'dark image correction', respectively. In tomography, the goal is to determine a measure of the interaction probability between the material and the neutron as a function of spatial coordinates. This quantity delivers the structural information about the interior of the sample. The reconstruction codes, such as the OCTOPUS reconstruction software, apply the inverse Radon-transformation and filtered back projection algorithms. The visualization of the dataset in 3D space (volume rendering) is carried out using VGStudio 2.1.

Reference:

Z. Kis, L. Szentmiklósi, T. Belgya: NIPS–NORMA station - A combined facility for neutron-based nondestructive element analysis and imaging at the Budapest Neutron Centre Nucl. Instr. Meth. A **779** (2015)116–123

Beam size for imaging:	up to 40×40 mm ²
Beam cross section for PGAA/PGAI:	continuously adjustable rectangular slit
Collimator ratio (L/D) :	233 – 2380
Beam energy distribution:	Cold beam
Thermal-equivalent flux at target:	≈2.7×10 ⁷ ·cm ⁻² ·s ⁻¹
Scintillator screen :	100 mm thick ⁶ Li/ZnS scintillator on an Al plate
Mirror:	Al coated quartz mirror set in 45° to the neutron beam
Lens:	Canon EF 85mm f1.2 L II USM
Standard imaging detector :	Back-illuminated Andor iKon-M 934 CCD camera with 1024×1024 pixels and 16-bit pixel depth
Spatial resolution:	230660 μm according to the 1.5100.5 mm distance from the scintillator screen
Sample stage:	XYZω motorized sample stage with a travel distance of 200 mm and a guaranteed precision of 15 μm
Sample chamber dimensions:	200×200×200 mm ³
Sample environment:	Ambient pressure and temperature

◀ **Table 1.**
Specifications of the
NORMA facility



▶ **Figure 1.**

a) The spatial distribution of the neutron beam intensity at the sample position of the NIPS/NORMA facility without the graphite scatterer and some flux values measured by gold foils; and b) the energy and wavelength distribution of the neutron beam. c) The spatial distribution of the neutron beam intensity at the sample position of the NIPS/NORMA facility with the graphite scatterer mounted at the end of the neutron guide.

6.12. BIO – BIOLOGICAL IRRADIATION CHANNEL

Instrument responsible: Balazs Zabori

Centre for Energy Research

Biological Irradiation Facility is existing at the Budapest Neutron Centre (BNC) in order to provide reliable platform for biological irradiation studies. The physical properties of the facility is described below.

The channel lock consists of 3 steel and heavy-concrete segments turnable by an excentrical axis to open and close the channel. There is an internal remotely controlled filter holder at a distance of 262 cm from the core which has six windows with the following materials: four Bi disks of 5, 10, 15 and 20 cm thick and one Pb disk of 20 cm, the 6th one is an open hole. At the orifice of the beam tube two cylindrical tanks were constructed of alumina to serve as a water shutter and its emergency water storage, respectively. The water can be pumped up from and released to a larger buffer tank located outside of the reactor shielding block by pressurized air. The construction materials inside the beam tube work as internal, not removable filters with total thickness of 18 mm Pb and 15 mm Al.

The irradiation cavity is situated outside of the shielding block of the reactor in a distance of 1400 mm, thus its surface-to-reactor core distance is 3100 mm including the exchangeable core window (65 mm) made either of beryllium (rolling as the fast neutron reflector, too) or of aluminum. The use of the aluminum window results in a hard

neutron spectrum. Between the shielding surface of the reactor and the cavity there is a borated water shielded collimator with a useful diameter of 10 cm. It is possible to use this collimator as a holder for outer filters of about 800 mm length. Presently, filters of plexi-glass, polyethylene, iron, aluminum and lead are available to decrease the gamma and neutron intensity or to modify the neutron spectrum and the neutron-to-gamma ratio. There are two changeable filter disks of boron-carbide working as thermal and epithermal absorbers. The collimator is movable on a rail. The samples to be irradiated can be rotated to achieve a uniform, homogeneous irradiation. Cadmium or Boron carbide filters are used, if required, for decreasing the thermal neutron contribution.

Three levels of the dosimetry system were developed: real time, active beam monitors; passive activation, track-etch and TL detectors and computer codes for spectrum and dose calculations. Each exposure is individually planned and continuously monitored during the procedure. Some typical dose and flux values are presented in 1. Table and the schematic view of the system is presented in 1. Figure.

The irradiation facility is applicable to study the effects of the neutron and gamma radiation and high dose rate on the living animals, cells, etc.

BIO – Biological irradiation channel >

Quantity	Energy range	Min	Max
Neutron dose rate (mGy/s)	$E > 0.5 \text{ eV}$	0.023	14
Gamma dose rate ($\mu\text{Gy/s}$)	-	1.5	2570
Fast neutron flux ($\text{cm}^{-2}\text{s}^{-1}$)	$E > 100 \text{ keV}$	2×10^6	2×10^9
Intermediar neutron flux ($\text{cm}^{-2}\text{s}^{-1}$)	$100 \text{ keV} > E > 0.5 \text{ eV}$	8×10^3	2×10^6
Thermal neutron flux ($\text{cm}^{-2}\text{s}^{-1}$)	$E < 0.5 \text{ eV}$	5×10^4	3×10^8

Table 1. Presently existing minimum and maximum dose and flux values.

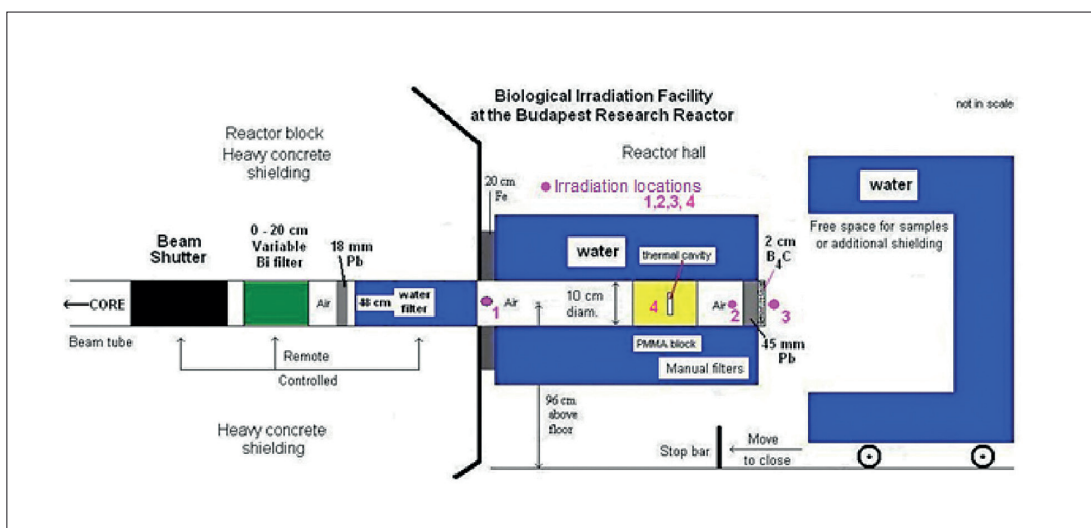


Figure 1. Schematic view of the Biological Irradiation Facility.

6.13. PGAA – PROMPT GAMMA ACTIVATION ANALYSIS

Instrument scientists: Zsolt Kasztovszky, László Szentmiklósi, Boglárka Maróti

Centre for Energy Research, Nuclear Analysis and Radiography Department

When a nucleus captures a neutron, the binding energy of the neutron is promptly emitted in the form of gamma radiation. The energies of the gamma photons are specific to the nucleus, while their numbers are proportional to the quantity of that nuclide. By analyzing the energy spectrum of these gamma rays, the isotopic and elemental contents of the irradiated sample can be determined. This is the principle of the prompt gamma activation analysis method.

The PGAA facility is located near the end position of the neutron guide No. 1. It is used for non-destructive elemental analysis of samples by detecting neutron-capture prompt gamma rays. The neutrons are guided from the cold neutron-source of the Budapest Research Reactor to the experimental positions by a neutron guide, which is slightly curved so that it decreases the background coming from the reactor core. Before the main beam enters to the experimental area, it is divided into two sub-beams (upper and lower) by suitable collimators, and the upper beam serves the PGAA facility. The neutron guide has been recently upgraded with $2\Theta_c$ supermirror guides that improved the thermal-equivalent neutron flux at the PGAA sample positions to $9.6 \times 10^7 \text{ cm}^{-2} \text{ s}^{-1}$. The beam can be collimated to a maximum cross-section of $2 \times 2 \text{ cm}^2$. The intensity of the incoming neutrons is monitored and recorded with an ORDELA Model 4511 N neutron detector throughout the whole reactor campaign.

For special experiments, a pulsed beam can also be used. Modulation in the order of milliseconds can be done by a revolving chopper blade, while longer on-off periods can be achieved with a fast beam shutter.

The experimental area is a $3 \times 6.5 \text{ m}^2$ space at the rear end of the guide hall (see Figure 1). The neutrons enter the cabin and fly along a 3 m long evacuated aluminum flight-tube across the experimental area, to the beam stop placed at the wall of the guide hall. A pneumatically actuated

instrument shutter is used to control the entry of the neutron beam into the cabin while two computer-controlled secondary shutters are in place to allow independent operation of the PGAA and NIPS/NORMA facilities. Independent sections of the modular aluminum flight tube can easily be removed and reinstalled as needed. A series of appropriate size collimators are used for each beams. At present, the upper beam is used for PGAA measurements while the lower beam is used for NIPS/NORMA experiments.

The PGAA target chamber is at 1.5 m distance from the end of the guide. The sample chamber can be evacuated or filled up with gases to decrease beam-induced background. To prevent scattering of neutrons to the PGAA sample from the lower beam, a layer of neutron absorber is placed below the sample. The targets are mounted on thin Al frames by Teflon strings. Optionally, an automated sample changer with a capacity of 16 samples can be used. A neutron absorber after the PGAA target chamber stops the upper beam.

The detector system of the PGAA facility consists of an n-type high-purity germanium (Canberra HPGe 2720/S) main detector with closed-end coaxial geometry, and a BGO Compton-suppressor surrounded by a 10 cm thick lead shielding. The sample-to-detector distance is adjustable, but it is typically 230 mm. By removing the front detector shielding, the HPGe main detector can be placed as close as 12 cm to the target.

The BGO annulus and catchers around the HPGe detect most of the scattered gamma photons. If the events from the HPGe and the BGO are collected in anticoincidence mode, Compton-suppressed spectra can be acquired. An analogue spectroscopy amplifier combined with an ADC and an Ethernet-based multichannel analyzer (Canberra AIM 556A) collects the counts. A CAEN N6724 digitizer card with 4-channel input and fibre optic link is an option for advanced list mode data acquisition.

A schematic drawing of the experimental area, the sample chambers and the HPGe-BGO detector assembly is shown in Figure 1. The main parameters of the PGAA system are collected in Table 1.

Reference:

L Szentmiklósi, T Belgya, Z Révay, Z Kis. (2010) Upgrade of the Prompt-Gamma Activation Analysis (PGAA) and the Neutron Induced Prompt-gamma Spectroscopy (NIPS) facilities at the Budapest Research Reactor. J Radioanal Nucl Chem. **286**:501-505.

Beam tube:	NG1 guide, end position
Distance from guide end:	1.5 m
Beam cross section (computer selectable):	2×2cm ² , 1.4×1.4cm ² , 1×1cm ² , 42mm ² , 23mm ² , 10mm ² , 5mm ² , 1/30 attenuator
Thermal-equivalent flux at target:	≈9.6×10 ⁷ cm ⁻² s ⁻¹ (in air)
Vacuum in target chamber (optional):	≈1 mbar
Target chamber Al-window thickness	0.5 mm
Form of target at room temperature:	Solid, powder, liquid; gas in a pressurized container
Target packing at atmospheric pressure:	sealed FEP Teflon bag or vial
Sample chamber dimensions:	4×4×10 cm ³
γ-ray detector	n-type coax. HPGe, with BGO shield
Distance from target to detector window:	230 mm
HPGe window:	Carbon epoxy, 0.5 mm
Relative efficiency:	27% at 1332 keV (⁶⁰ Co)
FWHM:	2.1 keV at 1332 keV (⁶⁰ Co)
Compton suppression factor:	≈5 (1332 keV) to ≈40 (7000 keV)

Table 1.
Specifications of the PGAA facility

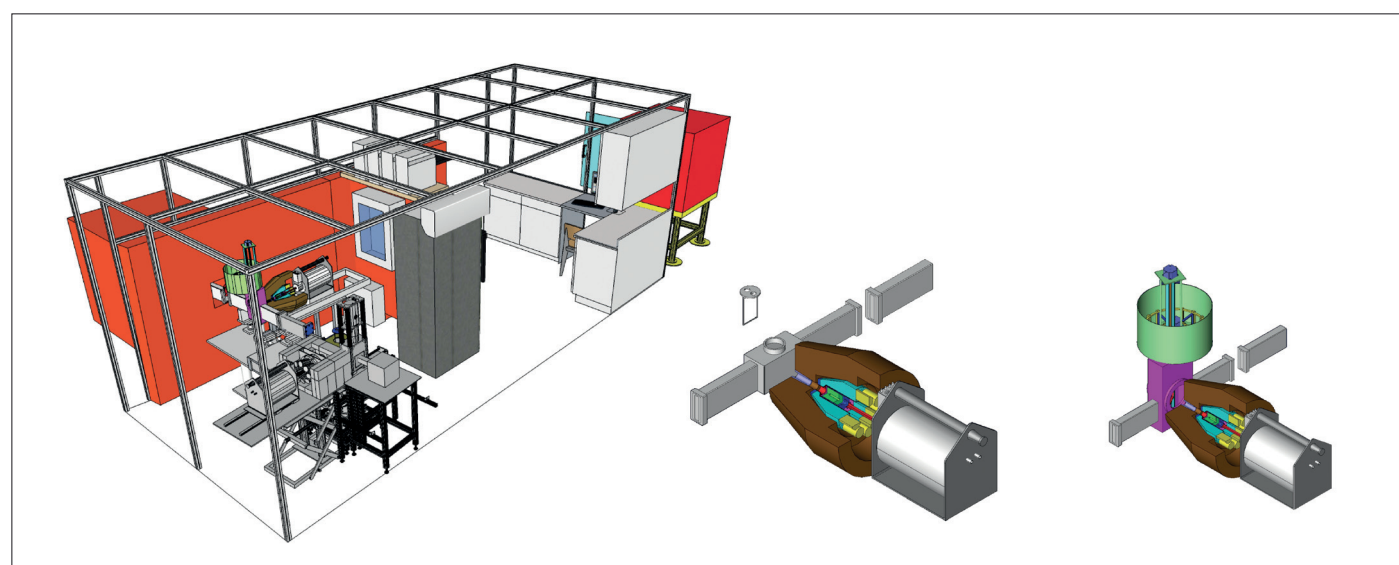


Figure 1.
Layout of the PGAA-NIPS experimental area (left). The PGAA facility, with the standard sample chamber (middle) and with the automated sample changer (right)

6.14. NIPS - NEUTRON-INDUCED PROMPT GAMMA-RAY SPECTROSCOPY

Instrument scientists: László Szentmiklósi, Zoltán Kis, Katalin Gméling

Centre for Energy Research, Nuclear Analysis and Radiography Department

The NIPS facility is located at the end position of the neutron guide No.1. It is designed for a wide range of experiments that involve nuclear reaction-induced prompt and delayed gamma radiations, γ - γ coincidences, large-sample PGAA, Prompt-Gamma Activation Imaging (PGAI).

From the cold neutron-source of the Budapest Research Reactor, the neutrons are guided to the experimental positions by the same curved neutron guides as for the PGAA facility. Before the beam enters to the experimental area, the beam is divided into two sub-beams (upper and lower) by suitable collimators, and the lower one operates the NIPS facility. The thermal-equivalent neutron flux at the NIPS sample positions is $2.7 \times 10^7 \text{ cm}^{-2} \text{ s}^{-1}$. The beam could be collimated to a maximum cross-section of $4 \times 4 \text{ cm}^2$. The intensity of the incoming neutron flux is monitored and recorded with an ORDELA Model 4511 N neutron detector throughout the whole reactor campaign.

The beam arrives through a flight tube of $5 \times 5 \text{ cm}^2$ cross section. If multiple detectors are to be placed close to the sample, a narrow aluminum tube with a $5 \times 5 \times 5 \text{ cm}^3$ sample chamber is available. Alternatively a sample chamber with dimensions of $20 \times 20 \times 20 \text{ cm}^3$ is available for large-sample PGAA and position-sensitive applications. It is made of AlMgSi alloy, and lined from inside with ^6Li -enriched polymer. By removing one or more side panels, larger objects up to 5 kg weight could also be analyzed (such as a sword, vase, stones, etc.). Samples can be loaded manually from the top, or placed onto an XYZw motorized sample stage with a travel distance of 200

mm and a guaranteed precision of $15 \mu\text{m}$, which is introduced from the bottom. If custom devices are to be built into the beam, a short flight tube without a sample chamber is the proper choice.

An n-type coaxial HPGe detector (Canberra GR 2318/S) equipped with a Scionix BGO Compton suppressor is used for the routine prompt gamma measurements. This latter can accommodate HPGe detectors with larger crystals (up to end cap diameter of 76 mm). The passive shielding is made of standard lead bricks in a thickness of 10 cm for each direction. A changeable gamma collimator system is available for PGAI measurements consisting of three different lead collimators with an opening of 30 mm in diameter, a $2 \times 20 \text{ mm}^2$ slit and a $5 \times 5 \text{ mm}^2$, respectively. The gamma detector systems are regularly calibrated for counting efficiency and non-linearity. This procedure results in a precision of about 0.5% for the relative efficiency curve, 1% for the absolute efficiency curve and a precision of 0.005-0.1 keV for energy determination of peaks. The complex γ -ray spectra are evaluated with the spectroscopy program Hypermet-PC.

A digital signal processor combined with an Ethernet-based multichannel analyzer module (Canberra AIM 556B) collects the counts. Alternatively, a four-channel, all-digital XIA Pixie 4 spectrometer can also be used. A user-friendly facility control program, "Budapest PGAA-NIPS Data Acquisition Software", has been written for manual, semi-automatic, and unattended automatic batch measurements. It controls the beam shutters, slits, the motorized sample stage and the gamma acquisition.

Reference:

L Szentmiklósi, Z Kis, T Belgya, AN Berlizov. (2013) On the design and installation of a Compton-suppressed HPGe spectrometer at the Budapest neutron-induced prompt gamma spectroscopy (NIPS) facility. J Radioanal Nucl Chem. **298**(3):1605-11.

Table 1.
Specifications of
NIPS facility

Beam tube:	NG1 guide, end position
Distance from guide end:	2.6 m
Beam cross section for PGAA/PGAI:	continuously adjustable rectangular slit
Beam cross section for imaging:	up to 40x40 mm ²
Thermal-equivalent flux at target:	$\approx 2.7 \times 10^7 \text{ cm}^{-2} \text{ s}^{-1}$
Vacuum in target chamber:	Not available
Form of target at room temperature:	Solid, powder, liquid; gas in a pressurized container
Target packing at atmospheric pressure:	sealed FEP Teflon bag or vial
Sample chamber dimensions:	5x5x5 cm ³ /20x20x20 cm ³
Distance from target to detector window:	minimum 25 mm, typical 280 mm
γ -ray detector	n-type coax. HPGe, with BGO shield
HPGe window:	Al, 0.5 mm
Relative efficiency:	23% at 1332 keV (⁶⁰ Co)
FWHM:	2.2 keV at 1332 keV (⁶⁰ Co)
Compton-suppression factor	≈ 3.5 (1332 keV) to ≈ 30 (7000 keV)

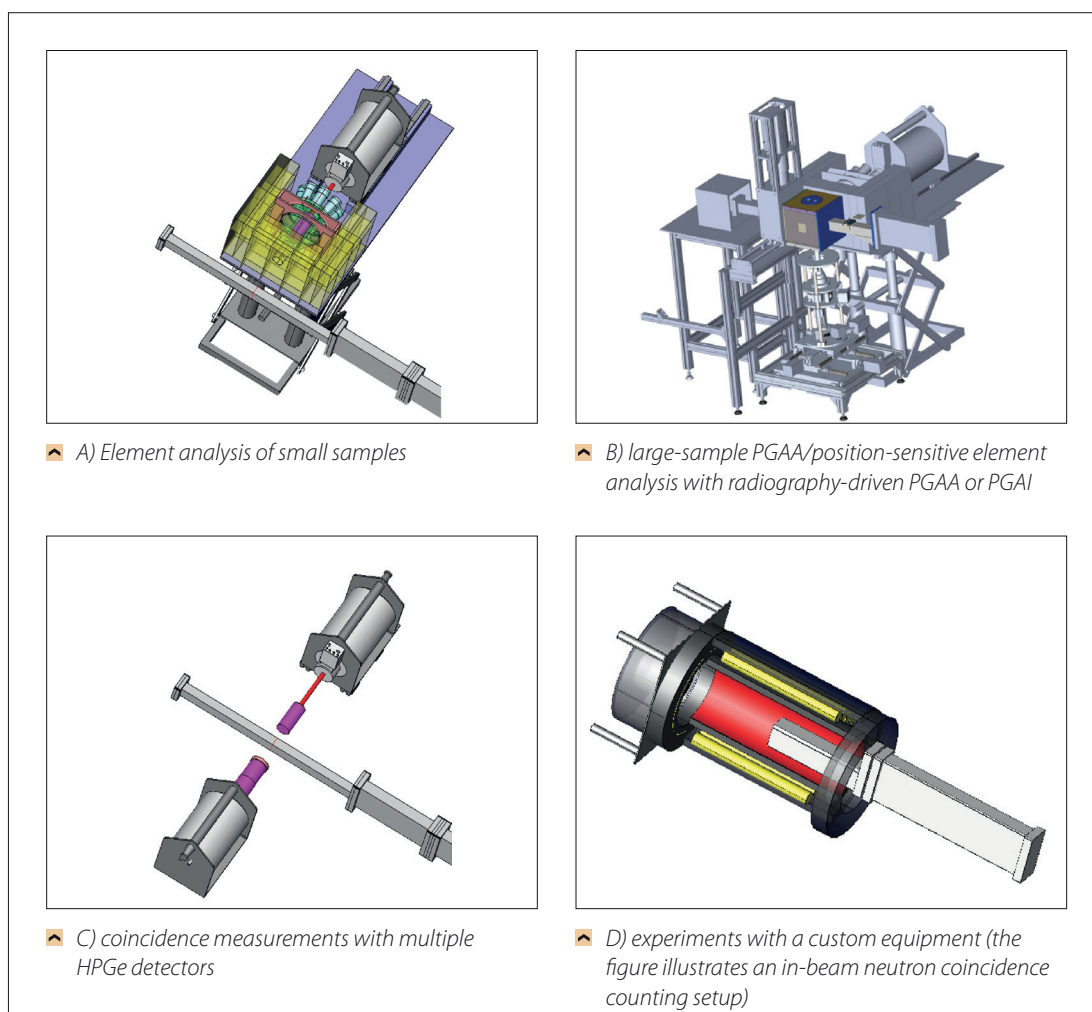


Figure 1.
Possible configurations
of the NIPS experimental
station. The beam arrives
from the lower-right corner
of the images.

6.15. DÖME LOW-LEVEL GAMMA-SPECTROSCOPY FACILITY

Instrument responsible: Zoltán KIS

Centre for Energy Research, Nuclear Analysis and Radiography Department

The increasing need for low-background counting led to the installation of a permanent counting station in the cold-neutron guide hall of Budapest Neutron Centre in 2010. The purpose of DÖME (DÖgnehéz Mérő Eszköz or “damn heavy measuring tool”) is to assist the in-beam activation measurements with off-line counting option on a routine basis, and to allow the measurement of environmental samples of low activities. The facility’s main features are the instant and local availability and the highly accurate activity measurement.

The low-level counting station consists of an iron chamber manufactured from pre-World War II iron (recycled material of the bombed Elisabeth-bridge, 1945), and is therefore free of any man-made radioactivity. The wall of the chamber is 155 mm thick and has a graded shielding (148.5 mm Fe, 5 mm Pb and 1.5 mm Cu layers). The chamber with an internal dimension of 800×800×800 mm³ accommodates a Canberra GR1319 HPGe detector of 13% relative efficiency with a BigMAC cryostat along its horizontal diagonal. This geometry allows sample-to-detector distances up to 250 mm.

As an option for targeted measurements of low-energy lines, a Canberra Low Energy HPGe (GL1018) detector is also available with better energy resolution but for a narrower energy range (up to

about 1 MeV). A Canberra DSA-2000 digital gamma spectrometer with 16k channels is used for the data collection. With the GR1319 detector the facility has a spectral background of about 1.39 cps over the energy range of 7-3150 keV, which compares to 211 cps outside the chamber (i.e. a reduction factor of 152). Dead-time losses during the experiments are typically below 1%.

In-beam activated powder samples can be measured in the Teflon bag used for the PGAA or NIPS-NORMA experiment. Solid samples can be analyzed as received. For powdered environmental samples an easily re-sealable, radon-gastight sample holder from high density polyethylene was fabricated.

The three main parameters of the facility are the detection efficiency, channel-to-energy calibration with nonlinearity and energy resolution. These are established using commercially available certified radioactive sources (¹⁵²Eu, ²⁰⁷Bi, ⁶⁰Co, ¹³³Ba, ²²⁶Ra). The system is calibrated for contact geometry as well as for 32, 167 and 237 mm distances. The EFFICIENCY, NONLINEARITY and FWHM ANALYSIS modules of the HYPERMET-PC software are used for such calculations, while for the efficiency determination of larger, close-to-detector samples the Excel based EFFTRAN efficiency-transfer program and its macros are used.

Reference:

Z Kis, P Völgyesi, Z Szabó. (2013) DÖME: Revitalizing a low-background counting chamber and developing a radon-tight sample holder for gamma-ray spectroscopy measurements. *J Radioanal Nucl Chem.* **298**(3):2029-35.

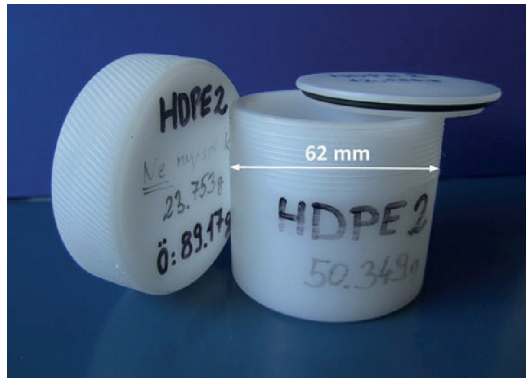
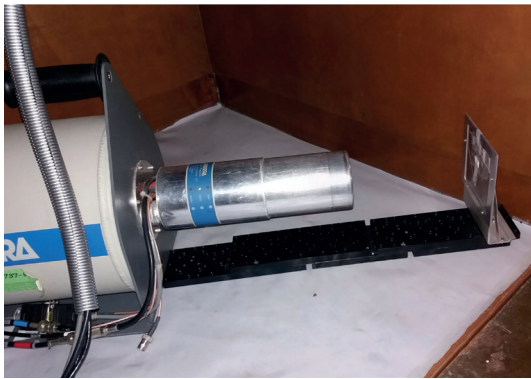


Figure 1. Sample geometries at the DÖME station (left: off-line counting of in-beam activated samples, right: HDPE container for environmental samples)

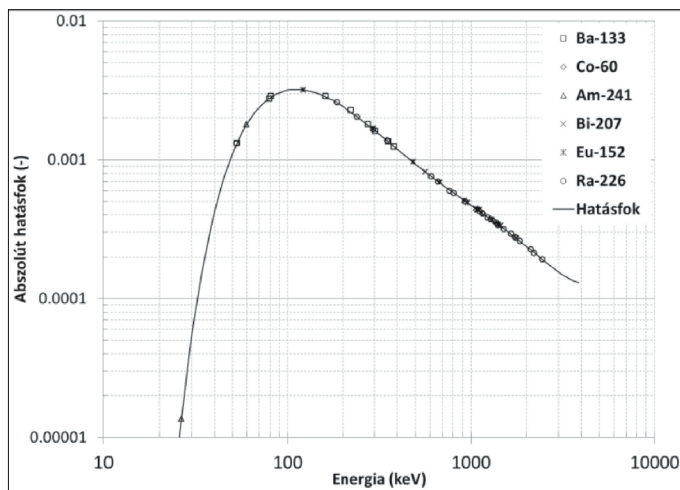


Figure 3. The absolute full-energy peak efficiency for point sources at 167 mm in the DÖME counting station.



Figure 2. The iron chamber of the DÖME counting station.

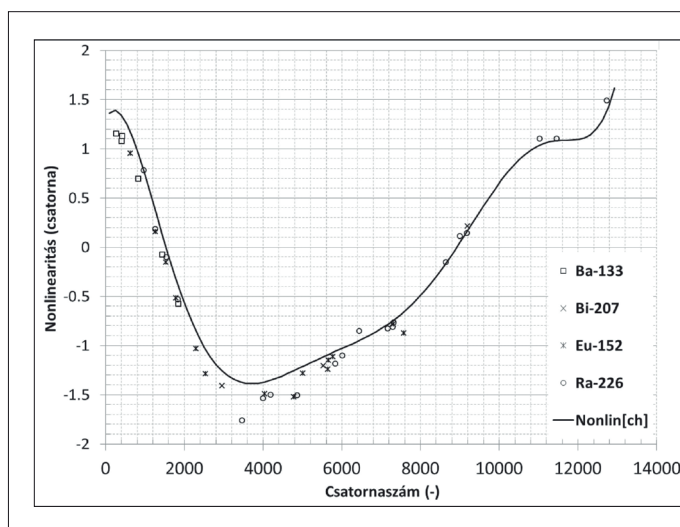
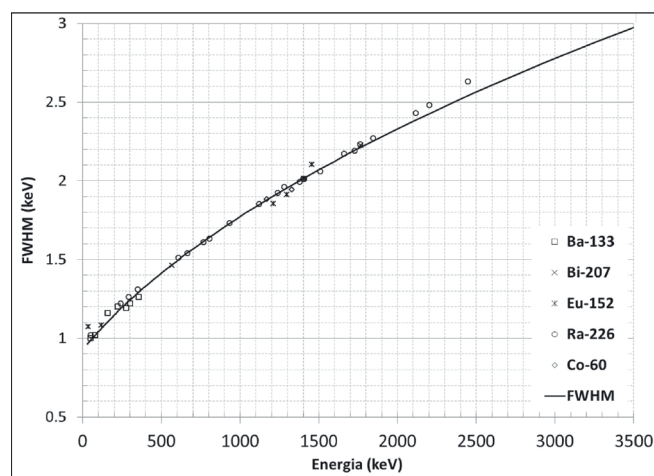


Figure 4. Nonlinearity and energy resolution of DÖME counting station



6.16. BAGIRA4 – REACTOR IRRADIATION LOOP

Instrument scientists: Attila Kovács, Ferenc Gillemot, Ákos Horváth

Centre for Energy Research

Objectives

At the Budapest Research Reactor, two gas cooled irradiation rigs (BAGIRA 1, 2 and 3) have been operated since 1998. Twenty seven different irradiation researches have been performed, testing irradiation ageing of reactor and fusion devices, structural materials, as low alloyed and stainless steels, Al, Ti and W alloys, ceramics etc. The devices served more than 17 years. The material aged by irradiation and corrosion, and their capacity cannot satisfy the up-to date requirements of the newly developing materials.

Presently the main interest of the nuclear industry is the development of fusion reactors and Generation

IV reactors. To increase the efficiency and decrease the impact on the environment, high operation temperature will be used. Consequently high temperature irradiation combined with in pile creep and fatigue testing are the future tasks of the irradiation devices.

Nowadays, there are only a few research reactors in Europe. With the new device in connection with the hot laboratory and with the existing know-how, we are capable of participating in international research projects, as well as customized irradiation and post irradiation examination in cooperation with several institutes and nuclear power industries worldwide.

Description of the new device

The new device is called Budapest Advanced Gas-cooled Irradiation Rig with Aluminium structure 4, BAGIRA4.

The main features of it are:

- The rig capacity is 24 Charpy size specimen (appr. 800 gr steel) or similar. The specimen sizes and shape can be varied according to the requirements, since only the target simple holder has to be changed.

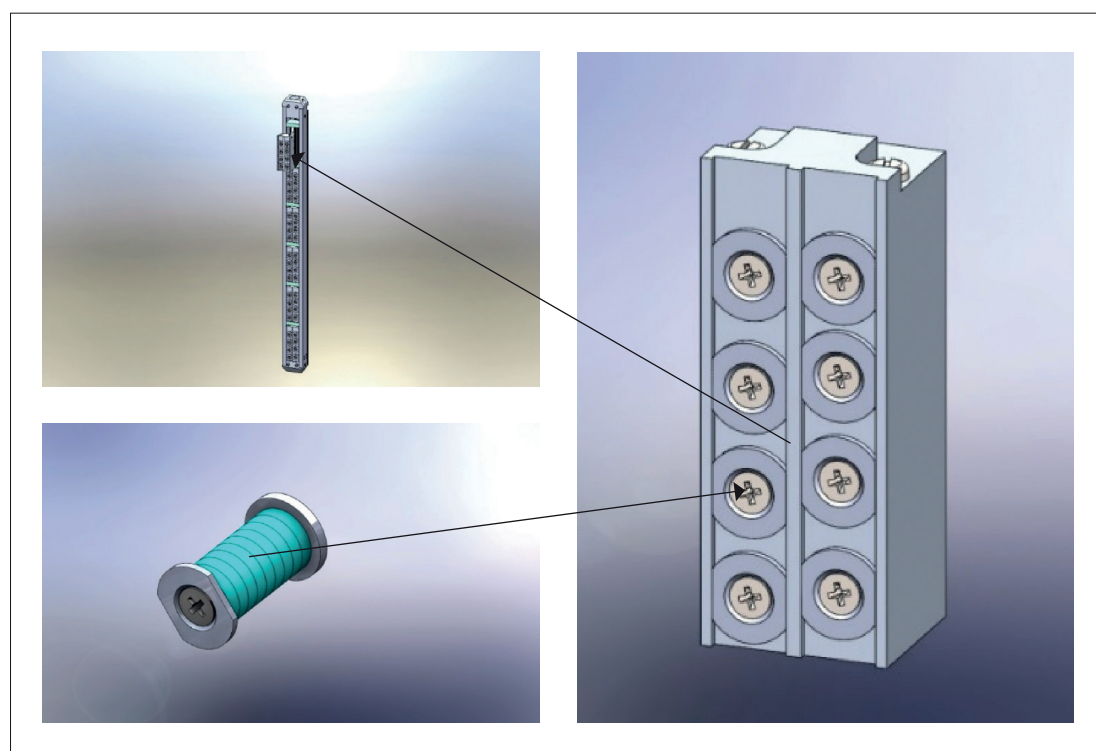


Figure 1. ▶
Full filled target,
with 6 adjustable thermal
control zone

- At each of the new six zones, the electric heating can be separately controlled, ensuring to keep the required irradiation temperature within $\pm 5^\circ\text{C}$. Irradiation temperature can be controlled between 150°C - 350°C with gamma and electric heating and helium-nitrogen gas mix cooling.
- The maximum fluence rate is $3 \cdot 10^{13} \text{ n/cm}^2 \text{ E} > 1\text{MeV}$ (approximately 1,5 dpa/year).
- The target holder is separated from the thermocouples and electric heating system. This way the cost of the heating elements and thermocouples decreasing, and only minor quantity of aluminium or titanium heat removal material goes into the radioactive waste.
- The new target pick up and eject system allows the quick target change during the operation pause of the reactor, and active target also can be used (e.g. irradiated and annealed material can be reirradiated)
- The device is designed for automatic operation, programmable, and it has several safety features, (including emergency passive cooling system, automatic reset in case of any malfunction of the control system, etc.)



◀ **Figure 2.**
Assembled Bagira4 head
with gas and electrical
connectors

The present situation and the remaining work

The equipment is ready and the control software is tested several hundred hours. Twelve different safety tests performed successfully, and the Hungarian National Safety Authority permitted the installation into the reactor.

From the second half of 2016 some functional materials: Spinel, Alumina, Diamond, YAG will be irradiated in the Bagira 4, under the Functional Materials (FM) subproject of European Consortium for the Development of Fusion Energy (Eurofusion).

References

Gillemot Ferenc: „Study of Irradiation Effects at the Research Reactor” Strengths of materials, Vol 42. No 1. 2010, Springer Science pp.78-83

6.17. RNAA – REACTOR-NEUTRON ACTIVATION ANALYSIS

Instrument scientists: Ibilya Sziklai-László, Dénes Párkányi

Centre for Energy Research, Nuclear Analysis and Radiography Department

Neutron activation analysis (NAA) is a method for quantitative composition analysis of chemical elements based on the conversion of stable nuclei in the sample to radioactive nuclei by nuclear reactions, followed by the quantitation of the reaction products via their gamma radiations. The k_0 -standardized neutron activation analysis (k_0 -NAA), combined with high-resolution and high-throughput gamma-ray spectrometry, offers mostly non-destructive, multi-elemental analysis for many branches of science and technology. NAA has inherently favorable characteristics, negligible matrix effect, excellent selectivity and high sensitivity. Even small amount (few tens of milligrams) of samples (mostly solid) can be measured, in which about 35-75 elements in less than 0.01 μg quantities can be determined.

Samples for NAA are irradiated with neutrons in the core of the reactor. Short and long time irradiations are also possible in two designated vertical channels of the reactor. Short irradiations are done by means of a pneumatic rabbit system,

whereas samples for long irradiations are loaded into the rotating channel.

The gamma-rays emitted from the sample are counted in low-level gamma-spectroscopic counting chamber to reduce the external background. In our NAA laboratory there are three low-level gamma-spectroscopic chambers, which are built from pre-World War II steel (free of any man-made radioactivity), have 10 cm thick wall covered with 2 mm thick Cu-layer inside to attenuate the X-rays. There are three different high-purity Ge detectors and two digital gamma spectrometers to detect the gamma-rays and collect the gamma spectra.

The spectra are evaluated with the gamma spectroscopy package Hyperlab 2013.1. This includes automatic peak search, energy calibration the nonlinearity option, and net peak area computation, efficiency correction. For quantitative evaluation, the KayZero for Windows 3 program is used, based on the k_0 standardization.

Reference:

László Szentmiklósi, Dénes Párkányi, Ibilya Sziklai-László, Upgrade of the Budapest neutron activation analysis laboratory, J. Radioanal. Nucl. Chem. (2016) online first, DOI 10.1007/s10967-016-4776-7



Figure 1. ▶
The "D5" gamma spectrometer of the NAA laboratory

Table 1.
Technical details of the irradiation and counting

	Short time irradiation	Long time irradiation
Irradiation time:	0.5 to 5 minutes	More than 1 hour (generally 2–24 hours)
Sample holder:	Powder samples wrapped in Whatmann41 paper and pressed to pellet, afterwards packed in polyethylene capsules	Dried, powdered samples placed into Suprasil AN quartz
Sample geometry:	Pellet: 5 mm diameter, 3 mm height	diameter 4–6 mm
Sample weight:	5–30 mg	30–200 mg
Thermal neutron flux	$5.7 \times 10^{13} \text{ cm}^{-2}\text{s}^{-1}$	$2.0 \times 10^{13} \text{ cm}^{-2}\text{s}^{-1}$
f (thermal to epithermal flux ratio)	37.9	51.2
α (flux parameter $1/E^{1+\alpha}$)	0.003	0.002
Measured elements:	Al, Ca, Cl, Cu, Dy, In, K, Mg, Mn, Na, Sm, Ti, V	As, Ag, Ba, Au, Br, Eu, K, La, Na, Ca, Cd, Ce, Co, Cr, Cs, Eu, Fe, Ga, Gd, Hf, Hg, Ho, Mo, Lu, Nd, Rb, Sb, Sc, Se, Sm, Sn, Sr, Ta, Tb, Th, Tm, U, Yb, W, Zn, Zr

Detectors	Efficiency	Resolution @ 59.5 keV	Resolution @ 1332.5 keV	Dewar
ORTEC PopTop 55195-P“D5”	55%	0.95 keV	1.75 keV	30 l
Canberra GC3618“D4”	36%	0.80 keV	1.80 keV	30 l
Canberra GC1318“D3”	13%	0.95 keV	1.80 keV	30 l

Digital spectrometers	Software (energy range)	Comment
ORTEC DSpecPlus	MAESTRO (30-2500 keV)	DSP-based, Zero-Deadtime Mode
ORTEC DSpec502	MAESTRO (30-3300 keV)	DSP-based, Two channel, Zero-Deadtime Mode

7. | *Education*

GRADUATE AND POSTGRADUATE COURSES

Nuclear analytical methods and applications in earth science and archeometry (Nukleáris elemanalitikai módszerek és alkalmazásaik a földtudományi és archeometriai kutatásokban) I. ELTE TTK, (Gméling Katalin, Belgya Tamás, Kasztovszky Zsolt, Kis Zoltán, Maróti Boglárka, Párkányi Dénes, Szentmiklósi László, Sziklainé László Ibolya) 2013-2014-2015.

Nuclear analytical methods and applications in earth science and archeometry II. (Nukleáris elemanalitikai módszerek és alkalmazásaik a földtudományi és archeometriai kutatásokban II.) ELTE TTK, (Gméling Katalin, Belgya Tamás, Kasztovszky Zsolt, Kis Zoltán, Maróti Boglárka, Párkányi Dénes, Szentmiklósi László, Sziklainé László Ibolya) 2013-2014-2015.

Control theory, University of Pécs, (János Füzi), 2013-2014-2015

Digital Control, University of Pécs, (János Füzi), 2013-2014-2015

Electronics, University of Pécs, (János Füzi), 2013-2014-2015

Neutron beam methods in materials science, BME (László Rosta), 2013-2014-2015

Research of materials structures by neutron scattering ELTE (László Rosta), 2013-2014-2015

LABORATORY PRACTICE AND SEMINARS

Nuclear analytical methods and applications in earth science and archeometry I. (Nukleáris elemanalitikai módszerek és alkalmazásaik a földtudományi és archeometriai kutatásokban I.) ELTE TTK, (Gméling Katalin, Belgya Tamás, Kasztovszky Zsolt, Kis Zoltán, Maróti Boglárka, Párkányi Dénes, Szentmiklósi László, Sziklainé László Ibolya) 2013-2014-2015.

Nuclear analytical methods and applications in earth science and archeometry II. (Nukleáris elemanalitikai módszerek és alkalmazásaik a földtudományi és archeometriai kutatásokban II.) ELTE TTK, (Gméling Katalin, Belgya Tamás, Kasztovszky Zsolt, Kis Zoltán, Maróti Boglárka, Párkányi Dénes, Szentmiklósi László, Sziklainé László Ibolya) 2013-2014-2015.

Level scheme determination of C and Be, lab practice for nuclear engineering students, BME NTI, 2013-2014-2015

PGAA lab practice, ELTE, 2013-2014,2015

PGAA lab practice, University of Debrecen, 2015

Nuclear fuel cycle course - Conditioning and storage of high level radioactive waste (lecture, Margit Fábíán) 2013-2014-2015

Control theory seminar , Univesity of Pécs, (János Füzi) 2013-2014-2015

Electronics laboratory practice, University of Pécs (János Füzi), 2013-2014-2015

PH.D. STUDENTS

M. Zagyvai, Gyors módszerek fejlesztése α -bomló radioizotópok meghatározására környezeti mintákban (Supervisor: N. Vajda)

D. Párkányi, Radioanalitikai módszerek fejlesztése nukleáris hulladékban előforduló hosszú felezési idejű radionuklidok meghatározására (Supervisor: L. Szentmiklósi)

B. Maróti, A prompt-gamma aktivációs analízis optimalizálása fémmintákra és kiegészítése komplementer vizsgálatokkal (Supervisor: T. Belgya)

DISSERTATIONS

M. Papp (ELTE) Elektronikai hulladékok vizsgálata nukleáris analitikai és szerkezetvizsgálati módszerekkel (Supervisor: L. Szentmiklósi)

L. Radnay (University of Debrecen) Investigation of steel structure critical stiffness: strengthening by posttensioning and stressed skin diaphragm design (Supervisors: M. Iványi, J. Füzi)

C. Genreith (Univ. Aachen) Bridging HCl and HBr Oxidation over Heterogeneous Catalysts for Halogen Production (Supervisor: J. Perez-Ramirez)

D. Turkoglu (Ohio State Univ.) Evaluation of prompt gamma-ray data and nuclear structure of Niobium-94 with statistical model calculations (I. Cao)

Events | **8.**

CONFERENCES AND WORKSHOPS

6th International k0-Users' Workshop was held in Budapest, between 22-27 September 2013, it was hosted by Budapest Neutron Centre – MTA EK. The k0 method was launched in the 1970s, jointly by András Simonits and Frans De Corte at the nuclear-analytical laboratories of the KFKI-Budapest and the INW-Gent in order to standardize the neutron activation analysis. The k0 factor contains the essential information for a gamma ray emitted by any nuclide produced by neutron activation. The first workshop among the k0 users was organised in 1992 by Frans De Corte in Belgium. Since then, it has been organized by laboratories dealing with the k0 method world-wide. In 2013 the conference was held in Budapest and organized by the laboratory of András Simonits, the other developer.

Neutrons – 80. A conference was organized by BNC devoted to the 80 years of discovery of neutrons at the Eötvös Loránd University Campus in Budapest on November 27th, 2012. In 1932 Cambridge physicist James Chadwick's famous Nobel Prize winning paper proving the existence of the neutron was published by the Royal Society. Chadwick's discovery led to the development of neutron research, which has been making breakthroughs across the sciences ever since. This historical event and the development of neutron sciences was marked by this event. Ferenc Mezei, László Rosta, Ákos Horváth, János Gadó, Rózsa Baranyai gave lectures on the progress in neutron research and the Budapest Research Reactor. Several young researchers of BNC presented highlight from their recent experiments. The event was attended by many colleagues of the Hungarian neutron user community, researchers from the academia, universities and even from industry.

ENSA. The European Neutron Scattering Association (ENSA) held its second annual Committee meeting on the 16th and 17th of October 2014 in Budapest, it was hosted by the Budapest Neutron Centre, and organized by the Neutron Spectroscopy Department. ENSA groups 24 countries as member organizations. The European user community is considered as a mature and well organized community so that neutron science and the utilization of neutron

beam facilities at neutron source centers have a healthy growth to reach by now a community as large as 6000 users in Europe. This meeting held in Budapest is a recognition that over the past two decades Hungary became an important part of the European neutron scattering landscape and BNC is one of the most reliable provider of access to its neutron beam facilities. This ENSA meeting was attended by 21 delegates and observers as well as 14 representatives of European neutron source facilities. Professor Christiane Alba-Simionesco was elected as the next chair of ENSA and Prof. Ferenc Mezei (Hungarian delegate) as co-chair.

ESS Steering Committee. The 21st Meeting of the European Spallation Source (ESS) Steering Committee – STC21 was organised by BNC-Wigner and held in Budapest, April 7-8, 2015. This important body of delegates of 17 member countries of the ESS consortium, observers of various organisations and the management of ESS – nearly 50 people – has discussed current issues of the construction of ESS, the world's most important neutron facility to be operated. This event was marked by the fact, that this was the last meeting of STC as the highest governance forum of ESS AB, since the European Commission has had awarded the status of ERIC to ESS, thus this body was transformed into the ESS Council playing the same role as of STC.

In-kind delivery meetings. Hungary joined ESS in July 2015, by signing the letter of intent to be a partner at a level of 1% contribution to the ESS investment as well as to become a founding member of ESS ERIC. In this way the path was opened for providing in-kind contributions from Hungarian institutions and industrial companies to the construction of ESS. In 2015 a series of in-kind delivery conferences were held at BNC with the wide participation of interested partners from Hungarian side together with ESS experts in different fields of ESS components, such as the accelerator, target, neutron scattering and control systems. The 6 meetings altogether was attended more than 80 people of nearly 30 organisations. As a result the in-kind delivery process to ESS has started very rapidly and the proper in-kind agreements are now being implemented covering nearly the totality of the time-proportional budget.

PROFESSIONAL TRAINING

Central European Training School on Neutron Techniques

Each year in May Budapest Neutron Centre organizes the only neutron school in the Central European region. From 2013 to 2015 BNC organized three introductory schools, the 2015 school was the 9th event organized in Budapest at the Research Reactor site. Every year the school brought together 25-30 university students, PhD students, young scientists and researchers wishing to deepen their knowledge in the field of materials research and neutron techniques. The majority of the participants came from the Central and Eastern European Region as Czech Republic, Slovakia, Italy, Poland, Romania, Turkey, Ukraine and Hungary, but participants from Germany, Portugal, Russia, UK, Morocco, India and China were also present.

The BNC introductory schools gave a theoretical introduction on neutron scattering techniques, the lectures besides the BNC instrument scientists were given by researchers from ILL-Grenoble, ESS-Lund, Vienna University, JINR, HZB. The 15 hours theoretical lessons in the different neutron scattering techniques, neutron imaging and activation analysis gave insight into the basics of the neutron techniques by approaching the theory from a more practical point of view, useful for the future users of the neutrons. The practical part consisted of 15 hours of training, the participants

could choose between the following neutron instruments: reflectometer, small angle neutron scattering instrument, three-axis spectrometer, neutron diffractometer, time of flight spectrometer, prompt gamma activation analysis station with neutron imaging, and neutron radiography. The experiments demonstrated the work on a large scale facility and showed several applications of neutron scattering in resolving interesting questions on material science.

An afternoon session of the schools was dedicated to the so called “flash-presentations and posters”. This event proved to be an important moment of the school. The participants had the opportunity to present their own research and their connecting point with neutrons, which was a starting for fruitful discussions about the possibilities in performing neutron scattering experiments in order to solve scientific questions.

The organizers are grateful to all lecturers and instrument scientists for their contribution as well as for the many discussions with the “students” leading to ideas for new experiments and collaborations. The organizers thank all students for their enthusiastic participation, which shows the increasing interest for the BNC neutron school.

Further details of the school: www.kfki.hu/~cets

9. | *Publications*

1. Eremin, R.A., Kholmurodov, K.T., Petrenko, V.I., Rosta, L., Avdeev, M.V.; Molecular dynamics simulations for small-angle neutron scattering: Scattering length density spatial distributions for mono-carboxylic acids in d-decalin; *Models in Bioscience and Materials Research: Molecular Dynamics and Related Techniques*, p.139-154, 2013
2. Bulavin, L.A., Nagornyi, A.V., Petrenko, V.I., Avdeev, M.V., Almásy, L., Rosta, L., Aksenov, V.L.; Neutron studies of the structure of non-polar magnetic fluids with surfactant excess; *Ukrainian Journal of Physics*; **58**(12): p.1143-1148, 2013
3. Rogante, M., Rosta, L., Heaton, M.E.; Neutron beam measurement of industrial polymer materials for composition and bulk integrity; *Measurement Science and Technology*; **24**(10), 105601, 2013
4. Eremin, R.A., Kholmurodov, K., Petrenko, V.I., Rosta, L., Avdeev, M.V.; Effect of the solute-solvent interface on small-angle neutron scattering from organic solutions of short alkyl chain molecules as revealed by molecular dynamics simulation; *Journal of Applied Crystallography*; **46**(2): p.372-378, 2013
5. Nagornyi, A.V., Petrenko, V.I., Avdeev, M.V., Bulavin, L.A., Rosta, L., Aksenov, V.L.; On determination of the structural parameters of polydisperse magnetic fluids by small-angle neutron scattering; *Journal of Surface Investigation*; **7**(1): p.99-104, 2013
6. Petrenko, V.I., Avdeev, M.V., Turcu, R., Nan, A., Vekas, L., Aksenov, V.L., Rosta, L., Bulavin, L.A.; Powder structure of magnetic nanoparticles with a substituted pyrrole copolymer shells according to small-angle neutron scattering; *Journal of Surface Investigation*; **7**(1): p. 5-9, 2013
7. Tropin, T.V., Kyrey, T.O., Kyzyma, O.A., Feoktistov, A.V., Avdeev, M.V., Bulavin, L.A., Rosta, L., Aksenov, V.L.; Experimental investigation of C₆₀/NMP/toluene solutions by UV-Vis spectroscopy and small-angle neutron scattering; *Journal of Surface Investigation*; **7**(1): p.1-4, 2013
8. Melnikova, L., Mitroova, Z., Timko, M., J. Kovač, Koralewski, M., Pochylski, M., Avdeev, M.V., Petrenko, V.I., Garamus, V.M., Almásy, L., Kopčanský, P.; Physical characterization of iron oxide nanoparticles in magnetoferritin; *Magnetohydrodynamics*; **49**: p. 293-296, 2013
9. Liu, F., Xiao, J., Garamus, V.M., Almásy, L., Willumeit, R., Mu, B., Zou, A. ; Interaction of the biosurfactant, surfactin with betaines in aqueous solution; *Langmuir*; **29**(34): p. 10648-10657, 2013
10. Yang, X., Zhao, L., Almásy, L., Garamus, V.M., Zou, A., Willumeit, R., Fan, S.; Preparation and characterization of 4-dedimethylamino sancycline (CMT-3) loaded nanostructured lipid carrier (CMT-3/NLC) formulations; *International Journal of Pharmaceutics*; **450**: p.225-234, 2013
11. Lebedev, V., Török, Gy., Vinogradova, L.; Regular star-shaped fullerene(C₆₀)-Containing polystyrenes in solutions: SANS aspect; *Journal of Macromolecular Science, Part B: Physics*; **52**(12): p.1736-1755, 2013
12. Tatár, L., Török, Gy., Smith, D.J., Do, S., Ohms, C., Kovács, L.; Manufacture, residual stress measurement and analysis of a WVER-440 nozzle mockup; *American Society of Mechanical Engineers, Pressure Vessels and Piping Division (Publication) PVP*; **6**(A), 2013
13. Lebedev, V.T., Török, Gy., Vinogradova, L.V.; Effect of fullerene C₆₀ branching center on the conformational properties of arms and the structure of star-shaped polystyrenes in solutions; *Polymer Science - Series A*; **55**(2): p. 65-74, 2013
14. Lebedev, V.T., Grushko, Y.S., Török, Gy.; Structure and self-assembly of fullerene-containing molecular systems; *Journal of Optoelectronics and Advanced Materials* ; **15**(4): p. 193-198, 2013
15. Száraz, Z., Török, Gy., Kršjak, V., Hähner, P.; SANS investigation of microstructure evolution in high chromium ODS steels after thermal ageing; *Journal of Nuclear Materials*; **435**(1): p. 56-62, 2013
16. Lebedev, V.T., Török, Gy., Vinogradova, L.V.; Structural features of fullerene-containing star-shaped polystyrene molecules with Oligomer arms in solutions; *Polymer Science - Series A*; **55**(1): p. 32-38, 2013
17. M. Fabian, E. Sváb, V. Pamukchieva, A. Szekeres, K. Todorova, S. Vogel, U. Ruett, Reverse Monte Carlo modeling of the neutron and X-ray diffraction data for new chalcogenide Ge-Sb-S(Se)-Te glasses, *Journal of Physics and Chemistry of Solids*, **74**:p. 1355-1362, 2013
18. M. Fábrián, E. Sváb, M. von Zimmermann; Structure study of new uranium loaded borosilicate glasses; *J. Non-Cryst. Solids* **380**: p. 71-77

19. SUN GuangAi*, WANG XiaoLin, WU ErDong, LI Jian, CHEN YanZhou, CHEN Bo, SHENG LiuSi, LUZIN Vladimir, GYULA Török; Three-dimensional stress distribution of surplus assembled 7050Al alloy ring and plug determined by neutron diffraction; *Chinese Science Bulletin*; **58** (11): p. 1000-1006 (2013)
20. Z. Száraz, Gy. Török, V. Kršjak, P. Hähner; SANS investigation of microstructure evolution in high chromium ODS steels after thermal ageing; *Journal of Nuclear Materials*; **435**: p. 56-62 (2013)
21. T. Veres, L. Cser, V. Bodnarchuk, V. Ignatovich, Z. E. Horváth, B. Nagy; Investigation of periodic Ni-Ti multilayers, *Thin Solid Films*; **540**, p. 69-72 (2013)
22. Bottyán L, Merkel D G, Nagy B, Füzi J, Sajti Sz, Deák L, Endrőczy G, Petrenko AV, Major J; GINA – A polarized neutron reflectometer at the Budapest Neutron Centre; *REVIEW OF SCIENTIFIC INSTRUMENTS*; **84**(1): p. 8, (2013)
23. Khaydukov YN, Nagy B, Kim J-H, Keller T, Rühm A, Nikitenko YV, Zhernenkov KN, Stahn J, Kiss LF, Csik A, Bottyán L, Aksenov VL; On the feasibility to study inverse proximity effect in a single S/F bilayer by Polarized Neutron Reflectometry; *JETP LETTERS* **98**(2): p. 107-110, (2013)
24. Merkel DG, Nagy B, Sajti Sz, Szilágyi E, Kovács-Mezei R, Bottyán L; Higher harmonics suppression in Fe/Si polarizing neutron monochromators; *NUCLEAR INSTRUMENTS & METHODS IN PHYSICS RESEARCH SECTION A-ACCELERATORS SPECTROMETERS DETECTORS AND ASSOCIATED EQUIPMENT* **704**: pp. 92-97. (2013)
25. Nagy B, Khaydukov YN, Kiss LF, Sajti S, Merkel DG, Tanczikó F, Vasenko AS, Tsaregorodsev RO, Rühm A, Keller T, Bottyán L; Controlling Exchange Coupling Strength in Ni_xCu_{1-x} Thin Films; **26**(5): pp. 1957-1961. (2013)
26. Veres T, Cser L, Bodnarchuk V, Ignatovich V, Horváth ZE, Nagy B; Investigation of periodic Ni-Ti multilayers, *THIN SOLID FILMS*; **540**: p. 69-72 (2013)
27. T. Rehren, T. Belgya, A. Jambon, G. Káli, Z. Kasztovszky, Z. Kis, I. Kovács, B. Maróti, M. Martinón-Torres, G. Miniaci, V.C. Pigott, M. Radivojević, L. Rosta, L. Szentmiklósi, and Z. Szokefalvi-Nagy; 5,000 years old Egyptian iron beads made from hammered meteoritic iron, *Journal of Archaeological Science*; **40**(12): p. 4785-4792. (2013)
28. Rosta L, Belgya T, Káli Gy, Kasztovszky Zs, Kis Z, Kovács I, Maróti B, Szentmiklósi L, Szökefalvi-Nagy Z, Alblbert Jambon, Thilo Rehren; „VASGYÖNGYÖK AZ ÉGBŐL” A legősibb ember által készített vastárgyak meteorit eredetének igazolása röntgen- és neutronanalízissel, *Magyar Régészet* (online magazin, 2013 tél).
29. Schwengner R, Beyer R, Junghans AR, Massarczyk R, Schramm G, Bemmerer D, Birgersson E, Ferrari A, Grosse E, Hannaske R, Kempe M, Kögler T, Matic A, Schilling KD, Wagner A, Rusev G, Makinaga A, Belgya T, Kis Z, Szentmiklósi L, Weil J, Becvar F, Krticka M, Experiments with neutrons and photons at ELBE, In: Garrett PE, Hadinia B (szerk.), Capture Gamma-Ray Spectroscopy and Related Topics: Proceedings of the Fourteenth International Symposium, Kanada, 2011.08.28-2011.09.02., New Jersey; London: World Scientific Pub Co Inc, 2013. pp. 465-474., (ISBN:978-981-4383-63-9)
30. Belgya T, Szentmiklósi L, Thermal neutron capture cross sections of $^{54,56,57}\text{Fe}$, In: Garrett PE, Hadinia B (szerk.), Capture Gamma-Ray Spectroscopy and Related Topics: Proceedings of the Fourteenth International Symposium, Kanada, 2011.08.28-2011.09.02., New Jersey; London: World Scientific Pub Co Inc, 2013. pp. 450-455. (ISBN:978-981-4383-63-9)
31. M. Balaskó, L. Horváth, Á. Horváth, A. Kiss, A. Aszódi: Study on the Properties of Supercritical Water Flowing in a Closed Loop using Dynamic Neutron Radiography *Physics Procedia*; **43**: p. 254-263. (2013)
32. Kis Z, Völgyesi P, Szabó Zs. DÖME - revitalizing a low-background counting chamber and developing a radon-tight sample holder for gamma-ray spectroscopy measurements; *Journal of Radioanalytical and Nuclear Chemistry*; **298**(3): p. 2029-2035 (2013)
33. László Szentmiklósi, Zoltán Kis, Tamás Belgya & Andrey N. Berlizov On the design and installation of a Compton-suppressed HPGe spectrometer at the Budapest neutron-induced prompt gamma spectroscopy(NIPS) facility; *Journal of Radioanalytical and Nuclear Chemistry* **298**: p.1605-1611 (2013)
34. Schillebeeck P, Belgya T, Borella A., Kopecky S., Mengoni A., Quérel C.R., Szentmiklósi L, Tressl I. and Wynants R., Neutron capture studies of ^{206}Pb at a cold neutron beam; *The European Physical Journal A*; **49**: 143; (2013)
35. Farra R., García-Melchor M., Eichelbaum M., Hashagen M., Frandsen W., Allan J., Girgsdies F., Szentmiklósi L, López N. and Teschner D. Promoted Ceria: a Structural, Catalytic and Computational Study; *ACS Catalysis*; p. 2256-2268 (2013)

36. Schulze R., Szentmiklósi L., Kudejova P., Canella L., Kis Z., Belgya T., Jolie J., Ebert M., Materna T., T. Bíró K., Hajnal Zs. The ANCIENT CHARM project at FRM II: threedimensional elemental mapping by prompt gamma activation imaging and neutron tomography; *Journal of Analytical Atomic Spectrometry*; p. 1508-1512 (2013)
37. Oberstedt A., Belgya T., Billnert R., Borcea R., Brys T., Geerts W., Göök A., Hambsch F.-J., Kis Z., Martinez T., Oberstedt S., Szentmiklósi L., Takács K., Vidali M., Improved values for the characteristics of prompt-fission gamma-ray spectra from the reaction $^{235}\text{U}(n_{\text{th}},f)$, *Physical Review C*; **87**: 051602. (2013)
38. Friedrich M., Villaseca S.A., Szentmiklósi L., Teschner D., Armbrüster M., Order-induced selectivity increase of $\text{Cu}_{60}\text{Pd}_{40}$ in the semi-hydrogenation of acetylene, *Materials*, **6**: p. 2958-2977. (2013)
39. Massarczyk R., Schramm G., Junghans A.R., Schwengner R., Anders M., Belgya T., Beyer R., Birgersson E., Ferrari A., Grosse E., Hannaske R., Kis Z., Kogler T., Kosev K., Marta M., Szentmiklósi L., Wagner A., Weil J.L. Electromagnetic dipole strength up to the neutron separation energy from Pt-196 (γ, γ') and Pt-195(n, γ) reactions, *Physical Review C Nuclear Physics* **87**: 044306. (2013)
40. Mödlinger M., Piccardo P., Kasztovszky Z., Kovács I., Szőkefalvi-Nagy Z., Káli G., Szilágyi V., Archaeometallurgical characterization of the earliest European metal helmets, *Materials Characterization*, **79**: p. 22-36. (2013)
41. Firestone R.B., Krticka M., Révay Zs., Szentmiklósi L., Belgya T., Thermal neutron capture cross sections of the potassium isotopes, *Physical Review C*; **87**: 024605. (2013)
42. Szabó Z., Völgyesi P., Nagy H.É., Szabó C., Kis Z., Csorba O., Radioactivity of natural and artificial building materials - a comparative study, *Journal of Environmental Radioactivity*, **118**: p. 64-74. (2013)
43. Mukherji D., Rösler J., Wehrs J., Strunz P., Beran P., Gilles R., Hofmann M., Hoelzel M., Eckerlebe H., Szentmiklósi L., Mácsik Z., Application of in situ neutron and X-ray measurements at high temperatures in the development of Co-Re based alloys for gas turbines, *Metallurgical and Materials Transactions A: Physical Metallurgy and Materials Science*, **44** : p. 22-30. (2013)
44. Moser M., Mondelli C., Schmidt T., Girgsdies F., Schuster M.E., Farra R., Szentmiklósi L., Teschner D., Pérez-Ramirez J., Supported CeO_2 catalysts in technical form for sustainable chlorine production, *Applied Catalysis B: Environmental*, **132-133** :p. 123-131. (2013)
45. Farra R., Eichelbaum M., Schlögl R., Szentmiklósi L., Schmidt T., Amrute A.P., Mondelli C., Pérez-Ramirez J., Teschner D., Do observations on surface coverage-reactivity correlations always describe the true catalytic process? A case study on ceria. *Journal of Catalysis*, **297**: p. 119-127. (2013)
46. Genreith C., Rossbach M., Mauerhofer E., Belgya T., Caspary G., Measurement of thermal neutron capture cross sections of ^{237}Np and ^{242}Pu using prompt gamma neutron activation, *Journal of Radioanalytical and Nuclear Chemistry*, **296**: p. 699-706. (2013)
47. Bernardini F., De Min A., Lenaz D., Kasztovszky Z., Turk P., Veluscek A., Szilágyi V., Tuniz C., Montagnari Kokelj E., Mineralogical and chemical constraints on the provenance of copper age polished stone axes of 'Ljubljana type' from caput Adriae, *Archaeometry*, DOI: 10.1111/arcm.12004 (2013)
48. K. T. Bíró, Zs. Kasztovszky: Obsidian Studies Using Nuclear Techniques in Hungary, Science for Heritage - IAEA TC RER0034 *Regional Project Enhancing the Characterization, preservation and protection of cultural heritage artefacts Newsletter*, Nr. **1**: p. 4-9. (2013)
49. Kasztovszky Zs., T. Dobosi V., T. Bíró K., Szilágyi V., Maróti B. Japán obszidiánok PGAA vizsgálata a Magyar Nemzeti Múzeum Litotéka gyűjteményéből / Prompt Gamma Activation Analysis of Japanese obsidians in the Lithotheca Collection of the HNM; *Archeometriai Műhely / Archaeometry Workshop*; **9**(4): p. 247–254. (2013)
50. Szakmány Gy., T. Bíró K., Kristály F., Bendő Zs., Kasztovszky Zs., Zajzon N. Távolsági import csiszolt kőeszközök nagynyomású metamorfitokból Magyarországon / Long distance import of polished stone artefacts: HP metamorphites in Hungary, *Archeometriai Műhely/Archaeometry Workshop*; **10**(1): p. 83-92. (2013)
51. Péterdi B., Szakmány, Gy., Judik, K., Dobosi, G., Kasztovszky, Zs., Szilágyi, V., Bendő, Zs., G. Gil: Késő rézkori nefrit vésőbalta kőzettani és geokémiai vizsgálatának eredményei – kitekintéssel az ismert európai nefritlelőhelyekre (Balatonőszöd – Temetői dűlő lelőhely, bádeni kultúra). In: Dályay V. – Sámson, M. – Hámos, G. (szerk.): *IV. Kőzettani és Geokémiai Vándorgyűlés Kiadványa*, Orfű, 2013. szeptember 12-14.; p. 100-105. (ISBN 978-963-8221-52-0)

52. Szakmány Gy, Bendő Zs., Kasztovszky Zs., Kristály F., Zajzon N.: Nagynyomású metaofiolit nyersanyagú csiszolt kőeszközök magyarországi régészeti leletanyagokban. In: Dályay V. – Sámson, M. – Hámos, G. (szerk.): *IV. Kőzettani és Geokémiai Vándorgyűlés Kiadványa*, Orfű, 2013. szeptember 12-14.; p. 95-99. (ISBN 978-963-8221-52-0)
53. Oláh I, Ligner J, Bendő Zs, Szakmány Gy, Szilágyi V. Különösen gazdag kőbalta és csiszolt kőeszköz leletegyüttes előzetes vizsgálati eredményei Diósvizlőről, *Archeometriai Műhely*; **10**(1): p. 67-82. (2013)

2014

54. Eremin, R.A., Kholmurodov, K.T., Petrenko, V.I., Rosta, L., Avdeev, M.V.; Molecular dynamics simulation analysis of small-angle neutron scattering by a solution of stearic acid in benzene; *Physics of the Solid State*; **56**(1): p.81-85 (2014)
55. Ünnep, R., Zsiros, O., Solymosi, K., Kovács, L., Lambrev, P.H., Tóth, T., Schweins, R., Posselt, D., Székely, N.K., Rosta, L., Nagy, G., Garab, G.; The ultrastructure and flexibility of thylakoid membranes in leaves and isolated chloroplasts as revealed by small-angle neutron scattering; *Biochimica et Biophysica Acta - Bioenergetics* ;**1837**(9): p. 1572-1580 (2014)
56. Melníková, L., Petrenko, V.I., Avdeev, M.V., Garamus, V.M., Almásy, L., Ivankov, O.I., Bulavin, L.A., Mitróová, Z., Kopčanský, P.; Effect of iron oxide loading on magnetoferritin structure in solution as revealed by SAXS and SANS; *Colloids and Surfaces B: Biointerfaces*; **123**: p. 82-88 (2014)
57. Drescher, S., Lechner, B.-D., Garamus, V.M., Almásy, L., Meister, A., Blume, A.; The headgroup (A)symmetry strongly determines the aggregation behavior of single-chain phenylene-modified bolalipids and their miscibility with classical phospholipids; *Langmuir*; **30**(31): p. 9273-9284 (2014)
58. Chen, Y., Yang, X., Zhao, L., Almásy, L., Garamus, V.M., Willumeit, R., Zou, A.; Preparation and characterization of a nanostructured lipid carrier for a poorly soluble drug; *Colloids and Surfaces A: Physicochemical and Engineering Aspects*; **455** (1): p. 36-43 (2014)
59. Tian, Q., Almásy, L., Yan, G., Sun, G., Zhou, X., Liu, J., Krakovsky, I., Veres, M., Rosta, L., Chen, B.; Small-angle neutron scattering investigation of polyurethane aged in dry and wet air ; *Express Polymer Letters*; **8**(5): p.345-351 (2014)
60. Xiao, J., Liu, F., Garamus, V.M., Almásy, L., Handge, U.A., Willumeit, R., Mu, B., Zou, A.; Insights into the interactions among surfactin, betaines, and PAM: Surface tension, small-Angle neutron scattering, and small-Angle x-ray scattering study; *Langmuir*; **30**(12): p. 3363-3372, (2014)
61. Khamova, T.V., Shilova, O.A., Kopitsa, G.P., Almásy, L., Rosta, L.; Small-angle neutron scattering study of the mesostructure of bioactive coatings for stone materials based on nanodiamond-modified epoxy siloxane sols ; *Physics of the Solid State*; **56**(1): p. 105-113 (2014)
62. Fagadar-Cosma, E., Dudás, Z., Birdeanu, M., Almásy, L.; Hybrid organic - Silica nanomaterials based on novel A$\langle 3 \rangle$B mixed substituted porphyrin; *Materials Chemistry and Physics*; **148**(2): p. 143-152 (2014)
63. Nagorny, A.V., Petrenko, V.I., Bulavin, L.A., Almásy, L., Kovalchuk, V.I., Moroz, K.O., Nedyak, S.P.; Neutron and thermodynamic studies of magnetic fluids stabilized by monocarboxylic acids; *Journal of Physical Studies*; **18**(3): p.1-6
64. Melníková, L., Mitróová, Z., Timko, M., Kováč, J., Avdeev, M.V., Petrenko, V.I., Garamus, V.M., Almásy, L., Kopčanský, P. ; Structural characterization of magnetoferritin; *Mendeleev Communications*; **24**(2): p.80-81 (2014)
65. Kiselev, M.A., Zemlyanaya, E.V., Ryabova, N.Y., Hauss, T., Almásy, L., Funari, S.S., Zbytovska, J., Lombardo, D.; Influence of ceramide on the internal structure and hydration of the phospholipid bilayer studied by neutron and X-ray scattering; *Applied Physics A: Materials Science and Processing*; **116**(1): p.319-325 (2014)
66. Michalcová, A., Svobodová, P., Nováková, R., Len, A., Heczko, O., Vojtěch, D., Marek, I., Novák, P.; Structure and magnetic properties of nickel nanoparticles prepared by selective leaching; *Materials Letters*; **137**: p. 221-224 (2014)

67. Lebedev, V.T., Török, Gy., Vinogradova, L.V.; Investigations of the structure and conformations of star-shaped polymers with fullerene branching centers: Polystyrenes with different structures and functionalities of the C₆₀ centers in toluene; *Physics of the Solid State* ; **56**(1):p. 190-198 (2014)
68. Lebedev, V.T., Török, Gy., Vinogradova, L.V.; Investigations of the structure and conformations of star-shaped polymers with fullerene branching centers functionalized by carbonyl groups; *Physics of the Solid State*; **56**(1): p. 183-189 (2014)
69. Shevtsov, M.A., Nikolaev, B.P., Marchenko, Y.Y., Yakovleva, L.Y., Dobrodumov, A.V., Török, Gy., Pitkin, E., Lebedev, V.T.; Magnetic Resonance Imaging of Rat C6 Glioma Model Enhanced by Using Water-Soluble Gadolinium Fullerene; *Applied Magnetic Resonance*; **45**(4): p. 303-314 (2014)
70. Gillemot, F., Horváth, Á., Horváth, M., Kovács, A., Radiguet, B., Cammelli, S., Pareige, P., Mayoral, M.H., Ulbricht, A., Kresz, N., Oszwald, F., Török, Gy.; Microstructural changes in highly irradiated 15Kh2MFA steel; *Effects of Radiation on Nuclear Materials*: **26**: p.45-56 (2014)
71. M. Fábrián, E. Sváb, K. Krezhov, Neutron diffraction and RMC modeling of new amorphous molybdate system, *Journal of Physics: Conference Series (JPCS)* **558**: 012017 (pp6) (2014)
72. M. A. Shevtsov • B. P. Nikolaev • Ya. Yu. Marchenko • L. Y. Yakovleva • A. V. Dobrodumov • Gy. Török • E. Pitkin • V. T. Lebedev ; Magnetic Resonance Imaging of Rat C6 Glioma Model Enhanced by Using Water-Soluble Gadolinium Fullerene ; *Applied Magnetic Resonance*; **45**(4), (2014)
73. Abraham E, Bessou M, Ziegler A , Herve MC , Szentmiklósi L, Kasztovszky ZS, Kis Z, Menu M, Terahertz, X-ray and neutron computed tomography of an Eighteenth Dynasty Egyptian sealed pottery, *APPLIED PHYSICS A - MATERIALS SCIENCE AND PROCESSING*; **117**(3): p. 963-972. (2014)
74. Basunia MS, Firestone RB, Révay Zs, Choi HD, Belgya T, Escher JE, Hurst AM, Krčička M, Szentmiklósi L, Sleaford B, Summers NC; Determination of the ¹⁵¹Eu(n,γ)Eu and ¹⁵³Eu(n,γ)¹⁵⁴Eu Reaction Cross Sections at Thermal Neutron Energy; *NUCLEAR DATA SHEETS* **119**: p. 88-90 (2014)
75. Belgya T; Uncertainty calculation of functions of γ-ray detector efficiency and its usage in comparator experiments, *JOURNAL OF RADIOANALYTICAL AND NUCLEAR CHEMISTRY*; **300**(2): p. 559-566 (2014)
76. Belgya T, Kis Z, Szentmiklósi L; Neutron Flux Characterization of the Cold Beam PGAA-NIPS Facility at the Budapest Research Reactor; *NUCLEAR DATA SHEETS*; **119**: p. 419-421 (2014)
77. Belgya T, Szentmiklósi L, Massarczyk R, Schwenger R, Schramm G, Birgersson E, Junghans A, Strength function from the ¹¹³Cd(n,γ) reaction, PROCEEDINGS OF THE ERINDA WORKSHOP, CERN, Geneva, Switzerland October 2013, edited by Enrico Chiaveri, *CERN-Proceedings-2014-002*: CERN Geneva: p. 119-126 (2014)
78. Belgya T, Révay Zs, Compendium of Neutron Beam Facilities for High Precision Nuclear Data Measurements , in *IAEA TECDOC 1743* (2014)
79. Benkó T , Beck A , Frey K , Srankó DF , Geszti O , Sáfrán Gy , Maróti B, Schay Z, Bimetallic Ag–Au/SiO₂ catalysts: Formation, structure and synergistic activity in glucose oxidation, *APPLIED CATALYSIS A-GENERAL*; **479**: p. 103-111 (2014)
80. Bernardini F , De Min A , Lenaz D , Kasztovszky Z, Turk P , Velušček A , Szilágyi V, Tuniz C , Montagnari Kokelj E, Mineralogical and Chemical Constraints on the Provenance of Copper Age Polished Stone Axes of ‚Ljubljana Type‘ from Caput Adriae, *ARCHAEOLOGY*; **56**(2): p. 175-202 (2014)
81. Bernardini F , De Min A , Lenaz D , Kasztovszky Z, Turk P , Velušček A , Tuniz C , Montagnari Kokelj E, Petrographic and geochemical comparison between the Copper Age “Ljubljana type” axes and similar lithotypes from Eisenkappler Diabaszug complex (southern Austria), *JOURNAL OF ARCHAEOLOGICAL SCIENCE*; **41**: p. 511-522 (2014)
82. Choi HD , Firestone RB , Basunia MS , Hurst A , Sleaford B , Summers N , Escher JE , Révay Zs, Szentmiklósi L, Belgya T, Krčička M, Radiative Capture Cross Sections of ^{155,157}Gd for Thermal Neutrons, *NUCLEAR SCIENCE AND ENGINEERING*; **177**(2): p. 219-232 (2014)
83. Firestone R B , Révay Zs, Belgya T, Thermal neutron capture cross sections and neutron separation energies for ²³Na(n,γ), *PHYSICAL REVIEW C NUCLEAR PHYSICS*; **89**(1): 014617 (2014)
84. Firestone RB , Abusaleem K , Basunia MS , Bečvář F , Belgya T, Bernstein LA , Choi HD , Escher JE , Genreith C , Hurst AM , Krčička M , Renne PR , Révay Zs, Rogers AM , Rossbach M , Siem S , Sleaford B , Summers NC, Szentmiklósi L, van Bibber K , Wiedeking M, EGAF: Measurement and Analysis of

- Gamma-ray Cross Sections, *NUCLEAR DATA SHEETS*; **119**: p. 79-87 (2014)
85. [Gmélíng K](#), [Simonits A](#), [Sziklai LL](#), [Párkányi D](#), Comparative PGAA and NAA results of geological samples and standards, *JOURNAL OF RADIOANALYTICAL AND NUCLEAR CHEMISTRY*; **300**(2): p. 507-516 (2014)
 86. [Hurst AM](#), [Firestone RB](#), [Sleaford BW](#), [Summers NC](#), [Révay Z](#), [Szentmiklosi L](#), [Basunia MS](#), [Belgya T](#), [Escher JE](#), [Krticka M](#), Investigation of the tungsten isotopes via thermal neutron capture, *PHYSICAL REVIEW C NUCLEAR PHYSICS* **89**(1): 014606 (2014)
 87. [Hurst AM](#), [Firestone RB](#), [Szentmiklősi L](#), [Révay Zs](#), [Basunia MS](#), [Belgya T](#), [Escher JE](#), [Krtička M](#), [Summers NC](#), [Sleaford BW](#), New Measurement of the Thermal-capture Cross Section for the Minor Isotope ¹⁸⁰W, *NUCLEAR DATA SHEETS*, **119**: p. 91-93 (2014)
 88. [Jacimovic R](#), [De Corte F](#), [Kennedy G](#), [Vermaercke P](#), [Révay Z](#), The 2012 recommended k(0) database, *JOURNAL OF RADIOANALYTICAL AND NUCLEAR CHEMISTRY* **300**(2): p. 589-592 (2014)
 89. [Kasztovszky Zs](#), Tűz és víz találkozása - obszidián kőszközők a Kárpátokon innen és túl, **ÉLET ÉS TUDOMÁNY 2014**: p. 38-40. (2014)
 90. [Kasztovszky Zs](#), [T Biro K](#), [Kis Z](#), Prompt Gamma Activation Analysis of the Nyírlugos obsidian core depot find, *JOURNAL OF LITHIC STUDIES* **1**(1): p. 151-163 (2014)
 91. [Mödlinger M](#), [Kasztovszky Zs](#), [Kis Z](#), [Maróti B](#), [Kovács I](#), [Szőkefalvi-Nagy Z](#), [Káli Gy](#), [Horváth E](#), [Sánta Zs](#), [El Morr Z](#), Non-invasive PGAA, PIXE and ToF-ND analyses on Hungarian Bronze Age defensive armour, *JOURNAL OF RADIOANALYTICAL AND NUCLEAR CHEMISTRY* **300**(2): p. 787-799 (2014)
 92. [Mukherji D](#), [Gilles R](#), [Karge L](#), [Strunz P](#), [Beran P](#), [Eckerlebe H](#), [Stark A](#), [Szentmiklosi L](#), [Macsik Z](#), [Schumacher G](#), [Zizak I](#), [Hofmann M](#), [Hoelzel M](#), [Rosler J](#), Neutron and synchrotron probes in the development of Co-Re-based alloys for next generation gas turbines with an emphasis on the influence of boron additives, *JOURNAL OF APPLIED CRYSTALLOGRAPHY*; **47**: p. 1417-1430 (2014)
 93. [Oberstedt A](#), [Belgya T](#), [Billnert R](#), [Borcea R](#), [Brys T](#), [Chaves C](#), [Gamboni T](#), [Geerts W](#), [Göök A](#), [Guerrero C](#), [Hamsch F-J](#), [Kis Z](#), [Martinez T](#), [Oberstedt S](#), [Szentmiklosi L](#), [Takács K](#), [Vidali M](#), Measurements of prompt fission gamma-rays and neutrons with lanthanide halide scintillation detectors, *PROCEEDINGS OF THE ERINDA WORKSHOP, CERN, Geneva, Switzerland October 2013*, edited by Enrico Chiaveri, *CERN-Proceedings-2014-002*: CERN Geneva, p. 79-86 (2014)
 94. [Oberstedt S](#), [Billnert R](#), [Belgya T](#), [Borcea R](#), [Bry's T](#), [Geerts W](#), [Göök A](#), [Hamsch F-J](#), [Kis Z](#), [Martinez Perez T](#), [Oberstedt A](#), [Szentmiklosi L](#), [Vidali M](#), New Prompt Fission γ -ray Data in Response to the OECD/NEA High Priority Request, *NUCLEAR DATA SHEETS* **119**: p. 225-228 (2014)
 95. [Oberstedt S](#), [Billnert R](#), [Belgya T](#), [Bry's T](#), [Geerts W](#), [Guerrero C](#), [Hamsch F-J](#), [Kis Z](#), [Moens A](#), [Oberstedt A](#), [Sibbens G](#), [Szentmiklosi L](#), [Vanleeuw D](#), [Vidali M](#), High-precision prompt- γ -ray spectral data from the reaction ²⁴¹Pu(nth, f), *PHYSICAL REVIEW C NUCLEAR PHYSICS* **90**(2): 024618 (2014)
 96. [Peterdi B](#), [Szakmany G](#), [Judik K](#), [Dobosi G](#), [Kasztovszky Z](#), [Szilagyi V](#), [Maroti B](#), [Bendo Z](#), [Gil G](#), Petrographic and geochemical investigation of a stone adze made of nephrite from the Balatonoszod - Temetoi dulo site (Hungary), with a review of the nephrite occurrences in Europe (especially in Switzerland and in the Bohemian Massif), *GEOLOGICAL QUARTERLY* **58**(1): p. 181-192 (2014)
 97. [Szentmiklosi L](#), [Belgya T](#), [Maroti B](#), [Kis Z](#), Characterization of HPGe gamma spectrometers by geant4 Monte Carlo simulations, *JOURNAL OF RADIOANALYTICAL AND NUCLEAR CHEMISTRY* **300**(2): p. 553-558 (2014)
 98. [Völgyesi P](#), [Kis Z](#), [Szabó Zs](#), [Szabó C](#), Using the 186-keV peak for Ra-226 activity concentration determination in Hungarian coal-slag samples by gamma-ray spectroscopy, *JOURNAL OF RADIOANALYTICAL AND NUCLEAR CHEMISTRY* **302**(1): p. 375-383 (2014)
 99. [Wallner A](#), [Belgya T](#), [Bichler M](#), [Buczak K](#), [Dillmann I](#), [Käppeler F](#), [Lederer C](#), [Mengoni A](#), [Quinto F](#), [Steier P](#), [Szentmiklosi L](#), Novel Method to Study Neutron Capture of U235 and U238 Simultaneously at keV Energies, *PHYSICAL REVIEW LETTERS* **112**(19): 192501 (2014)
 100. [Watkinson D](#), [Rimmer M](#), [Kasztovszky Z](#), [Kis Z](#), [Maróti B](#), [Szentmiklősi L](#), The Use of Neutron Analysis Techniques for Detecting The Concentration And Distribution of Chloride Ions in Archaeological Iron, *ARCHAEOLOGY* **56**(5): p. 841-859 (2014)

101. Eremin, R.A., Kholmurodov, K.T., Petrenko, V.I., Rosta, L., Grigoryeva, N.A., Avdeev, M.V. On the microstructure of organic solutions of mono-carboxylic acids: Combined study by infrared spectroscopy, small-angle neutron scattering and molecular dynamics simulations; *Chemical Physics*, **461**: p. 1-10 (2015)
102. Almeida, J.C., Wacha, A., Bóta, A., Almásy, L., Vaz Fernandes, M.H., Margaça, F.M.A., Miranda Salvado, I.M. PDMS-SiO₂/hybrid materials - A new insight into the role of Ti and Zr as additives; *Polymer (United Kingdom)*; **72**(17951): p. 40-51 (2015)
103. Marczak, W., Hołaj-Krzak, J.T., Lodowski, P., Almásy, L., Fadda, G.C. Hydrogen-bonded aggregates in the mixtures of piperidine with water: Thermodynamic, SANS and theoretical studies; *Chemical Physics Letters* **619**: p. 77-83 (2015)
104. Tian, Q., Takács, E., Krakovský, I., Horváth, Z.E., Rosta, L., Almásy, L.; Study on the microstructure of polyester polyurethane irradiated in air and water; *Polymers*, **7**(9): p. 1755-1766 (2015)
105. Lancastre, J.J.H., Falcão, A.N., Margaça, F.M.A., Ferreira, L.M., Miranda Salvado, I.M., Casimiro, M.H., Almásy, L., Meiszterics, A.; Influence of the polymer molecular weight on the microstructure of hybrid materials prepared by γ -irradiation; *Radiation Physics and Chemistry*, **106**: p. 126-129 (2015)
106. Putz, A.-M., Cecilia, S., Ianăși, C., Dudás, Z., Székely, K.N., Plocek, J., Sfârloagă, P., Săcărescu, L., Almásy, L.; Pore ordering in mesoporous matrices induced by different directing agents; *Journal of Porous Materials*, **22**(2): p. 321-331 (2015)
107. Gubanova, N.N., Baranchikov, A.Ye., Kopitsa, G.P., Almásy, L., Angelov, B., Yapryntsev, A.D., Rosta, L., Ivanov, V.K.; Combined SANS and SAXS study of the action of ultrasound on the structure of amorphous zirconia gels; *Ultrasonics Sonochemistry*, **24**: p. 230-237 (2015)
108. Lancastre, J.J.H., Falcão, A.N., Margaça, F.M.A., Ferreira, L.M., Miranda Salvado, I.M., Almásy, L., Casimiro, M.H., Meiszterics, A.; Nanostructure of PDMS-TEOS-PrZr hybrids prepared by direct deposition of gamma radiation energy; *Applied Surface Science*, **352**: p. 91-94 (2015)
109. Kyzyma, E.A., Tomchuk, A.A., Bulavin, L.A., Petrenko, V.I., Almásy, L., Korobov, M.V., Volkov, D.S., Mikheev, I.V., Koshlan, I.V., Koshlan, N.A., Bláha, P., Avdeev, M.V., Aksenov, V.L.; Structure and toxicity of aqueous fullerene C₆₀ solutions; *Journal of Surface Investigation*, **9**(1): p. 1-5 (2015)
110. Darnay, L., Len, A., Koncz, Á., Friedrich, L., Rosta, L.; Small angle neutron scattering study of nanostructural changes in microbial transglutaminase-treated low-fat yogurt during fermentation; *Food Science and Biotechnology*, **24**(6): p. 2125-2128 (2015)
111. Kulvelis, Yu.V., Ivanchev, S.S., Lebedev, V.T., Primachenko, O.N., Likhomanov, V.S., Török, Gy.; Structure characterization of perfluorosulfonic short side chain polymer membranes; *RSC Advances*, **5**(90): p. 73820-73826 (2015)
112. Kulvelis, Yu.V., Lebedev, V.T., Kononova, S.V., Török, Gy.; Effect of the fullerene C₆₀ on the structure of asymmetric microporous membranes based on polyamidoimide; *Journal of Surface Investigation*, **9**(1): p.6-11 (2015)
113. Bergner, F., Gillemot, F., Hernández-Mayoral, M., Serrano, M., Török, Gy., Ulbricht, A., Altstadt, E.; Contributions of Cu-rich clusters, dislocation loops and nanovoids to the irradiation-induced hardening of Cu-bearing low-Ni reactor pressure vessel steels; *Journal of Nuclear Materials*, **461**: p.37-44(2015)
114. Fábián M., Atomerőművi hulladékok kezelése 1., *Fizikai Szemle* **LXV** (7-8.): p. 241-244 (2015)
115. Fábián M., Atomerőművi hulladékok kezelése 2., *Fizikai Szemle* **LXV** (9.): p. 311-314 (2015)
116. Veres, T. & Cser, L.; Comparison of periodic and aperiodic supermirrors, *Pollack Periodica* **10**: p. 71-80. (2015)
117. R Angelova, V Groudeva, L Slavov, M Iliev, I Nedkov, Sziklai-László, K Krezhov. (2015) Investigation of iron-containing products from natural and laboratory cultivated Sphaerotilus-Leptothrix bacteria. *J Biol Phys.* 41(4):367-75.
118. T Belgya, R Massarzyk, L Szentmiklósi, G Schramm, R Schwengner, AR Junghans, A Wagner, E Grosse; Combined study of the gamma-ray strength function of ¹¹⁴Cd with (n,g) and (g,g') reactions.; *EPJ Web of Conferences*. **93**(01012) (2015)
119. J Corsi, B Maroti, A Re, Z Kasztovszky, L Szentmiklósi, M Torbagyi, A Agostino, D Angelici, S Allegretti; Compositional analysis of a historical collection of Cisalpine Gaul's coins kept at the Hungarian National Museum; *J Anal At Spectrom.* **30**(3):730-7. (2015)

120. D Edge, A Williams, Zs Kasztovszky, Z Kis, I Kovács, L Rosta, Z Szókefalvi-Nagy, Gy Káli; NONDESTRUCTIVE METHODS OF ANALYSIS APPLIED TO ORIENTAL SWORDS; *Gladius*; **139**(58) (2015)
121. AM Hurst, RB Firestone, L Szentmiklosi, BW Sleaford, MS Basunia, T Belgya, JE Escher, M Krticka, Z Revay, NC Summers; Radiative thermal neutron-capture cross sections for the W-180(n, gamma) reaction and determination of the neutron-separation energy; *Phys Rev C*. **92**(3):034615. (2015)
122. AM Hurst, NC Summers, L Szentmiklosi, RB Firestone, MS Basunia, JE Escher, BW Sleaford; Determination of the effective sample thickness via radiative capture; *Nuclear Instruments & Methods in Physics Research Section B-Beam Interactions with Materials and Atoms*; **362**: p. 38-44. (2015)
123. Zs Kasztovszky, B Maróti; Ezüsttárgyak neutronos vizsgálatának lehetőségei és nehézségei (in Hungarian); *Archeometriai Műhely*; **12**(1): p. 25-31. (2015)
124. Z Kis, L Szentmiklosi, T Belgya; NIPS-NORMA station-A combined facility for neutron-based non-destructive element analysis and imaging at the Budapest Neutron Centre; *Nuclear Instruments & Methods in Physics Research Section A-Accelerators Spectrometers Detectors and Associated Equipment*. **779**: p.116-23. (2015)
125. V Kiss, KP Fischl, E Horvath, Gy Kali, Zs Kasztovszky, Z Kis, B Maróti, G Szabo; Non-destructive analyses of bronze artefacts from Bronze Age Hungary using neutron-based methods; *J Anal At Spectrom* **30**(3):685-693. (2015)
126. Ch. Lorenz, R. John, R. Massarczyk, R. Schwengner, A. Blanc, G. de France, M. Jentschel, U. Köster, P. Mutti, G. Simpson, T. Soldner, W. Urban, S. Valenta and T. Belgya; Neutron-capture experiment on ⁷⁷Se with EXILL at ILL Grenoble; *EPJ Web of Conferences*; **93**. (2015)
127. M Moser, G Vile, S Colussi, F Krumeich, D Teschner, L Szentmiklosi, A Trovarelli, J Perez-Ramirez; Structure and reactivity of ceria-zirconia catalysts for bromine and chlorine production via the oxidation of hydrogen halides; *Journal of Catalysis* **331**: p. 128-37. (2015)
128. M Prudêncio, M Dias, C Burbidge, Zs Kasztovszky, R Marques, J Marques, G Cardoso, M Trindade, B Maróti, F Ruiz, L Esteves, M Matos, A Pais; PGAA, INAA and luminescence to trace the "history" of "The Panoramic View of Lisbon": Lisbon before the earthquake of 1755 in painted tiles (Portugal); *J Radioanal Nucl Chem* **304**. (2015)
129. M Rossbach, C Genreith, T Randriamalala, E Mauerhofer, Zs Revay, P Kudejova, S Söllradl, T Belgya, L Szentmiklosi, RB Firestone, AM Hurst, LA Bernstein, B Sleaford, JE Escher; TANDEM: a mutual cooperation effort for transactinide nuclear data evaluation and measurement; *JOURNAL OF RADIOANALYTICAL AND NUCLEAR CHEMISTRY- LETTERS* **303**. (2015)
130. E Starnini, G Szakmány, S Józsa, Zs Kasztovszky, V Szinger-Szilágyi, B Maróti, B Voytek, F Horváth; Lithics from the Tell Site Hódmezővásárhely-Gorzsa (Southeast Hungary): Typology, Technology, Use and Raw Material Strategies during the Late Neolithic (Tisza Culture).
131. L Szentmiklosi, Z Kis; Characterizing nuclear materials hidden in lead containers by neutron-tomography-driven prompt gamma activation imaging (PGAI-NT); *Analytical Methods* **7**(7): p. 3157-3163. (2015)
132. K T. Bíró, Zs Kasztovszky, Gy Káli, Z Kis, A Len, B Maróti, M Molnár, D Párkányi, L Rosta, L Szentmiklosi, Z Szikszai, A Kovács, I Kovács, S-N Z.; TC RER/0/039 – "Enhancing the Characterization, Preservation and Protection of Cultural Heritage Artefacts" Country Report – Hungary. (2014-2015).
133. K.T. Bíró, LM Szabó, L Szentmiklosi, C Korom, I Salamon; 3D MEGJELÉNÍTÉSI TECHNIKÁK ÉS LEHETSÉGES ARCHEOMETRIAI ALKALMAZÁSUK A MAGYAR NEMZETI MÚZEUM MŰTÁRGYAIN. *Archeometriai Műhely*. (2015)
134. G Zerovnik, B Becker, T Belgya, C Genreith, H Harada, S Kopecky, V Radulovic, T Sano, P Schillebeeckx, A Trkov; Systematic effects on cross-section data derived from reaction rates at a cold neutron beam; *Nuclear Instruments & Methods in Physics Research Section a-Accelerators Spectrometers Detectors and Associated Equipment*; **799**: p. 29-36. (2015).
135. Z Pécskay, K Gméling, F Molnár, Z Benkó; Neogene calc-alkaline intrusive magmatism of post-collisional origine along the outer Carpathians: A comparative study of the Pieniny Mountains and the adjacent areas; *Annales Societatis Geologorum Poloniae*. **85**: p. 77-89.
136. J. Sztáncsuj, Katalin T. Bíró, Zs. Kasztovszky, S. Józsa, K. Gméling, B. Maróti; Lithic Implements At Ariuşd (Erőd) A Preliminary Report, *Communications Archaeologiae Hungariae* 2014, p. 19-36. (2015).

Appendix

EXPERIMENTAL STATIONS AT BNC

	Acronym	Instrument	Responsible person phone: +361 392 2222 /EXT, e-mail
1	PSD	Powder diffractometer, Thermal beam No.9	Margit FÁBIÁN/1965 fabian@bnc.hu
2	MTEST	Materials test diffractometer, Thermal beam No.6	László TEIMLEITNER /1469 temleitner@bnc.hu
3	TOF	Time-of-flight diffractometer, Thermal beam No.1	György KÁLI/1439 kali@bnc.hu
4	YS-SANS	Small angle scattering spectrometer (Yellow Submarine), Cold guide No.2	Laszlo ALMÁSY/1447 almasy@bnc.hu
5	F-SANS	Focusing small angle scattering spectrometer, Cold guide No.3/2	Adél LEN/ 1447 len@bnc.hu
6	REFL	Neutron reflectometer, Cold guide No.1/2	Tamás VERES /1738 veres@szfki.hu
7	GINA	Polarised neutron reflectometer, Cold guide No.3/1	Laszlo Bottyan/2761 bottyan@bnc.hu
8	ATHOS	Three-axis spectrometer, Cold guide No.1/1	Gyula TÖRÖK/1439 torok@bnc.hu
9	TAST	Three-axis spectrometer on a thermal beam, Thermal beam No.8	Alex SZAKAL/1416 szakal@bnc.hu
10	RAD	Dynamic/static radiography, Thermal beam No.2/3	Zoltán KIS/ 3311 kis@bnc.hu
11	NORMA	Neutron Tomography, Cold guide No.1/4	Zoltán KIS/ 3311 kis@bnc.hu
12	BIO	Biological irradiations, Thermal beam No.5	Balázs ZÁBORI/1341 zabori@bnc.hu
13	PGAA	Prompt gamma activation analysis, Cold guide No.1/3	László SZENTMIKLÓSI /3143 szentmiklosi@bnc.hu
14	NIPS	Neutron Induced Prompt-Gamma Spectroscopy, Cold guide No.1/4	Zsolt KASZTOVSZKY /3234 kasztovszky@bnc.hu
15	DÖME	The Low-Level gamma-spectroscopy facility	Zoltán KIS/ 3311 kis@bnc.hu
16	BAGIRA	Controlled temperature irradiation rig, Reactor tank	Attila KOVÁCS/1420 kovacs.attila.gy@energia.mta.hu
17	RNAA	Fast-rabbit system and activation analysis, Reactor tank	Dénes PÁRKÁNYI /1411 parkanyi@bnc.hu

An accurate and comprehensive event recording system with absolute and high resolution timestamps

- ⌘ Timestamp resolution: 100 ns

Typical DAQ events to be recorded from the experiments:

- ⌘ Neutron events
- ⌘ Zero time events
- ⌘ Chopper events
- ⌘ Monitor events
- ⌘ Stroboscopic events
- ⌘ Sample environment data

Event	Start	Stop	Channel	Value	Unit	Resolution
START	00000000	00000000	START	1	ns	100
STOP	00000000	00000000	STOP	1	ns	100
CHOPPER	00000000	00000000	CHOPPER	1	ns	100
DETECTOR	00000000	00000000	DETECTOR	1	ns	100
MONITOR	00000000	00000000	MONITOR	1	ns	100
STROBOSCOPIC	00000000	00000000	STROBOSCOPIC	1	ns	100
SAMPLE ENVIRONMENT	00000000	00000000	SAMPLE ENVIRONMENT	1	ns	100

DAQ Solutions for any neutron spectrometers
Event list from FPGA electronics

DAQ Software

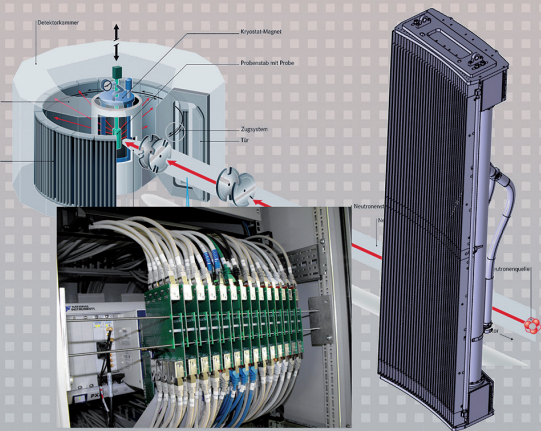
- ⌘ Comprehensive event records
- ⌘ Real time wavelength evaluation
- ⌘ Hidden list mode: immediate spectrum outputs available
- ⌘ Support for dynamic measurements:
e.g. time dependent or stroboscopic experiments

Signal Processing and Data Acquisition System for Large Area PSD

- ⌘ 400+ He-3 PSD tubes
- ⌘ 800+ channels of sampling ADC based signal processing
- ⌘ Up to 50k events/s per tube
- ⌘ Novel algorithm for neutron event qualification
- ⌘ TOF with 7 choppers, 100 ns flight time resolution

Reference:

- ⌘ NEAT-II instrument at Helmholtz-Zentrum Berlin, Germany

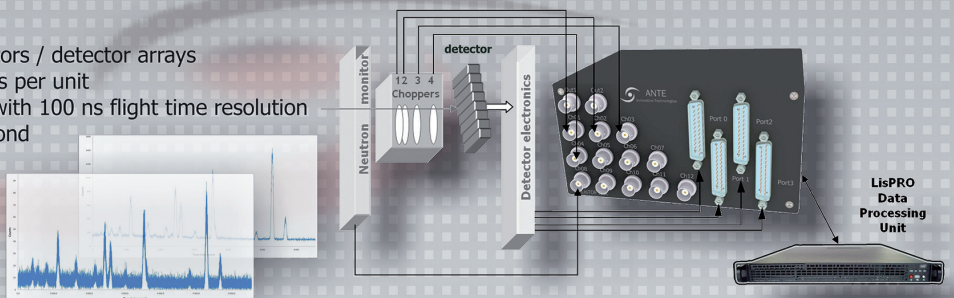


LisTOF Solution

- ⌘ Scalable solution for multidetectors / detector arrays
- ⌘ Can handle up to 8000 detectors per unit
- ⌘ For Time-of-Flight instruments with 100 ns flight time resolution
- ⌘ Up to 2,500,000 events per second

Reference:

- ⌘ Time-of-Flight Diffractometer at BNC, Budapest, Hungary

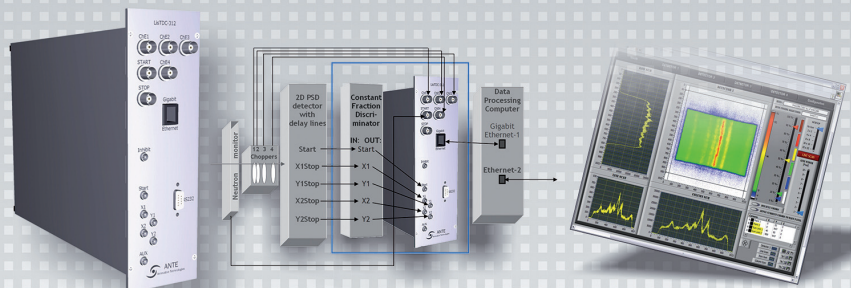


LisTDC Solution

- ⌘ For 2D PSD wire detector
- ⌘ 82.3 ps time to digital resolution
- ⌘ Up to 500,000 hits per second
- ⌘ TOF with 100 ns flight time resolution

References:

- ⌘ Instruments at INPC, Mian Yang, China (RSND, TPNR, SANS, CNTAS)
- ⌘ Bilby Instrument at ANSTO, Australia



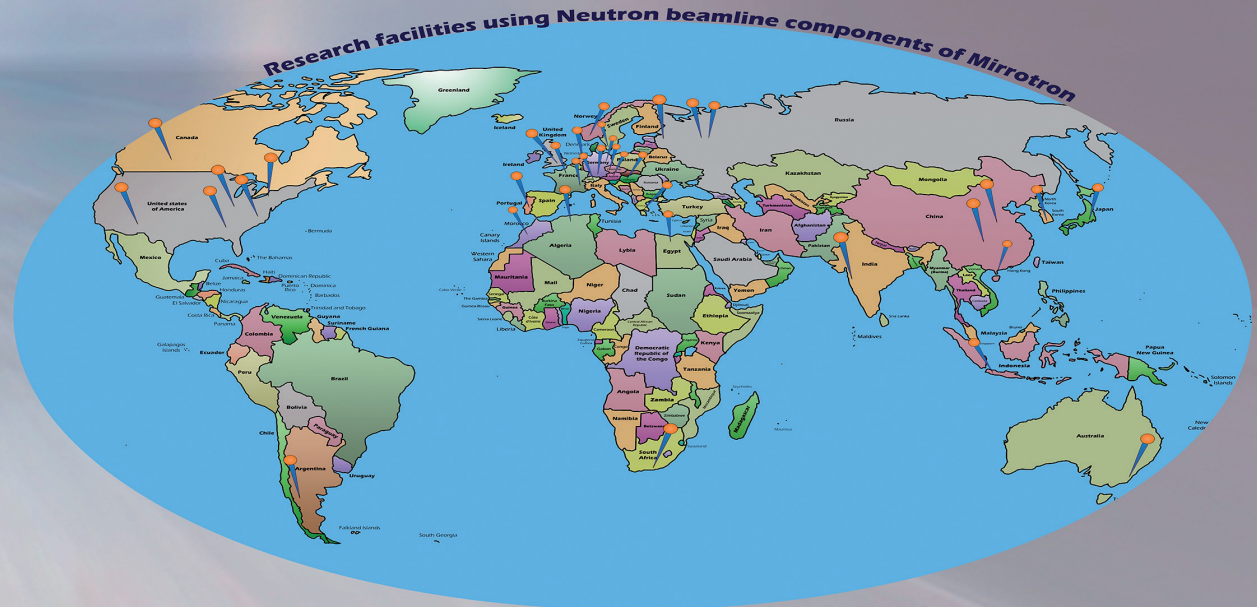
ANTE Innovative Technologies Ltd
KFKI Building 6. Konkoly Thege út 29-33
H-1121 Budapest, HUNGARY

e-mail:
neutron@ante.hu

Partners

- ⌘ HZB, Berlin
- ⌘ Mirrotron, Ltd, Budapest
- ⌘ National Instruments
- ⌘ Budapest Neutron Center
- ⌘ IFE, Kjeller

25 years experience in Neutron Optics & Instrumentation



Supermirror neutron guides total of 1654 meters

Supermirror coating up to $m=5.5$ QC

- 938 meters of guides supplied in vacuum housing,
- 261 meters are made to superpolished substrates,
- 84 meters of In-pile & Shutter guides,
- 36 meters of Bender / Cavity guides,
- 672 meters of glass-sandwich neutron guides,
- 236 meters of metal-glass sandwich neutron guides,
- 367 meters of tapered & elliptic neutron guides,

Neutron Polarizers: 20 equipment

- 4 complete Polarizer-Analyzer systems
- 13 transmission polarizer-analyzer guide units
- 11 pcs RF Spin Flipper
- 14 pcs RF Current / Power Supply
- 3 pcs S-Bender

Neutron Detection & Monitoring Devices: 42 units

Filled inside ~ 720 liter 3-Helium gas

- 23 pcs 2D Position Sensitive Detector
- 11 pcs MK-200 2D PSD
- 2 pcs MK-300 2D PSD
- 7 pcs Large Area 2D PSD
- 3 pcs 2D PS Beam Monitor
- 16 pcs Beam Monitor
- 20 pcs Beam Monitor Electronic unit
- 3 pcs Test "Black" Detector

Neutron Disc Choppers: 50 units

Speed up to 250Hz

- 56 Chopper Disc units
- 44 pcs Single Disc Chopper
- 6 pcs Double Disc Chopper
- 11 pcs Servo Drive System
- 39 pcs Magnetic Bearing Levitated

Neutron Fermi Chopper: 12 units

- Speed up to 600Hz
- 8 pcs complete system
 - 4 pcs Replacement rotor
 - 9 pcs Single Slit Package
 - 3 pcs Double Slit Package

Neutron Velocity Selector: 32 units

- 29 pcs Multi-Disk model – 125Hz
- 3 pcs Multi-Blade model – 200Hz

Neutron Guide Exchanger: 8 systems

- Total length of 75 meters:
- Precise translation mechanism
 - Vacuum vessel

Radiation Shielding

- MirroBor: High B4C=80% content flexible neutron shielding
- 2mm thick MirroBor: 261,5m²
 - 5mm thick MirroBor: 306,75m²
- MirroBor-H: High B4C=82% content solid/hard neutron shielding
- Rotating Monochromator Shielding: 2 assemblies

Neutron Beam Shaping Devices: 125 units

Beam Shutter: 13 units:

- 8 units by motorized movements
- 5 units by pneumatic movements

Beam Slit: 25 units

- 6 units with single - symmetrical movement blades
- 13 units with double - individual movement blades
- 6 units with double manual movement blades

Focusing monochromator: 7 units

Flat analyzer: 2 units

Aperture/diaphragm changer: 15 units

Collimator: 63 units

- 30 sets of motorized multi-pin collimator
- 2 sets of multi-beam guide (17meters)
- 21 units of Soller collimator
- 4 units oscillating Radial collimator

Complete Beamline Instrument: 11 systems

- 6 Spectrometers
- 3 Reflectometers
- 2 Diffractometers

